
Electronic Thesis and Dissertation Repository

9-3-2020 9:45 AM

Human Genetic Variation in Na⁺-Taurocholate Co-transporting Polypeptide (NTCP; SLC10A1) and Targeted Slc10a1 Disruption in Mice: Effects on Bile Acid and Rosuvastatin Transport

Laura E. Russell, *The University of Western Ontario*

Supervisor: Kim, Richard B., *The University of Western Ontario*

A thesis submitted in partial fulfillment of the requirements for the Doctor of Philosophy degree in Physiology and Pharmacology

© Laura E. Russell 2020

Follow this and additional works at: <https://ir.lib.uwo.ca/etd>



Part of the [Medical Pharmacology Commons](#)

Recommended Citation

Russell, Laura E., "Human Genetic Variation in Na⁺-Taurocholate Co-transporting Polypeptide (NTCP; SLC10A1) and Targeted Slc10a1 Disruption in Mice: Effects on Bile Acid and Rosuvastatin Transport" (2020). *Electronic Thesis and Dissertation Repository*. 7311.
<https://ir.lib.uwo.ca/etd/7311>

This Dissertation/Thesis is brought to you for free and open access by Scholarship@Western. It has been accepted for inclusion in Electronic Thesis and Dissertation Repository by an authorized administrator of Scholarship@Western. For more information, please contact wlsadmin@uwo.ca.

Abstract

Sodium-taurocholate co-transporting polypeptide (NTCP, *SLC10A1*) is the central bile acid uptake transporter on the basolateral membrane of hepatocytes. Pharmacological inhibition of NTCP is also being used to treat Hepatitis B and D, and NTCP transports a variety of drugs including cholesterol-lowering statins. Despite these crucial roles, limited knowledge exists regarding the effects of genetic variation in *SLC10A1* on bile acid and rosuvastatin transport.

To address this, we characterized activity and protein expression of genetically variant *SLC10A1 in vitro*. Seven *SLC10A1* genetic variants displayed robust reductions in NTCP-mediated transport of taurocholic acid and rosuvastatin and virtually absent NTCP protein expression at the plasma membrane. *In silico* tools were employed to assess their performance to predict deleterious function, however these did not generate robust enough predictions to replace *in vitro* studies.

To elucidate the *in vivo* effects of targeted *Slc10a1* disruption, serum bile acid composition and hepatic, renal, and ileal gene expression were assessed in male *Slc10a1^{-/-}* mice. Conjugated serum hypercholanemia and absence of *Oatp1a1* (*Slco1a1*) mRNA were observed in a subset of *Slc10a1^{-/-}* mice. Additional changes in gene mRNA expression and mouse necropsy studies suggest these mice were unable to thrive as a result of nutrient malabsorption and disrupted nuclear receptor signaling.

Sex-related differences were evaluated in serum bile acid composition and hepatic gene expression in *Slc10a1^{-/-}* mice. No important sex-related differences

were observed in serum bile acid composition. *Oatp1a1* mRNA was nearly undetectable in both male and female hypercholanemic mice. Sex associated differences in hepatic gene expression in control and normocholanemic *Slc10a1*^{-/-} mice were consistent with literature, however these sex-specific differences were reversed for certain bile acid genes in hypercholanemic mice.

These findings identify novel loss of function genetic variants in the *SLC10A1* gene *in vitro*. Additionally, our studies in *Slc10a1*^{-/-} mice provide evidence of altered nuclear receptor signaling that may have important implications on bile acid physiology and drug response.

Keywords

Na⁺-taurocholate co-transporting polypeptide (NTCP), *SLC10A1*, bile acids, bile acid transporters, drug transporters, hepatic uptake transport, rosuvastatin, *Slc10a1*^{-/-} mice, genetic variation

Summary for Lay Audience

Bile acids are important in digesting food but also play important roles in liver and intestinal health. Genetic changes that affect bile acid movement throughout the gastrointestinal tract can therefore have important implications on health and disease. Specifically, proteins located on the outer membranes of cells in the liver and intestine act as entry and exit points for the movement of bile acids through these tissues. These proteins are called transporters and are also involved in cellular entry and exit of drugs in clinical use. Of importance to this thesis is the commonly prescribed drug rosuvastatin, known by its brand name Crestor™. The ability of rosuvastatin to enter into liver cells is important for its cholesterol-lower capabilities. Therefore, in addition to transporter proteins being important in gastrointestinal health, they are important in drug response. Genetic changes that affect transporters can decrease entry of rosuvastatin into the liver, thereby reducing its cholesterol-lowering benefit. Moreover, reduced entry of rosuvastatin into the liver increases rosuvastatin concentrations in the blood, which has been associated with the adverse drug event of muscle pain and weakness.

Limited information is available regarding the effects of genetic variation in a specific transporter protein that is expressed on the outer cellular membrane of liver cells. This thesis aimed to gather information related to bile acid and drug transport into the liver by using cellular and mouse models to study the effects of genetic changes in our transporter protein of interest. Results from these studies indicate that previously untested genetic changes in our transporter protein result

in reduced protein function and expression, reflected by reduced transport of a bile acid and of the drug rosuvastatin. Furthermore, we genetically disrupted our transporter of interest in mice and identified important changes in bile acid physiology and signaling. We did not observe any differences in rosuvastatin concentrations in the blood or livers of these genetically modified mice, as additional transport proteins are sufficient to maintain rosuvastatin uptake into the liver.

Taken together, these studies used cellular and animal models to identify important effects of genetic changes in our transporter protein. Future studies should assess these effects in humans to determine the overall clinical relevance of our findings. These studies will help contribute to better understanding bile acid transport, signaling, and drug response.

Co-Authorship Statements

Chapter 1: Sections on rare genetic variation and computational prediction were adapted and reprinted with permission (approval listed in Appendix D)

Russell LE and Schwarz UI. 2020. Variant discovery using next-generation sequencing and its future role in pharmacogenetics. *Pharmacogenomics* 21(7):471-86. Copyright 2020 Pharmacogenomics Future Medicine Ltd.

LER wrote the reprinted sections. LER and UIS edited and approved the final version of the manuscript.

Chapter 3: Primary article adapted and reprinted with permission (approval listed in Appendix D)

Russell LE, Zhou Y, Lauschke VM, Kim RB. 2020. *In vitro* functional characterization and *in silico* prediction of rare genetic variation in the bile acid and drug transporter, Na⁺-taurocholate co-transporting polypeptide (NTCP, *SLC10A1*). *Mol Pharm* 17(4):1170-81. Copyright 2020 American Chemical Society.

LER and RBK designed the experiments. LER conducted the *in vitro* experiments. LER and YZ generated the *in silico* predictions. LER, VML, and RBK analyzed and interpreted the data. LER and RBK wrote the manuscript and LER, VML, and RBK edited the manuscript. All authors approved the final version of the manuscript.

Chapter 4: Primary article in preparation

Russell LE, Schmerk CS, Mansell SE, Almousa AA, and Kim RB. Evaluating serum bile acid composition, transporter gene expression, and hepatic rosuvastatin uptake in *Slc10a1*^{-/-} mice. Manuscript in preparation, 2020.

LER, CSS, and RBK were involved in study concept and design. LER, CSS, SEM, and AAA were involved in experimental execution. LER and RBK analyzed and interpreted data. LER and RBK wrote the manuscript, and all authors edited and approved the final version of the manuscript.

Chapter 5: Primary article in preparation

Russell LE, Schmerk CS, Mansell SE, Almousa AA, and Kim RB. Investigating sex-related effects of *Slc10a1* disruption on serum bile acids and hepatic gene expression. Manuscript in preparation, 2020.

LER, CSS, and RBK were involved in study concept and design. LER, CSS, SEM, and AAA were involved in experimental execution. LER and RBK analyzed

and interpreted data. LER and RBK wrote the manuscript, and all authors edited and approved the final version of the manuscript.

Acknowledgments

I would like to thank my supervisor, Dr. Richard Kim, for his guidance throughout this PhD. Dr. Kim, I have learned so much from you. Thank you for sharing your wisdom related to Precision Medicine; I am eternally grateful for this opportunity. I would also like to express my gratitude to Dr. Lina Dagnino, who provided helpful feedback in the final stages of my thesis. Thanks to Dr. Rommel Tirona, Dr. Robert Gros, Dr. Donglin Bai, and Dr. Michael Poulter, for serving as advisors on my thesis committee.

Many thanks to members of the Kim, Tirona, and Schwarz Labs for their support and friendship throughout my PhD. To Dr. Markus Gulilat and Michelle Kim, the lab would not have been the same without you and I am so happy to have met you and continued our friendships. To Dr. Crystal Schmerk, Sara Mansell, and Dr. Ahmed Almousa, the mouse experiments would not have been possible without you and I am very appreciative of your assistance. To Dr. Ute Schwarz, thank you for thoughtful discussions over the years. Cam Ross and Heidi Liao, thanks for being great lab technicians and all-around great people! To Dr. Wendy Teft and Dr. Aze Wilson, thank you for being awesome coworkers and for sharing your scientific knowledge during my journey. To Brad Linton, Dr. Adrienne Borrie, Dr. Sam Medwid, Theo Wigle, and Jaymie Mailloux, it was a pleasure to work alongside you.

Further, my PhD experience was enriched by various members of the scientific community. I feel very fortunate to have completed an internship at Genentech during my studies. To my Genentech supervisor, Dr. Edna Choo, I

look back on my experience in South San Francisco fondly. I would like to thank Justin Ly and everyone in the Drug Metabolism and Pharmacokinetics department at Genentech for contributing to the experience that sparked my interest in pursuing a career in industry. Further, California would not have been so unforgettable without my fellow interns, Dr. Lydia Dewis and Dr. Jasmine Bickel. Thank you, ladies, for being so amazing.

I would like to acknowledge members of the International Society for the Study of Xenobiotics for their contributions to my career development. To my mentors, Dr. Sonia De Moraes and Dr. Franz Schuler, and to members of the ISSX New Investigators Group, especially Jasleen Sodhi: thank you. Additionally, I was fortunate to be part of the Drug Safety and Effectiveness Cross Disciplinary Training (DSECT) Program for two years, which helped deepen my understanding of a broad range of topics in drug safety and effectiveness research. I am grateful to the program trainees and Dr. Lisa Dolovich & Andrea Massey for making this such a positive experience.

Last but not least, thank you to my family, friends, fellow graduate students, and yoga community who have supported me so graciously from (before) the beginning to the end of my PhD. To my mother, Debbie Russell, your unwavering support does not go unnoticed; you have been a pillar in my achievements. To my father, Geoff Russell, your love and encouragement have been instrumental in this journey. To my best friends Madi Borland and Kristen Hajpel, thank you for all of your kind words and for being there through the good and the bad. I cannot adequately express my appreciation for you all.

Table of contents

Abstract	<i>i</i>
Summary for Lay Audience	<i>iii</i>
List of Figures	<i>xiii</i>
List of Appendices	<i>xvi</i>
1 Introduction	1
1.1 The Liver	1
1.2 Organization, architecture, and cell biology of hepatocytes	5
1.3 Physiological roles of bile acids	6
1.4 Primary bile acid synthesis	7
1.5 Secondary bile acid synthesis	10
1.6 Bile acid detoxification	12
1.7 Transporters maintain enterohepatic circulation of bile acids	12
1.8 Pathology associated with disruption of bile acid transport and synthesis 16	
1.9 Nuclear receptors in bile acid homeostasis.....	17
1.10 FXR regulation of bile acid synthesis and transport	23
1.11 Role of bile acid transporters in statin transport.....	27
1.12 Rosuvastatin transport and genetic variation.....	28
1.13 Na ⁺ -taurocholate co-transporting polypeptide (NTCP, <i>SLC10A1</i>)	29
1.14 Rare genetic variation and next-generation sequencing	31
1.15 Computational prediction of rare variant function	33
1.16 References.....	35
2 Rationale, Specific Aims, Hypotheses	44
2.1 Thesis Rationale	44
2.2 Governing hypothesis	44
2.3 Specific Aim 1	44
2.4 Specific Aim 2	45
2.5 Specific Aim 3	46
2.6 References.....	47
3 In vitro functional characterization and in silico prediction of rare genetic variation in the bile acid and drug transporter, Na⁺-taurocholate co-transporting polypeptide (NTCP, <i>SLC10A1</i>) (Russell et al., 2020)	49
3.1 Introduction	50

3.2	Methods & Materials	54
3.2.1	Materials	54
3.2.2	Identification of single nucleotide variants in <i>SLC10A1</i>	54
3.2.3	<i>In silico</i> functional prediction of genetic variants in NTCP	55
3.2.4	Wild type and variant plasmid construction	58
3.2.5	Transient expression of NTCP in cultured cells	61
3.2.6	Single timepoint <i>in vitro</i> transport of taurocholic acid and rosuvastatin	63
3.2.7	Characterization of transport kinetics	64
3.2.8	Western blot analysis	65
3.2.9	Cell surface biotinylation	66
3.2.10	Cell surface deglycosylation assay	67
3.2.11	Immunofluorescence confocal microscopy	68
3.2.12	Predictive performance of <i>in silico</i> tools	69
3.2.13	Predicted structures of NTCP	70
3.2.14	Statistics	70
3.3	Results	72
3.3.1	Identifying <i>SLC10A1</i> variants	72
3.3.2	<i>In vitro</i> transport and protein expression	74
3.3.3	Transport kinetics	85
3.3.4	Determining the proximity of NTCP variants to amino acid residues important in NTCP function	89
3.3.5	Predictive performance of algorithms	97
3.4	Discussion	104
3.5	References	112
4	<i>Evaluating serum bile acid composition, bile acid gene expression, and rosuvastatin disposition in <i>Slc10a1</i>^{-/-} mice</i>	119
4.1	Introduction	120
4.2	Methods & Materials	124
4.2.1	Materials	124
4.2.2	Animal use approval	124
4.2.3	Liver-specific targeted disruption of <i>Slc10a1</i> in C57BL/6 mice	124
4.2.4	Quantification of serum total bile acids by colorimetric assay	127
4.2.5	Quantification of serum individual bile acids by LC-MS/MS	127
4.2.6	Quantification of mRNA in mouse tissues	130
4.2.7	Mouse necropsy	132
4.2.8	Rosuvastatin studies	132
4.2.9	Statistics	133
4.3	Results	135
4.3.1	Mouse phenotype	135
4.3.2	Serum total bile acid concentrations	141
4.3.3	Serum conjugated and unconjugated bile acids	143
4.3.4	Relative mRNA levels of hepatic bile acid uptake transporters	149
4.3.5	Relative mRNA levels of bile acid efflux transporters	151
4.3.6	Relative mRNA levels of hepatic bile acid synthesis genes	155
4.3.7	Relative mRNA levels of bile acid genes in the ileum	157
4.3.8	Relative mRNA levels of bile acid transporter genes in the kidney	160
4.3.9	Hepatic uptake of rosuvastatin	163
4.4	Discussion	166
4.5	References	174

5	<i>Investigating sex-related effects of <i>Slc10a1</i> disruption in mice on serum bile acids and hepatic bile acid gene expression</i>	179
5.1	Introduction	180
5.2	Methods & Materials	182
5.2.1	Materials	182
5.2.2	Animal use approval	182
5.2.3	Liver-specific targeted disruption of <i>Slc10a1</i> in C57BL/6 mice	182
5.2.4	Quantification of serum total bile acids by colorimetric assay	182
5.2.5	Quantification of serum individual bile acids by LC-MS/MS	183
5.2.6	Quantification of hepatic mRNA expression by qPCR	183
5.2.7	Control, normocholanemic, and hypercholanemic mice	183
5.2.8	Statistics	183
5.3	Results	185
5.3.1	Total serum bile acids	185
5.3.2	Individual serum unconjugated bile acids	187
5.3.3	Individual serum conjugated bile acids	189
5.3.4	Overall serum unconjugated and conjugated bile acid profiles	191
5.3.5	Overall serum muricholic acid and cholic acid profiles	195
5.3.6	Hepatic bile acid synthesis gene expression	199
5.3.7	Hepatic expression of hepatic bile acid uptake transporters	205
5.3.8	Hepatic expression of hepatic bile acid efflux transporters	209
5.4	Discussion	214
5.5	References	219
6	<i>Summary, future directions & conclusions</i>	223
6.1	Conclusions	237
6.2	References	239
7	<i>Appendices</i>	242
	<i>Curriculum Vitae</i>	256

List of Tables

Table 1.1. Nuclear receptors and their target bile acid-related genes	22
Table 3.1. <i>In silico</i> tools used to predict effects of SLC10A1 genetic variation on NTCP protein function	57
Table 3.2. Primers used to clone NTCP and create variants	59
Table 3.3. Primers used to clone NTCP and create variants continued	60
Table 3.4. <i>SLC10A1</i> variants for <i>in vitro</i> characterization and <i>in silico</i> prediction	73
Table 3.5. Performance of <i>in silico</i> tools to predict taurocholic acid and rosuvastatin uptake.	103
Table 4.1. Bile acid mass spectrometry parameters	129
Table 4.2. Primers used for qPCR	131
Table 5.1. Statistical differences in serum unconjugated and conjugated bile acid species	194
Table 5.2. Sex-related differences in unconjugated and conjugated serum bile acids	194
Table 5.3. Statistical differences in overall serum muricholic acid and cholic acid species	198
Table 5.4. Sex-related differences in overall serum muricholic acid and cholic acid	198

List of Figures

Figure 1.1. Liver anatomy	2
Figure 1.2. Organization of hepatocytes and cholangiocytes within the liver.....	4
Figure 1.3. Primary bile acid synthesis	9
Figure 1.4. Formation of secondary bile acids	11
Figure 1.5. Transporters in bile acid enterohepatic circulation	15
Figure 1.6. Interplay between bile acids, nuclear receptor regulation, and bile acid and drug metabolism.	18
Figure 1.7. FXR binds to response elements in target genes to induce their transcription.....	21
Figure 1.8. FXR regulation of bile acid synthesis and transport	26
Figure 3.1. An overview of cloning, transfection, and transport experiments.....	62
Figure 3.2. Determining the effect of the V5 epitope on substrate transport.....	75
Figure 3.3. Substrate uptake and whole-cell NTCP protein expression of <i>SLC10A1</i> variants in HEK293T cells.	78
Figure 3.4. Whole-cell and plasma membrane expression of variant NTCP protein in HEK293T cells	80
Figure 3.5. Immunofluorescence confocal microscopy of wild type and variant NTCP.....	81
Figure 3.6. Whole-cell protein expression of NTCP in HeLa cells.	83
Figure 3.7. Cell surface NTCP protein deglycosylation in HEK293T cells	84
Figure 3.8. Determining linear substrate uptake timepoints for NTCP-mediated transport	86
Figure 3.9. Transport kinetics for wild type and variant NTCP.....	88
Figure 3.10. Predicted topologies for NTCP with residues for TCA transport activity and binding sites identified.	90
Figure 3.11. Predicted topologies for NTCP with residues for rosuvastatin transport activity and binding sites identified.	91
Figure 3.12. Predicted three dimensional structures for NTCP with loss of activity variants identified.....	92
Figure 3.13. Predicted 3D structure of NTCP with identified binding sites and loss of activity but not expression variants I279T and A64T.	94
Figure 3.14. Sequence alignment for human, mouse, and rat NTCP and human ASBT	96
Figure 3.15. Performance of <i>in silico</i> tools optimized for evolutionary conservation and amino acid properties to predict <i>in vitro</i> NTCP variant transport activity	100
Figure 3.16. Performance of <i>in silico</i> tools optimized using outputs from multiple <i>in silico</i> scoring tools to predict <i>in vitro</i> NTCP variant transport activity	101
Figure 3.17. Performance of the ADME-optimised <i>in silico</i> tool to predict <i>in vitro</i> NTCP variant transport activity	102
Figure 4.1. Liver-specific targeted disruption <i>Slc10a1</i>	126
Figure 4.2. Relative mRNA levels in the livers of floxed control mice, <i>Slc10a1</i> ^{+/-} mice, and <i>Slc10a1</i> ^{-/-} mice.	137
Figure 4.3. Mouse survival over the first eight weeks of life	138

Figure 4.4. Weekly mouse body weights from week one to week eight.....	140
Figure 4.5. Total serum bile acid concentrations	142
Figure 4.6. Individual serum bile acid concentrations	145
Figure 4.7. Percentages of unconjugated and conjugated bile acids.....	146
Figure 4.8. Percentages of muricholic acid and cholic acid species	148
Figure 4.9. Relative mRNA expression of bile acid uptake transporters in the liver	150
Figure 4.10. Relative mRNA expression of canalicular efflux transporters in the liver.....	152
Figure 4.11. Relative mRNA expression of basolateral efflux transporters in the liver.....	154
Figure 4.12. Relative mRNA levels of bile acid synthesis genes in the liver.....	156
Figure 4.13. Relative mRNA levels of transporters and repressors of bile acid synthesis and uptake in the ileum.....	159
Figure 4.14. Relative mRNA levels of bile acid transporters in the kidney.....	162
Figure 4.15. Hepatic disposition of orally administered rosuvastatin (10mg/kg) in control and <i>Slc10a1</i> ^{-/-} mice.	164
Figure 4.16. Hepatic mRNA expression of bile acid uptake and efflux transporters in ten-week-old mice.....	165
Figure 4.17. Hypothesized alterations in nuclear receptor signaling in our hypercholanemic <i>Slc10a1</i> ^{-/-} mice.....	173
Figure 5.1. Total serum total bile acid concentrations grouped by biological sex	186
Figure 5.2. Individual unconjugated serum bile acid concentrations grouped by sex.....	188
Figure 5.3. Individual conjugated serum bile acid concentrations grouped by sex	190
Figure 5.4. Overall serum unconjugated and conjugated bile acids	193
Figure 5.5. Overall serum muricholic acid species (MCAs) and cholic acid species (CAs)	197
Figure 5.6. Hepatic mRNA expression of bile acid synthesis gene <i>Cyp7a1</i> its transcriptional repressor <i>Shp</i>	201
Figure 5.7. Hepatic mRNA expression of bile acid synthesis genes <i>Cyp8b1</i> and <i>Cyp27a1</i>	204
Figure 5.8. Hepatic mRNA expression of bile acid uptake transporter genes <i>Ntcp</i> and <i>Oatp1b2</i>	206
Figure 5.9. Hepatic mRNA expression of bile acid uptake transporter genes <i>Oatp1a1</i> and <i>Oatp1a4</i>	208
Figure 5.10. Hepatic mRNA expression of canalicular bile acid efflux transporter genes <i>Bsep</i> and <i>Mrp2</i>	210
Figure 5.11. Hepatic mRNA expression of basolateral bile acid efflux transporter genes <i>Mrp3</i> and <i>Ostβ</i>	213
Figure 6.1. Rare genetic variant discovery and characterization: from next- generation sequencing to <i>in vivo</i> clinical relevance	227
Figure 6.2. Hypothesized alterations in nuclear receptor signaling in our hypercholanemic <i>Slc10a1</i> ^{-/-} mice.....	229

Figure 6.3. Female-dominant gene expression in healthy and hypercholanemic mice..... 235

List of Appendices

Appendix A. Supplemental data	242
Appendix B. Mouse necropsy reports.....	246
Appendix C. Ethics & Animal Use Approvals.....	251
Appendix D. Permission to reproduce published articles.....	254

Abbreviations

ABC	ATP-binding cassette
ADE	Adverse drug event
ADME	Absorption, distribution, metabolism, excretion
ASBT	Apical sodium-dependent bile acid transporter
ATP	Adenosine triphosphate
AUC _{ROC}	Area under the receiver operating characteristic curve
BAAT	Bile acid CoA:amino acid N-acyltransferase
BARE	Bile acid response element
BCA	Bicinchoninic assay
BSEP	Bile salt export pump
BSH	Bile salt hydrolase
CA	Cholic acid
CADD	Combined annotation-dependent depletion
CAR	Constitutive androstane receptor
CDCA	Chenodeoxycholic acid
cDNA	Complementary deoxyribonucleic acid
CYP	Cytochrome P450
CYP27A1	Sterol 27-hydroxylase
CYP7A1	Cholesterol 7 α -hydroxylase
CYP7B1	Oxysterol and steroid 7-alpha-hydroxylase
CYP8B1	Sterol 12 α -hydroxylase
DCA	Deoxycholic acid
DMSO	Dimethyl sulfoxide
DNA	Deoxyribonucleic acid
EDTA	Ethylenediaminetetraacetic acid
ER	Estrogen receptor
FBS	Fetal Bovine Serum
FGF15	Fibroblast growth factor 15
FGF19	Fibroblast growth factor 19
FGFR4	Fibroblast growth factor receptor 4
FXR	Farnesoid X receptor
FXRE	Farnesoid X receptor response element
GCA	Glycocholic acid
GCDCA	Glycochenodeoxycholic acid
GDCA	Glycodeoxycholic acid
GR	Glucocorticoid receptor
HMG-CoA	3-hydroxy-3-methylglutaryl coenzyme A
HNF	Hepatocyte nuclear factor
HSDH	Hydroxysteroid dehydrogenase
K _m	Substrate concentration producing 50% maximal velocity
LCA	Lithocholic acid
LDS	Lithium dodecyl sulfate
LXR	Liver X receptor
m/z	Mass-to-charge ratio

MetaLR	Meta Logistic Regression
MCA	Muricholic acid
MDR	Multidrug resistance
mRNA	Messenger ribonucleic acid
MRP	Multidrug resistance-associated protein
NTCP	Na ⁺ -taurocholate co-transporting polypeptide
OATP	Organic anion transporting polypeptide
OST	Organic solute transporter
P-gp	P-glycoprotein
PBS	Phosphate buffered saline
PPAR	Peroxisome proliferator-activated receptor
PXR	Pregnane X receptor
RIPA	Radioimmunoprecipitation assay
RNA	Ribonucleic acid
SD	Standard deviation
SDS-PAGE	Sodium dodecyl sulfate polyacrylamide gel electrophoresis
SEM	Standard error of the mean
SHP	Small heterodimer partner
SIFT	Sorting Intolerant From Tolerant
SLC	Solute carrier
t _{1/2}	Elimination half life
TBA	Total bile acids
TBS	Tris buffered saline
TCA	Taurocholic acid
TCDCA	Taurochenodeoxycholic acid
TDCA	Taurodeoxycholic acid
UDCA	Ursodeoxycholic acid
VDR	Vitamin D receptor
V _{max}	Maximal velocity
WT	Wild type

1 Introduction

1.1 The Liver

The liver is responsible for many integral homeostatic and physiological functions. The liver is a bidirectional biological filter; it filters blood from the portal circulation as well as from the systemic circulation. The portal vein and the hepatic artery supply hepatocytes with blood. The portal vein carries nutrients, xenobiotics, and toxins absorbed from the gastrointestinal tract. The hepatic artery stems from the lungs and delivers oxygen to the liver. The hepatic veins are responsible for draining blood from the liver into the inferior vena cava, thus reaching the systemic circulation (Nagy et al., 2020). The filtration achieved by the liver is an active process, where many exogenous substances are metabolized and subsequently excreted. The biliary system is a main component of the liver. The biliary system removes hydrophobic substances including bile acids, drugs, and metabolites from hepatocytes by draining into the gallbladder followed by secretion into the intestinal lumen and fecal excretion (Nagy et al., 2020). A gross overview of these important structures in hepatic anatomy are depicted in Figure 1.1.

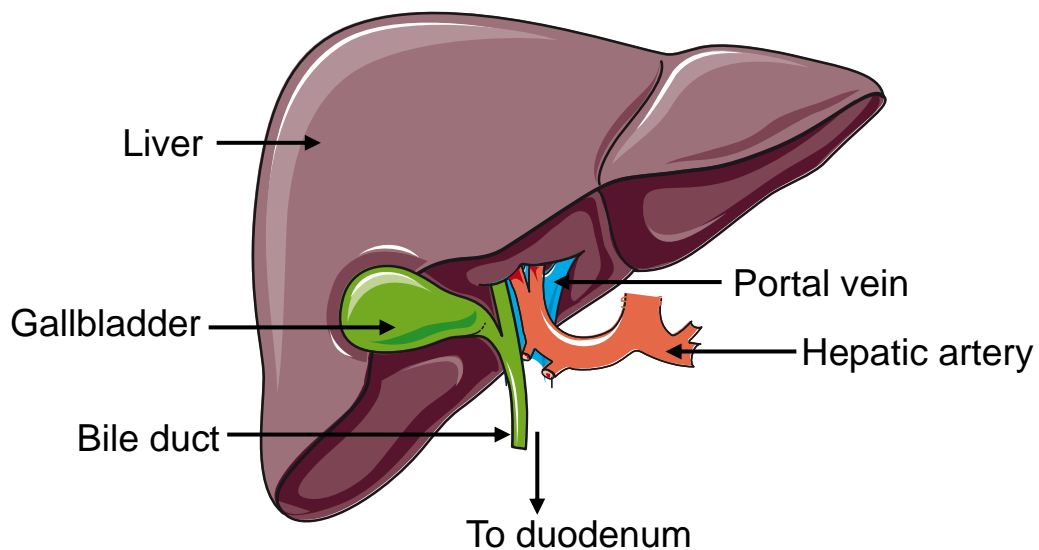


Figure 1.1. Liver anatomy

The liver is a large gastrointestinal organ with a variety of physiological functions. Blood is delivered to the liver via the hepatic artery and is drained from the liver via the portal vein. Endogenous and exogenous compounds extracted from the blood into the liver can be excreted into the bile, which is stored in the gallbladder. Upon hormonal signaling, the contents of the gallbladder are released into the duodenum, which is the proximal segment of the small intestine. From the duodenum, compounds can be reabsorbed or will be subject to fecal excretion. This diagram was adapted from Servier Medical Art (<https://smart.servier.com>).

The liver is composed of several cell types including two main epithelial cells: hepatocytes and bile duct cells, also known as cholangiocytes (Müsch and Arias, 2020). Hepatocytes are parenchymal cells of the liver and account for 70-80% of liver's mass. Hepatocytes are responsible for bile formation. They secrete and extract a variety of molecules from the blood into the liver and vice versa (Müsch and Arias, 2020). Cholangiocytes are located in the biliary tree and form tube-like networks responsible for draining hepatocytes and maintaining bile flow. Cholangiocytes are polarized epithelial cells capable of altering bile composition and mediating hepatic tissue repair.

The functions of hepatocytes and cholangiocytes are dependent on supporting cells such as the endothelial cells, myofibroblasts, and immune cells. Sinusoidal endothelial cells are characterized by distinctive fenestrae that promote exposure of hepatocytes to substances in the blood for extraction. Also located within the sinusoids are various subpopulations of myofibroblasts which provide mechanical support and are reservoirs for growth factors, cytokines, and vitamins. Various immune cells including Kupffer cells, hepatic stellate cells, and dendritic cells are present within the liver to defend against pathogens and help filter blood. The organization of the hepatocytes, liver sinusoids with fenestrated endothelial cells, and afferent and efferent vessels allow for very efficient exchange between the blood and hepatocytes (Nagy et al., 2020). An overview of the cellular organization of hepatocytes and cholangiocytes is depicted in Figure 1.2.

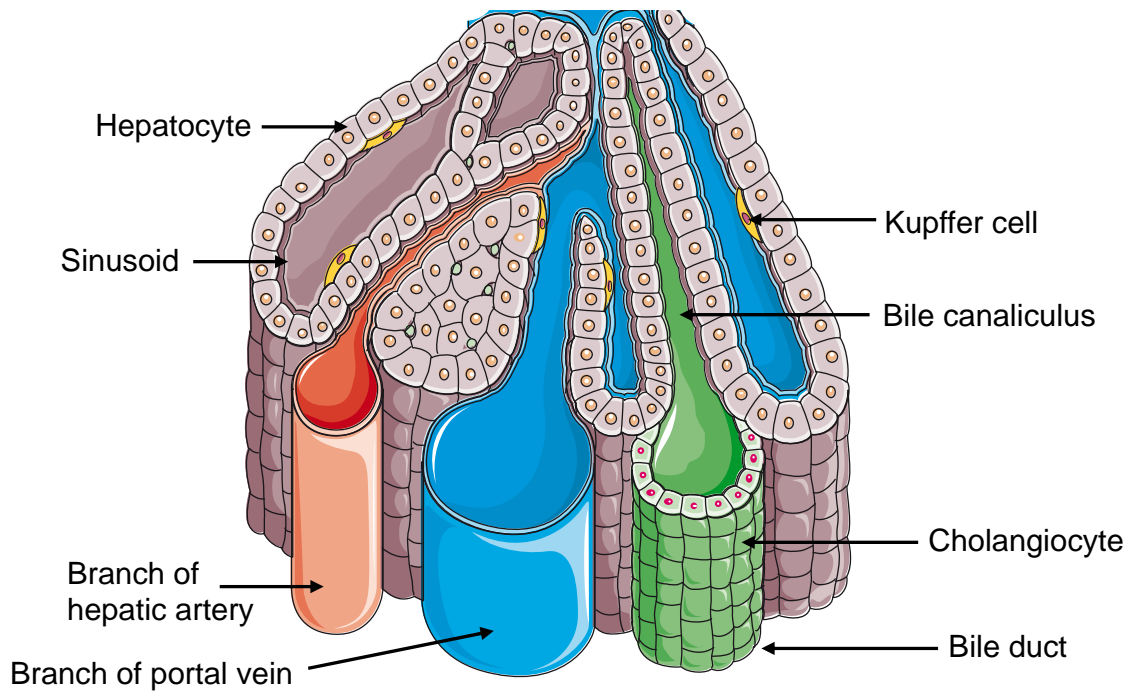


Figure 1.2. Organization of hepatocytes and cholangiocytes within the liver

Hepatocytes are the most prominent functional cells of the liver and conduct a variety of metabolic functions. The liver sinusoids provide blood to hepatocytes. Sinusoids are vascular channels that receive blood from branches of the hepatic artery. Hepatocytes are in direct contact with endothelial cells that line the liver sinusoids, and this proximity to blood allows movement of compounds from the blood into hepatocytes and vice versa. The portal vein drains blood from the liver. Bile canaliculi are important, tube-like structures that collect bile into the bile ducts. Cholangiocytes are the main cell types within the bile canaliculi and bile ducts. Kupffer cells are immune cells within the liver. This diagram was adapted from Servier Medical Art (<https://smart.servier.com>).

1.2 Organization, architecture, and cell biology of hepatocytes

Hepatocytes fulfill the majority of liver functions, including metabolism of macronutrients and drugs, as well as cholesterol and bile acid synthesis and excretion (Trefts et al., 2017). Hepatocytes are large, polarized polygon-shaped cells with several distinct surfaces. The hepatocyte is characterized by three separate membrane regions: the basolateral domain, the lateral domain, and the bile canalicular domain. The basolateral domains of portal hepatocytes are in contact with the vasculature of the liver sinusoids, allowing for exchange of endogenous and exogenous compounds between the blood and hepatocytes. The lateral domain is the least complex and contains a variety of junction proteins for cell-cell adherence and gap junctions that permit the intercellular transfer of small molecules and communication signals (Nagy et al., 2020). The lateral membrane domains of adjacent hepatocytes are discontinuous to allow the formation of a bile canalicular domain. Canalicular domains connect a network of hepatocytes to form bile canaliculi, which are small tube-like structures that empty bile from hepatocytes into a series of progressively larger ducts (Musch and Arias, 2020). The bile canalicular membrane domains contain transport proteins that actively secrete bile acids, phospholipids, cholesterol, drugs, and metabolites from hepatocytes into the biliary network.

Microtubules, microfilaments, and motor proteins are essential for cell polarity and protein trafficking; their regulation dictates protein sorting and delivery to apical and basolateral domains (Kumar et al., 2020). The selective

absorption and secretion exhibited by hepatocytes is dependent on cell polarity. Although hepatocytes exhibit a unique multipolar phenotype, they express similar polarization complexes observed in monopolar epithelial cells. Therefore, these same polarization mechanisms may be regulated in a distinctive manner within hepatocytes (Müsch and Arias, 2020).

1.3 Physiological roles of bile acids

Bile acids, cholesterol and phospholipids are key components of bile. The biosynthesis of bile acids represents a major mechanism of cholesterol turnover, and secretion of bile acids from hepatocytes regulates bile flow. The most well-known role of bile acids is to facilitate digestion in the gut. They also regulate metabolic functions through nuclear receptor and G protein-coupled receptor-mediated signaling in the enterohepatic system. Bile acids are amphipathic molecules and contain hydrophobic and hydrophilic faces. The hydrophobic region aids in cholesterol and fat emulsification in the gut, assisting digestive enzymes in nutrient extraction for subsequent absorption. The hydrophilic region increases bile acid solubility (de Aguiar Vallim et al., 2013).

Bile acids undergo enterohepatic circulation, which is an efficient type of recycling. A postprandial rise in fat and amino acids within the intestinal lumen stimulates duodenal endocrine cells to secrete the hormone cholecystokinin. Cholecystokinin signals to contract the smooth muscle cells surrounding the gallbladder, causing release of gallbladder contents. Cholecystokinin is also responsible for relaxation of the sphincter of Oddi, which controls bile release

from bile ducts into the duodenum (Otsuki, 2000). Following their secretion into the intestine, most bile acids are actively reabsorbed in the terminal ileum and secreted into the systemic circulation for redistribution to the liver and uptake into hepatocytes. About 95% of the bile acid pool is recycled through enterohepatic circulation, and the rest is excreted (Li and Chiang, 2020).

1.4 Primary bile acid synthesis

In hepatocytes, cholesterol is catabolized in a multistep fashion which includes hydroxylation and reduction to form bile acids. There are two main pathways of bile acid production: the classical pathway and the alternative pathway (Li and Chiang, 2020).

The rate-limiting and initiating enzyme in the classical pathway is cholesterol 7 α -hydroxylase (CYP7A1), found in the endoplasmic reticulum of hepatocytes. CYP7A1 catalyzes hydroxylation of cholesterol at the C-7 α position to form 7 α -hydroxycholesterol (Myant and Mitropoulos, 1977). Subsequently, one of two primary bile acids, cholic acid (CA) or chenodeoxycholic acid (CDCA), will be produced. Production of CA is mediated by sequential hydroxylation via microsomal sterol 12 α -hydroxylase (CYP8B1) and mitochondrial sterol 27-hydroxylase (CYP27A1). Alternatively, CYP27A1 will produce CDCA when CYP8B1 metabolism does not occur. The activity of CYP8B1 therefore influences the ratio of CA:CDCA in the bile acid pool, where increased CYP8B1 activity will yield increased concentrations of CA. Within peroxisomes, CA and CDCA will be conjugated to taurine or glycine prior to secretion across the bile canalicular

membrane. The alternative bile acid synthesis pathway is achieved by hydroxylation through CYP27A1 and oxysterol and sterol 7 α -hydroxylase (CYP7B1). The key enzymes involved in the alternative and classical pathways of bile acid synthesis are presented in Figure 1.3.

Of note, the classical pathway is under tight control by bile acid-mediated nuclear receptor signaling, whereas the alternative pathway is constitutively active, independent of bile acid signaling. The alternative pathway is especially important in neonates which do not express CYP7A1 until weaning, whereas the classical pathway is the predominant cascade for bile acid production in adults (Li and Chiang, 2020).

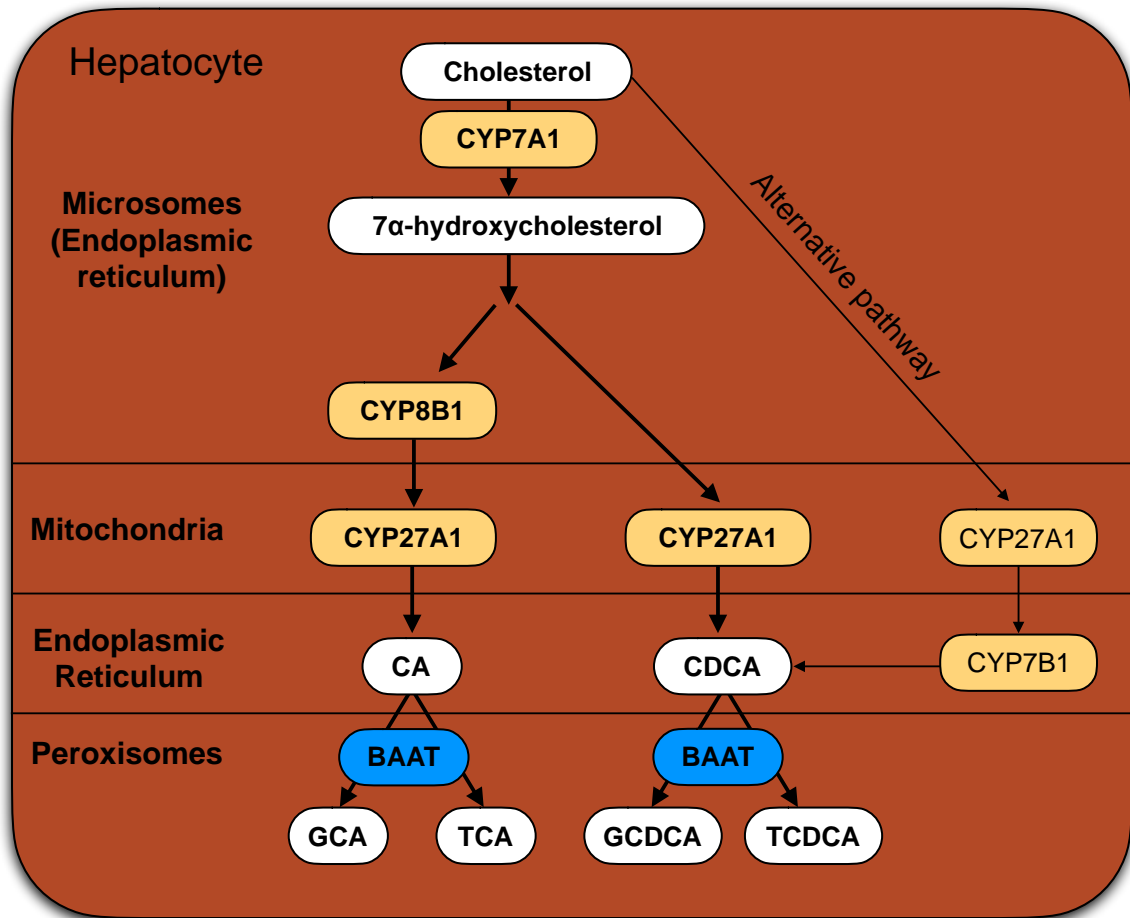


Figure 1.3. Primary bile acid synthesis

Within hepatocytes, the classical primary bile acid synthetic pathway is initiated in liver microsomes of the endoplasmic reticulum, where cholesterol 7 α hydroxylase (CYP7A1) hydroxylates cholesterol to form 7 α -hydroxycholesterol. Hydroxylation by microsomal sterol 12 α -hydroxylase (CYP8B1) and subsequently mitochondrial CYP27A1 will yield cholic acid (CA), whereas metabolism by CYP27A1, bypassing CYP8B1, yields chenodeoxycholic acid (CDCA). Within peroxisomes, bile acid CoA:amino acid N-acyltransferase (BAAT) amidates CA and CDCA with glycine or taurine to form glycocholic acid (GCA) taurocholic acid (TCA), glycochenodeoxycholic acid (GCDCA) and taurochenodeoxycholic acid (TCDCA). The alternative pathway is independent of CYP7A1 and mainly produces CDCA through CYP27A1 followed by CYP7B1.

1.5 Secondary bile acid synthesis

Subsequent to bile release into the small intestine, primary bile acids are modified by gut microbiota to produce secondary bile acids. Bile salt hydrolase hydrolyzes the amide bond that links taurine or glycine to the bile acid, thus reverting conjugated bile acids to their unconjugated forms. In the colon, hydroxysteroid dehydrogenase partially dehydroxylates unconjugated CA and CDCA to form secondary bile acids deoxycholic acid (DCA) and lithocholic acid (LCA), respectively (Ridlon et al., 2006). The most abundant secondary bile acid is DCA, whereas LCA is only present in trace amounts. Secondary bile acid synthesis is presented in Figure 1.4.

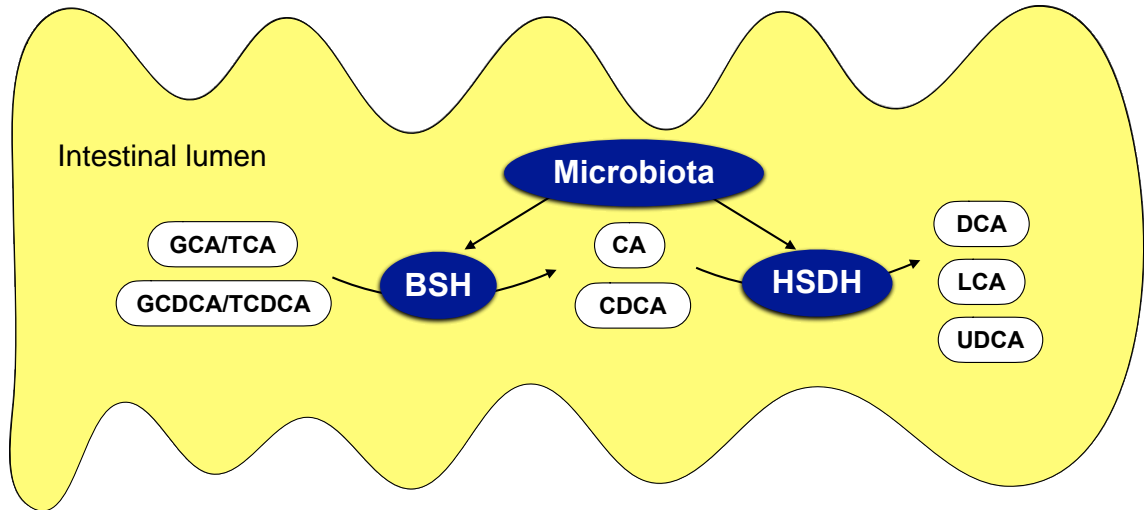


Figure 1.4. Formation of secondary bile acids

Conjugated primary bile acids GCA, TCA, GCDCA, and TCDCA that were synthesized in the liver are released into the small intestine. Within the intestine, microbiota produce bacterial enzymes called bile salt hydrolases (BSHs), which deconjugate primary bile acids to their unconjugated forms, CA and CDCA. Microbiota also produce hydroxysteroid dehydrogenases (HSDHs) which partially dehydroxylate unconjugated primary bile acids to form the secondary bile acids deoxycholic acid (DCA), lithocholic acid (LCA) and ursodeoxycholic acid (UDCA). Deoxycholic acid is produced from cholic acid, and LCA and UDCA are formed from CDCA.

1.6 Bile acid detoxification

Bile acid detoxification occurs through sulfation and hydroxylation within hepatocytes. Metabolism via sulfation and/or hydroxylation increases the hydrophilicity of bile acids and promotes their excretion. The majority of bile acids excreted in the feces are mainly unconjugated, as bacterial hydrolases deconjugate bile acids in the colon. Although minimal urinary bile acid excretion occurs under physiological conditions, sulfation is upregulated under high bile acid conditions and promotes urinary excretion (Li and Chiang, 2020). Under physiological conditions, glucuronidation is a negligible mechanism of bile acid detoxification. However, glucuronidation may become a more prominent mode of bile acid metabolism and excretion during cholestasis (Javitt, 2002).

1.7 Transporters maintain enterohepatic circulation of bile acids

The vast majority of bile acid circulation through the enterohepatic system is dependent on transporter proteins expressed at the plasma membranes of hepatocytes and enterocytes. Two types of transporters are involved in this process: solute carrier transporters and ATP-binding cassette (ABC) transporters. Solute carrier (SLC) transporters can be classified as either Na⁺-dependent or Na⁺-independent. ABC transporters utilize ATP hydrolysis to harness energy for the translocation of a substrate against its concentration gradient (Giacomini et al., 2010).

The secretion of bile acids from hepatocytes into the bile canaliculi is mediated by ABC transporters. The major canalicular membrane transporter for canalicular bile acid efflux is the bile salt export pump (BSEP, encoded by the *ABCB11* gene). Also on the canalicular membrane, multidrug resistance-associated protein 2 (MRP2, encoded by the *ABCC2* gene) can transport bile acids but plays a more important role in sulfated bile acid export (Dawson et al., 2009).

As bile acids flow through the intestine, active reuptake occurs in the ileum through the apical sodium-dependent bile acid transporter (ASBT, encoded by the *SLC10A2* gene), which is a Na⁺-dependent SLC transporter. On the basolateral membrane of enterocytes, efflux of bile acids into portal blood is facilitated by the Na⁺-independent SLC transporter heterodimer organic solute transporter $\alpha\beta$ (OST α and OST β , encoded by the *SLC51A* and *SLC51B* genes, respectively) and the ABC transporter, multidrug resistance-associated protein 3 (MRP3, encoded by gene *ABCC3*) (Dawson et al., 2009).

Once secreted into the blood, bile acids recirculate to the liver where they are taken up at the basolateral membrane of hepatocytes. The central hepatic bile acid uptake transporter is the SLC transporter Na⁺-taurocholate co-transporting polypeptide (NTCP, encoded by the *SLC10A1* gene), which preferentially transports conjugated bile acids. Additionally, organic anion transporting polypeptides (OATPs, gene family *SLCO*) are important Na⁺-independent SLC bile acid uptake transporters on the basolateral membranes of hepatocytes. Organic anion transporting polypeptides involved in bile acid uptake

from the sinusoidal blood into hepatocytes are OATP1B1 (encoded by the *SLCO1B1* gene) and OATP1B3 (encoded by the *SLCO1B3* gene) (Dawson et al., 2009).

The aforementioned transporters maintain enterohepatic circulation under physiological conditions. However, under cholestatic conditions, altered nuclear receptor signaling promotes hepatocellular bile acid efflux to prevent toxic bile acid buildup. In this case, hepatic expression of bile acid transporters OST $\alpha\beta$ and multidrug resistance-associated protein 4 (MRP4, encoded by gene *ABCC4*) 4 (MRP3 and MRP4, genes *ABCC3* and *ABCC4*) at the basolateral membrane of hepatocytes, which are not typically abundant in liver under physiological conditions, are induced (Halilbasic et al., 2013). A graphical depiction of bile acid transporters in the enterohepatic system is presented in Figure 1.5.

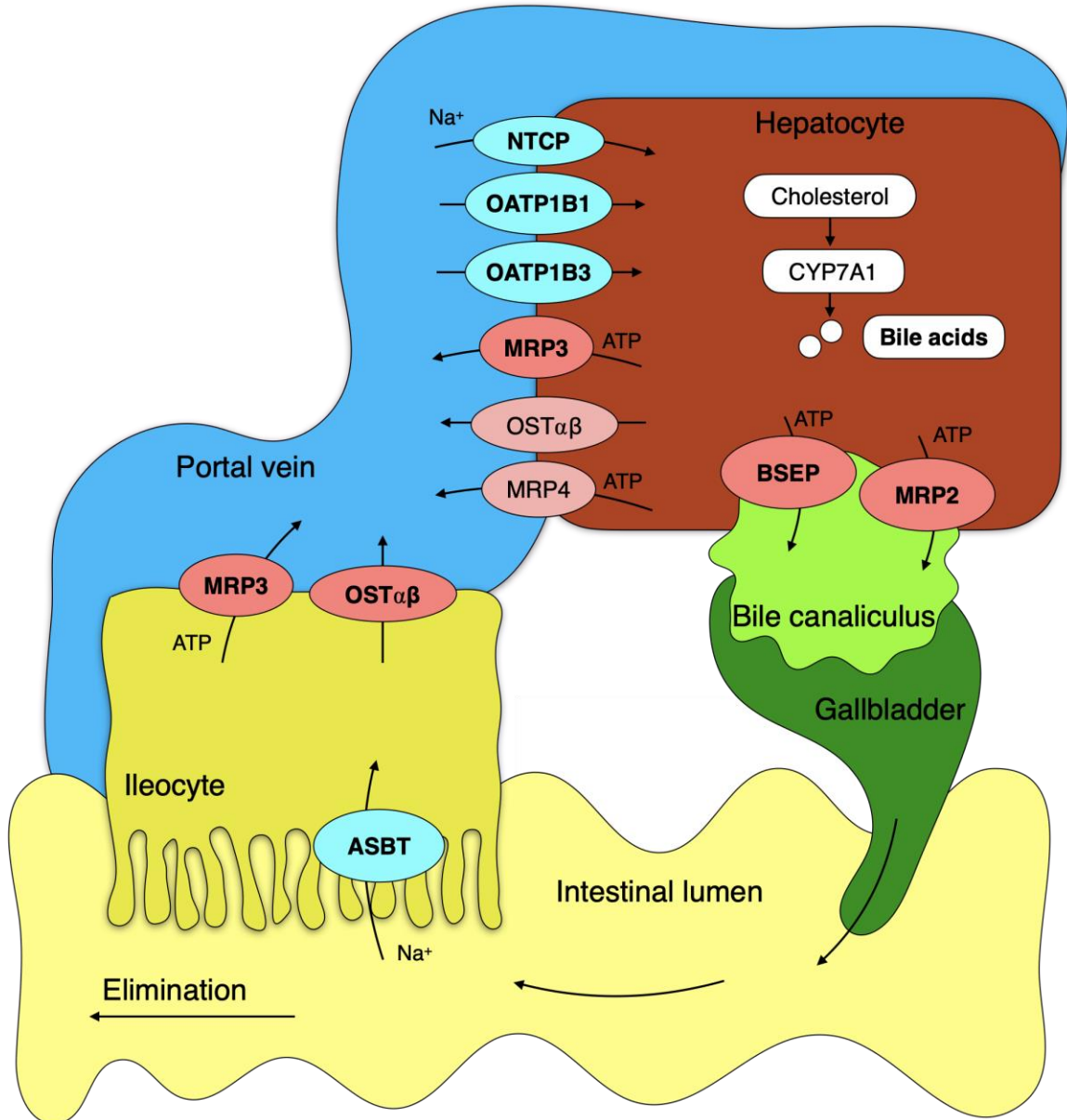


Figure 1.5. Transporters in bile acid enterohepatic circulation

Uptake transporters are shaded light blue and efflux transporters are shaded pink. Subsequent to bile acid synthesis and conjugation in hepatocytes, bile acids are secreted into bile canaliculi by ATP-dependent transporters, bile salt export pump (BSEP) and multidrug resistance-associated protein 2 (MRP2). Bile acids concentrate in the gallbladder, are released upon hormonal signaling to aid in emulsification of dietary lipids and are largely reabsorbed in the terminal ileocytes by the apical sodium-dependent bile acid transporter (ASBT). Bile acids are secreted into portal circulation by organic solute transporters (OST) α/β and MRP3. Bile acids can then recirculate to the liver for uptake by Na⁺-taurocholate co-transporting polypeptide (NTCP) or the sodium-independent organic anion transporting polypeptides OATP1B1 and OATP1B3 on the basolateral membranes of hepatocytes. Hepatic efflux of bile acids into sinusoidal blood is mediated by MRP3. Under pathological conditions including hepatic cholestasis, MRP4 and OST $\alpha\beta$ are upregulated to aid in secreting bile acids from hepatocytes into the blood.

1.8 Pathology associated with disruption of bile acid transport and synthesis

Bile acid synthesis and transport are tightly regulated to avoid bile acid accumulation; when this homeostasis is disrupted, cholestasis can ensue. Cholestasis is a chronic liver condition characterized by bile acid accumulation in the liver and/or elevated bile acids in the serum. It is characterized by decreased bile flow and can result from genetic variation in bile acid transporters, biliary obstruction, or autoimmune-mediated destruction of bile ducts. Cholestasis can progress to fibrosis, cirrhosis, and liver failure. Chronic cholestasis is a common cause of liver transplantation and has been associated with increased incidences of hepatocellular and cholangiocellular carcinomas (Wikström Shemer et al., 2015).

Dysregulation of bile acid signaling can also mediate serum hypercholanemia. Hypercholanemia is characterized by excessive accumulation of bile acids in the blood, causing itching and fat malabsorption, and can be an indicator of liver pathology (Neale et al., 1971; Luo et al., 2018). Genetic variation that alters bile acid transport or synthesis can result in serum hypercholanemia (Carlton et al., 2003; Vaz et al., 2015; Deng et al., 2016). Implications of serum hypercholanemia include increased incidence of cholelithiasis, known as gallstone formation, due to impeded bile flow (Fisher and Yousef, 1973). Elevated serum bile acids may also be indicative of decreased intestinal bile acids, which is linked to fat malabsorption, decreased absorption of fat-soluble vitamins, and failure to thrive (Carlton et al., 2003).

1.9 Nuclear receptors in bile acid homeostasis

Nuclear receptors are key transcription factors that modify the expression of their target genes. Nuclear receptors are generally activated upon binding of ligands or through post-translational modification and recruitment of transcriptional co-factors. A variety of nuclear receptors including farnesoid X receptor (FXR, encoded by gene *NR1H4*), pregnane X receptor (PXR, encoded by gene *NR1I2*), vitamin D receptor (VDR, encoded by gene *NR1I1*), and constitutive androstane receptor (CAR, encoded by gene *NR1I3*) are directly or indirectly responsive to bile acids and initiate signaling to regulate bile acid synthesis, transport, and detoxification (Claudel and Trauner, 2020). These pathways are not only involved in bile acid metabolism but also drug metabolism, and their regulation contribute to overall liver functions. Dysregulation of these nuclear receptors subsequent to altered bile acid signaling can result in liver pathology or adverse drug events (Li and Chiang, 2013). A brief overview of the interplay between bile acids, nuclear receptors, and liver functions including bile acid and drug metabolism is presented in Figure 1.6.

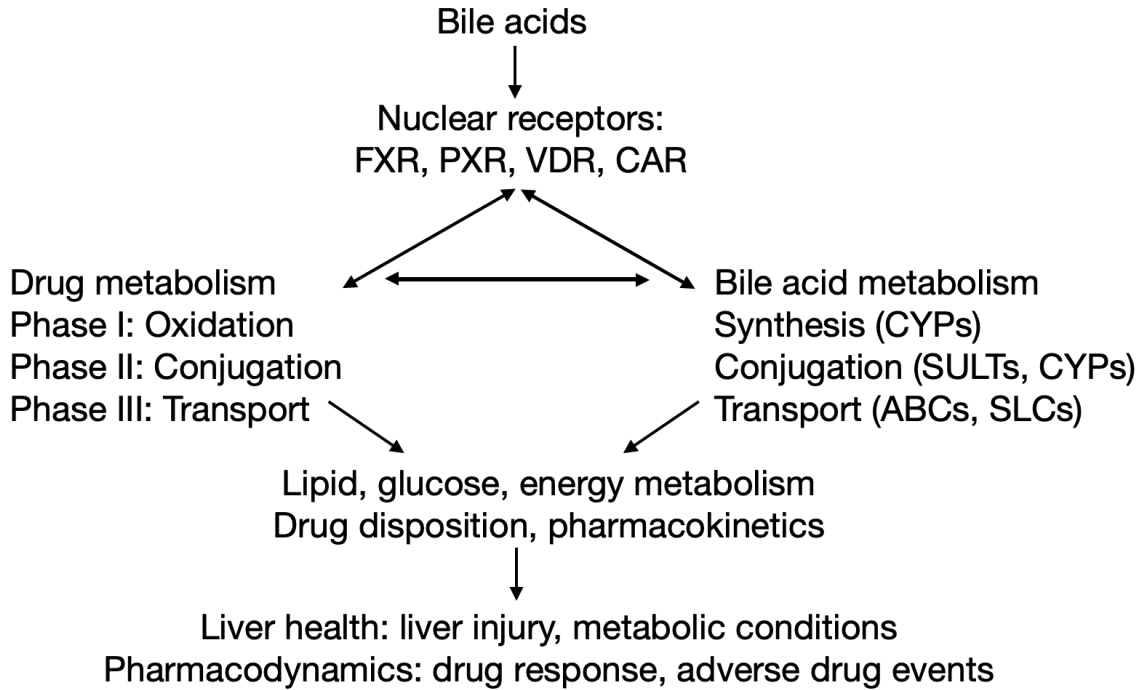


Figure 1.6. Interplay between bile acids, nuclear receptor regulation, and bile acid and drug metabolism.

Bile acids are ligands for nuclear receptors. Bile acids bind directly to FXR, PXR and VDR, and indirectly to CAR, to elicit nuclear receptor signaling that regulates the various phases of drug metabolism and bile acid metabolism. Moreover, the nuclear receptor target genes involved in these processes also regulate processes that control downstream nuclear receptor signaling. This dynamic process is involved in the major metabolic functions of the liver, including lipid, glucose, and energy metabolism and drug disposition. Ultimately, dysregulation of these processes can affect liver health, contributing to disease such as cholestatic insult or metabolic conditions, and can affect the handling and response to drugs. Adapter from Li & Chiang (Li and Chiang, 2013).

Farnesoid X receptor is mainly expressed in hepatocytes and enterocytes (Li and Li, 2017), and bile acids are the central ligands for FXR activation (Makishima et al., 1999). Farnesoid X receptor can function as a heterodimer with retinoic acid receptor α (RXR α , gene *NR2B1*). Upon activation, the FXR-RXR α complex binds to FXR response elements to induce transcription of target genes (Caudel and Trauner, 2020). Farnesoid X Receptor can also bind to DNA as a monomer to either repress (Caudel et al., 2002) or stimulate (Barbier et al., 2003) gene transcription. FXR response elements are typically located within two kilobases of transcriptional start sites of genes involved in fatty acid, lipid, steroid, and bile acid metabolism (Chong et al., 2010). Genetic defects in FXR are associated with a severe form of inherited cholestasis known as progressive familial intrahepatic cholestasis (Gomez-Ospina et al., 2016), and can predispose pregnant women to intrahepatic cholestasis of pregnancy (Van Mil et al., 2007).

Similar to FXR, nuclear receptors PXR, CAR, and VDR are expressed in the liver and intestine and form heterodimers with RXR (Baes et al., 1994; Jones et al., 1998; Kliewer et al., 1998). Bile acid structure dictates their efficacy for nuclear receptor activation. The most potent activator of FXR is CDCA, followed by DCA, CA, and LCA. The most efficacious ligand for the activation of both PXR and VDR is LCA. Bile acids do not directly bind to or activate CAR. As the master regulator of bile acid homeostasis, FXR is imperative in the regulation of bile acid synthesis, oxidation, conjugation, and transport. Additionally, PXR, CAR, and VDR play important roles in bile acid oxidation (phase I metabolism), conjugation (phase II metabolism), and transport (phase III metabolism) (Li and

Chiang, 2013). A summary of how FXR activates its target genes is presented in Figure 1.7. Specific FXR, PXR, VDR, and CAR target genes of relevance to this thesis are presented in Table 1.1.

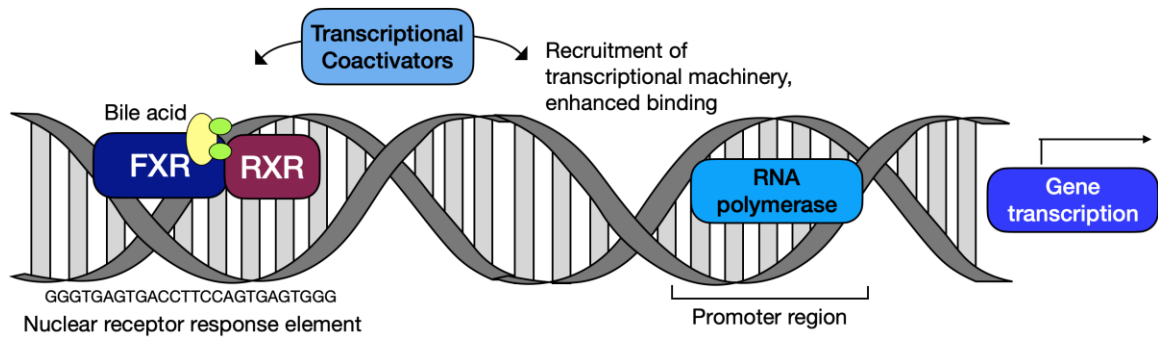


Figure 1.7. FXR binds to response elements in target genes to induce their transcription

When FXR is activated by bile acids, it can heterodimerize or act as a monomer to bind DNA response elements upstream of its target genes. The response element for FXR is an inverted nucleotide repeat. Once FXR binds to this recognition sequence, transcriptional activator proteins will initiate the FXR response by recruiting and stabilizing transcriptional machinery so that RNA polymerase II can enhance the transcription of the target gene.

Table 1.1. Nuclear receptors and their target bile acid-related genes

Human Gene	Human Protein	Mouse Gene	Mouse Protein	Tissue(s)	Membrane localization	Function	Major regulatory nuclear receptor
<i>SLCO1B1</i>	OATP1B1	<i>Slco1b2</i>	OATP1B2	Liver	Basolateral	Uptake	FXR, SHP, HNF4 α
<i>SLCO1B3</i>	OATP1B3	<i>Slco1b2</i>	OATP1B2	Liver	Basolateral	Uptake	FXR, SHP, HNF4 α
		<i>Slco1a1</i>	OATP1A1	Liver	Basolateral	Uptake	PXR, CAR
		<i>Slco1a4</i>	OATP1A4	Liver	Basolateral	Uptake	PXR, CAR
<i>SLC10A1</i>	NTCP	<i>Slc10a1</i>	NTCP	Liver	Basolateral	Uptake	FXR, SHP, HNF4 α
<i>ABCC3</i>	MRP3	<i>Abcc3</i>	MRP3	Liver, intestine	Basolateral	Efflux	CAR, PXR, VDR
<i>ABCC4</i>	MRP4	<i>Abcc4</i>	MRP4	Liver	Basolateral	Efflux	CAR
<i>SLC51A/B</i>	OST $\alpha\beta$	<i>Slc51a/b</i>	OST $\alpha\beta$	Liver, Intestine	Basolateral	Efflux	FXR
<i>ABCB11</i>	BSEP	<i>Abcb11</i>	BSEP	Liver	Canalicular	Efflux	
<i>ABCC2</i>	MRP2	<i>Abcc2</i>	MRP2	Liver	Canalicular	Efflux	FXR, CAR, PXR
<i>SLC10A2</i>	ASBT	<i>Slc10a2</i>	ASBT	Intestine	Apical Endoplasmic	Uptake	FXR, SHP
<i>CYP7A1</i>	CYP7A1	<i>Cyp7a1</i>	CYP7A1	Hepatic	reticulum	Synthesis	FXR, SHP
<i>NR0B2</i>	SHP	<i>Nr0b2</i>	SHP	Hepatic	Cytosolic	Regulation	FXR
<i>FGF19</i>	FGF19	<i>Fgf15</i>	FGF15	Intestine, liver	Cytosolic	Regulation	FXR, SHP

Adapted from Li & Chiang and Halilbasic et al. (Halilbasic et al., 2013; Li and Chiang, 2013).

The nuclear receptor regulation of bile acid transport is a complex process. In addition to the nuclear receptors already described, the nuclear receptors peroxisome proliferator activator α (PPAR α , encoded by gene *NR1C1*), liver X receptor (LXR, encoded by gene *NR1H3*), glucocorticoid receptor (GR, encoded by gene *NR3C1*), estrogen receptor, and hepatocyte nuclear factors 1 α , 3 β , and 4 α (HNF1 α , HNF3 β , and HNF4 α , encoded by genes *HNF1A*, *HNF3B*, and *NR2A1*, respectively) contribute to regulating bile acid transporters to maintain enterohepatic circulation (Halilbasic et al., 2013).

1.10 FXR regulation of bile acid synthesis and transport

Bile acid synthesis is largely controlled by *CYP7A1*. The *CYP7A1* promoter contains two bile acid response elements (BAREs), BARE-1 and BARE-2 which are regulated by transcription factors. In humans and mice, transcriptional coactivators HNF4 α and liver-related homolog 1 (LRH-1, encoded by gene *NR5A2*) bind to BARE-1 to induce *CYP7A1*. Hepatocyte nuclear factor 4 α and LRH-1 are thought to be constitutively active in hepatocytes to control basal expression of *CYP7A1*. Bile acids mediate negative feedback regulation of their own synthesis. Through binding to HNF4 α and LRH-1, bile acids prevent *CYP7A1* transcription. However, the fundamental mechanism of *CYP7A1* repression is attributed to bile acid-mediated activation FXR.

There are two major inhibitory pathways that act through FXR to repress *CYP7A1* when intracellular concentrations of bile acids rise (Li and Chiang, 2020). One pathway originates in enterocytes, where bile acids directly bind to

FXR, and activated FXR binds an FXR response element in the fibroblast growth factor 19 (*FGF19*) gene. The mouse ortholog of *FGF19* is *Fgf15*. Fibroblast Growth Factor 19/FGF15 is released from enterocytes for circulation to the liver, where it binds to the fibroblast growth factor receptor 4 (FGFR4) located on the basolateral membrane of hepatocytes. This event recruits the co-receptor β -Klotho, and the activated FGFR4- β -Klotho complex initiates a cascade to signal through c-Jun N terminal kinase (Holt et al., 2003) and induces the orphan nuclear receptor, small heterodimer partner (SHP, gene *NR0B2*) (Inagaki et al., 2005).

The second homeostatic pathway governed through FXR occurs within hepatocytes, where bile acids bind and activate FXR which promotes the transcription of *SHP*. SHP is a transcriptional co-repressor that inhibits bile acid synthesis. Specifically, SHP indirectly represses *CYP7A1* gene transcription by inhibiting HNF4 α and LRH-1 at the protein level (Goodwin et al., 2000). However, under physiological conditions, bile acid concentrations within hepatocytes may not be sufficient to elicit FXR activation. Importantly, studies showed that infusing taurocholic acid into the duodenum caused inhibition of bile acid synthesis, whereas intravenous taurocholic acid infusion did not. This suggests that intestinal signaling through FXR and FGF19 may be the rate-limiting mechanism driving this negative feedback loop, rather than hepatic bile acid concentrations (Pandak et al., 1995; Li and Dawson, 2019).

Bile acid secretion into the canaliculi and bile acid reuptake in the ileum are two driving forces of bile acid enterohepatic circulation. After bile acids are

synthesized in hepatocytes, FXR induces *BSEP* transcription through direct binding to the FXRE in the *BSEP* promoter, leading to enhanced bile acid secretion across the canalicular membrane (Ananthanarayanan et al., 2001). Bile acid mediated FXR activation inhibits the transcription of *NTCP* via SHP (Denson et al., 2001). In enterocytes, FXR activation similarly inhibits bile acid uptake by inhibiting *ASBT* gene transcription (Neimark et al., 2004), possibly via SHP. Furthermore, FXR directly induces bile acid efflux genes *OST α* and *OST β* (Lee et al., 2006) by binding directly to their promoters. In response to high bile acid concentrations, the overall regulation of transporters favours a decrease in intracellular bile acid concentrations. This is achieved by the upregulation of efflux transporters and the downregulation of uptake transporters and genes involved in bile acid synthesis. The regulatory pathways governed by FXR activation in enterocytes and hepatocytes are shown in Figure 1.8.

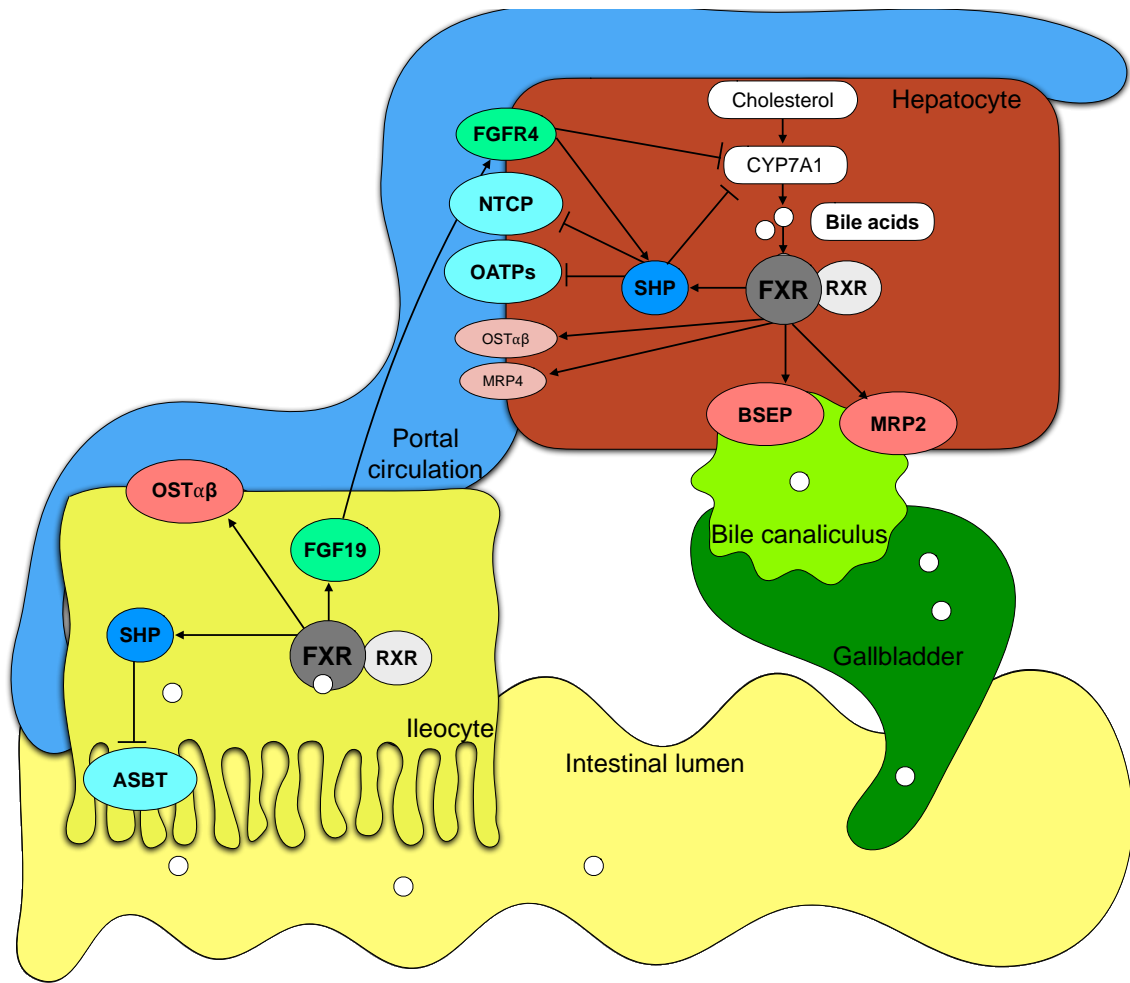


Figure 1.8. FXR regulation of bile acid synthesis and transport

In enterocytes, bile acids bind and activate farnesoid X receptor (FXR), which stimulates production of fibroblast growth factor 19 (FGF19, FGF15 in mice). FGF19 travels to hepatocytes where it binds to the fibroblast growth factor receptor 4 (FGFR4), which signals to induce SHP. SHP protein interferes with coactivators of CYP7A1 to inhibit CYP7A1 transcription. Also, within enterocytes, FXR activation directly induces organic solute transporters $\alpha\beta$ (OST $\alpha\beta$) and FXR inhibits apical sodium-dependent bile acid transporter (ASBT) via SHP. In hepatocytes, FXR activation directly induces bile salt export pump (BSEP) and multidrug resistance-associated protein 2 (MRP2) on the bile canalicular membrane. On the hepatic basolateral membrane, OST $\alpha\beta$ and MRP4 are typically not expressed abundantly, but can become upregulated upon FXR activation. FXR also induces SHP to inhibit bile acid uptake by Na⁺-taurocholate co-transporting polypeptide (NTCP) and organic anion transporting polypeptides OATP1B1 and OATP1B3 at the basolateral membrane of hepatocytes.

1.11 Role of bile acid transporters in statin transport

In addition to their roles in enterohepatic circulation of bile acids, many of these transporters are also important in the disposition of xenobiotics including statins. Statins are lipid-lowering drugs that competitively inhibit 3-hydroxy-3-methylglutaryl coenzyme A (HMG-CoA) reductase, the rate-limiting enzyme in cholesterol synthesis in hepatocytes (Istvan, 2002). Statins are often prescribed to hypercholesterolemic patients to prevent cardiovascular disease, providing their primary therapeutic benefit by reducing total and low-density lipoprotein cholesterol in the plasma (Collins et al., 2016).

Importantly, transporters also regulate statin pharmacodynamics. Efficient uptake into hepatocytes is imperative for therapeutic efficacy (Rocha et al., 2018). Decreased hepatic uptake of statins can result in increased systemic concentrations, which has been associated with elevated risk of the most common statin-induced adverse event, myopathy (Tomaszewski et al., 2011; Nigam, 2015). A high degree of interindividual variability in plasma statin concentrations has been documented. Variability up to 45-fold has been observed in patients taking the same dose of atorvastatin or rosuvastatin (DeGorter et al., 2013).

There are various statins on the market, all of which maintain the same therapeutic effect and share similar pharmacophore structures that mimic HMG-CoA. Statins are amphiphilic and differ in ring structures attached to the pharmacophore, which change their chemical properties and determine their hydrophilicity. Statins with more hydrophobic properties are atorvastatin,

simvastatin, fluvastatin, and lovastatin, whereas rosuvastatin, pitavastatin, and pravastatin are more hydrophilic (Fong, 2014). Statins are administered orally and exhibit rapid intestinal absorption. Hydrophobic statins are capable of plasma membrane diffusion, whereas hydrophilic statins are highly dependent on transporters for their absorption (Schachter, 2005).

1.12 Rosuvastatin transport and genetic variation

Rosuvastatin displays high selectivity for hepatocytes and, due to its minimal metabolism, is not prone to cytochrome P450-mediated drug-drug interactions (Cheng-Lai, 2003). Due to its low passive membrane permeability, rosuvastatin disposition is nearly entirely dependent on uptake and efflux transporters. *In vitro*, hepatic uptake transporters OATP1B1, OATP1B3, OATP2B1, and NTCP can transport rosuvastatin (Ho et al., 2006; Kitamura et al., 2008; Choi et al., 2011; Bi et al., 2013). In human hepatocytes, OATP1B1 and OATP1B3 mediate high affinity and capacity rosuvastatin transport, accounting for approximately 55% of rosuvastatin uptake, whereas NTCP shows high capacity but lower affinity and is responsible for up to 35% of hepatic rosuvastatin uptake (Ho et al., 2006; Bi et al., 2013). *In vitro* and *in vivo* studies provide evidence that bile canalicular efflux transporters breast cancer resistance protein (BCRP, gene *ABCG2*) and MRP2 mediate biliary secretion of rosuvastatin (Kitamura et al., 2008; Hu et al., 2010; DeGorter et al., 2013).

Genetic polymorphisms in hepatic uptake transporters and bile canalicular efflux transporters have been associated with altered plasma rosuvastatin

concentrations. Variability up to 45-fold was observed in plasma statin concentration between patients taking the same dose. This study identified genetic variants in *SLCO1B1* and *ABCG2* that decrease statin transport by OATP1B1 and BCRP, respectively, and are associated with increased plasma rosuvastatin concentrations (DeGorter et al., 2013). The low degree of metabolism and high degree of facilitated and active transport of rosuvastatin implies that variation in other rosuvastatin transporters, such as NTCP, might also play a role in the observed interpatient variability in plasma statin concentrations.

1.13 Na⁺-taurocholate co-transporting polypeptide (NTCP, *SLC10A1*)

NTCP is a key bile acid transporter located on the basolateral membrane of hepatocytes. Conjugated bile acid uptake from the blood into hepatocytes is largely mediated by NTCP (Hagenbuch et al., 1991; Hagenbuch and Meier, 1994). NTCP works by secondary active transport, facilitating the symport of one bile acid molecule per two sodium ions (Weinman, 1997; Anwer and Stieger, 2014).

Genetic variation resulting in deficient NTCP expression and/or activity can result in serum hypercholanemia (Vaz et al., 2015; Mao et al., 2019). Over the past five years, various case reports of NTCP deficiency in humans have been published. Individuals deficient in NTCP present with elevated bile acids in the serum, which is most prominent in pediatric subjects (Vaz et al., 2015; Liu et

al., 2017; Qiu et al., 2017). In some NTCP deficient mice and humans, serum bile acids normalization occurs over time. This is thought to occur via compensation of bile acid uptake by other transporters, including hepatic OATPs. However, in some subjects, serum hypercholanemia persist into adulthood (Deng et al., 2016; Liu et al., 2017; Mao et al., 2019). Although serum hypercholanemia does not cause the progressive liver damage seen with intrahepatic cholestasis, serum cholestasis affects the enterohepatic circulation of bile acids. Vitamin D deficiency and decreased bone mineral density have been reported in individuals with homozygous loss of function genetic variation in *SLC10A1* (Liu et al., 2017), which may indicate reduced bile acid secretion into the gut.

In *Slc10a1*^{-/-} mice, serum hypercholanemia and altered bile acid transporter expression has been observed in some but not all animals (Slijepcevic et al., 2015). It remains unclear why certain mice appear near-normal in terms of bile acid physiology, whereas others are severely impacted by the disruption of *Slc10a1*.

NTCP is also the receptor for the entry of hepatitis B and D viruses into hepatocytes (Yan et al., 2012), and the NTCP-specific inhibitor, Bulevirtide (formerly Myrcludex B), has recently been approved for the treatment of Hepatitis B and D. Clinical trials have shown no serious acute adverse events with Myrcludex B administration (Blank et al., 2016; Bogomolov et al., 2016). However, serum bile acids, particularly conjugated species, were significantly elevated in individuals administered the NTCP inhibitor. Due to the detergent properties of bile acids and their ability to digest cellular membranes causing

toxicity, long-term implications of persistent serum hypercholanemia are unknown and warrant further investigation (Blank et al., 2018).

1.14 Rare genetic variation and next-generation sequencing

Next-generation sequencing (NGS) is a powerful tool that provides the opportunity for the discovery of common as well as rare variants. However, elucidating functional effects of rare variants, particularly with regard to drug response, lack thereof, or adverse drug events (ADEs), remains a major challenge.

Costs of genome sequencing have declined exponentially over the past decade, with the current average cost of sequencing one human genome at approximately \$1,000 US dollars, compared to over \$100,000 in 2009 (Hayden, 2014). This has fostered rapid uptake of genomic sequencing for both research and clinical purposes. However, the rate at which we are discovering variants far exceeds our ability to characterize their function, let alone understand their clinical relevance.

The abundance of rare variants has been confirmed by numerous studies characterizing large genomic datasets from initiatives including The 1000 Genomes Project (Genomes Project et al., 2012) and the Exome Aggregation Consortium (ExAC) (Lek et al., 2016), the latter combining sequencing data of more than 60,000 individuals. A high prevalence (97.5%) of very rare variation was discovered in 628 known drug-target genes, leading researchers to predict that approximately 80% of patients may harbour a variant that affects a gene involved

in response to commonly prescribed drugs (Scharfe et al., 2017). A recent study noted high frequencies of rare variants in genes of drug transporters belonging to the solute carrier (SLC) superfamily, where 99.8% of single nucleotide variants were found to be rare (Schaller and Lauschke, 2019).

Despite the sustained reduction in cost, genome-wide sequencing of larger patient populations remains challenging for most research institutions due to the increased cost, time, data storage capacity, and bioinformatics pipelines required to carefully analyze the vast number of data generated while ensuring assay quality and technical as well as clinical validity of detected variants (DePristo et al., 2011; Rehm et al., 2013; Richards et al., 2015). Alternatively, targeted exome sequencing panels focus on a small number of genes of interest (~100) but can also target specific noncoding regions of known functional relevance. Such gene panels generally facilitate “deeper” sequencing with a higher read coverage, also known as read depth, and therefore sequencing data can be interpreted with greater confidence (Gulilat et al., 2019).

In comparison to more cost-effective array-based genotyping platforms focused on common variation with established functional effects, targeted next-generation sequencing allows for the discovery of novel, mostly rare genetic variation. Consequently, sequencing data can be utilized to assess specific genotypes that may be clinically actionable or to perform a more comprehensive pharmacogenetic analysis for subsequent research. While increasingly robust sequencing technologies have identified many rare and very rare genetic variants, most remain of unknown functional and clinical significance. Currently,

computational (*in silico*) and *in vitro* approaches are employed as the first steps in defining which variants have altered function such that rigorous *in vivo* testing can be pursued to determine potential clinical implications in disease and pharmacotherapy.

1.15 Computational prediction of rare variant function

A variety of computational algorithms have been developed and optimized to predict whether genetic variants will affect the function of a given protein. Variants predicted to have an altered function are classified as deleterious or damaging, and those predicted to maintain physiological function are classified as benign or tolerated. These *in silico* prediction tools are especially important for the classification of rare variants, where population scale and genome-wide association studies (GWAS) are often underpowered to associate rare variation to drug-associated phenotypes such as toxicity (Speed et al., 2012; Visscher et al., 2017).

Commonly used algorithms for variants in coding regions of the genome base their predictions on evolutionary conservation and/or amino acid physicochemical properties (Grantham, 1974; Cooper et al., 2005; Kumar et al., 2009; Adzhubei et al., 2010). Other *in silico* tools aggregate prediction scores from multiple algorithms to generate one ensemble prediction score in an attempt to improve their predictive accuracy (Kircher et al., 2014; Ioannidis et al., 2016).

While the open-access nature of such prediction tools allows easy access to score variants of interest, predictions from different tools often produce

conflicting results: one tool may classify a variant as deleterious when another tool may predict no functional effect, thus classifying the same variant as tolerated or benign. Though some of these differences may be expected given the diverse methodologies employed by each algorithm to derive their respective scores, such conflicting and potentially incorrect results undoubtedly degrade the confidence in these algorithms for variant interpretation (Han et al., 2017; Gulilat et al., 2019). Particularly, if such functional predictions lack the required sensitivity (proportion of true positives that are correctly identified by a score) and specificity (proportion of true negatives correctly identified by a score) to forecast functionality of a particular variant, they cannot be trusted clinically.

One well-known caveat of applying these *in silico* tools to predict functional effects of variations in drug transport or metabolism genes, known as pharmacogenes, is that most algorithms are trained using data on evolutionary conservation and disease. Typically, genetic variants in pharmacogenes are not associated with disease; they display lower evolutionary conservation in contrast to disease-associated genes which are under higher evolutionary pressure to retain endogenous function (Fujikura et al., 2015; Lauschke et al., 2017; Zhou et al., 2018; Schaller and Lauschke, 2019). Recently, an *in silico* tool was specifically optimized using drug transport and metabolism data. Overall, this algorithm showed more accurate predictions for functional effects in pharmacogenes compared to conventional *in silico* tools developed based on sequence homology and disease (Zhou et al., 2019).

1.16 References

- Adzhubei IA, Schmidt S, Peshkin L, Ramensky VE, Gerasimova A, Bork P, Kondrashov AS, and Sunyaev SR (2010) A method and server for predicting damaging missense mutations. *Nature Methods* **7**:248-249.
- Ananthanarayanan M, Balasubramanian N, Makishima M, Mangelsdorf DJ, and Suchy FJ (2001) Human bile salt export pump promoter is transactivated by the farnesoid X receptor/bile acid receptor. *J Biol Chem* **276**:28857-28865.
- Anwer MS and Stieger B (2014) Sodium-dependent bile salt transporters of the SLC10A transporter family: more than solute transporters. *Pflugers Arch* **466**:77-89.
- Baes M, Gulick T, Choi HS, Martinoli MG, Simha D, and Moore DD (1994) A new orphan member of the nuclear hormone receptor superfamily that interacts with a subset of retinoic acid response elements. *Molecular and cellular biology* **14**:1544-1552.
- Barbier O, Torra IP, Sirvent A, Claudel T, Blanquart C, Duran-Sandoval D, Kuipers F, Kosykh V, Fruchart JC, and Staels B (2003) FXR induces the UGT2B4 enzyme in hepatocytes: a potential mechanism of negative feedback control of FXR activity. *Gastroenterology* **124**:1926-1940.
- Bi YA, Qiu X, Rotter CJ, Kimoto E, Piotrowski M, Varma MV, Ei-Kattan AF, and Lai Y (2013) Quantitative assessment of the contribution of sodium-dependent taurocholate co-transporting polypeptide (NTCP) to the hepatic uptake of rosuvastatin, pitavastatin and fluvastatin. *Biopharm Drug Dispos* **34**:452-461.
- Blank A, Eidam A, Haag M, Hohmann N, Burhenne J, Schwab M, van de Graaf S, Meyer MR, Maurer HH, Meier K, Weiss J, Bruckner T, Alexandrov A, Urban S, Mikus G, and Haefeli WE (2018) The NTCP-inhibitor Myrcludex B: Effects on Bile Acid Disposition and Tenofovir Pharmacokinetics. *Clin Pharmacol Ther* **103**:341-348.
- Blank A, Markert C, Hohmann N, Carls A, Mikus G, Lehr T, Alexandrov A, Haag M, Schwab M, Urban S, and Haefeli WE (2016) First-in-human application of the novel hepatitis B and hepatitis D virus entry inhibitor myrcludex B. *J Hepatol* **65**:483-489.
- Bogomolov P, Alexandrov A, Voronkova N, Macievich M, Kokina K, Petrachenkova M, Lehr T, Lempp FA, Wedemeyer H, Haag M, Schwab M, Haefeli WE, Blank A, and Urban S (2016) Treatment of chronic hepatitis D

with the entry inhibitor myrcludex B: First results of a phase Ib/IIa study. *J Hepatol* **65**:490-498.

Carlton VEH, Harris BZ, Puffenberger EG, Batta AK, Knisely AS, Robinson DL, Strauss KA, Shneider BL, Lim WA, Salen G, Morton DH, and Bull LN (2003) Complex inheritance of familial hypercholanemia with associated mutations in TJP2 and BAAT. *Nature Genetics* **34**:91-96.

Cheng-Lai A (2003) Rosuvastatin: a new HMG-CoA reductase inhibitor for the treatment of hypercholesterolemia. *Heart disease (Hagerstown, Md)* **5**:72-78.

Choi MK, Shin HJ, Choi YL, Deng JW, Shin JG, and Song IS (2011) Differential effect of genetic variants of Na(+)-taurocholate co-transporting polypeptide (NTCP) and organic anion-transporting polypeptide 1B1 (OATP1B1) on the uptake of HMG-CoA reductase inhibitors. *Xenobiotica* **41**:24-34.

Chong HK, Infante AM, Seo YK, Jeon TI, Zhang Y, Edwards PA, Xie X, and Osborne TF (2010) Genome-wide interrogation of hepatic FXR reveals an asymmetric IR-1 motif and synergy with LRH-1. *Nucleic Acids Res* **38**:6007-6017.

Claudel T, Sturm E, Duez H, Torra IP, Sirvent A, Kosykh V, Fruchart JC, Dallongeville J, Hum DW, Kuipers F, and Staels B (2002) Bile acid-activated nuclear receptor FXR suppresses apolipoprotein A-I transcription via a negative FXR response element. *J Clin Invest* **109**:961-971.

Claudel T and Trauner M (2020) *Bile Acids as Signaling Molecules*. John Wiley & Sons, Inc.

Collins R, Reith C, Emberson J, Armitage J, Baigent C, Blackwell L, Blumenthal R, Danesh J, Smith GD, DeMets D, Evans S, Law M, MacMahon S, Martin S, Neal B, Poulter N, Preiss D, Ridker P, Roberts I, Rodgers A, Sandercock P, Schulz K, Sever P, Simes J, Smeeth L, Wald N, Yusuf S, and Peto R (2016) Interpretation of the evidence for the efficacy and safety of statin therapy. *Lancet (London, England)* **388**:2532-2561.

Cooper GM, Stone EA, Asimenos G, Green ED, Batzoglou S, Sidow A, and Progra NCS (2005) Distribution and intensity of constraint in mammalian genomic sequence. *Genome Research* **15**:901-913.

Dawson PA, Lan T, and Rao A (2009) Bile acid transporters. *J Lipid Res* **50**:2340-2357.

de Aguiar Vallim TQ, Tarling EJ, and Edwards PA (2013) Pleiotropic roles of bile acids in metabolism. *Cell metabolism* **17**:657-669.

- DeGorter MK, Tirona RG, Schwarz UI, Choi YH, Dresser GK, Suskin N, Myers K, Zou G, Iwuchukwu O, Wei WQ, Wilke RA, Hegele RA, and Kim RB (2013) Clinical and pharmacogenetic predictors of circulating atorvastatin and rosuvastatin concentrations in routine clinical care. *Circ Cardiovasc Genet* **6**:400-408.
- Deng M, Mao M, Guo L, Chen FP, Wen WR, and Song YZ (2016) Clinical and molecular study of a pediatric patient with sodium taurocholate cotransporting polypeptide deficiency. *Exp Ther Med* **12**:3294-3300.
- Denson LA, Sturm E, Echevarria W, Zimmerman TL, Makishima M, Mangelsdorf DJ, and Karpen SJ (2001) The orphan nuclear receptor, shp, mediates bile acid-induced inhibition of the rat bile acid transporter, ntcp. *Gastroenterology* **121**:140-147.
- DePristo MA, Banks E, Poplin R, Garimella KV, Maguire JR, Hartl C, Philippakis AA, del Angel G, Rivas MA, Hanna M, McKenna A, Fennell TJ, Kernytsky AM, Sivachenko AY, Cibulskis K, Gabriel SB, Altshuler D, and Daly MJ (2011) A framework for variation discovery and genotyping using next-generation DNA sequencing data. *Nat Genet* **43**:491-498.
- Fisher MM and Yousef IM (1973) Sex differences in the bile acid composition of human bile: studies in patients with and without gallstones. *Canadian Medical Association journal* **109**:190-193.
- Fong CW (2014) Statins in therapy: understanding their hydrophilicity, lipophilicity, binding to 3-hydroxy-3-methylglutaryl-CoA reductase, ability to cross the blood brain barrier and metabolic stability based on electrostatic molecular orbital studies. *European journal of medicinal chemistry* **85**:661-674.
- Fujikura K, Ingelman-Sundberg M, and Lauschke VM (2015) Genetic variation in the human cytochrome P450 supergene family. *Pharmacogenet Genomics* **25**:584-594.
- Genomes Project C, Abecasis GR, Auton A, Brooks LD, DePristo MA, Durbin RM, Handsaker RE, Kang HM, Marth GT, and McVean GA (2012) An integrated map of genetic variation from 1,092 human genomes. *Nature* **491**:56-65.
- Giacomini KM, Huang S-M, Tweedie DJ, Benet LZ, Brouwer KLR, Chu X, Dahlin A, Evers R, Fischer V, Hillgren KM, Hoffmaster KA, Ishikawa T, Keppler D, Kim RB, Lee CA, Niemi M, Polli JW, Sugiyama Y, Swaan PW, Ware JA, Wright SH, Wah Yee S, Zamek-Gliszczyński MJ, Zhang L, and The International Transporter C (2010) Membrane transporters in drug development. *Nature Reviews Drug Discovery* **9**:215-236.

- Gomez-Ospina N, Potter CJ, Xiao R, Manickam K, Kim MS, Kim KH, Shneider BL, Picarsic JL, Jacobson TA, Zhang J, He W, Liu P, Knisely AS, Finegold MJ, Muzny DM, Boerwinkle E, Lupski JR, Plon SE, Gibbs RA, Eng CM, Yang Y, Washington GC, Porteus MH, Berquist WE, Kambham N, Singh RJ, Xia F, Enns GM, and Moore DD (2016) Mutations in the nuclear bile acid receptor FXR cause progressive familial intrahepatic cholestasis. *Nature communications* **7**:10713.
- Goodwin B, Jones SA, Price RR, Watson MA, McKee DD, Moore LB, Galardi C, Wilson JG, Lewis MC, Roth ME, Maloney PR, Willson TM, and Kliewer SA (2000) A regulatory cascade of the nuclear receptors FXR, SHP-1, and LRH-1 represses bile acid biosynthesis. *Molecular cell* **6**:517-526.
- Grantham R (1974) Amino-Acid Difference Formula to Help Explain Protein Evolution. *Science* **185**:862-864.
- Gulilat M, Lamb T, Teft WA, Wang J, Dron JS, Robinson JF, Tirona RG, Hegele RA, Kim RB, and Schwarz UI (2019) Targeted next generation sequencing as a tool for precision medicine. *BMC Med Genomics* **12**:81.
- Hagenbuch B and Meier PJ (1994) Molecular cloning, chromosomal localization, and functional characterization of a human liver Na⁺/bile acid cotransporter. *J Clin Invest* **93**:1326-1331.
- Hagenbuch B, Stieger B, Foguet M, Lubbert H, and Meier PJ (1991) Functional expression cloning and characterization of the hepatocyte Na⁺/bile acid cotransport system. *Proc Natl Acad Sci U S A* **88**:10629-10633.
- Halilbasic E, Claudel T, and Trauner M (2013) Bile acid transporters and regulatory nuclear receptors in the liver and beyond. *J Hepatol* **58**:155-168.
- Han SM, Park J, Lee JH, Lee SS, Kim H, Han H, Kim Y, Yi S, Cho JY, Jang IJ, and Lee MG (2017) Targeted Next-Generation Sequencing for Comprehensive Genetic Profiling of Pharmacogenes. *Clin Pharmacol Ther* **101**:396-405.
- Hayden EC (2014) Technology: The \$1,000 genome. *Nature* **507**:294-295.
- Ho RH, Tirona RG, Leake BF, Glaeser H, Lee W, Lemke CJ, Wang Y, and Kim RB (2006) Drug and bile acid transporters in rosuvastatin hepatic uptake: function, expression, and pharmacogenetics. *Gastroenterology* **130**:1793-1806.
- Holt JA, Luo G, Billin AN, Bisi J, McNeill YY, Kozarsky KF, Donahee M, Wang DY, Mansfield TA, Kliewer SA, Goodwin B, and Jones SA (2003) Definition of a novel growth factor-dependent signal cascade for the

- suppression of bile acid biosynthesis. *Genes & development* **17**:1581-1591.
- Hu M, Lui SS, Mak VW, Chu TT, Lee VW, Poon EW, Tsui TK, Ko GT, Baum L, Tam LS, Li EK, and Tomlinson B (2010) Pharmacogenetic analysis of lipid responses to rosuvastatin in Chinese patients. *Pharmacogenet Genomics* **20**:634-637.
- Inagaki T, Choi M, Moschetta A, Peng L, Cummins CL, McDonald JG, Luo G, Jones SA, Goodwin B, Richardson JA, Gerard RD, Repa JJ, Mangelsdorf DJ, and Kliewer SA (2005) Fibroblast growth factor 15 functions as an enterohepatic signal to regulate bile acid homeostasis. *Cell metabolism* **2**:217-225.
- Ioannidis NM, Rothstein JH, Pejaver V, Middha S, McDonnell SK, Baheti S, Musolf A, Li Q, Holzinger E, Karyadi D, Cannon-Albright LA, Teerlink CC, Stanford JL, Isaacs WB, Xu J, Cooney KA, Lange EM, Schleutker J, Carpten JD, Powell IJ, Cussenot O, Cancel-Tassin G, Giles GG, MacInnis RJ, Maier C, Hsieh CL, Wiklund F, Catalona WJ, Foulkes WD, Mandal D, Eeles RA, Kote-Jarai Z, Bustamante CD, Schaid DJ, Hastie T, Ostrander EA, Bailey-Wilson JE, Radivojac P, Thibodeau SN, Whittemore AS, and Sieh W (2016) REVEL: An Ensemble Method for Predicting the Pathogenicity of Rare Missense Variants. *Am J Hum Genet* **99**:877-885.
- Istvan ES (2002) Structural mechanism for statin inhibition of 3-hydroxy-3-methylglutaryl coenzyme A reductase. *American heart journal* **144**:S27-32.
- Javitt NB (2002) Cholesterol, hydroxycholesterols, and bile acids. *Biochemical and biophysical research communications* **292**:1147-1153.
- Jones G, Strugnell SA, and DeLuca HF (1998) Current understanding of the molecular actions of vitamin D. *Physiol Rev* **78**:1193-1231.
- Kircher M, Witten DM, Jain P, O'Roak BJ, Cooper GM, and Shendure J (2014) A general framework for estimating the relative pathogenicity of human genetic variants. *Nat Genet* **46**:310-315.
- Kitamura S, Maeda K, Wang Y, and Sugiyama Y (2008) Involvement of Multiple Transporters in the Hepatobiliary Transport of Rosuvastatin. *Drug Metabolism and Disposition* **36**:2014.
- Kliewer SA, Moore JT, Wade L, Staudinger JL, Watson MA, Jones SA, McKee DD, Oliver BB, Willson TM, Zetterström RH, Perlmann T, and Lehmann JM (1998) An orphan nuclear receptor activated by pregnanes defines a novel steroid signaling pathway. *Cell* **92**:73-82.

- Kumar M, Gupta A, and Mallik R (2020) *Cytoskeletal Motors*. John Wiley & Sons, Incorporated.
- Kumar P, Henikoff S, and Ng PC (2009) Predicting the effects of coding non-synonymous variants on protein function using the SIFT algorithm. *Nat Protoc* **4**:1073-1081.
- Lauschke VM, Milani L, and Ingelman-Sundberg M (2017) Pharmacogenomic Biomarkers for Improved Drug Therapy-Recent Progress and Future Developments. *AAPS J* **20**:4.
- Lee H, Zhang Y, Lee FY, Nelson SF, Gonzalez FJ, and Edwards PA (2006) FXR regulates organic solute transporters alpha and beta in the adrenal gland, kidney, and intestine. *J Lipid Res* **47**:201-214.
- Lek M, Karczewski KJ, Minikel EV, Samocha KE, Banks E, Fennell T, O'Donnell-Luria AH, Ware JS, Hill AJ, Cummings BB, Tukiainen T, Birnbaum DP, Kosmicki JA, Duncan LE, Estrada K, Zhao F, Zou J, Pierce-Hoffman E, Berghout J, Cooper DN, Deflaux N, DePristo M, Do R, Flannick J, Fromer M, Gauthier L, Goldstein J, Gupta N, Howrigan D, Kiezun A, Kurki MI, Moonshine AL, Natarajan P, Orozco L, Peloso GM, Poplin R, Rivas MA, Ruano-Rubio V, Rose SA, Ruderfer DM, Shakir K, Stenson PD, Stevens C, Thomas BP, Tiao G, Tusie-Luna MT, Weisburd B, Won HH, Yu D, Altshuler DM, Ardissino D, Boehnke M, Danesh J, Donnelly S, Elosua R, Florez JC, Gabriel SB, Getz G, Glatt SJ, Hultman CM, Kathiresan S, Laakso M, McCarroll S, McCarthy MI, McGovern D, McPherson R, Neale BM, Palotie A, Purcell SM, Saleheen D, Scharf JM, Sklar P, Sullivan PF, Tuomilehto J, Tsuang MT, Watkins HC, Wilson JG, Daly MJ, MacArthur DG, and Exome Aggregation C (2016) Analysis of protein-coding genetic variation in 60,706 humans. *Nature* **536**:285-291.
- Li J and Dawson PA (2019) Animal models to study bile acid metabolism. *Biochim Biophys Acta Mol Basis Dis* **1865**:895-911.
- Li J and Li T (2017) Bile acid receptors link nutrient sensing to metabolic regulation. *Liver Res* **1**:17-25.
- Li T and Chiang JY (2013) Nuclear receptors in bile acid metabolism. *Drug Metab Rev* **45**:145-155.
- Li T and Chiang JYL (2020) *Bile Acid Metabolism in Health and Disease: An Update*. John Wiley & Sons, Inc.
- Liu R, Chen C, Xia X, Liao Q, Wang Q, Newcombe PJ, Xu S, Chen M, Ding Y, Li X, Liao Z, Li F, Du M, Huang H, Dong R, Deng W, Wang Y, Zeng B, Pan Q, Jiang D, Zeng H, Sham P, Cao Y, Maxwell PH, Gao ZL, Peng L, and Wang Y (2017) Homozygous p.Ser267Phe in SLC10A1 is associated with

a new type of hypercholanemia and implications for personalized medicine. *Sci Rep* **7**:9214.

Luo L, Aubrecht J, Li D, Warner RL, Johnson KJ, Kenny J, and Colangelo JL (2018) Assessment of serum bile acid profiles as biomarkers of liver injury and liver disease in humans. *PLoS One* **13**:e0193824.

Makishima M, Okamoto AY, Repa JJ, Tu H, Learned RM, Luk A, Hull MV, Lustig KD, Mangelsdorf DJ, and Shan B (1999) Identification of a nuclear receptor for bile acids. *Science* **284**:1362-1365.

Mao F, Liu T, Hou X, Zhao H, He W, Li C, Jing Z, Sui J, Wang F, Liu X, Han J, Borchers CH, Wang JS, and Li W (2019) Increased sulfation of bile acids in mice and human subjects with sodium taurocholate cotransporting polypeptide deficiency. *J Biol Chem* **294**:11853-11862.

Müsch A and Arias IM (2020) *Hepatocyte Surface Polarity*. John Wiley & Sons, Inc.

Myant NB and Mitropoulos KA (1977) Cholesterol 7 alpha-hydroxylase. *J Lipid Res* **18**:135-153.

Nagy P, Thorgeirsson SS, and Grisham JW (2020) *Organizational Principles of the Liver*. John Wiley & Sons, Inc.

Neale G, Lewis B, Weaver V, and Panveliwalla D (1971) Serum bile acids in liver disease. *Gut* **12**:145-152.

Neimark E, Chen F, Li X, and Shneider BL (2004) Bile acid-induced negative feedback regulation of the human ileal bile acid transporter. *Hepatology* **40**:149-156.

Nigam SK (2015) What do drug transporters really do? *Nat Rev Drug Discov* **14**:29-44.

Otsuki M (2000) Pathophysiological role of cholecystokinin in humans. *J Gastroenterol Hepatol* **15 Suppl**:D71-83.

Pandak WM, Heuman DM, Hylemon PB, Chiang JY, and Vlahcevic ZR (1995) Failure of intravenous infusion of taurocholate to down-regulate cholesterol 7 alpha-hydroxylase in rats with biliary fistulas. *Gastroenterology* **108**:533-544.

Qiu JW, Deng M, Cheng Y, Atif RM, Lin WX, Guo L, Li H, and Song YZ (2017) Sodium taurocholate cotransporting polypeptide (NTCP) deficiency: Identification of a novel SLC10A1 mutation in two unrelated infants presenting with neonatal indirect hyperbilirubinemia and remarkable hypercholanemia. *Oncotarget* **8**:106598-106607.

- Rehm HL, Bale SJ, Bayrak-Toydemir P, Berg JS, Brown KK, Deignan JL, Friez MJ, Funke BH, Hegde MR, Lyon E, Working Group of the American College of Medical G, and Genomics Laboratory Quality Assurance C (2013) ACMG clinical laboratory standards for next-generation sequencing. *Genet Med* **15**:733-747.
- Richards S, Aziz N, Bale S, Bick D, Das S, Gastier-Foster J, Grody WW, Hegde M, Lyon E, Spector E, Voelkerding K, Rehm HL, and Committee ALQA (2015) Standards and guidelines for the interpretation of sequence variants: a joint consensus recommendation of the American College of Medical Genetics and Genomics and the Association for Molecular Pathology. *Genet Med* **17**:405-424.
- Ridlon JM, Kang DJ, and Hylemon PB (2006) Bile salt biotransformations by human intestinal bacteria. *J Lipid Res* **47**:241-259.
- Rocha KCe, Pereira BMV, and Rodrigues AC (2018) An update on efflux and uptake transporters as determinants of statin response. *Expert Opinion on Drug Metabolism & Toxicology* **14**:613-624.
- Schachter M (2005) Chemical, pharmacokinetic and pharmacodynamic properties of statins: an update. *Fundamental & clinical pharmacology* **19**:117-125.
- Schaller L and Lauschke VM (2019) The genetic landscape of the human solute carrier (SLC) transporter superfamily. *Hum Genet*.
- Scharfe CPI, Tremmel R, Schwab M, Kohlbacher O, and Marks DS (2017) Genetic variation in human drug-related genes. *Genome Med* **9**:117.
- Slijepcevic D, Kaufman C, Wichers CG, Gilgioni EH, Lempp FA, Duijst S, de Waart DR, Elferink RP, Mier W, Stieger B, Beuers U, Urban S, and van de Graaf SF (2015) Impaired uptake of conjugated bile acids and hepatitis b virus pres1-binding in na(+)-taurocholate cotransporting polypeptide knockout mice. *Hepatology* **62**:207-219.
- Speed D, Hemani G, Johnson MR, and Balding DJ (2012) Improved heritability estimation from genome-wide SNPs. *Am J Hum Genet* **91**:1011-1021.
- Tomaszewski M, Stępień KM, Tomaszewska J, and Czuczwar SJ (2011) Statin-induced myopathies. *Pharmacological reports : PR* **63**:859-866.
- Trefts E, Gannon M, and Wasserman DH (2017) The liver. *Current biology : CB* **27**:R1147-r1151.
- Van Mil SW, Milona A, Dixon PH, Mullenbach R, Geenes VL, Chambers J, Shevchuk V, Moore GE, Lammert F, Glantz AG, Mattsson LA, Whittaker J, Parker MG, White R, and Williamson C (2007) Functional variants of the

central bile acid sensor FXR identified in intrahepatic cholestasis of pregnancy. *Gastroenterology* **133**:507-516.

Vaz FM, Paulusma CC, Huidekoper H, de Ru M, Lim C, Koster J, Ho-Mok K, Bootsma AH, Groen AK, Schaap FG, Oude Elferink RP, Waterham HR, and Wanders RJ (2015) Sodium taurocholate cotransporting polypeptide (SLC10A1) deficiency: conjugated hypercholanemia without a clear clinical phenotype. *Hepatology* **61**:260-267.

Visscher PM, Wray NR, Zhang Q, Sklar P, McCarthy MI, Brown MA, and Yang J (2017) 10 Years of GWAS Discovery: Biology, Function, and Translation. *Am J Hum Genet* **101**:5-22.

Weinman SA (1997) Electrogenicity of Na(+)-coupled bile acid transporters. *Yale J Biol Med* **70**:331-340.

Wikström Shemer EA, Stephansson O, Thuresson M, Thorsell M, Ludvigsson JF, and Marschall HU (2015) Intrahepatic cholestasis of pregnancy and cancer, immune-mediated and cardiovascular diseases: A population-based cohort study. *J Hepatol* **63**:456-461.

Yan H, Zhong GC, Xu GW, He WH, Jing ZY, Gao ZC, Huang Y, Qi YH, Peng B, Wang HM, Fu LR, Song M, Chen P, Gao WQ, Ren BJ, Sun YY, Cai T, Feng XF, Sui JH, and Li WH (2012) Sodium taurocholate cotransporting polypeptide is a functional receptor for human hepatitis B and D virus. *Elife* **1**.

Zhou Y, Fujikura K, Mkrтчian S, and Lauschke VM (2018) Computational Methods for the Pharmacogenetic Interpretation of Next Generation Sequencing Data. *Front Pharmacol* **9**:1437.

Zhou Y, Mkrтчian S, Kumondai M, Hiratsuka M, and Lauschke VM (2019) An optimized prediction framework to assess the functional impact of pharmacogenetic variants. *Pharmacogenomics J* **19**:115-126.

2 Rationale, Specific Aims, Hypotheses

2.1 Thesis Rationale

NTCP (*SLC10A1*) is central to the hepatic uptake of conjugated bile acids (Dawson et al., 2009). Genetic disruption of NTCP function can result in serum hypercholanemia (Vaz et al., 2015; Deng et al., 2016; Liu et al., 2017; Qiu et al., 2017), which may alter nuclear receptor signaling and gene expression. Further, the additional roles of NTCP in hepatic uptake of rosuvastatin (Ho et al., 2006; Bi et al., 2013), and hepatitis B and D viruses (Yan et al., 2012) underline its importance in drug transport and disease. Despite these important physiological roles, limited data exist regarding the effects of genetic variation in *SLC10A1* on bile acid dynamics and rosuvastatin transport. The goals of this study are to assess *in vitro* and *in vivo* effects of genetic disruption of *SLC10A1* on bile acid and rosuvastatin transport.

2.2 Governing hypothesis

Genetic variation in NTCP (*SLC10A1*) decreases hepatic bile acid and rosuvastatin uptake

2.3 Specific Aim 1

A. To test the functional effects of uncharacterized genetic variants in *SLC10A1* on NTCP transport activity and protein expression *in vitro*

B. To determine the performances of *in silico* algorithms to predict the effects of genetic variation on NTCP-mediated transport activity

Rationale: Many studies have characterized the transport activity and protein expression of genetically variant forms bile acid transporters OATP1B1 and OATP1B3 (Tirona et al., 2001; Schwarz et al., 2011; DeGorter et al., 2012), however, few studies have done so for NTCP. *In vitro* characterization is an important step in understanding which variants may be critical to study *in vivo*. Genetic variation in *SLC10A1* is rare, thus *in silico* prediction presents an attractive approach to prioritize variants for subsequent *in vitro* characterization.

My hypothesis is that genetic variation in *SLC10A1* will decrease taurocholic acid and/or rosuvastatin transport *in vitro*. Additionally, I hypothesize that common *in silico* tools will accurately predict deleterious NTCP-mediated transport of the endogenous substrate and that the pharmacogenetic-optimized tool will accurately predict NTCP-mediated transport of rosuvastatin.

2.4 Specific Aim 2

- A. To examine bile acid composition and expression of genes involved in bile acid synthesis and transport in *Slc10a1*^{-/-} mice**
- B. To determine hepatic uptake of rosuvastatin in *Slc10a1*^{-/-} mice**

Rationale: Although NTCP is an important rosuvastatin transporter *in vitro*, the importance of NTCP to rosuvastatin uptake *in vivo* has not been assessed. Additionally, limited data exist regarding effects of *Slc10a1* disruption in a mouse model (Slijepcevic et al., 2015; Mao et al., 2019). **My hypothesis is that *Slc10a1*^{-/-} mice are unable to compensate for disrupted *Slc10a1*, resulting in serum conjugated hypercholanemia and an altered hepatic gene expression. Additionally, I hypothesize that the liver-to-serum rosuvastatin concentration ratios will be decreased in *Slc10a1*^{-/-} mice.**

2.5 Specific Aim 3

To investigate sex-related differences in bile acid composition and expression of bile acid synthesis and transporter genes in *Slc10a1*^{-/-} mice

Rationale: Sex-related differences in bile acid synthesis and transport have been described in humans and animals (Phelps et al., 2019). Moreover, female mice may be more susceptible to persistent hypercholanemia (Mao et al., 2019), however sex-related differences have not been extensively investigated in *Slc10a1*^{-/-} mice. **My hypothesis is that female *Slc10a1*^{-/-} mice will display increased serum bile acid concentrations and hepatic *Cyp7a1* mRNA expression.**

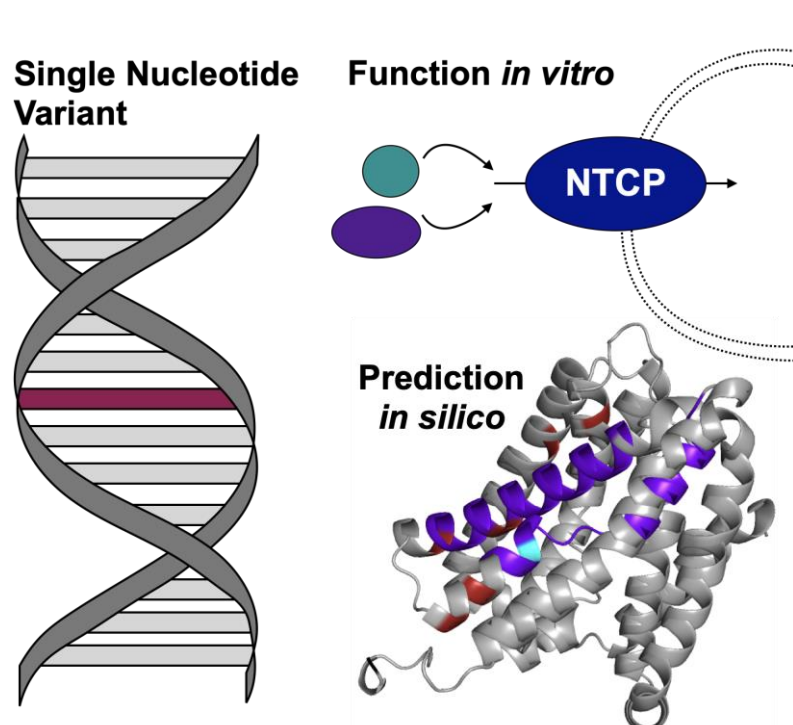
2.6 References

- Bi YA, Qiu X, Rotter CJ, Kimoto E, Piotrowski M, Varma MV, Ei-Kattan AF, and Lai Y (2013) Quantitative assessment of the contribution of sodium-dependent taurocholate co-transporting polypeptide (NTCP) to the hepatic uptake of rosuvastatin, pitavastatin and fluvastatin. *Biopharm Drug Dispos* **34**:452-461.
- Dawson PA, Lan T, and Rao A (2009) Bile acid transporters. *J Lipid Res* **50**:2340-2357.
- DeGorter MK, Ho RH, Leake BF, Tirona RG, and Kim RB (2012) Interaction of three regiospecific amino acid residues is required for OATP1B1 gain of OATP1B3 substrate specificity. *Mol Pharm* **9**:986-995.
- Deng M, Mao M, Guo L, Chen FP, Wen WR, and Song YZ (2016) Clinical and molecular study of a pediatric patient with sodium taurocholate cotransporting polypeptide deficiency. *Exp Ther Med* **12**:3294-3300.
- Ho RH, Tirona RG, Leake BF, Glaeser H, Lee W, Lemke CJ, Wang Y, and Kim RB (2006) Drug and bile acid transporters in rosuvastatin hepatic uptake: function, expression, and pharmacogenetics. *Gastroenterology* **130**:1793-1806.
- Liu R, Chen C, Xia X, Liao Q, Wang Q, Newcombe PJ, Xu S, Chen M, Ding Y, Li X, Liao Z, Li F, Du M, Huang H, Dong R, Deng W, Wang Y, Zeng B, Pan Q, Jiang D, Zeng H, Sham P, Cao Y, Maxwell PH, Gao ZL, Peng L, and Wang Y (2017) Homozygous p.Ser267Phe in SLC10A1 is associated with a new type of hypercholanemia and implications for personalized medicine. *Sci Rep* **7**:9214.
- Mao F, Liu T, Hou X, Zhao H, He W, Li C, Jing Z, Sui J, Wang F, Liu X, Han J, Borchers CH, Wang JS, and Li W (2019) Increased sulfation of bile acids in mice and human subjects with sodium taurocholate cotransporting polypeptide deficiency. *J Biol Chem* **294**:11853-11862.
- Phelps T, Snyder E, Rodriguez E, Child H, and Harvey P (2019) The influence of biological sex and sex hormones on bile acid synthesis and cholesterol homeostasis. *Biol Sex Differ* **10**:52.
- Qiu JW, Deng M, Cheng Y, Atif RM, Lin WX, Guo L, Li H, and Song YZ (2017) Sodium taurocholate cotransporting polypeptide (NTCP) deficiency: Identification of a novel SLC10A1 mutation in two unrelated infants presenting with neonatal indirect hyperbilirubinemia and remarkable hypercholanemia. *Oncotarget* **8**:106598-106607.

- Schwarz UI, Meyer zu Schwabedissen HE, Tirona RG, Suzuki A, Leake BF, Mokrab Y, Mizuguchi K, Ho RH, and Kim RB (2011) Identification of novel functional organic anion-transporting polypeptide 1B3 polymorphisms and assessment of substrate specificity. *Pharmacogenet Genomics* **21**:103-114.
- Slijepcevic D, Kaufman C, Wichers CG, Gilgioni EH, Lempp FA, Duijst S, de Waart DR, Elferink RP, Mier W, Stieger B, Beuers U, Urban S, and van de Graaf SF (2015) Impaired uptake of conjugated bile acids and hepatitis b virus pres1-binding in na(+) -taurocholate cotransporting polypeptide knockout mice. *Hepatology* **62**:207-219.
- Tirona RG, Leake BF, Merino G, and Kim RB (2001) Polymorphisms in OATP-C: identification of multiple allelic variants associated with altered transport activity among European- and African-Americans. *J Biol Chem* **276**:35669-35675.
- Vaz FM, Paulusma CC, Huidekoper H, de Ru M, Lim C, Koster J, Ho-Mok K, Bootsma AH, Groen AK, Schaap FG, Oude Elferink RP, Waterham HR, and Wanders RJ (2015) Sodium taurocholate cotransporting polypeptide (SLC10A1) deficiency: conjugated hypercholanemia without a clear clinical phenotype. *Hepatology* **61**:260-267.
- Yan H, Zhong GC, Xu GW, He WH, Jing ZY, Gao ZC, Huang Y, Qi YH, Peng B, Wang HM, Fu LR, Song M, Chen P, Gao WQ, Ren BJ, Sun YY, Cai T, Feng XF, Sui JH, and Li WH (2012) Sodium taurocholate cotransporting polypeptide is a functional receptor for human hepatitis B and D virus. *Elife* **1**.

3 *In vitro* functional characterization and *in silico* prediction of rare genetic variation in the bile acid and drug transporter, Na⁺-taurocholate co-transporting polypeptide (NTCP, *SLC10A1*)

(Russell et al., 2020)



Adapted & reprinted with permission from: Russell LE, Zhou Y, Lauschke VM, Kim RB. 2020. *In vitro* functional characterization and *in silico* prediction of rare genetic variation in the bile acid and drug transporter, Na⁺-taurocholate co-transporting polypeptide (NTCP, *SLC10A1*). *Mol Pharm* 17(4):1170-81. Copyright 2020 American Chemical Society.

3.1 Introduction

Bile acids are essential to digestion and absorption of dietary lipids, fat-soluble vitamins, and xenobiotics (Hofmann and Mysels, 1992; Chiang, 2013). Importantly, bile acids serve as key signaling molecules. The direct binding of bile acids to nuclear receptors such as farnesoid X receptor regulates expression of a medley of genes involved in bile acid biosynthesis and transport (Makishima et al., 1999; Tu et al., 2000). Bile acid homeostasis is maintained by membrane-bound transporters which facilitate enterohepatic recycling and prevent toxic intracellular and extracellular bile acid accumulation (Hofmann, 1999; Dawson et al., 2009). Bile acid transporters are also involved in the disposition of drugs including the cholesterol-lowering drug rosuvastatin (McTaggart et al., 2001; Martin et al., 2003; Ho et al., 2006; DeGorter et al., 2013). Rosuvastatin exerts its effect in the liver by preventing the conversion of 3-hydroxy-3-methylglutaryl-CoA to mevalonate, the rate-limiting step in cholesterol biosynthesis. Due to the hydrophilic nature of rosuvastatin, this statin is dependent on drug transporters for optimal hepatic uptake, a prerequisite for therapeutic benefit at its site of action (McTaggart et al., 2001; Martin et al., 2003).

First cloned from rat liver in 1991 and from human liver in 1994, Na⁺-taurocholate co-transporting polypeptide (NTCP, *SLC10A1*) is a key hepatic bile acid uptake transporter that also mediates transport of substrate drugs from the sinusoidal blood into hepatocytes (Hagenbuch et al., 1991; Hagenbuch and Meier, 1994; Ho et al., 2006). NTCP is the only sodium-dependent bile acid transporter in the liver and is localized exclusively to the basolateral membrane

of hepatocytes (Hagenbuch and Meier, 1994; Anwer and Stieger, 2014). NTCP uses secondary active transport to symport one bile acid molecule per two ions sodium from portal blood into the liver (Weinman, 1997; Anwer and Stieger, 2014). NTCP favors uptake of conjugated bile acids, can be inhibited or induced by a number of clinically used drugs, and is thought to contribute to up to 35% of hepatic rosuvastatin uptake (Meier et al., 1997; Kim et al., 1999; McTaggart et al., 2001; Martin et al., 2003; Ho et al., 2006).

Given the central role of NTCP in the maintenance of bile acid homeostasis, clinical cases of variation inducing complete deficiency of NTCP-mediated bile acid transport are extremely rare. However, a few causative genetic variants have been observed in greater abundance in East Asian or African American populations (Ho et al., 2004; Pan et al., 2011; Cunningham et al., 2019). NTCP-deficient individuals present with persistent elevations in serum bile acid concentrations, particularly of the conjugated nature (Vaz et al., 2015; Deng et al., 2016; Liu et al., 2017; Qiu et al., 2017). Additionally, NTCP deficiency may be associated with deficits in bone mineral density and fat-soluble vitamins due to impaired absorption at the intestine (Vaz et al., 2015; Deng et al., 2016; Liu et al., 2017). Studies of NTCP deficiency in knockout mouse models report marked elevations in serum bile acid concentrations along with dysregulated expression of bile acid transporters and increased serum concentrations of sulfated bile acids (Slijepcevic et al., 2015; Slijepcevic et al., 2017; Mao et al., 2019). More recently, NTCP was identified as a receptor for the entry of Hepatitis B and D viruses (HBV and HDV) into hepatocytes (Yan et al., 2012; Ni et al., 2014). Since

then, there has been growing interest in studying genetic influences on HBV and HDV infection.

Next-generation sequencing (NGS) has revealed vast amounts of rare variation in the human genome. Most of these genetic variants remain of uncertain clinical significance (Nelson et al., 2012; Fujikura et al., 2015). Solute carrier (SLC) transporters were found to be among the gene families with most variations, with each individual harbouring on average 30 genetic variants in the SLC superfamily (Schaller and Lauschke, 2019). It is expected that rare variants in genes involved in absorption, distribution, metabolism, and excretion (ADME) of drugs account for 30-40% of genetically induced adverse drug events (Kozyra et al., 2017). A major challenge with genomic datasets at present is the inability to interpret which rare variants may be clinically important, as classical functional assays *in vitro* are not feasible for the large number of rare variants that continue to be discovered (Lauschke and Ingelman-Sundberg, 2019; Lauschke et al., 2019; Zhou et al., 2019). Various algorithms have been developed to predict the consequences of genetic variation for which no functional data exist. However, different *in silico* algorithms often generate conflicting results (Gulilat et al., 2019). Moreover, most algorithms have been trained using evolutionary conservation and disease and thus are often poor predictors of functional variation related to drug transport or metabolism (Zhou et al., 2018).

Due to the vital roles of NTCP in bile acid homeostasis, statin transport, and HBV and HDV infection and treatment, functional characterization of rare *SLC10A1* variants may help identify genetic variants that increase susceptibility

to disease and/or adverse drug events. Furthermore, comparing observed transport *in vitro* to *in silico* predicted function will help elucidate the relevance of using *in silico* tools to predict rare *SLC10A1* variation. In the present study, we assessed 35 previously uncharacterized, rare, missense *SLC10A1* variants by determining *in vitro* expression, cellular localization and transport of the endogenous substrate taurocholic acid (TCA) and the xenobiotic substrate rosuvastatin. We also compared the *in silico* scores with the observed functional effects *in vitro* to assess the performances of seven algorithms to predict TCA and rosuvastatin uptake by genetically variant NTCP.

3.2 Methods & Materials

3.2.1 Materials

[³H]-Taurocholic acid (20 Ci/mmol) was purchased from American Radiolabeled Chemicals (St. Louis, MO). Taurocholic acid, rosuvastatin, and d6-rosuvastatin were purchased from Toronto Research Chemicals (Toronto, ON). All other chemicals, unless otherwise stated, were obtained from Millipore Sigma (St. Louis, MO).

3.2.2 Identification of single nucleotide variants in *SLC10A1*

The Ensembl Genome Browser (<https://www.ensembl.org>, accessed February 2019) was used to identify rare, missense genetic variants in *SLC10A1*. For this study, a rare variant was defined as displaying a minor allele frequency (MAF) <0.5%. Additional variants were identified from targeted next-generation sequencing of 235 local patients on heterogeneous pharmacotherapy regimens at London Health Sciences Centre, Canada (Gulilat et al., 2019). The genomics component of our study was approved by the Research Ethics Board of Western University, London, Canada (Appendix C). All subjects provided written informed consent. The DNA from patients was sequenced on the basis of having an adverse drug reaction or having measured drug concentrations outside of the expected range as identified by therapeutic drug monitoring. ClinVar (<https://www.ncbi.nlm.nih.gov/clinvar/>) and Single Nucleotide Polymorphism (https://www.ncbi.nlm.nih.gov/projects/SNP/snp_summary.cgi)

databases from the National Centre for Biotechnology Information as well as the Online Mendelian Inheritance in Man (<https://omim.org/>) database were searched for publications that assessed *SLC10A1* variant function. Variants for which no data were found for taurocholic acid uptake, rosuvastatin uptake, or protein expression were deemed novel for the purpose of this study and were selected for characterization *in vitro*.

3.2.3 *In silico* functional prediction of genetic variants in NTCP

Using the Ensembl Genome Browser database (<https://ensembl.org/>), *in silico* functional prediction scores for genetic variants of *SLC10A1* were obtained from the following tools: Combined Annotation-Dependent Depletion (CADD) (Kircher et al., 2014), Sorting Intolerant From Tolerant (SIFT) (Kumar et al., 2009), PolyPhenotyping-2 (PolyPhen-2) (Adzhubei et al., 2013), Mutation Assessor (Reva et al., 2007), Rare Exome Variant Ensemble Learner (REVEL) (Ioannidis et al., 2016), and MetaLR (Meta Logistic Regression) (Dong et al., 2015). One additional *in silico* algorithm optimized for pharmacogenes, further referred to as ADME-optimized, was independently employed to generate predictive scores for *SLC10A1* variants (Zhou et al., 2019). For ease of interpretation, predictions for functional impact of genetic variants were classified under one of two categories: deleterious (D) or tolerated (T). To classify variants as deleterious, the following threshold values were used: SIFT < 0.05, CADD > 20, and > 0.5 for PolyPhen-2, Mutation Assessor, REVEL, MetaLR, and ADME-optimized. Variants with SIFT > 0.05, CADD < 20, and scores < 0.5 for PolyPhen-2, Mutation Assessor, REVEL,

MetaLR, and ADME-optimized were classified as tolerated (T). An overview of methodologies used by individual tools to generate their predictions is presented in Table 3.1.

Table 3.1. *In silico* tools used to predict effects of SLC10A1 genetic variation on NTCP protein function

Tool	Acronym definition	Main prediction parameter(s)	Genomic region(s)	Publication
SIFT	Sorting Intolerant From Tolerant	Sequence homology	Coding	2009. Kumar et al., Nat Protocols
Mutation Assessor	NA	Sequence homology	Coding	2007. Reva et al., Genome Biol
PolyPhen-2	PolyPhenotyping version 2	Sequence homology, amino acid physicochemical properties	Coding	2013. Adzhubei et al., Curr Pro Hum Genet
Meta LR	Meta Logistic Regression	Ensemble method including inputs from 14 tools	Coding	2015. Dong et al. Hum Mol Genet.
CADD	Combined Annotation-Dependent Depletion	Ensemble method including inputs from 63 tools	Condng and noncoding	2014. Kircher et al., Nat Genet
REVEL	Rare Exome Variant Ensemble Learner	Ensemble method including inputs from 13 tools	Coding	2016. Ioannidis et al., Am J Hum Genet
ADME-optimized	Absorption, Distribution, Metabolism, Excretion	Ensemble method including inputs from 5 tools	Coding	2019. Zhou et al., Pharmacogenomics J

3.2.4 Wild type and variant plasmid construction

The open reading frame of *SLC10A1* was amplified by PCR from cDNA of pooled healthy human liver samples obtained through the Liver Tissue Cell Distribution System (Minneapolis, MN; funded by National Institutes of Health Contract N01DK70004/HHSN267200700004C) using primers listed in Table 3.1 (NTCP F and NTCP R). The PCR product was subcloned into the pCR2.1-TOPO cloning plasmid (Thermo Fisher Scientific). The NTCP open reading frame was then transferred to the pEF6/V5-His-TOPO expression plasmid (Thermo Fisher Scientific). Missense mutations were introduced using site-directed mutagenesis (QuikChange II, Agilent Technologies, Cedar Creek, TX). The stop codon of NTCP was mutated to ensure the translation of the V5 tag for subsequent analysis of protein expression. Constructs were verified using dideoxy sequencing at Robarts Research Institute. Primer pairs for mutating the stop codon and for creating each of the missense variants are listed in Tables 3.2 & 3.3.

Table 3.2. Primers used to clone NTCP and create variants

Primer name	Nucleotide Change	Forward or Reverse?	Oligonucleotide
Wild Type	NA	Forward	ATGGAGGCCCAACGCGTCTGC
NTCP	NA	Reverse	CCAGGCCACCAGGGGAAGGGCTAG
A3T	c.7G>A	Forward	ATTGCCCTTATGGAGACCCACAACGCGTCTG
		Reverse	CAGACGCGTTGTGGGTCCCATAAGGGCAAT
R21C	c.61C>T	Forward	CCAACTTTGGCAAGTGCCCCACAGACCTGGC
		Reverse	GCCAGGTCTGTGGGCACTTGCCAAAGTTGG
V29I	c.85G>A	Forward	CCTGGCACTGAGCATCATCCTGGTGTTC
		Reverse	GAACACCAGGATGATGCTCAGTGCCAGG
M39T	c.116T>C	Forward	GTTGTTCTTCATCACGCTCTCGCTGGGC
		Reverse	GCCCAGCGAGAGCGTGATGAAGAACAAC
S41L	c.122C>T	Forward	CATGTTGTTCTTCATCATGCTCTTGCTGGGCTGCAC
		Reverse	GTGACGCCAGCAAGAGCATGATGAAGAACAACATG
K52N	c.156G>C	Forward	GTTTCAGCAAGATCAACGCTCACTTATGGAAGC
		Reverse	GCTTCCATAAGTGAGCGTTGATCTTGCTGAACT
A64T	c.190G>A	Forward	GGGCTGGCCATCACCTGGTGGCAC
		Reverse	GTGCCACCAGGGTGATGGCCAGCCC
P73T	c.217C>A	Forward	CAGTATGGCATCATGACCCTCACGGCCTTTG
		Reverse	CAAAGCCGTGAGGGTCATGATGCCATACTG
I88T	c.263T>C	Forward	AGGTCTTCCGGCTGAAGAACACTGAGGCACTGG
		Reverse	CCAGTGCCTCAATGTTCTTCAGCCGGAAGACCT
I93V	c.277G>A	Forward	CATTGAGGCACTGGCCGCTTGGTCTGTGGCTGC
		Reverse	GCAGCCACAGACCAAGACGGCCAGTGCCTCAATG
L138P	c.413T>C	Forward	GCCTCTCCTCCCGTACATCTACTCC
		Reverse	GGAGTAGATGTACGGGAGGAGAGGGC
I159M	c.477C>G	Forward	GCCCTATAAAGGCATGGTGATATCACTGGTCC
		Reverse	GGACCAGTGATATCACCATGCCTTATAGGGC
T171I	c.512C>T	Forward	GGTTCATTCCCTTGATCATAGGGATCGTCCTCA
		Reverse	TGAGGACGATCCCTATGATGCAAGGAATGAGAACC
R180Q	c.539G>A	Forward	CGTCTCAAATCCAAACAGCCACAATACATGCGC
		Reverse	GCGCATGTATTGTGGCTGTTTGGATTTGAGGACG
M184T	c.551T>C	Forward	ATCCAAACGGCCACAATACACGCGCTATGTCATCA
		Reverse	TGATGACATAGCGCGTGATTGTGGCCGTTTGGAT
V187L	c.559G>C	Forward	CAATACATGCGCTATCTCATCAAGGGAGGG
		Reverse	CCCTCCCTTGATGAGATAGCGCATGTATTG
G190E	c.569G>A	Forward	GCGCTATGTCATCAAGGAAGGGATGATCATCATT
		Reverse	GAATGATGATCATCCCTTCCCTTGATGACATAGCGC

Table 3.3. Primers used to clone NTCP and create variants continued

Primer name	Nucleotide Change	Forward or Reverse?	Oligonucleotide
G191R	c.571G>A	Forward Reverse	GCGCTATGTCATCAAGGGAAGGATGATCATCATTC GAATGATGATCATCCTTCCCTTGATGACATAGCGC
I195L	c.583A>C	Forward Reverse	GGAGGGATGATCATCCTTCTCTTGTGCAGTG CACTGCACAAGAGAAGGATGATCATCCCTCC
V200M	c.598G>A	Forward Reverse	ATTCTCTGTGCAGTATGGCCGTCACAGTTC GAACTGTGACGGCCATACTGCACAAGAGAAT
V202I	c.604G>A	Forward Reverse	CTTGTGCAGTGTGGCCATCACAGTTCTCTCTGCC GGCAGAGAGAACTGTGATGGCCACACTGCACAAG
L205F	c.613C>T	Forward Reverse	GGCCGTCACAGTTTTCTCTGCCATCAATGTGGGG CCCCACATTGATGGCAGAGAAAAGTGTGACGGCC
I232T	c.695T>C	Forward Reverse	CCTCCTCCCTGATGCCTTTTACTGGCTTTCTGCTG CAGCAGAAAGCCAGTAAAAGGCATCAGGGAGGAGG
F234L	c.702T>G	Forward Reverse	GCCTTTTATTGGCTTGTGCTGGGTTATGTTC GAACATAACCCAGCAGCAAGCCAATAAAAGGC
S241F	c.722C>T	Forward Reverse	GGGTTATGTTCTCTTTGCTCTCTCTTGCC GGCAGAAGAGAGCAAAGAGAACATAAACC
R249W	c.745C>T	Forward Reverse	CTGCCTCAATGGATGGTGCAGACGCAC GTGCGTCTGCACCATCCATTGAGGCAG
R252S	c.754C>A	Forward Reverse	CAATGGACGGTGCAGAAGCACTGTCAGCATGGAG CTCCATGCTGACAGTGTCTTGCACCGTCCATTG
R252C	c.754C>T	Forward Reverse	CAATGGACGGTGCAGATCGACTGTCAGCATGGAG CTCCATGCTGACAGTGTCTTGCACCGTCCATTG
T258S	c.773G>C	Forward Reverse	CGCACTGTCAGCATGGAGAGTGGATGCCAAAATGTCC GGACATTTTGGCATCCACTCTCCATGCTGACAGTGCG
I279T	c.836T>C	Forward Reverse	CCACCTGAAGTCACTGGACCACITTTT GAAAAGTGGTCCAGTGACTTCAGGTGG
Q293E	c.877C>G	Forward Reverse	CCTCTACATGATTTTCGAGCTTGGAGAAGGGC GCCCTTCTCCAAGCTCGAAAATCATGTAGAGG
M319I	c.957G>A	Forward Reverse	TCAAGACTCCCAAGGATAAAAACAAAATAATCTACACAGCTGCC GGCAGCTGTGTAGATTATTTTGTTTTATCCTTGGGAGTCTTGA
E328K	c.982G>A	Forward Reverse	CAGCTGCCACAACCTGAAAAACAATTCCAGGAGCT AGCTCCTGGAATTGTTTTTTCAGTTGTGGCAGCTG
E328Q	c.982G>C	Forward Reverse	GCTGCCACAACCTGAACAAACAATTCCAGGAGC GCTCCTGGAATTGTTTGTTCAGTTGTGGCAGC
E342K	c.1024G>A	Forward Reverse	GCACCTACAAAGGGAAGGACTGCTCCCT AGGGGAGCAGTCTCCCTTTGTAGGTGC
Mutate stop codon	c.1047G>C	Forward Reverse	CCCCTTGCACAGCCTACAAGGGCAATTCTGC GCAGAATTGCCCTTGTAGGCTGTGCAAGGGG

3.2.5 Transient expression of NTCP in cultured cells

Transient transfection was performed in human embryonic kidney 293 type T (HEK293T) cells, obtained from American Type Culture Collection (Manassas, VA). HEK293T cells were cultured in Dulbecco's Modified Eagle's Medium (MEM) (Thermo Fisher Scientific, Grand Island, NY) supplemented with 10% FBS and 2 mM L-glutamine (Thermo Fisher Scientific) at 37°C and 5% CO₂. For transport experiments and protein analysis, HEK293T cells were seeded at 2.0 x 10⁵ cells/well on 12-well plates coated with poly-D-lysine-hydrobromide. After 24 hours, Lipofectamine 3000 (Thermo Fisher Scientific) diluted in Opti-MEM medium (Thermo Fisher Scientific) was used to transiently transfect 1 µg per well of empty vector cDNA (control) or plasmid containing NTCP cDNA inserts, wild type (WT) or variant. Cells were cultured for 16 hours prior to transport and protein assays. An overview of cloning, transfection, and transport assays is depicted in Figure 3.1.

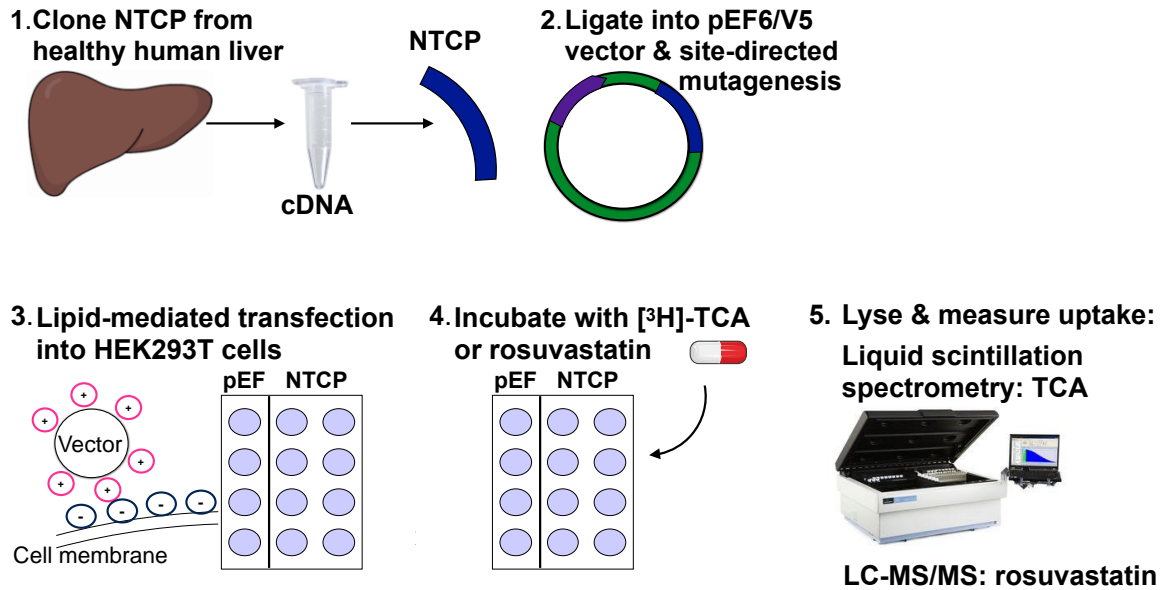


Figure 3.1. An overview of cloning, transfection, and transport experiments

Human NTCP was cloned from healthy hepatic tissue. 2. The NTCP open reading frame was ligated into the pEF-V5-His/TOPO expression vector, and site-directed mutagenesis was used to introduce missense mutations into the plasmid. 3. Vector control (pEF empty vector) or pEF-NTCP (pEF with the NTCP open reading frame, wild type or mutant, inserted) was transiently transfected into human embryonic kidney 293 type T (HEK293T) cells using Lipofectamine 3000, a lipid reagent that coats the DNA plasmid with lipids, creating a positive charge surrounding the plasmid DNA which is then attracted to the plasma membrane of cells for fusion and uptake of the DNA. 4. Transfected cells were incubated with a specified concentration of radiolabelled [³H] taurocholic acid (TCA) or unlabelled rosuvastatin. 5. At a specified timepoint, cells were washed with phosphate buffered saline to remove media containing the substrate, and cells were lysed for measurement of taurocholic acid uptake using liquid scintillation spectrometry or rosuvastatin by liquid chromatography tandem mass spectrometry (LC-MS/MS).

3.2.6 Single timepoint *in vitro* transport of taurocholic acid and rosuvastatin

For taurocholic acid (TCA) uptake, cells were incubated with 5 μM taurocholic acid supplemented with [^3H]-taurocholic acid for 5 min to yield 100,000 disintegrations per minute (DPM) per dose (400 μL). Transport was quenched by washing wells 3x with 1 mL ice-cold 1x PBS. Cells were lysed in 1% SDS in water (v/v), and uptake was assessed using liquid scintillation spectrometry (Tri-Carb 3900TR; Perkin Elmer, Waltham, MA).

For rosuvastatin uptake, transfected cells were incubated with 1 μM rosuvastatin for 5 min, washed 3x with 1 mL ice-cold 1x PBS, and lysed in 400 μL ice-cold acetonitrile supplemented with the internal standard d6-rosuvastatin. Cell lysates were centrifuged at 10,000 $\times g$ for 10 min at 4°C to pellet cell debris. The supernatant was diluted in H₂O supplemented with 0.1% formic acid (2:1 v/v). The concentration of rosuvastatin was quantified based on a previously reported method (DeGorter et al., 2013). Solutes were separated by reversed-phase chromatography on a Hypersil GOLD C18 column (50 \times 3 mm, 5 μm ; ThermoFisher Scientific) with 0.1% formic acid/water and acetonitrile solvent gradient. After electrospray ionization, mass spectrometric detection (TSQ Vantage) was performed in positive mode with transitions 482.1 \rightarrow 258.2 m/z for rosuvastatin and 488.0 \rightarrow 264.3 m/z for d6-rosuvastatin. Calibration curves were linear with rosuvastatin concentrations between 0 and 1000 ng/mL. Inter-day assay accuracy and precision were 5.8% and 8.9%, respectively, and the lower limit of quantitation was 1 ng/mL.

Cellular uptake was corrected for protein content per well as determined by the Pierce Bicinchoninic Acid (BCA) Protein Assay Kit (Thermo Fisher Scientific). Passive diffusion was accounted for by determining the difference in uptake between cells transfected with WT or variant NTCP plasmids and empty vector-transfected cells. For single time-point transport experiments, cellular uptake was normalized to uptake by WT NTCP-transfected cells (% WT). Experiments were performed in duplicate on three to four experimental days (n=3-4).

3.2.7 Characterization of transport kinetics

Three variants were selected for kinetic analysis based on the results from the single time point uptake assays. These include one variant that displayed substrate specificity (NTCP G191R) and two variants with reduced transport activity for TCA and rosuvastatin (NTCP R21C and K52N). To determine the transport kinetics for taurocholic acid and rosuvastatin uptake, a timepoint of 2 was selected based on linear substrate uptake at this timepoint. Uptake of 0.5, 1, 2, 5, 10, 20, 50, and 100 μM taurocholic acid and 1, 2, 5, 10, 20, 50, 100, and 200 μM rosuvastatin were assessed at 2 min. Michaelis-Menten nonlinear curve-fitting was performed with GraphPad Prism 6 (GraphPad, San Diego, CA) to determine the maximal uptake velocity (V_{max}) and the concentration at which half-maximal uptake occurred (K_m). Cellular uptake was corrected for protein content per well as determined by the Pierce BCA Protein Assay Kit (Thermo Fisher Scientific). Passive diffusion was accounted for by determining the difference in uptake between cells transfected with WT or variant NTCP plasmids and empty

vector-transfected cells. For kinetic experiments, the rates of substrate uptake were calculated by determining picomoles of substrate transported per milligram of protein per well per minute (pmol/mg protein/min). Experiments were performed in duplicate on 3 experimental days (n=3).

3.2.8 Western blot analysis

Transfected HEK293T cells were lysed in Pierce IP Lysis Buffer (Thermo Fisher Scientific) and 15 µg protein/well, as quantified using a BCA assay (Thermo Fisher Scientific), were separated by SDS-PAGE using 10% NuPAGE Bis-Tris gels (Thermo Fisher Scientific). Gels were transferred to polyvinylidene difluoride membranes and probed with antibodies. The loading control was probed first by incubating membranes for 16 hr at 4°C with rabbit polyclonal anti-Na⁺/K⁺-ATPase antibody (Cell Signaling Technology, Danvers, MA; catalogue number 3010S) diluted 1:1000 in TBS-T (20mM Tris, 150mM NaCl, 0.1% Tween 20, pH 7.4). Membranes were washed with 1x TBS-T for 10 min, 3x, at room temperature prior to a 1 hr incubation at room temperature with horseradish peroxidase-labeled anti-rabbit antibody (Cell Signaling Technology, Danvers, MA). Membranes were washed with 1x TBS-T for 10 min, three times, and the loading control was visualized by enhanced chemiluminescence (Amersham ECL Select; GE Healthcare, Mississauga, ON). Subsequently, to probe for NTCP expression using an antibody for the V5 tag, membranes were incubated for 1 hr at room temperature with mouse monoclonal anti-V5 antibody (Thermo Fisher; catalogue number R960-25), diluted 1:5000 in 1x TBS-T. The anti-V5 antibody was

selected to probe for NTCP expression due to the lack of a high-affinity NTCP antibody. Blots were washed with 1x TBS-T for 10 min, 3x, prior to incubation with horseradish peroxidase-labeled anti-mouse antibody (Bio-Rad, Hercules, CA) for 1 hr at room temperature. Blots were washed with 1x TBS-T at room temperature for 10 min, 3x, and expression of the V5 was visualized using enhanced chemiluminescence (Amersham ECL Select; GE Healthcare, Mississauga, ON). Western blots for HeLa cells were performed as stated above, with the exception of the use of a β -actin antibody (sc-1615-HRP, Santa Cruz Biotechnology, Dallas, TX) at 1:1000 dilution in TBS-T to probe the loading control.

3.2.9 Cell surface biotinylation

Plasma membrane protein expression was carried out for *SLC10A1* variants that displayed reduced substrate transport or reduced NTCP protein expression in whole-cell lysates. HEK293T cells were transfected as previously described for transport experiments. Sixteen hours post-transfection, cells were washed with 1x PBS. Cells were treated with membrane impermeable biotinylating reagent, Sulfo-NHS-SS-Biotin (EZ-Link, Thermo Fisher Scientific) at 0.5 mg/mL/well in 1x PBS supplemented with 100 μ M CaCl_2 and 2.12 mM MgCl_2 (PBS/Mg/Ca), and were rocked gently for 1 hr at 4°C. Cells were washed 3x with 1 mL PBS/Mg/Ca supplemented with 50 μ M glycine (PBS/Mg/Ca/glycine) and then incubated with 1 mL PBS/Mg/Ca/glycine, rocking at 4°C. After 20 min, cells were washed with PBS/Mg/Ca and lysed in 700 μ L radioimmunoprecipitation (RIPA) buffer (10 mM

Tris, 150 mM NaCl, 1.27 mM EDTA, 0.1% (w/v) SDS, and 10% (v/v) Triton X-100), supplemented with protease inhibitor cocktail. After sonication and 10,000 x *g* centrifugation for 5 mins at 4°C, 80 µL Streptavidin Agarose Resin (Thermo Fisher Scientific) was added to 600 µL cell lysate. Samples were mixed on an end-over-end rocker for 1 hr at room temperature, centrifuged at 10,000 x *g* for 3 min, and the supernatants were discarded. The pellets were washed three times with ice-cold RIPA buffer, and biotinylated proteins were released by incubating each sample with 100 µL 4x Lithium Dodecyl Sulfate (LDS) Sample Buffer (NuPAGE, Thermo Fisher Scientific) supplemented with 5% (v/v) 2-mercaptoethanol, mixing on an end-over-end rocker for 30 min at room temperature. Samples were centrifuged and the supernatants were subject to Western blot analysis as described above.

3.2.10 Cell surface deglycosylation assay

Protein deglycosylation was performed in HEK293T cell lysates enriched for the plasma membrane fraction using the biotinylation method previously described. Deglycosylation was achieved using the Glycoprofile II Enzymatic in-Solution N-Deglycosylation Kit. The kit protocol was modified as described below. Ten µg of HEK293T plasma membrane protein fraction were added to tubes containing 22.5 µL RNase B standard solution (22.5 µg/µL w/v) and 10 µL 1x reaction buffer. One µL aliquots of the denaturant solution containing 2% octyl B-D glycopyranoside with 100 mM 2-mercaptoethanol were added to the solution containing plasma membrane cell fractions and RNase B. One µL H₂O was

added to the control sample, and 1 μL PNGase F enzyme at 500 units of enzyme/mL was added to the experimental sample. Samples were mixed by vortexing and were incubated at 37°C for 1 hr. Samples were allowed to cool and were subsequently subjected to SDS-PAGE and Western blotting for NTCP protein expression using the V5 epitope tag as previously described.

3.2.11 Immunofluorescence confocal microscopy

HEK293T cells were plated on lysine-coated 4-well culture slides at 2.0×10^5 cells per 1.7 cm^2 well (2.35×10^4 cells/ mm^2) and were transiently transfected with plasmids encoding V5-tagged WT or variant NTCP. Culture slides were washed with room temperature 1x PBS, fixed in 4% paraformaldehyde for 10 min, permeabilized with 0.3% Triton X-100 in 1x PBS for 10 min, and washed in 1x PBS for 5 min. Slides were then blocked with 2% bovine serum albumin (BSA) in 1x PBS for 2 hr. Slides were incubated with mouse monoclonal anti-V5 diluted 1:2000 in 2% BSA/PBS for 1 hr at room temperature, then subjected to three, 5 min washes in 1x PBS supplemented with 0.05% Tween-20 (PBS-T). Slides were incubated with secondary Alexa 488-conjugated goat anti-mouse antibody diluted 1:1000 in PBST for 30 min at 37°C and were kept covered from light for subsequent steps. Slides were washed for 5 min, 3x, with 1x PBS-T. All liquid was removed from slides and a culture slide tool was used to remove culture slide walls. One drop of VECTASHIELD (Vector Labs, Burlington, Canada) mounting medium containing DAPI nuclear stain was added to each section of interest. A Corning No.1 (22x50 mm) cover glass was sealed over the regions of

interest. The samples were visualized using a TSC-SP8 confocal microscope by Leica Microsystems (Wetzlar, Germany). A 63x objective lense with oil immersion was used, and samples were observed at 405 nm using a 50 mW diode laser and 488 nm using a 20 mW optically pumped semiconductor laser for DAPI and V5-NTCP, respectively.

3.2.12 Predictive performance of *in silico* tools

Receiver operating characteristic (ROC) curves were generated to analyze the performance of algorithms to predict observed TCA and rosuvastatin uptake. Variants defined as tolerated *in vitro* were those with > 25% WT substrate uptake. Variants with < 25% WT uptake activity were defined as deleterious. Prediction scores from *in vitro* tolerated variants were compared to prediction scores from *in vitro* deleterious variants using ROC curves generated using GraphPad Prism 6. Area under the curve for receiver operating characteristic curves (AUC_{ROC}) was used as a measure of predictive performance. Sensitivity was determined by the true positive (TP) rate. True positives reflect variants with deleterious transport *in vitro* that were predicted to be deleterious by the *in silico* tool. False negatives (FN) are defined as having deleterious transport *in vitro* but predicted tolerated by the *in silico* tool. Specificity was determined by calculating the true negative (TN) rate. True negatives have no effect on transport activity *in vitro* and were predicted to be tolerated by the *in silico* tool. False positives (FP) are variants that display no change in transport activity *in vitro* yet are predicted deleterious by the *in silico* tool.

$$Sensitivity = \frac{\Sigma TP}{\Sigma TP + \Sigma FN} \quad Specificity = \frac{\Sigma TN}{\Sigma TN + \Sigma FP}$$

Σ : Sum, TP: true positive, FN: false negative

3.2.13 Predicted structures of NTCP

The 2D predicted membrane topologies of NTCP were visualized using the web application Protter (Omasits et al., 2014). The 3D predicted structure of NTCP was generated using Phyre2 (Kelley et al., 2015) and visualized using PyMOL (version 1.7.4, Schrödinger, LLC). Regions involved in sodium- and bile acid-binding were identified by previous biochemical studies of NTCP (Hallen et al., 2002; Mareninova et al., 2005).

3.2.14 Statistics

To determine statistical significance between transport activities for WT NTCP and wild type NTCP expressing the V5 epitope, unpaired, two-tailed Student's t tests were performed. One-way ANOVA with Dunnett's multiple comparisons tests were used to determine statistical differences between the transport activities of WT and variant NTCP. One-way ANOVA with Dunnett's multiple comparisons tests were also used to determine statistical differences in Michaelis-Menten K_m and V_{max} values between transport activities of WT and variant NTCP. For *in silico* predictive algorithm performance, Mann-Whitney tests were used to determine statistical differences AUC_{ROC} values, sensitivities, and specificities of

the various *in silico* predictions. Statistical significance was set at $P < 0.05$. All statistical analyses were performed using GraphPad Prism 6 (La Jolla, CA).

3.3 Results

3.3.1 Identifying *SLC10A1* variants

A total of 35 uncharacterized *SLC10A1* variants were identified for functional assessment. Thirty-one missense variants were identified using the Ensembl Genome Browser (<http://ensembl.org>) with filters set to identify rare, missense variants (< 0.5% minor allele frequency). Four additional variants were identified by next-generation sequencing of 235 patients from London Health Sciences Centre, Canada. All variants were scored for their predicted deleteriousness using *in silico* algorithms (Table 3.4).

Table 3.4. SLC10A1 variants for *in vitro* characterization and *in silico* prediction

NTCP (<i>SLC10A1</i>) variant information				<i>in silico</i> predictions						
rs ID	Nucleotide change	AA change	MAF ID (%)	SI	PP	MA	CA	RE	LR	AD
rs201910047	c.7G>A	A3T	E 0.005	T	T	T	T	T	T	T
rs200758433	c.61C>T	R21C	E 0.009	D	D	D	D	T	T	D
rs148905100	c.85G>A	V29I	E 0.007	T	T	T	T	T	T	T
rs536458730	c.116T>C	M39T	E 0.003	D	D	D	D	D	T	D
rs111885789	c.122C>T	S41L	N 0.055	D	D	D	D	D	T	D
rs569402278	c.156G>C	K52N	E 0.005	D	D	D	D	T	T	D
rs202018997	c.190G>A	A64T	E 0.004	D	D	D	D	D	T	D
rs763683476	c.217C>A	P73T	N 0.001	D	D	D	D	D	T	D
rs148467625	c.263T>C	I88T	E 0.119	T	T	D	T	T	T	T
rs200105842	c.277G>A	I93V	E 0.033	T	T	T	T	T	T	T
rs543063679	c.413T>C	L138P	E 0.002	D	D	D	D	D	T	D
rs144006534	c.477C>G	I159M	E 0.001	D	D	T	T	T	T	D
rs202007233	c.512C>T	T171I	E 0.002	T	T	T	T	T	T	T
rs571796903	c.539G>A	R180Q	E 0.01	D	D	D	D	T	T	T
rs766070047	c.551T>C	M184T	N 0.001	T	T	T	T	T	T	T
rs199771927	c.559G>C	V187L	E 0.001	T	T	D	T	T	T	T
rs553948182	c.569G>A	G190E	E 0.02*	T	T	D	T	T	T	T
rs202246109	c.571G>A	G191R	E 0.003	D	D	D	D	D	T	D
rs145747967	c.583A>C	I195L	E 0.001	T	T	D	T	T	T	T
rs202213974	c.598G>A	V200M	E 0.022	D	D	D	D	T	T	D
rs146868379	c.604G>A	V202I	E 0.007	T	T	D	T	T	T	T
rs142448421	c.613C>T	L205F	N 0.001	D	D	D	D	T	T	D
rs190268737	c.695T>C	I232T	E 0.021	T	T	T	T	T	T	T
rs139931299	c.702T>G	F234L	E 0.028	D	D	D	D	T	T	D
rs150579813	c.722C>T	S241F	E 0.001	D	T	D	D	T	T	D
rs76966244	c.745C>T	R249W	E 0.2*	D	D	D	D	D	D	D
rs141269120	c.754C>A	R252S	E 0.02*	D	D	D	D	D	D	D
rs141269120	c.754C>T	R252C	E 0.02*	D	D	D	D	D	D	D
rs541801766	c.773G>C	T258S	E 0.001	D	D	D	D	D	D	D
rs72547507	c.836T>C	I279T	E 0.014	D	D	D	D	T	T	D
rs189313778	c.877C>G	Q293E	E 0.017	D	D	D	D	T	T	D
rs149272163	c.957G>A	M319I	E 0.019	T	T	T	T	T	T	T
rs571658472	c.982G>A	E328K	E 0.002	D	D	D	D	T	T	T
rs571658472	c.982G>C	E328Q	E 0.002	D	T	D	D	T	T	T
rs375849915	c.1024G>A	E342K	E 0.004	T	T	T	T	T	T	T

Acronyms and short forms: rs ID, reference single nucleotide polymorphism identification; AA, amino acid; ID, identification; E, Ensembl genome browser; N, or next-generation sequencing; MAF, minor allele frequency; SI, Sorting Intolerant From Tolerant (SIFT); PP, PolyPhenotyping Version 2 (PolyPhen-2); MA, Mutation Assessor; CA, Combined Annotation-Dependent Depletion (CADD); RE, Rare Exome Variant Ensemble Learner (REVEL); LR, Meta Logistic Regression (MetaLR); AD, Absorption Distribution Metabolism Excretion (ADME) pharmacogenetics-optimized algorithm; T, tolerated; D, deleterious. Minor allele frequencies were obtained from the Exome Aggregation Consortium (ExAC) database (<http://exac.broadinstitute.org/>) except where denoted by *, where frequency was determined using the 1000 Genomes database. Classifications by these algorithms were simplified to tolerated (T) for variants predicted to have no functional consequence and deleterious (D) for variants predicted to affect protein function.

3.3.2 *In vitro* transport and protein expression

To assess the impact of these genetic variations on NTCP activity and expression, transport assays and evaluation of NTCP protein expression and localization were performed in transiently transfected HEK293T cells.

Stop codons for NTCP plasmids were mutated to express the 14 amino acid V5 epitope tag for subsequent protein expression assays. Therefore, to determine any difference in transport activities for TCA and rosuvastatin uptake, transport by wild type (WT) NTCP expressing the stop codon and WT NTCP expressing the V5 epitope were compared. Expression of the V5 epitope had no measurable effect on NTCP-mediated transport of taurocholic acid and rosuvastatin (Fig. 3.2).

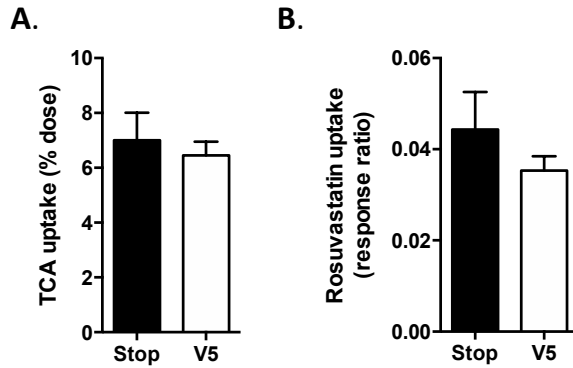


Figure 3.2. Determining the effect of the V5 epitope on substrate transport.

HEK293T cells transfected with the pEF-NTCP-Stop or pEF-NTCP-V5 plasmid were administered 5 μ M TCA or 1 μ M rosuvastatin and uptake was quantified at 5 min using liquid scintillation spectroscopy or LC-MS/MS, respectively. A. TCA transport expressed as percentage of dose administered. B. Rosuvastatin transport expressed as ratio of rosuvastatin uptake relative to d6-rosuvastatin internal standard uptake. A standard curve was not used to determine concentration of rosuvastatin uptake. Experiments were performed in duplicate on three experimental days, n=3 and results represent mean \pm SEM. Statistical significance was determined using Student's t tests.

After establishing no detectable difference between transport activity of NTCP expressing the stop codon and NTCP expressing the V5 epitope, all subsequent experiments were performed using constructs expressing the V5 epitope. To screen variants for their transport activity, uptake of 5 μ M TCA and 1 μ M rosuvastatin were determined (Figure 3.3).

Significantly increased transport of TCA was observed for two *SLC10A1* variants, A3T and E342K (Fig. 3.3 A), which exhibited 127 ± 10 -17% of WT NTCP activity ($P < 0.05$). Taurocholic acid transport was significantly reduced for 19 *SLC10A1* variants (Fig. 3.3 A). Uptake by these variants ranged from 0 to 73% of WT NTCP TCA uptake activity ($P < 0.05$). Among these 19 variants, robust reductions in TCA transport were observed for P73T, L138P, F234L, S241F, R249W, R252S, and R252C (0 -13 \pm 0-3% of WT NTCP uptake activity, $P < 0.0001$, Fig. 3.3 A).

These same seven variants also showed marked reduction in rosuvastatin transport, where 0 -4 \pm 0-3% of WT rosuvastatin uptake activity was observed (Fig. 3.3 B). Rosuvastatin transport was significantly increased for the T171I variant, which displayed $194 \pm 17\%$ of WT NTCP rosuvastatin uptake ($P < 0.0001$, Fig. 3.3 B).

One variant, G191R, displayed substrate specificity; transport of TCA was comparable to WT NTCP activity ($89 \pm 7\%$), however rosuvastatin transport was significantly decreased to $8 \pm 2\%$ of WT NTCP uptake ($P < 0.0001$).

With regard to protein expression in HEK293T whole-cell lysates, three distinct NTCP protein bands were observed. One band each at molecular weights of approximately 32, 38, and 52 kDa were detected (Fig. 3.3 C).

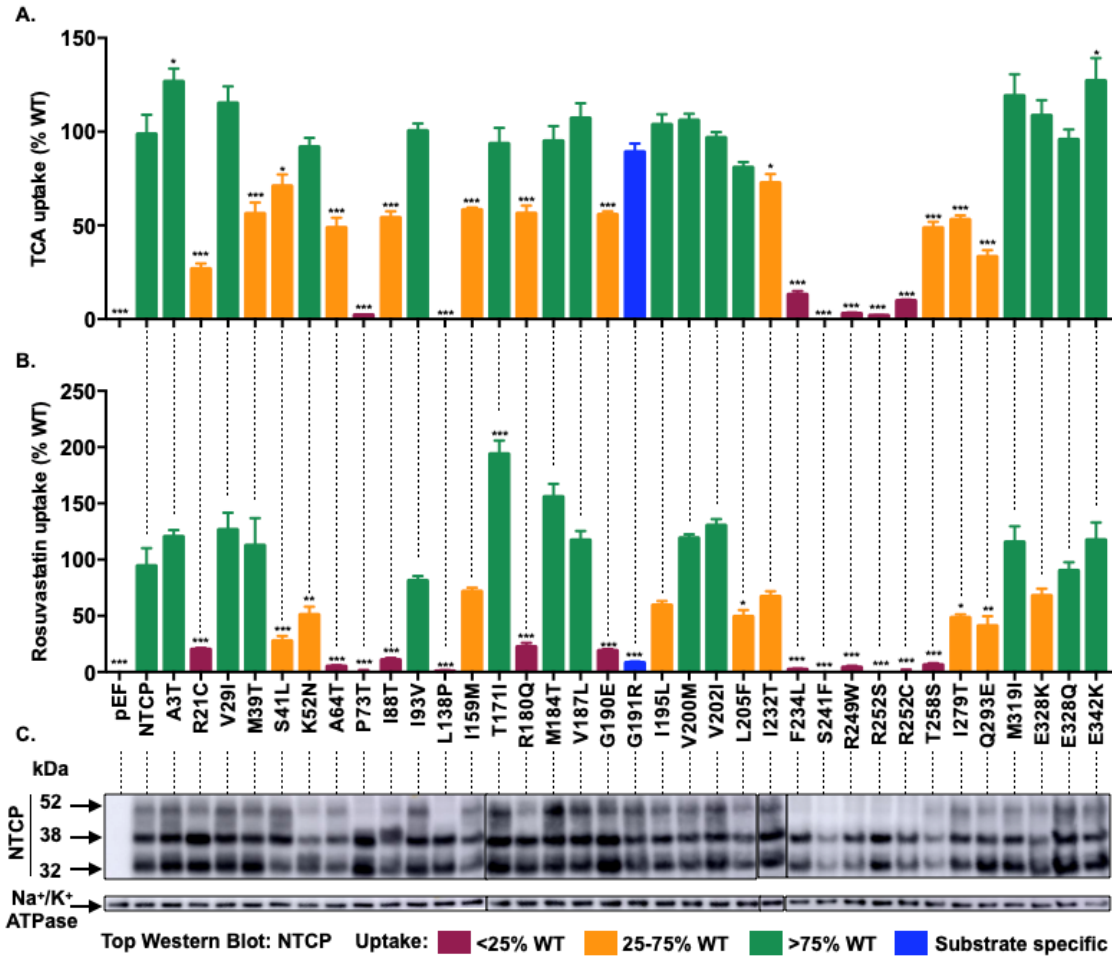


Figure 3.3. Substrate uptake and whole-cell NTCP protein expression of *SLC10A1* variants in HEK293T cells.

A. & B. Single timepoint substrate uptake in transfected HEK293T cells after 5 min incubation with A. 5 μ M TCA or B. 1 μ M rosuvastatin. C. Whole-cell protein expression of NTCP from transfected HEK293T lysates. Transport experiments were performed in duplicate on 3-4 experimental days and are expressed as mean percentage of wild type uptake \pm SEM. Statistical significance was assessed using one-way ANOVA with Dunnett's multiple comparison tests, * $P < 0.05$, ** $P < 0.01$, *** $P < 0.0001$.

As NTCP exerts its function at the plasma membrane, cell surface biotinylation and subsequent Western blotting were performed to determine the extent of NTCP protein at the cell surface. Protein expression was quantified for WT NTCP and select variants that displayed reductions in taurocholate and rosuvastatin transport. The three-band pattern for NTCP expression was again observed in whole-cell HEK293T lysates for WT NTCP and variants R21C, A64T, and T258S (Fig. 3.5 A). For plasma membrane-enriched samples (Fig. 3.5 B), the 52 kDa bands increased in intensity and the 32 and 38 kDa bands decreased in intensity for NTCP, R21C, A64T, and T258S. This suggests that the 52 kDa band represents NTCP protein expressed at the cell surface.

In contrast, no bands were observed at 52 kDa for the seven variants with robust reductions in transport activity for both substrates. This was observed in whole-cell (Fig. 3.5 A) and plasma membrane-enriched fractions (Fig. 3.5 B), suggesting these variant proteins are not abundantly expressed at the cell surface. Additionally, using immunofluorescence microscopy, plasma membrane localization was detected for WT NTCP, whereas intracellular retention of NTCP protein was observed for all variants with nearly undetectable transport activity (Fig. 3.6).

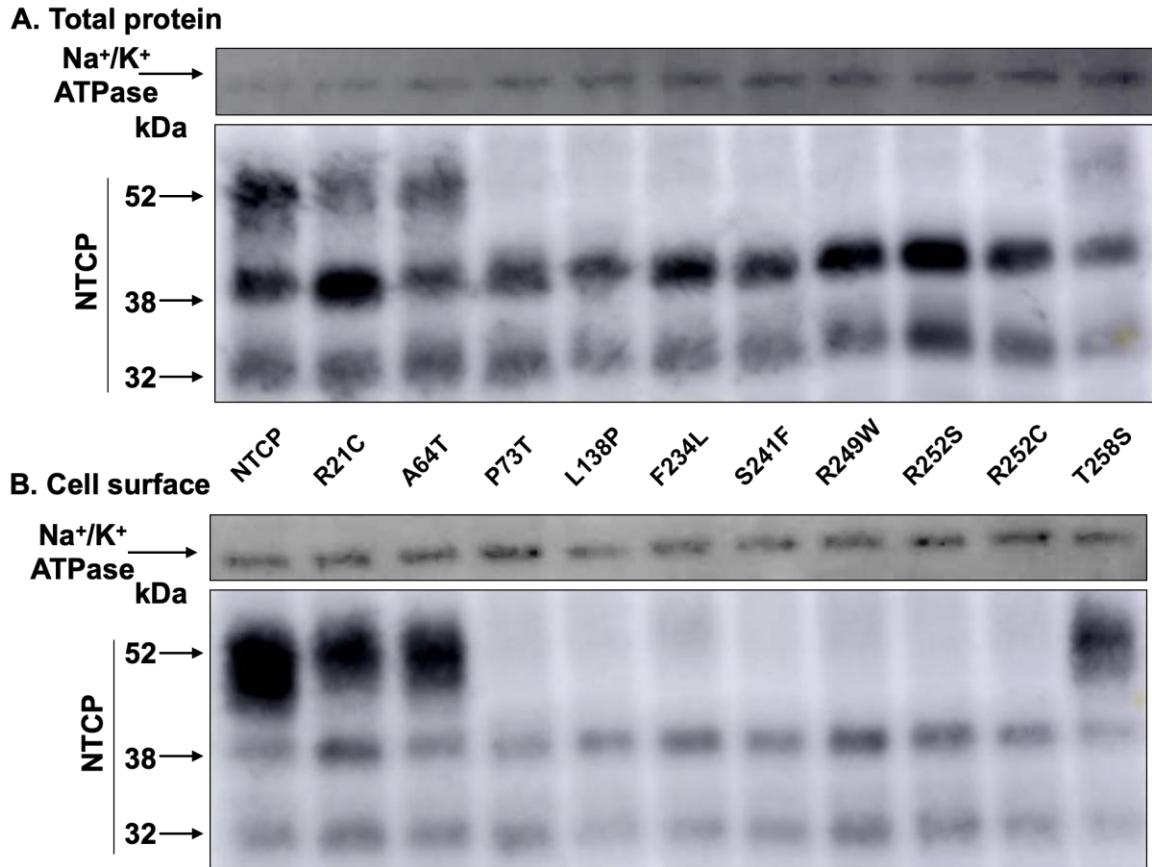


Figure 3.4. Whole-cell and plasma membrane expression of variant NTCP protein in HEK293T cells

Variants with reduced transport activity: R21C A64T, and T258S. Variants with nearly undetectable transport activity: P73T, L138P, F234L, S241F, R249W, R252S, and R252C. A. NTCP protein expression in whole-cell HEK293T lysates. B. NTCP protein expression in plasma membrane-enriched fractions of HEK293T cells, obtained using cell surface biotinylation..

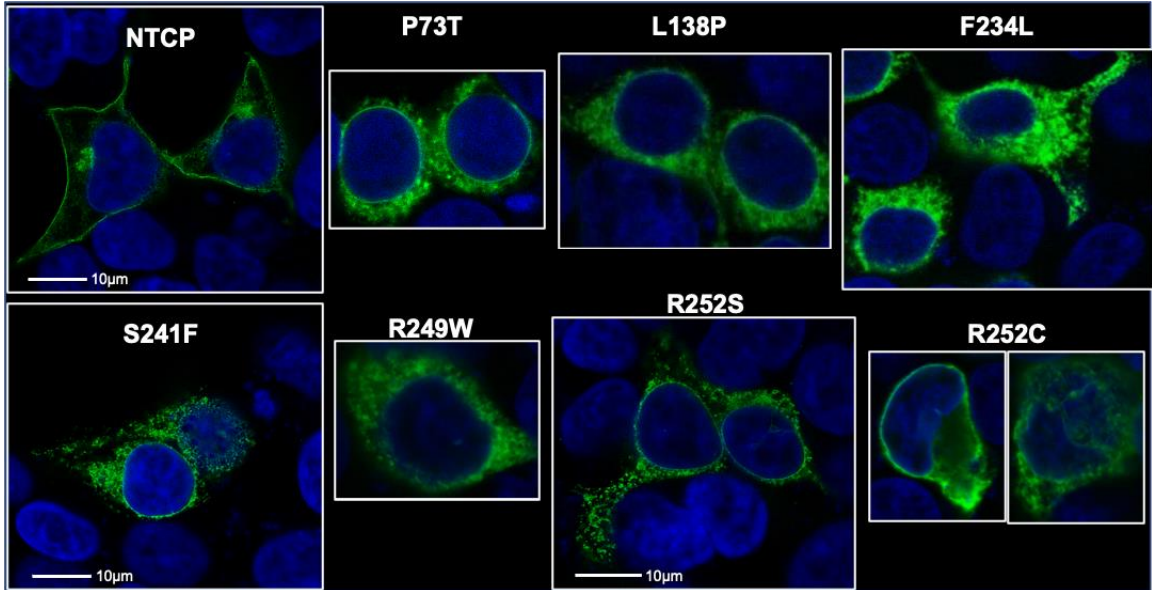


Figure 3.5. Immunofluorescence confocal microscopy of wild type and variant NTCP. All variants in this figure displayed nearly absent transport for taurocholate and rosuvastatin. DAPI was used to stain nuclei blue and Alexa-488 fluorophore was used to stain wild type and variant NTCP fluorescent green. Scale bars represent 10 μm and were obtained for WT NTCP, and NTCP variants S241F and R252S. Scale bars are not available for variants P73T, L138P, F234L, R249W, and R252C.

The three band NTCP protein expression pattern is unique to our studies. Previous *in vitro* studies consistently identify two protein bands for NTCP expression. However, these studies typically use HeLa, HepG2, or HepaRG cell lines (Ho et al., 2004; Appelman et al., 2017; Lee et al., 2018). The detected molecular weight of NTCP protein bands in these studies range from 32-39 kDa for the lower band and 45-65 kDa for the upper band. No additional studies assessing NTCP protein expression in transiently transfected HEK293T cells were identified upon literature search.

In human liver samples, NTCP protein migrates as a broad band of approximately 56 kDa, which is reduced to 37 kDa upon deglycosylation (Shneider et al., 1997). In HeLa cells, a band at 50 kDa was deglycosylated to 37 kDa (Ho et al., 2004). NTCP protein bands from HepG2 and HepaRG cells treated with a deglycosylating agent shifted from 45-60 kDa to 32 kDa (Lee et al., 2018). To elucidate whether the three band NTCP protein expression pattern observed in our HEK293T cells was unique to HEK293T cells, we quantified WT and variant NTCP protein expression in HeLa cells. Consistent with literature, we observed a two-band pattern for NTCP in HeLa cells (Fig. 3.7).

To determine whether the three bands in HEK293T cells represent different extents of NTCP glycosylation, a deglycosylation assay was performed in plasma membrane enriched HEK293T samples (Fig. 3.8). Deglycosylation shifted the plasma membrane NTCP protein band from 52 kDa to protein streak migrating around 38 kDa, and to a sharp band at 32 kDa.

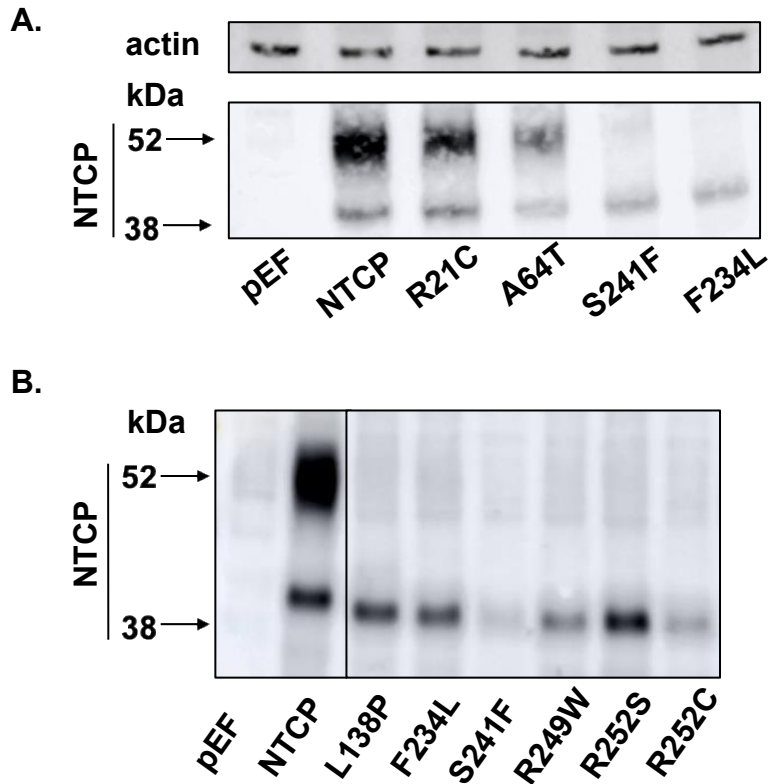


Figure 3.6. Whole-cell protein expression of NTCP in HeLa cells.

A. Lane 1 represents vector only control (pEF), lane 2 is WT NTCP, Lanes 3-4 are NTCP variant proteins R21C and A64T with reduced transport activity, and lanes 5-6 are variants S241F and F234L which show nearly abolished transport activity. Actin was used as the loading control for this blot. B. Lane 1 represents vector only control (pEF), lane 2 is WT NTCP, Lanes 3-8 are NTCP variant proteins L138P, F234L, S241F, R249W, R252S, and R252C which show nearly abolished transport activity. A loading control was not performed for this blot; however, the purpose of this blot is to indicate the two-band pattern of WT NTCP and the one band pattern observed for loss of activity NTCP variants. This is in contrast to the three-band pattern observed for WT NTCP and 2 band pattern observed for loss of activity variants in HEK293T cells (Fig. 3.3 C).

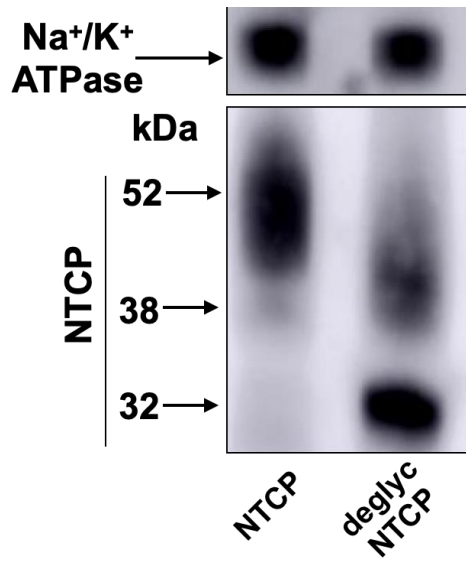


Figure 3.7. Cell surface NTCP protein deglycosylation in HEK293T cells

Lane one (NTCP) represents the control sample, where the NTCP cell-surface fraction was not treated with deglycosylating agent. Lane two (deglyc NTCP) represents an aliquot of this same NTCP plasma membrane fraction treated with the deglycosylating agent, PNGase F.

3.3.3 Transport kinetics

Transport kinetics were assessed for select variants to determine whether variant activity is altered due to differences in affinity of NTCP for the substrate (K_m), rate of transport by NTCP (V_{max}), or both. First, to determine the optimal timepoint to conduct kinetic studies, time course uptake experiments were performed. The objectives of these experiments were to determine timepoints at which uptake is linear, which reflects that transport is not yet saturated. Uptake of taurocholic acid and rosuvastatin occurred rapidly (Fig. 3.8). An incubation period of 2 min was selected for subsequent kinetic studies.

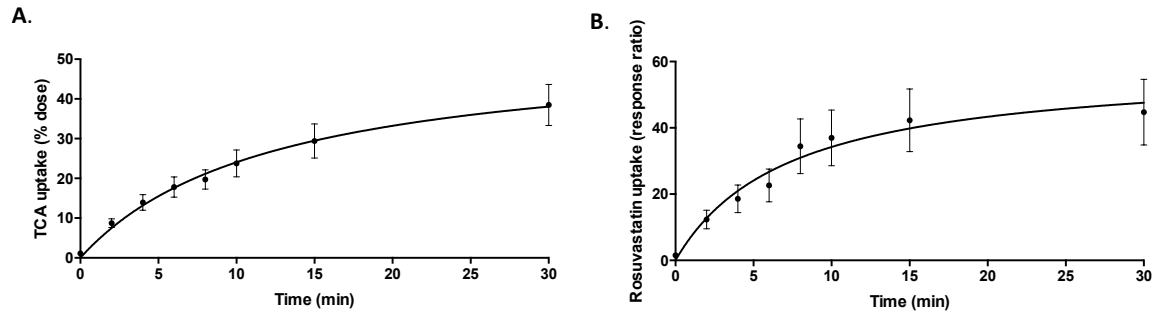


Figure 3.8. Determining linear substrate uptake timepoints for NTCP-mediated transport
 Doses of A. 5 μ M TCA (A) or B. 1 μ M rosuvastatin were administered to HEK293T cells expressing pEF-NTCP-V5. Uptake was quantified at 0, 2, 4, 6, 8, 10, 15, and 30 min. Studies were conducted in duplicate on three experimental days and results are presented as mean \pm SEM.

Three variants were selected for kinetic analysis based on the results from the single time point substrate uptake assays. These include G191R, which displayed substrate specificity (decreased rosuvastatin uptake but TCA uptake similar to WT NTCP), and R21C and K52N, for which reduced uptake of TCA and rosuvastatin were observed.

The V_{\max} for TCA uptake was significantly increased for NTCP G191R relative to WT NTCP ($P < 0.0001$, Fig. 3.9 A). The V_{\max} for TCA uptake was significantly reduced for NTCP R21C ($P < 0.05$, Fig. 3.9 A). For rosuvastatin transport, V_{\max} values for NTCP R21C, NTCP K52N, and NTCP G191R were all significantly decreased compared to WT NTCP (Fig. 3.9 B, $P < 0.0001$). No significant differences were observed between WT and variant NTCP K_m values for TCA or rosuvastatin transport (Fig. 3.9).

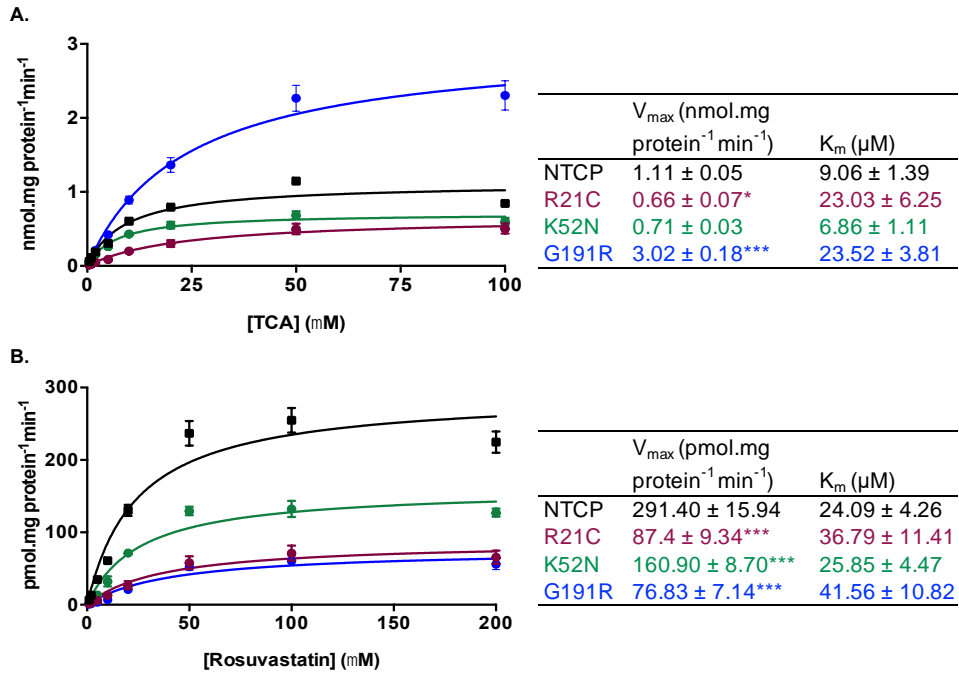


Figure 3.9. Transport kinetics for wild type and variant NTCP.

A. TCA transport kinetics after 2 min incubation with 0.5-100 μ M TCA. B. Rosuvastatin transport kinetics after 2 min incubation with 1-200 μ M rosuvastatin. All experiments were performed in duplicate on 3 experimental days and are expressed as mean \pm SEM. V_{max} and K_m values were determined by Michaelis-Menten nonlinear curve fitting using GraphPad Prism 6. Statistical significance was assessed using one-way ANOVA with Dunnett's multiple comparison tests, * $P < 0.05$, *** $P < 0.0001$.

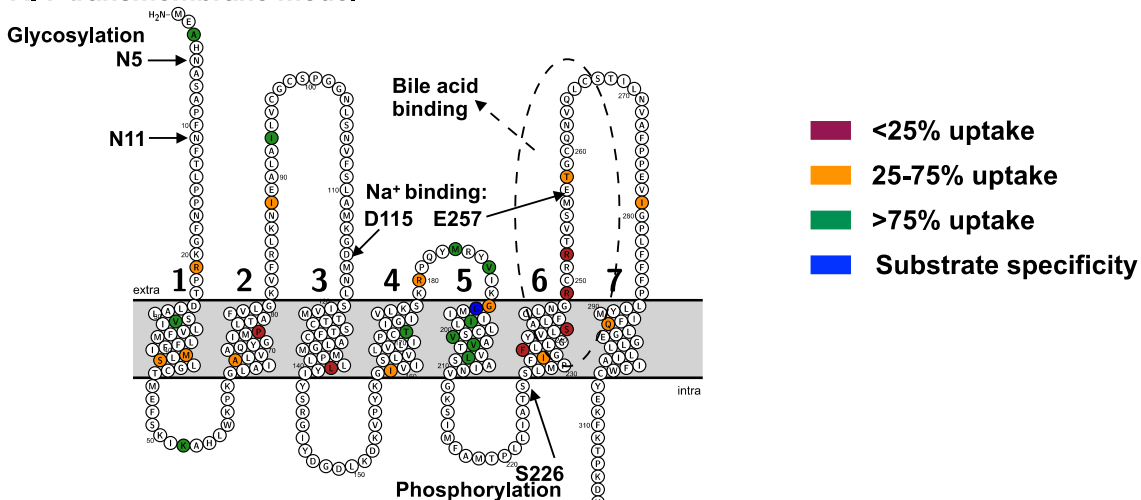
3.3.4 Determining the proximity of NTCP variants to amino acid residues important in NTCP function

To assess whether loss of activity variants may affect amino acid residues with important functions such as sodium- or bile acid-binding, variants were mapped onto predicted two-dimensional and three-dimensional NTCP structures (Figures 3.10-3.12). The number of transmembrane domains for NTCP remains controversial, where some sources predict seven (Mareninova et al., 2005) and others predict nine (Hallen et al., 2002) transmembrane domains. The seven transmembrane model predicts sodium- and bile acid-binding sites are located extracellularly. The nine transmembrane model predicts sodium- and bile acid-binding sites to be located intracellularly or within the membrane domain (Fig. 3.10 & 3.11).

None of the loss of activity variants directly affected amino acid residues involved in post-translational modifications such as phosphorylation or glycosylation (Fig. 3.10 & 3.11). Five of the loss of function and loss of plasma membrane expression variants (F234L, S241F, R249W, R252S, and R252C) were located within the putative bile acid-binding region of residues 221-274 (Mareninova et al., 2005) (Fig. 3.10-3.12). These variants were also in close proximity to one of the putative Na⁺-binding residues, E257 (Fig. 3.10-3.12).

NTCP with TCA uptake activity

A. 7 transmembrane model



B. 9 transmembrane model

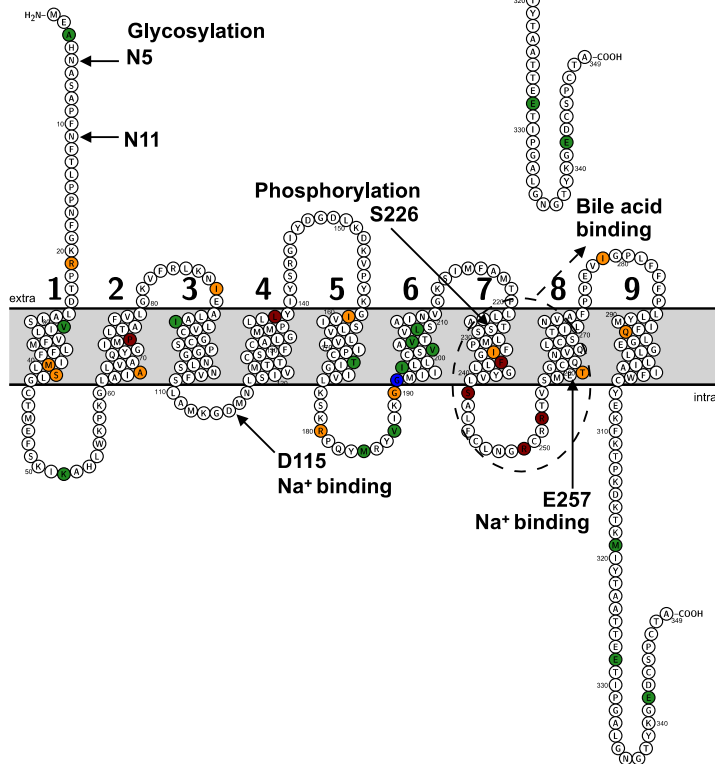
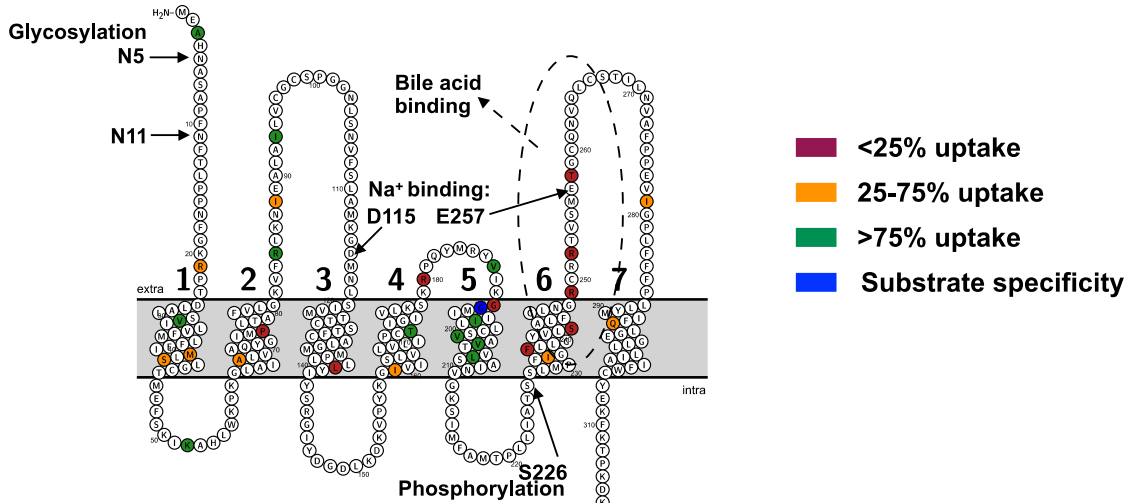


Figure 3.10. Predicted topologies for NTCP with residues for TCA transport activity and binding sites identified.

Residues involved in post-translational modifications and substrate binding are identified. Residues mutated in this study and their corresponding transport activity for taurocholic acid are also identified A. Predicted seven transmembrane model B. Predicted nine transmembrane model.

NTCP with rosuvastatin uptake activity

A. 7 transmembrane model



B. 9 transmembrane model

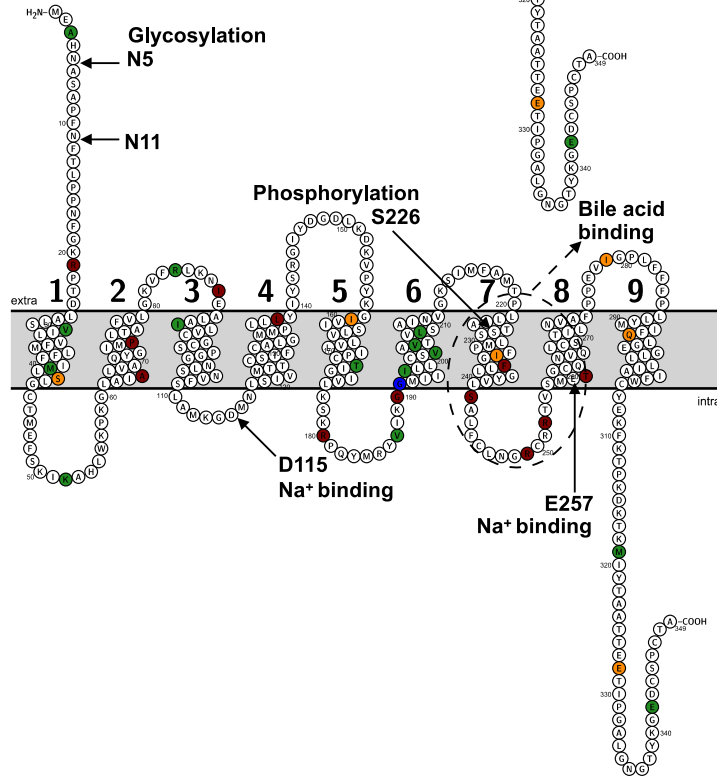


Figure 3.11. Predicted topologies for NTCP with residues for rosuvastatin transport activity and binding sites identified.

Residues involved in post-translational modifications and substrate binding are identified. Residues mutated in this study and their corresponding transport activity for rosuvastatin are also identified A. Predicted seven transmembrane model B. Predicted nine transmembrane model.

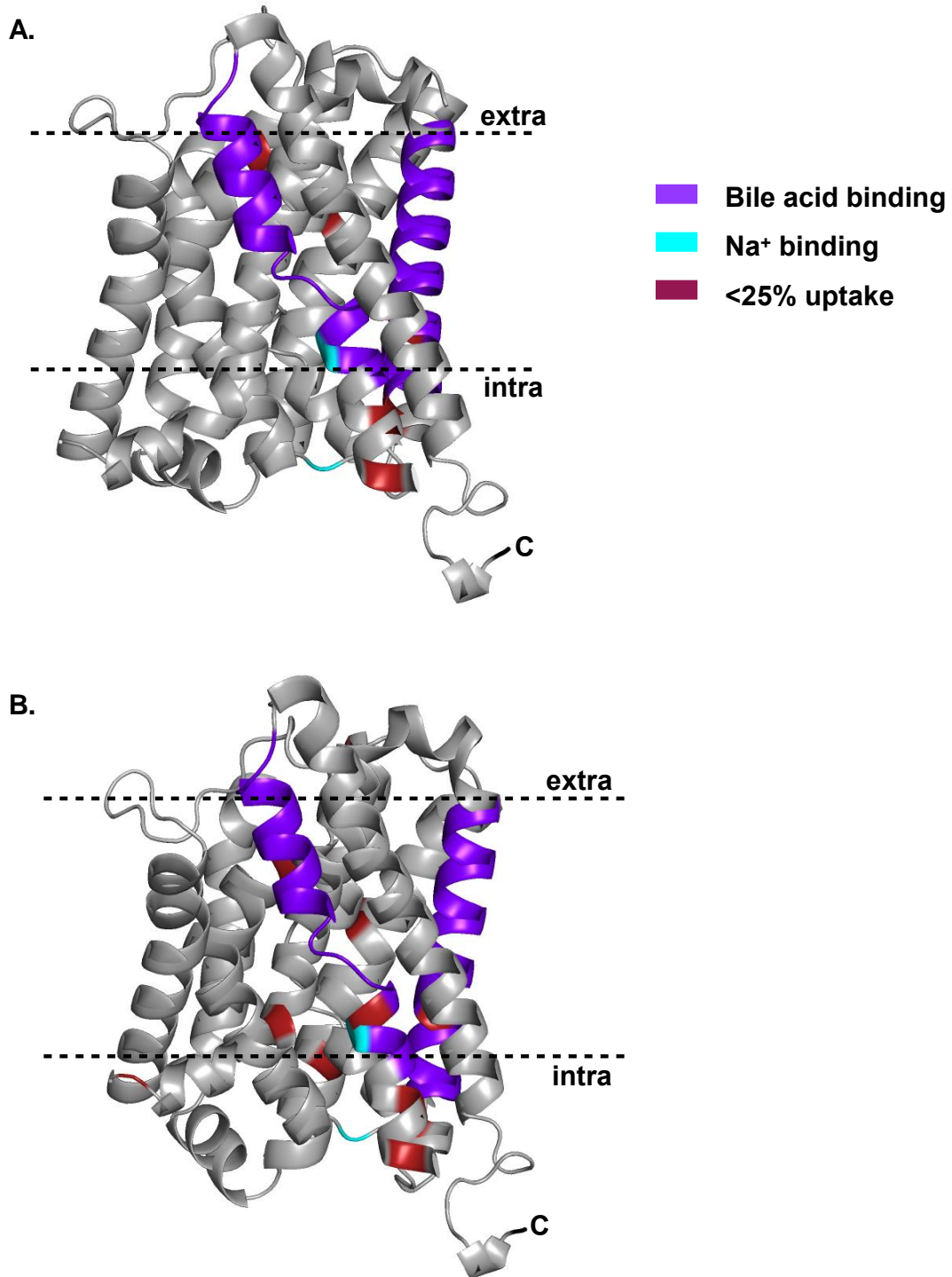


Figure 3.12. Predicted three dimensional structures for NTCP with loss of activity variants identified.

Loss of activity and expression variants for A. taurocholic acid transport and B. rosuvastatin are illustrated in red. Purple-coloured regions depict the predicted bile acid binding site (Mareninova et al., 2005). Cyan regions are residues D115 and E257, critical for TCA uptake by rat NTCP and putative sodium sensors (Zahner et al., 2003).

For NTCP variants A64T and I279T, protein expression similar to WT NTCP was detected, however transport of both TCA and rosuvastatin were significantly decreased. To determine whether these variants may be within important substrate binding regions of NTCP, A64T and I279T were mapped onto the predicted 3D structure of NTCP. Both A64T and I279T are in close proximity to residues important for sodium- and bile acid-binding (Figure 3.13).

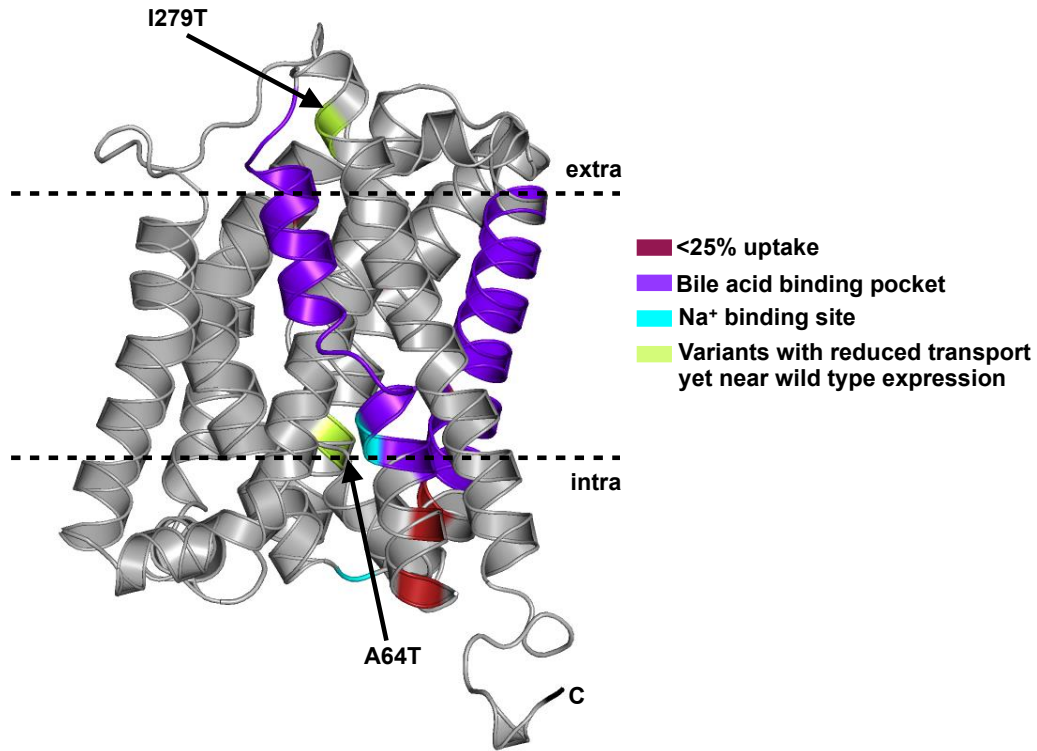


Figure 3.13. Predicted 3D structure of NTCP with identified binding sites and loss of activity but not expression variants I279T and A64T.

Purple-coloured regions depict the predicted bile acid-binding site (Mareninova et al., 2005). Cyan regions are residues D115 and E257, critical for TCA uptake by rat NTCP and putative sodium sensors (Zahner et al., 2003). Red regions depict the seven variants from our study with nearly undetectable transport activity and undetectable levels of protein expression at the plasma membrane. Light green regions depict two NTCP variants, A64T and I279T, which show normal protein expression yet significantly reduced transport of both TCA and rosuvastatin.

To determine whether our loss of activity and plasma membrane expression variants were located within amino acid residues that are evolutionarily conserved, the human NTCP amino acid sequence was aligned with sequences from rat and mouse NTCP orthologs, as well as the human paralog ASBT. Six of the seven loss of activity and cell surface expression variants (P73T, L138P, S235L, S241F, R252S, and R252C) are located at residues conserved between a minimum of three of the four aligned sequences. The only loss of activity and expression variant that is located at an amino acid residue not conserved between species orthologs and protein paralogs is R249W.

```

NTCP 1 -----MEAHNASAPFNFTLPNFGKRPTDLALSVLVFM LFFIMLSLGCTM 46
rNtcp 1 -----MEVHNVSAPFNFS LPPGFGHRATDKALSII LVLMLLLIMLSLGCTM 46
mNtcp 1 -----MEAHNVSAPFNFS LPPGFGHRATDTALSVLVVM LLLIMLSLGCTM 46
ASBT 1 MNDPNSCVDNATVCSGASC VVPE SNFNFI LSVVLS TVLT ILLALVMFSMGCNV 53

NTCP 47 EFSK IKAHLWKP KGLA IALVAQY GIMP LTA FVLGKV FR LKNI EALAI LVC GCS 99
rNtcp 47 EFSK IKAHLWKP KGV IVALVAQ FGI MP LAA FLLGKI FHLSNI EALAI LIC GCS 99
mNtcp 47 EFSK IKAHFWKP KGV IIAIVAQ YGI MP LSA FLLGKV FH LTSIEALAI LIC GCS 99
ASBT 54 EIKK FLGH IKR PWG ICVGF LCF GIM PLTGFI LSVAF DILPLQAVV VLIIGCC 106

NTCP 100 PGGNLSNVFSLAMK GDMNLSIVMTTCS TFCALGMMP LLLYIYSRGIYDGD LKD 152
rNtcp 100 PGGNLSNLF TLAMK GDMNLSIVMTTCS SFSALGMMP LLLYVYSKGIYDGD LKD 152
mNtcp 100 PGGNLSNLF TLAMK GDMNLSIVMTTCS SFTALGMMP LLLYIYSKGIYDGD LKD 152
ASBT 107 PGGTASN I LAYWVD GDM DLSVSM T TCS TLLALGMMP LCLLIYTKMWV DS-GSI 158

NTCP 153 KVPYKGI V I S L V L V L I P C T I G I V L K S K R P Q Y M R Y V I K G G M I I I L L C S V A V T V L 205
rNtcp 153 KVPYKGI M I S L V I V L I P C T I G I V L K S K R P H Y V P Y I L K G G M I I T F L L S V A V T A L 205
mNtcp 153 KVPYKGI M L S L V M V L I P C A I G I F L K S K R P H Y V P Y V L K A G M I I T F S L S V A V T V L 205
ASBT 159 V I P Y D N I G T S L V S L V V P V S I G M F V N H K W P Q K A K I I L K I G S I A G A I L I V L I A V V 211

NTCP 206 SA I NVGKS I M F A M T P L L I A T S S L M P F I G F L L G Y V L S A L F C L N G R C R R T V S M E T 258
rNtcp 206 S V I NVGNS I M F V M T P H L L A T S S L M P F S G F L M G Y I L S A L F Q L N P S C R R T I S M E T 258
mNtcp 206 S V I NVGNS I M F V M T P H L L A T S S L M P F T G F L M G Y I L S A L F R L N P S C R R T I S M E T 258
ASBT 212 G G I L - - Y Q S A W I I A P K L W I G T I F P V A G Y S L G F L L A R I A G L P W Y R C R T V A F E T 262

NTCP 259 G C O N V Q L C S T I L N V A F P P E V I G P L F F F P L L Y M I F Q L A E G L L I I A I F W C Y E K F K 311
rNtcp 259 G F Q N I Q L C S T I L N V T F P P E V I G P L F F F P L L Y M I F Q L A E G L L I I I I F R C Y E K I K 311
mNtcp 259 G F Q N V Q L C S T I L N V T F P P E V I G P L F F F P L L Y M I F Q L A E G L L F I I I F R C Y L K I K 311
ASBT 263 G M Q N T Q L C S T I V Q L S F T P E E L N V V F T F P L I Y S I F Q L A F A A I F L G F Y V A Y K K C H 315

NTCP 312 T P K D K T K M I Y T A A T T E E T I P G A L G N G T Y K G E D C S P C T A - - - - - 349
rNtcp 312 P P K D Q T K I T Y K A A A T E D A T P A A L E K G T H N G N I P P L Q P G P S P N G L N S G Q M A N 362
mNtcp 312 P Q K D Q T K I T Y K A A A T E D A T P A A L E K G T H N G N N P P T Q P G L S P N G L N S G Q M A N 362
ASBT 316 G K N K A E I P E S K E N G T E P E S S F Y K A N G G F Q P D E K - - - - - 348

```

Figure 3.14. Sequence alignment for human, mouse, and rat NTCP and human ASBT
Sequence alignment of NTCP (*SLC10A1*, UniProt: Q14973) to rat NTCP (rNtcp, P26435), mouse NTCP (mNtcp, O08705), and human ASBT (*SLC10A2*, Q12908). Residues in cyan denote putative sodium-binding sites, D114 and E257 (Zahner et al., 2003), which are conserved between all species. Light blue and darker blue-coloured residues share 75% and 100% sequence identity, respectively. The NTCP phosphorylation site, S226 (Anwer et al., 2005), is coloured pink and is conserved by NTCP, rNtcp, and mNtcp. The seven variants identified in this study to have loss of activity and loss of plasma membrane expression are coloured red: P73T, L138P, F234L, S241F, R249W, R252S, R252C. The predicted bile acid-binding region spanning NTCP residues 221-274 (Mareninova et al., 2005) is denoted by a purple box.

3.3.5 Predictive performance of algorithms

Next, we compared *in silico* predicted function from a battery of seven *in silico* tools to *in vitro* transport activities determined experimentally (Fig. 13.15-13.17). Performance of *in silico* tools to predict reduced NTCP-mediated transport of taurocholic acid and rosuvastatin was evaluated by determining sensitivities, specificities, and area under the receiver operating characteristic curves (AUC_{ROC}) (Table 3.5).

In silico tools SIFT and Mutation Assessor use evolutionary conservation to generate predictions of genetic variation on protein function. PolyPhen-2 uses evolutionary conservation and physicochemical properties of reference versus mutant amino acids to predict effects on protein function. Among these three algorithms, SIFT and Mutation Assessor predicted deleterious NTCP function for TCA uptake with 100% sensitivity, which reflects the true positive rate (Fig. 13.15 & Table 3.5). Sensitivity of PolyPhen-2 to predict TCA transport by variant NTCP was slightly lower at 86%. True negative rates, as reflected by specificities, ranged from 46-50%. Overall performances to predict TCA uptake by variant NTCP as reflected by AUC_{ROC} were 0.85, 0.69, and 0.87 for SIFT, PolyPhen-2, and Mutation Assessor, respectively. For each of these three algorithms, performance to predict decreased rosuvastatin transport by variant NTCP was reduced relative to performance of TCA transport by variant NTCP. AUC_{ROC} values reflective of rosuvastatin transport by variant NTCP were 0.72, 0.76, and 0.80 for SIFT, PolyPhen-2, and Mutation Assessor, respectively, and sensitivities

and specificities ranged from 86-93% and 52-57%, respectively (Fig. 13.5 & Table 3.5).

CADD, REVEL, and MetaLR are considered ensemble predictions methods; they generate their predictions by aggregating predictive outputs from various *in silico* tools. AUC_{ROC} values for CADD, REVEL, and MetaLR to predict deleterious TCA uptake by NTCP were 0.78, 0.93, and 0.97, respectively (Fig. 3.16 & Table 3.5). CADD displayed 100% sensitivity and 50% specificity for predicting reduced TCA transport (Fig. 3.16 & Table 3.5). Sensitivity and specificity of REVEL to predict decreased TCA transport were 71% and 82%, respectively. Sensitivity and specificity to predict decreased TCA transport were 43% and 96%, respectively (Fig. 3.16 & Table 3.5).

With regard to rosuvastatin transport by variant NTCP, CADD AUC_{ROC} was 0.79, which was similar to predictive performance of CADD for TCA transport. Sensitivity and specificity were 86% and 57%, respectively (Fig. 3.16 & Table 3.5). Performances of REVEL and MetaLR to predict rosuvastatin transport by variant NTCP were 0.84, which were lower than their AUC_{ROC} scores for TCA transport. Sensitivity and specificity of REVEL were 57% and 90%, and sensitivity and specificity were 29% and 100% for MetaLR (Fig. 3.16 & Table 3.5).

Performances of the ADME-optimized algorithm to predict TCA and rosuvastatin uptake by variant NTCP were 0.87 and 0.78, respectively. Sensitivities were 100% and 79% and specificities were 57% and 62% to predict TCA and rosuvastatin uptake, respectively (Fig. 13.17 & Table 3.5).

Overall, no algorithm was able to predict taurocholic acid and rosuvastatin uptake with 100% accuracy (Fig. 3.15-3.17 and Table 3.5). Ranked performance, for predicting variant NTCP uptake of TCA based on AUC_{ROC} was as follows: MetaLR > REVEL > Mutation Assessor > ADME-optimized > SIFT > CADD > PolyPhen-2. For predicting rosuvastatin uptake, ranked performance based on AUC_{ROC} was as follows: MetaLR = REVEL > Mutation Assessor > CADD > ADME-optimized > PolyPhen-2 > SIFT. Sensitivities (true positive rates) to predict TCA uptake were 100% for SIFT, Mutation Assessor, CADD, and ADME, and specificities (false positive rates) for these algorithms ranged from 46-59%. No algorithm predicted rosuvastatin uptake with 100% sensitivity.

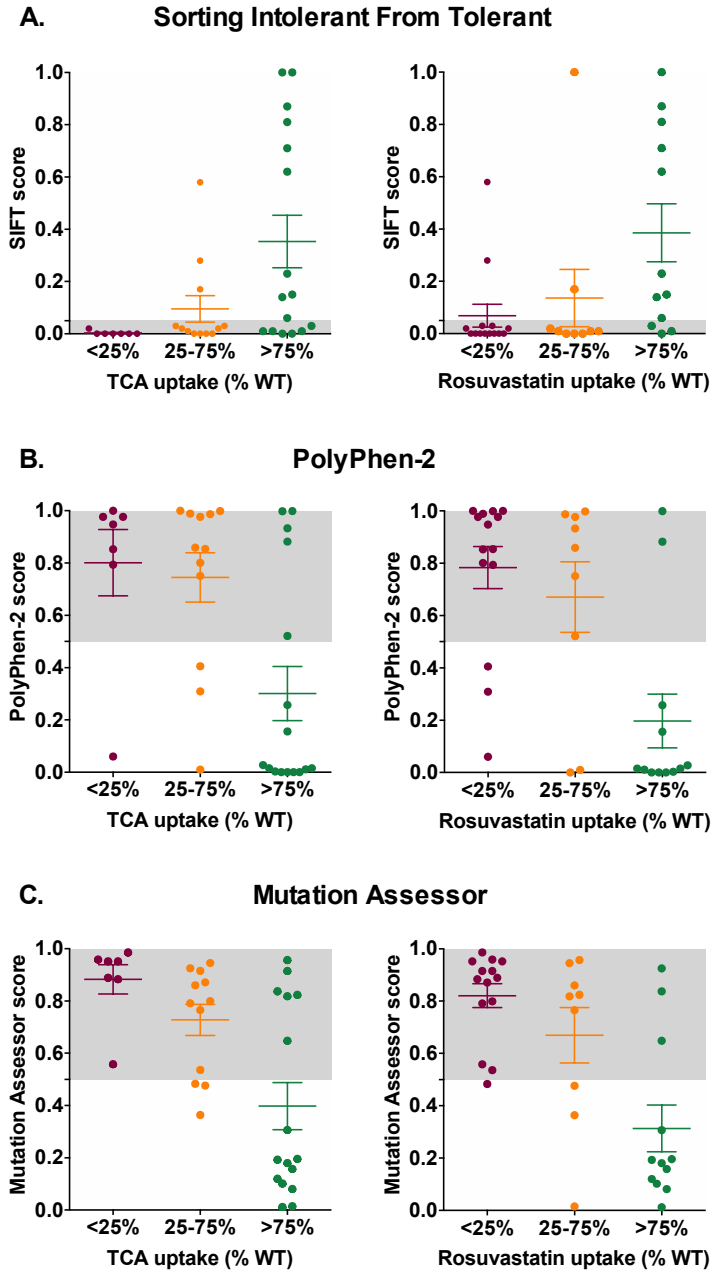


Figure 3.15. Performance of *in silico* tools optimized for evolutionary conservation and amino acid properties to predict *in vitro* NTCP variant transport activity

Variants were grouped by uptake activity *in vitro*, depicted as mean percentages of wild type (WT) uptake along the x-axes. Uptake $<25\%$ is depicted in red, 25-75% in orange, and $>75\%$ in green. *In silico* scores are plotted on the y-axes. True positives (accurate predictions) are represented by red circles within the gray shaded areas. True negatives (accurate predictions) are represented by green and orange circles that fall outside the gray area. False negatives (inaccurate predictions) are depicted when red circles fall outside the gray area. False positives (inaccurate predictions) are illustrated when green and orange circles fall within the gray area. Threshold for deleterious scores by algorithm are A. SIFT (sorting intolerant from tolerant): < 0.05 B. PolyPhen-2: > 0.5 , and C. Mutation Assessor: > 0.5 . Mean prediction score per group is indicated \pm SEM.

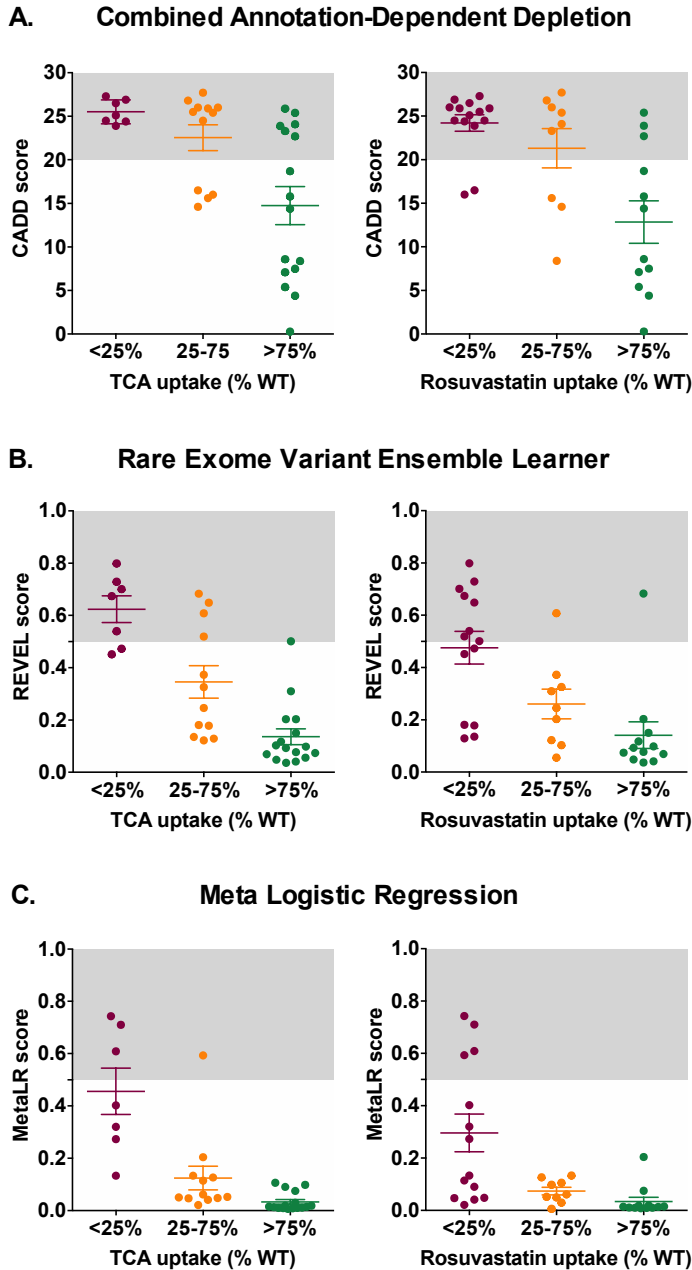


Figure 3.16. Performance of *in silico* tools optimized using outputs from multiple *in silico* scoring tools to predict *in vitro* NTCP variant transport activity

Variants were grouped by uptake activity *in vitro*, depicted as mean percentages of wild type (WT) uptake along the x-axes. Uptake <25% is depicted in red, 25-75% in orange, and >75% in green. *In silico* scores are plotted on the y-axes. True positives (accurate predictions) are represented by red circles within the gray shaded areas. True negatives (accurate predictions) are represented by green and orange circles that fall outside of gray area. False negatives (inaccurate predictions) are depicted when red circles fall outside the gray area. False positives (inaccurate predictions) are illustrated when green and orange circles fall within the gray area. Threshold for deleterious scores by algorithm are A. Combined Annotation-Dependent Depletion (CADD): > 20, B. Rare Exome Variant Ensemble Learner (REVEL): > 0.5, C. Meta Logistic Regression (MetaLR): > 0.5. Mean prediction score per group is indicated \pm SEM.

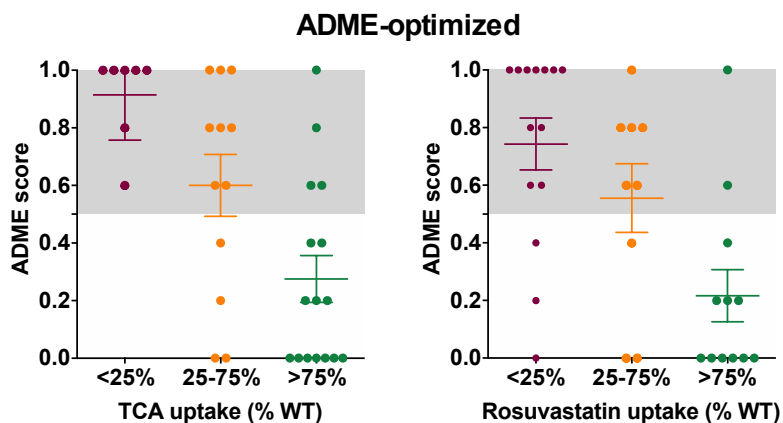


Figure 3.17. Performance of the ADME-optimised *in silico* tool to predict *in vitro* NTCP variant transport activity

Variants were grouped by uptake activity *in vitro*, depicted as mean percentages of wild type (WT) uptake along the x-axes. Uptake <25% is depicted in red, 25-75% in orange, and >75% in green. *In silico* scores are plotted on the y-axes. True positives (accurate predictions) are represented by red circles within the gray shaded areas. True negatives (accurate predictions) are represented by green and orange circles that fall outside of gray area. False negatives (inaccurate predictions) are depicted when red circles fall outside the gray area. False positives (inaccurate predictions) are illustrated when green and orange circles fall within the gray area. Scores were generated from the ADME-optimized prediction framework (Zhou et al., 2019). Deleterious predictions: scores > 0.5. Mean prediction score per group is indicated \pm SEM.

Table 3.5. Performance of *in silico* tools to predict taurocholic acid and rosuvastatin uptake.

Algorithm	Category	Threshold	TCA uptake			Rosuvastatin uptake		
			Predictive performance (AUC _{ROC})	Sensitivity (%)	Specificity (%)	Predictive performance (AUC _{ROC})	Sensitivity (%)	Specificity (%)
SIFT	Functionality	<0.05	0.85	100	46	0.72	86	52
PolyPhen-2	prediction	>0.5	0.69	86	50	0.76	79	57
Mutation Assessor		>0.5	0.87	100	46	0.80	93	57
CADD	Aggregate	>20	0.78	100	50	0.79	86	57
REVEL	scores	>0.5	0.93	71	82	0.84	57	90
MetaLR		>0.5	0.97	43	96	0.84	29	100
ADME	PGx optimized	>0.5	0.87	100	57	0.78	79	62

Threshold values are expressed as arbitrary units and are indicative of scores that predict a variant to be deleterious by each algorithm. Area under the receiver operating characteristic curve (AUC_{ROC}) values were calculated using GraphPad Prism 6. Sensitivity and specificity were calculated using the following equations:

$$Sensitivity = \frac{\sum TP}{\sum TP + \sum FN} \quad Specificity = \frac{\sum TN}{\sum TN + \sum FP}$$

3.4 Discussion

NTCP plays a central role in bile acid and rosuvastatin transport, as well as HBV and HDV infection; thus, genetic variation in *SLC10A1* may contribute to disease and adverse drug events (Ho et al., 2004; Yan et al., 2012). However, there is a paucity of information regarding effects of human *SLC10A1* genetic variation on NTCP function. Furthermore, next generation sequencing has revealed a vast extent of rare genetic variants of unknown clinical significance within the human genome. Prioritization of rare variants for functional study based on the likelihood of altered protein function is therefore an important part of streamlining their characterization. Our study was designed to determine effects of rare, missense genetic variation in *SLC10A1* on NTCP transport activity and protein expression.

Of thirty-five previously uncharacterized NTCP variants, we identified seven with nearly absent transport of the endogenous and drug substrates taurocholic acid and rosuvastatin. These seven genetic variants produced the following amino acid substitutions: P73T, L138P, F234L, S241F, R249W, R252S, R252C. Although variant NTCP protein was detected in whole-cell lysates, their expression was virtually undetectable at the plasma membrane, which likely explains the loss of transport of both substrates. Amino acid sequence alignments reveal that six of these seven residues are located in highly conserved regions, indicating their relative importance in NTCP protein function. Two variants, A3T and E342K showed modest but significant increases in taurocholic acid. Nearly 2-fold higher rosuvastatin uptake was observed for the

T171I variant. Interestingly, a substrate-specific effect was observed for the G191R variant; this variation did not affect TCA uptake, however rosuvastatin uptake was markedly reduced.

In silico tools were moderate to good predictors of *in vitro* taurocholic acid transport. Four of the seven employed tools accurately predicted deleterious activity for all of the seven of the loss of activity and loss of plasma membrane expression variants. The ADME-optimized *in silico* tool was no better than other tools for predicting uptake of rosuvastatin by variant forms of NTCP. These results suggest that *in silico* predictions are not robust enough to replace functional assessment of *SLC10A1* genetic variation *in vitro*. Although the ADME-optimized tool was developed using data for a variety of pharmacogenes, including *SLC10A2*, further optimization for predicted function to transport a specific class of drug by structure-function and drug binding studies may improve predictions for substrate-specific functional effects.

Although statistically significant differences in activity were found for 19 variants, intrinsic variability typical of heterologous expression systems may account for moderate changes in transport activity. Therefore, the most conclusive findings of our study centralize around the variants that displayed < 25% wild type NTCP activity.

Genetic variation in *SLC10A1* is dependent on ethnicity (Ho et al., 2004; Pan et al., 2011). The most common missense variant, NTCP S267F, is present in 5.0-7.5% of East Asian populations, with a global MAF <1% (Ho et al., 2004; Pan et al., 2011; Cunningham et al., 2019). This variant was reported to be protective

against HBV and HDV infection and showed nearly abolished TCA uptake, however transport of rosuvastatin was markedly increased (Ho et al., 2004; Ho et al., 2006; Hu et al., 2016; An et al., 2018; Chuaypen et al., 2019).

Adding to the previous observation that the I279T variant was normally expressed *in vitro* yet displayed reduced bile acid transport (Ho et al., 2004), we now show significantly reduced rosuvastatin transport by this variant. In 2011, Pan et al. reported decreased uptake of TCA and rosuvastatin, as well as ethnicity-dependent allele frequencies for NTCP A64T (Pan et al., 2011). Findings from our study add that both whole-cell and plasma membrane expression of this variant are comparable to expression of WT NTCP. We therefore speculate that decreased transport may be the result of decreased substrate affinity or rate of translocation.

NTCP is glycosylated at residues N5 and N11, and plasma membrane expression relies on glycosylation of at least one of these sites (Hagenbuch, 1997; Appelman et al., 2017). *In vitro* studies noted that the NTCP variant R252H displayed insufficient glycosylation and lack of expression at the plasma membrane (Vaz et al., 2015). Our results depict a pattern of three NTCP protein bands in transiently transfected HEK293T cells, whereas our study and others report a two band NTCP protein expression pattern in other cell lines. Our results suggest that the lowest molecular weight protein band in HEK293T cells represents fully deglycosylated NTCP protein. We therefore speculate that the process of glycosylation may be differ in HEK293T cells relative to HeLa or

HepG2 cells. This is supported by findings that cellular repertoires can produce different glycosylation patterns (Goh and Ng, 2018).

Studies suggest the highest molecular weight NTCP protein band represents fully mature glycosylated protein (Ananthanarayanan et al., 1994; Ho et al., 2004; Appelman et al., 2017). This mature glycosylated form of protein is absent for the seven variants that also display reduced transport of both substrates. Structural changes induced by the variations may interfere with NTCP glycosylation, leading to intrinsic instability and rapid degradation by proteases. Alternatively, these variations may alter plasma membrane trafficking of NTCP protein. In addition to glycosylation, NTCP undergoes a variety of post-translational modifications that affect plasma membrane expression and substrate transport, including phosphorylation and S-nitrosylation (Anwer et al., 2005; Schonhoff et al., 2011; Ramasamy et al., 2013; Anwer and Stieger, 2014). Though none of the genetic variants in our study directly affect residues important in post-translational modifications, it is possible these variations induce structural changes that interfere with modifications of these sites. Further studies will be necessary to determine mechanisms altering plasma membrane expression of these variants.

Biochemical studies predict NTCP to be a seven- or nine-transmembrane domain protein. The seven transmembrane structure predicts extracellular Na⁺- and bile acid-binding sites and an intracellular phosphorylation site, whereas the nine-transmembrane model predicts intracellular localization of Na⁺- and bile acid-binding sites (Hagenbuch et al., 1991; Hallen et al., 2002; Mareninova et al.,

2005). These notions suggest that the seven transmembrane model is likely a more accurate depiction of the membrane topology of NTCP. Interestingly, a region recognized as crucial for bile acid-binding and transport spans amino acids 221-274 of NTCP (Mareninova et al., 2005), the same region where five of the seven loss of function variants identified by our study reside. Further, mutagenesis studies show that residues S267 and C266 are required for bile acid transport, and E257 is necessary for optimal sodium-binding (Saeki et al., 2002; Zahner et al., 2003; Ho et al., 2004). When mapped onto the predicted 3D structure of NTCP another putative sodium sensor, D115, is in close proximity to the bile acid-binding region. Taken together, many of the loss of activity and expression variants are located within a region integral to the physiological function of NTCP, providing further support that these mutations are likely to play a functional role.

Though we were able to successfully characterize 35 missense variants, this is only a fraction of the 279 missense *SLC10A1* variants that have been reported to date in the Genome Aggregate Database (<https://gnomad.broadinstitute.org>, accessed November 2019). One remaining challenge in functional characterization of variants is that *in vitro* testing remains time and resource consuming. High-throughput assays present an attractive solution to the traditional low-throughput approach. These methodologies are conducted by introducing a pooled library of genetic variants into cultured mammalian cells, with each cell expressing a single genetic variation. Subsequently, phenotypic assessment is carried out using protein abundance, stability, or toxicity assays

(Starita et al., 2017; Weile and Roth, 2018). However, high-throughput characterization remains technically challenging. Furthermore, these methodologies are often inadequate to study protein localization and post-translational modifications, which are highly relevant to the function of many transporter proteins (Fowler and Fields, 2014; Starita et al., 2015; Ipe et al., 2017). Accordingly, robust *in silico* algorithms with high predictive power are becoming increasingly important to identify potential loss of activity rare variants. One remaining limitation to this approach is that, for the most part, these algorithms have been optimized to reflect effects related to physiological function. Few *in silico* tools have been optimized with respect to drug transport or metabolism, and predictions become even more complicated when variations display substrate-dependent effects (Gulilat et al., 2019; Zhou et al., 2019).

Functionality predictions by algorithms chosen in this study display some concordance. SIFT, Mutation Assessor, CADD, and ADME were 100% sensitive at predicting TCA uptake. These algorithms generated deleterious predictions for all seven loss of activity and loss of expression variants. Furthermore, four of these seven variants were predicted deleterious by all seven algorithms. When comparing prediction sensitivities for TCA uptake to prediction sensitivities for rosuvastatin uptake, each algorithm predicted transport of the endogenous substrate, TCA, with a higher degree of sensitivity. These data emphasize complexities of applying *in silico* algorithms to predict pharmacogenetic effects, as results can vary depending on the substrate.

Results from the current study show that algorithms that portrayed high sensitivity had low specificity, and vice versa. This is exemplified by MetaLR which showed 100% specificity to predict TCA and rosuvastatin uptake, yet sensitivities were limited to 50% and 29%, respectively. To optimize an algorithm, it is important to consider the threshold used to define a deleterious variant (Berrar and Flach, 2012). In our study, variants were defined as deleterious with a threshold of < 25% wild type NTCP activity, which is lower than the < 50% activity threshold used for the ADME-optimized algorithm (Zhou et al., 2019). Using this < 50% activity threshold, specificity of ADME to predict TCA uptake increases from 57% to 66%, and sensitivity and specificity to predict rosuvastatin uptake increase from 79% to 83% and 62% to 76%, respectively. This highlights the importance of selecting the threshold that classifies a variant as deleterious. The ideal threshold will give the best compromise between sensitivity and specificity (Berrar and Flach, 2012).

In conclusion, we identified seven previously uncharacterized, rare, missense *SLC10A1* variants with reduced transport activity for NTCP substrates taurocholic acid and rosuvastatin, likely subsequent to their inability to traffic or be retained at the plasma membrane. We also identified one variant that maintained taurocholic acid uptake but for which rosuvastatin transport was nearly absent. The *in vivo* relevance of these genetic variations remains unclear, however we expect that homozygous carriers of these loss of activity variants would display hypercholanemia as observed for variant carriers of NTCP S267F (Vaz et al., 2015; Deng et al., 2016; Liu et al., 2017; Qiu et al., 2017). We reveal

that currently available *in silico* algorithms do not adequately predict variant NTCP activity, thus *in vitro* functional assessment remains an important first step in determining which variants may be of clinical importance. These findings suggest that further optimization of *in silico* prediction tools is required to enhance their applicability for classifying rare variants as deleterious or tolerated.

3.5 References

- Adzhubei I, Jordan DM, and Sunyaev SR (2013) Predicting functional effect of human missense mutations using PolyPhen-2. *Curr Protoc Hum Genet* **Chapter 7:Unit7** 20.
- An P, Zeng Z, and Winkler CA (2018) The Loss-of-Function S267F Variant in HBV Receptor NTCP Reduces Human Risk for HBV Infection and Disease Progression. *J Infect Dis* **218**:1404-1410.
- Ananthanarayanan M, Ng OC, Boyer JL, and Suchy FJ (1994) Characterization of cloned rat liver Na(+)-bile acid cotransporter using peptide and fusion protein antibodies. *Am J Physiol* **267**:G637-643.
- Anwer MS, Gillin H, Mukhopadhyay S, Balasubramaniyan N, Suchy FJ, and Ananthanarayanan M (2005) Dephosphorylation of Ser-226 facilitates plasma membrane retention of Ntcp. *J Biol Chem* **280**:33687-33692.
- Anwer MS and Stieger B (2014) Sodium-dependent bile salt transporters of the SLC10A transporter family: more than solute transporters. *Pflugers Arch* **466**:77-89.
- Appelman MD, Chakraborty A, Protzer U, McKeating JA, and van de Graaf SF (2017) N-Glycosylation of the Na⁺-Taurocholate Cotransporting Polypeptide (NTCP) Determines Its Trafficking and Stability and Is Required for Hepatitis B Virus Infection. *PLoS One* **12**:e0170419.
- Berrar D and Flach P (2012) Caveats and pitfalls of ROC analysis in clinical microarray research (and how to avoid them). *Brief Bioinform* **13**:83-97.
- Chiang JY (2013) Bile acid metabolism and signaling. *Compr Physiol* **3**:1191-1212.
- Chuaypen N, Tuyapala N, Pinjaroen N, Payungporn S, and Tangkijvanich P (2019) Association of NTCP polymorphisms with clinical outcome of hepatitis B infection in Thai individuals. *BMC Med Genet* **20**:87.
- Cunningham F, Achuthan P, Akanni W, Allen J, Amode MR, Armean IM, Bennett R, Bhai J, Billis K, Boddu S, Cummins C, Davidson C, Dodiya KJ, Gall A, Giron CG, Gil L, Grego T, Haggerty L, Haskell E, Hourlier T, Izuogu OG, Janacek SH, Juettemann T, Kay M, Laird MR, Lavidas I, Liu Z, Loveland JE, Marugan JC, Maurel T, McMahon AC, Moore B, Morales J, Mudge JM, Nuhn M, Ogeh D, Parker A, Parton A, Patricio M, Abdul Salam AI, Schmitt BM, Schuilenburg H, Sheppard D, Sparrow H, Stapleton E, Szuba M, Taylor K, Threadgold G, Thormann A, Vullo A, Walts B, Winterbottom A, Zadissa A, Chakiachvili M, Frankish A, Hunt SE, Kostadima M,

- Langridge N, Martin FJ, Muffato M, Perry E, Ruffier M, Staines DM, Trevanion SJ, Aken BL, Yates AD, Zerbino DR, and Flicek P (2019) Ensembl 2019. *Nucleic Acids Res* **47**:D745-D751.
- Dawson PA, Lan T, and Rao A (2009) Bile acid transporters. *J Lipid Res* **50**:2340-2357.
- DeGorter MK, Tirona RG, Schwarz UI, Choi YH, Dresser GK, Suskin N, Myers K, Zou G, Iwuchukwu O, Wei WQ, Wilke RA, Hegele RA, and Kim RB (2013) Clinical and pharmacogenetic predictors of circulating atorvastatin and rosuvastatin concentrations in routine clinical care. *Circ Cardiovasc Genet* **6**:400-408.
- Deng M, Mao M, Guo L, Chen FP, Wen WR, and Song YZ (2016) Clinical and molecular study of a pediatric patient with sodium taurocholate cotransporting polypeptide deficiency. *Exp Ther Med* **12**:3294-3300.
- Dong C, Wei P, Jian X, Gibbs R, Boerwinkle E, Wang K, and Liu X (2015) Comparison and integration of deleteriousness prediction methods for nonsynonymous SNVs in whole exome sequencing studies. *Hum Mol Genet* **24**:2125-2137.
- Fowler DM and Fields S (2014) Deep mutational scanning: a new style of protein science. *Nature Methods* **11**:801-807.
- Fujikura K, Ingelman-Sundberg M, and Lauschke VM (2015) Genetic variation in the human cytochrome P450 supergene family. *Pharmacogenet Genomics* **25**:584-594.
- Goh JB and Ng SK (2018) Impact of host cell line choice on glycan profile. *Crit Rev Biotechnol* **38**:851-867.
- Gulilat M, Lamb T, Teft WA, Wang J, Dron JS, Robinson JF, Tirona RG, Hegele RA, Kim RB, and Schwarz UI (2019) Targeted next generation sequencing as a tool for precision medicine. *BMC Med Genomics* **12**:81.
- Hagenbuch B (1997) Molecular properties of hepatic uptake systems for bile acids and organic anions. *J Membr Biol* **160**:1-8.
- Hagenbuch B and Meier PJ (1994) Molecular cloning, chromosomal localization, and functional characterization of a human liver Na⁺/bile acid cotransporter. *J Clin Invest* **93**:1326-1331.
- Hagenbuch B, Stieger B, Foguet M, Lubbert H, and Meier PJ (1991) Functional expression cloning and characterization of the hepatocyte Na⁺/bile acid cotransport system. *Proc Natl Acad Sci U S A* **88**:10629-10633.

- Hallen S, Mareninova O, Branden M, and Sachs G (2002) Organization of the membrane domain of the human liver sodium/bile acid cotransporter. *Biochemistry* **41**:7253-7266.
- Ho RH, Leake BF, Roberts RL, Lee W, and Kim RB (2004) Ethnicity-dependent polymorphism in Na⁺-taurocholate cotransporting polypeptide (SLC10A1) reveals a domain critical for bile acid substrate recognition. *J Biol Chem* **279**:7213-7222.
- Ho RH, Tirona RG, Leake BF, Glaeser H, Lee W, Lemke CJ, Wang Y, and Kim RB (2006) Drug and bile acid transporters in rosuvastatin hepatic uptake: function, expression, and pharmacogenetics. *Gastroenterology* **130**:1793-1806.
- Hofmann AF (1999) The continuing importance of bile acids in liver and intestinal disease. *Arch Intern Med* **159**:2647-2658.
- Hofmann AF and Mysels KJ (1992) Bile acid solubility and precipitation in vitro and in vivo: the role of conjugation, pH, and Ca²⁺ ions. *J Lipid Res* **33**:617-626.
- Hu HH, Liu J, Lin YL, Luo WS, Chu YJ, Chang CL, Jen CL, Lee MH, Lu SN, Wang LY, You SL, Yang HI, Chen CJ, and Group R-HS (2016) The rs2296651 (S267F) variant on NTCP (SLC10A1) is inversely associated with chronic hepatitis B and progression to cirrhosis and hepatocellular carcinoma in patients with chronic hepatitis B. *Gut* **65**:1514-1521.
- Ioannidis NM, Rothstein JH, Pejaver V, Middha S, McDonnell SK, Baheti S, Musolf A, Li Q, Holzinger E, Karyadi D, Cannon-Albright LA, Teerlink CC, Stanford JL, Isaacs WB, Xu J, Cooney KA, Lange EM, Schleutker J, Carpten JD, Powell IJ, Cussenot O, Cancel-Tassin G, Giles GG, MacLinnis RJ, Maier C, Hsieh CL, Wiklund F, Catalona WJ, Foulkes WD, Mandal D, Eeles RA, Kote-Jarai Z, Bustamante CD, Schaid DJ, Hastie T, Ostrander EA, Bailey-Wilson JE, Radivojac P, Thibodeau SN, Whittemore AS, and Sieh W (2016) REVEL: An Ensemble Method for Predicting the Pathogenicity of Rare Missense Variants. *Am J Hum Genet* **99**:877-885.
- Ipe J, Swart M, Burgess KS, and Skaar TC (2017) High-Throughput Assays to Assess the Functional Impact of Genetic Variants: A Road Towards Genomic-Driven Medicine. *Cts-Clin Transl Sci* **10**:67-77.
- Kelley LA, Mezulis S, Yates CM, Wass MN, and Sternberg MJ (2015) The Phyre2 web portal for protein modeling, prediction and analysis. *Nat Protoc* **10**:845-858.
- Kim RB, Leake B, Cvetkovic M, Roden MM, Nadeau J, Walubo A, and Wilkinson GR (1999) Modulation by drugs of human hepatic sodium-dependent bile

- acid transporter (sodium taurocholate cotransporting polypeptide) activity. *J Pharmacol Exp Ther* **291**:1204-1209.
- Kircher M, Witten DM, Jain P, O'Roak BJ, Cooper GM, and Shendure J (2014) A general framework for estimating the relative pathogenicity of human genetic variants. *Nat Genet* **46**:310-315.
- Kozyra M, Ingelman-Sundberg M, and Lauschke VM (2017) Rare genetic variants in cellular transporters, metabolic enzymes, and nuclear receptors can be important determinants of interindividual differences in drug response. *Genet Med* **19**:20-29.
- Kumar P, Henikoff S, and Ng PC (2009) Predicting the effects of coding non-synonymous variants on protein function using the SIFT algorithm. *Nat Protoc* **4**:1073-1081.
- Lauschke VM and Ingelman-Sundberg M (2019) Prediction of drug response and adverse drug reactions: From twin studies to Next Generation Sequencing. *Eur J Pharm Sci* **130**:65-77.
- Lauschke VM, Zhou Y, and Ingelman-Sundberg M (2019) Novel genetic and epigenetic factors of importance for inter-individual differences in drug disposition, response and toxicity. *Pharmacol Ther* **197**:122-152.
- Lee J, Zong L, Krotow A, Qin Y, Jia L, Zhang J, Tong S, and Li J (2018) N-Linked Glycosylation Is Not Essential for Sodium Taurocholate Cotransporting Polypeptide To Mediate Hepatitis B Virus Infection &em>In Vitro&/em>. *Journal of Virology* **92**:e00732-00718.
- Liu R, Chen C, Xia X, Liao Q, Wang Q, Newcombe PJ, Xu S, Chen M, Ding Y, Li X, Liao Z, Li F, Du M, Huang H, Dong R, Deng W, Wang Y, Zeng B, Pan Q, Jiang D, Zeng H, Sham P, Cao Y, Maxwell PH, Gao ZL, Peng L, and Wang Y (2017) Homozygous p.Ser267Phe in SLC10A1 is associated with a new type of hypercholanemia and implications for personalized medicine. *Sci Rep* **7**:9214.
- Makishima M, Okamoto AY, Repa JJ, Tu H, Learned RM, Luk A, Hull MV, Lustig KD, Mangelsdorf DJ, and Shan B (1999) Identification of a nuclear receptor for bile acids. *Science* **284**:1362-1365.
- Mao F, Liu T, Hou X, Zhao H, He W, Li C, Jing Z, Sui J, Wang F, Liu X, Han J, Borchers CH, Wang JS, and Li W (2019) Increased sulfation of bile acids in mice and human subjects with sodium taurocholate cotransporting polypeptide deficiency. *J Biol Chem* **294**:11853-11862.
- Mareninova O, Shin JM, Vagin O, Turdikulova S, Hallen S, and Sachs G (2005) Topography of the membrane domain of the liver Na⁺-dependent bile acid transporter. *Biochemistry* **44**:13702-13712.

- Martin PD, Warwick MJ, Dane AL, Hill SJ, Giles PB, Phillips PJ, and Lenz E (2003) Metabolism, excretion, and pharmacokinetics of rosuvastatin in healthy adult male volunteers. *Clin Ther* **25**:2822-2835.
- McTaggart F, Buckett L, Davidson R, Holdgate G, McCormick A, Schneck D, Smith G, and Warwick M (2001) Preclinical and clinical pharmacology of Rosuvastatin, a new 3-hydroxy-3-methylglutaryl coenzyme A reductase inhibitor. *Am J Cardiol* **87**:28B-32B.
- Meier PJ, Eckhardt U, Schroeder A, Hagenbuch B, and Stieger B (1997) Substrate specificity of sinusoidal bile acid and organic anion uptake systems in rat and human liver. *Hepatology* **26**:1667-1677.
- Nelson MR, Wegmann D, Ehm MG, Kessner D, St Jean P, Verzilli C, Shen J, Tang Z, Bacanu SA, Fraser D, Warren L, Aponte J, Zawistowski M, Liu X, Zhang H, Zhang Y, Li J, Li Y, Li L, Woollard P, Topp S, Hall MD, Nangle K, Wang J, Abecasis G, Cardon LR, Zollner S, Whittaker JC, Chissoe SL, Novembre J, and Mooser V (2012) An abundance of rare functional variants in 202 drug target genes sequenced in 14,002 people. *Science* **337**:100-104.
- Ni Y, Lempp FA, Mehrle S, Nkongolo S, Kaufman C, Falth M, Stindt J, Koniger C, Nassal M, Kubitz R, Sultmann H, and Urban S (2014) Hepatitis B and D Viruses Exploit Sodium Taurocholate Co-transporting Polypeptide for Species-Specific Entry into Hepatocytes. *Gastroenterology* **146**:1070-U1301.
- Omasits U, Ahrens CH, Muller S, and Wollscheid B (2014) Protter: interactive protein feature visualization and integration with experimental proteomic data. *Bioinformatics* **30**:884-886.
- Pan W, Song IS, Shin HJ, Kim MH, Choi YL, Lim SJ, Kim WY, Lee SS, and Shin JG (2011) Genetic polymorphisms in Na⁺-taurocholate co-transporting polypeptide (NTCP) and ileal apical sodium-dependent bile acid transporter (ASBT) and ethnic comparisons of functional variants of NTCP among Asian populations. *Xenobiotica* **41**:501-510.
- Qiu JW, Deng M, Cheng Y, Atif RM, Lin WX, Guo L, Li H, and Song YZ (2017) Sodium taurocholate cotransporting polypeptide (NTCP) deficiency: Identification of a novel SLC10A1 mutation in two unrelated infants presenting with neonatal indirect hyperbilirubinemia and remarkable hypercholanemia. *Oncotarget* **8**:106598-106607.
- Ramasamy U, Anwer MS, and Schonhoff CM (2013) Cysteine 96 of Ntcp is responsible for NO-mediated inhibition of taurocholate uptake. *Am J Physiol Gastrointest Liver Physiol* **305**:G513-519.

- Reva B, Antipin Y, and Sander C (2007) Determinants of protein function revealed by combinatorial entropy optimization. *Genome Biol* **8**:R232.
- Russell LE, Zhou Y, Lauschke VM, and Kim RB (2020) In Vitro Functional Characterization and in Silico Prediction of Rare Genetic Variation in the Bile Acid and Drug Transporter, Na(+)-Taurocholate Cotransporting Polypeptide (NTCP, SLC10A1). *Mol Pharm* **17**:1170-1181.
- Saeki T, Kuroda T, Matsumoto M, Kanamoto R, and Iwami K (2002) Effects of Cys mutation on taurocholic acid transport by mouse ileal and hepatic sodium-dependent bile acid transporters. *Biosci Biotechnol Biochem* **66**:467-470.
- Schaller L and Lauschke VM (2019) The genetic landscape of the human solute carrier (SLC) transporter superfamily. *Hum Genet.*
- Schonhoff CM, Ramasamy U, and Anwer MS (2011) Nitric oxide-mediated inhibition of taurocholate uptake involves S-nitrosylation of NTCP. *Am J Physiol Gastrointest Liver Physiol* **300**:G364-370.
- Shneider BL, Fox VL, Schwarz KB, Watson CL, Ananthanarayanan M, Thevananther S, Christie DM, Hardikar W, Setchell KD, Mieli-Vergani G, Suchy FJ, and Mowat AP (1997) Hepatic basolateral sodium-dependent-bile acid transporter expression in two unusual cases of hypercholanemia and in extrahepatic biliary atresia. *Hepatology* **25**:1176-1183.
- Slijepcevic D, Abbing RLPR, Katafuchi T, Blank A, Donkers JM, van Hoppe S, de Waart DR, Tolenaars D, van der Meer JHM, Wildenberg M, Beuers U, Elferink RPJO, Schinkel AH, and van de Graaf SFJ (2017) Hepatic Uptake of Conjugated Bile Acids Is Mediated by Both Sodium Taurocholate Cotransporting Polypeptide and Organic Anion Transporting Polypeptides and Modulated by Intestinal Sensing of Plasma Bile Acid Levels in Mice. *Hepatology* **66**:1631-1643.
- Slijepcevic D, Kaufman C, Wichers CG, Gilglioni EH, Lempp FA, Duijst S, de Waart DR, Elferink RP, Mier W, Stieger B, Beuers U, Urban S, and van de Graaf SF (2015) Impaired uptake of conjugated bile acids and hepatitis b virus pres1-binding in na(+)-taurocholate cotransporting polypeptide knockout mice. *Hepatology* **62**:207-219.
- Starita LM, Ahituv N, Dunham MJ, Kitzman JO, Roth FP, Seelig G, Shendure J, and Fowler DM (2017) Variant Interpretation: Functional Assays to the Rescue. *Am J Hum Genet* **101**:315-325.
- Starita LM, Young DL, Islam M, Kitzman JO, Gullingsrud J, Hause RJ, Fowler DM, Parvin JD, Shendure J, and Fields S (2015) Massively Parallel Functional Analysis of BRCA1 RING Domain Variants. *Genetics* **200**:413-422.

- Tu H, Okamoto AY, and Shan B (2000) FXR, a bile acid receptor and biological sensor. *Trends Cardiovas Med* **10**:30-35.
- Vaz FM, Paulusma CC, Huidekoper H, de Ru M, Lim C, Koster J, Ho-Mok K, Bootsma AH, Groen AK, Schaap FG, Oude Elferink RP, Waterham HR, and Wanders RJ (2015) Sodium taurocholate cotransporting polypeptide (SLC10A1) deficiency: conjugated hypercholanemia without a clear clinical phenotype. *Hepatology* **61**:260-267.
- Weile J and Roth FP (2018) Multiplexed assays of variant effects contribute to a growing genotype-phenotype atlas. *Hum Genet* **137**:665-678.
- Weinman SA (1997) Electrogenicity of Na(+)-coupled bile acid transporters. *Yale J Biol Med* **70**:331-340.
- Yan H, Zhong GC, Xu GW, He WH, Jing ZY, Gao ZC, Huang Y, Qi YH, Peng B, Wang HM, Fu LR, Song M, Chen P, Gao WQ, Ren BJ, Sun YY, Cai T, Feng XF, Sui JH, and Li WH (2012) Sodium taurocholate cotransporting polypeptide is a functional receptor for human hepatitis B and D virus. *Elife* **1**.
- Zahner D, Eckhardt U, and Petzinger E (2003) Transport of taurocholate by mutants of negatively charged amino acids, cysteines, and threonines of the rat liver sodium-dependent taurocholate cotransporting polypeptide Ntcp. *Eur J Biochem* **270**:1117-1127.
- Zhou Y, Fujikura K, Mkrтчian S, and Lauschke VM (2018) Computational Methods for the Pharmacogenetic Interpretation of Next Generation Sequencing Data. *Front Pharmacol* **9**:1437.
- Zhou Y, Mkrтчian S, Kumondai M, Hiratsuka M, and Lauschke VM (2019) An optimized prediction framework to assess the functional impact of pharmacogenetic variants. *Pharmacogenomics J* **19**:115-126.

- 4 Evaluating serum bile acid composition, bile acid gene expression, and rosuvastatin disposition in *Slc10a1*^{-/-} mice

4.1 Introduction

In addition to their well-known roles in digestive processes, bile acids are important signaling molecules that modulate bile acid synthesis and transport within the enterohepatic system. Bile acids are synthesized in hepatocytes, secreted into bile, and released into the duodenum to facilitate solubilization of lipids and xenobiotics for nutrient absorption. Bile acids are efficiently circulated throughout the enterohepatic system by plasma membrane-bound uptake and efflux transport proteins in enterocytes and hepatocytes (Dawson et al., 2009). Due to their detergent properties, excessive extracellular or intracellular accumulation of bile acids, known as hypercholanemia and cholestasis, respectively, can mediate toxicity by breaking down cellular membranes. Additionally, different bile acids have different capacities to mediate toxicity; cholic acids are more toxic to lipid membranes than are muricholic acids (Li and Dawson, 2019).

Bile acid homeostasis is controlled by nuclear receptor signaling. Bile acids are ligands for nuclear receptors including the farnesoid X receptor (FXR), the pregnane X receptor (PXR), and the vitamin D receptor (VDR). Additionally, bile acids indirectly activate the constitutive androstane receptor (CAR). These nuclear receptors are ligand-activated transcription factors that regulate transcription of genes involved in bile acid synthesis, transport, and detoxification (Chiang, 2013). Genetic variation in bile acid transporters and the resulting dysregulation of nuclear receptor signaling have been linked to a variety of cholestatic and metabolic conditions (Kosters and Karpen, 2008).

Sodium taurocholate co-transporting polypeptide (NTCP; *SLC10A1*) is a key hepatic bile acid uptake transporter with preference for conjugated bile acids (Dawson et al., 2009). In humans, homozygous missense mutations in *SLC10A1* have been associated with vitamin D deficiency and persistent serum hypercholanemia, with bile acid concentrations reaching as high as 1531 μM (normal range: 0-16 μM) (Vaz et al., 2015; Deng et al., 2016; Liu et al., 2017; Qiu et al., 2017).

Two independent mouse lines in which the *Slc10a1* gene was targeted have been generated (Slijepcevic et al., 2015; Mao et al., 2019). The first study reported a surprising bimodal phenotype in *Slc10a1*^{-/-} mice; serum bile acid concentrations were highly elevated and bile acid transporter expression was altered in 30-35% of adult *Slc10a1*^{-/-} mice. The remaining mice displayed physiological serum bile acid concentrations and expression of bile acid transporters comparable to control animals (Slijepcevic et al., 2015).

The second study of *Slc10a1*^{-/-} mice observed a similar hypercholanemic phenotype in some animals aged four and eight weeks, noting important differences in expression of hepatic genes that control bile acid synthesis, transport, and detoxification. Following mice over time, investigators reported that serum bile acid concentrations decreased with age. Furthermore, hepatic bile acid transporter gene expression tended to normalize to levels seen in control animals by 20 months of age. Importantly, however, some mice remained hypercholanemic even at 20-month age mark (Mao et al., 2019). Authors also quantified serum bile acids in NTCP-deficient humans over time and noted that

bile acid concentrations are highest within the first three months of life and typically decline over time. However, some NTCP-deficient humans also remained hypercholanemic, with bile acid concentrations over 100 μM in certain individuals seven years of age (Mao et al., 2019).

In addition to its central role in bile acid uptake, NTCP is also capable of drug transport and may be important in hepatic uptake of rosuvastatin (Ho et al., 2006). Statins are a common class of lipid-lowering drugs. Their primary therapeutic effect is lowering cholesterol. This is achieved by inhibiting the rate-limiting enzyme in hepatic cholesterol synthesis, 3-hydroxy-3-methylglutaryl-coenzyme A (HMG-CoA) reductase. Rosuvastatin is a commonly prescribed, hydrophilic statin that is minimally metabolized in the liver. Hepatic disposition of rosuvastatin is therefore highly dependent on transporters (Stancu and Sima, 2001). Further, increased plasma concentrations of statin in the blood has been linked to increased risk of statin-induced myopathy (Link et al., 2008; DeGorter et al., 2013). Studies in human hepatocytes have identified OATP1B1, OATP1B3, OATP2B1, and NTCP as rosuvastatin transporters (Ho et al., 2006). Genetic polymorphisms in OATP transporters explain some of the variability seen in plasma rosuvastatin concentrations (DeGorter et al., 2013). However, the remaining unexplained variability in rosuvastatin concentrations in the plasma may contribute to adverse events. Investigation into additional factors influencing statin disposition will help maximize their safety and efficacy (Link et al., 2008).

Despite recent advancements in studying mouse models of NTCP deficiency, information regarding differences between normocholanemic and

hypercholanemic phenotypes induced by *Slc10a1* disruption remains limited. Moreover, although the impact of OATP deficiency on rosuvastatin disposition has been evaluated in a variety of OATP-null mouse models (Chen et al., 2008; Zaher et al., 2008; van de Steeg et al., 2010; DeGorter et al., 2012; Medwid et al., 2019), the relative importance of NTCP to rosuvastatin disposition has not yet been elucidated *in vivo*.

This study was designed to evaluate serum bile acid composition and hepatic, ileal, and renal mRNA levels in a third, independent *Slc10a1*^{-/-} mouse model. Additionally, this study aimed to assess the role of *Slc10a1* gene disruption on hepatic rosuvastatin disposition in mice.

4.2 Methods & Materials

4.2.1 Materials

Rosuvastatin, d6-rosuvastatin, and d5-Taurocholic acid were purchased from Toronto Research Chemicals (Toronto, ON). All other chemicals, unless otherwise stated, were obtained from Millipore-Sigma (St. Louis, MO).

4.2.2 Animal use approval

All animal experiments were approved by the University of Western Ontario Animal Care Committee (Protocol No. 2015-011), according to regulations and guidelines of the Canadian Council on Animal Care. Approval is listed in Appendix C.

4.2.3 Liver-specific targeted disruption of *Slc10a1* in C57BL/6 mice

The approach used to disrupt the mouse *Slc10a1* gene is depicted in Figure 4.1. A targeting vector designed by the Mouse Biology Program and UC Davis (Davis, CA) was injected into C57BL/6 embryos, where homologous recombination resulted in the insertion of a LoxP site between exons 1 and 2, and insertion of a neomycin cassette followed by a second LoxP site between exons 2 and 3. Selection of embryos with the integrated target vector was performed using diphtheria toxin A (DTA). Floxed mice were mated with mice expressing Cre

recombinase driven by the liver-specific Albumin promoter, B6.Cg-Tg(Alb-cre)21Mgn/J (The Jackson Laboratory, stock number 003574). Exon 2 of *Slc10a1* was replaced by the PGK-NEO cassette located in the targeting vector to generate *Slc10a1*^{-/-} mice.

Mice homozygous for the LoxP-flanked *Slc10a1* gene were mated with mice homozygous for the liver-specific Cre transgene to generate *Slc10a1*^{-/-} mice. Heterozygous *Slc10a1*^{+/-} mice were generated by crossing mice heterozygous for the LoxP flanked *Slc10a1* gene with mice homozygous for the liver-specific Cre transgene. Mice homozygous for the LoxP-flanked *Slc10a1* gene mated with animals that do not express the Cre transgene were used as wild type control animals and will be hereafter referred to as controls.

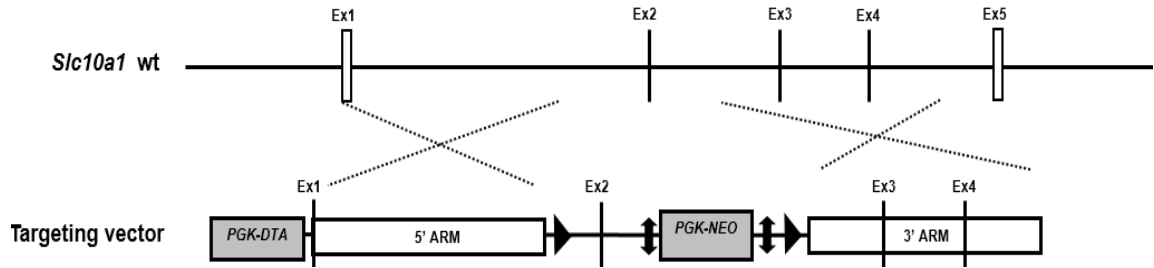


Figure 4.1. Liver-specific targeted disruption *Slc10a1*.

A schematic of the wild type (wt) mouse *Slc10a1* gene and the targeting vector for disruption of the mouse *Slc10a1* gene. PGK-DTA: Diphtheria Toxin A driven by the phosphoglycerate kinase (PGK) promoter, used for negative selection; PGK-NEO: neomycin selection cassette driven by the PGK promoter. Black horizontal arrows represent LoxP sites for Cre recombinase recognition.

4.2.4 Quantification of serum total bile acids by colorimetric assay

Immediately following isoflurane overdose, blood was collected from mice using cardiac puncture and was incubated at room temperature for 15 min to allow for clotting. Blood was then centrifuged for 10 min at 2,000 x *g* and 4°C. The supernatant was used to measure bile acids in the serum immediately or was stored at -20°C for bile acid quantification within 3 months of sample collection. Total serum bile acids were quantified following the protocol for the Total Bile Acids Assay Kit (Diazyme Laboratories Inc., Poway, CA).

4.2.5 Quantification of serum individual bile acids by LC-MS/MS

Individual serum bile acids were quantified using ultra-high-performance liquid chromatography tandem mass spectrometry (UHPLC-MS/MS). On the day of measurement, samples were thawed at 4°C and 50 µL were transferred to clean microcentrifuge tubes. Calibration curves were prepared in 1:1 (v/v) methanol:acetonitrile supplemented with various concentrations of bile acids: cholic acid (CA), deoxycholic acid (DCA), taurocholic acid (TCA), taurodeoxycholic acid (TDCA), α and β muricholic acids (α MCA, β MCA), tauro- α -muricholic acid (T α MCA) and tauro- β -muricholic acid (T β MCA). The internal standard (IS) solution was composed of TCA-d5 in 1:1 (v/v) MeOH:ACN. One hundred µL of ice-cold IS solution were added to each mouse blood and standard curve sample. Samples were mixed at 1400 RPM in a shaker placed at 4°C for 15 min. To induce protein precipitation, samples were incubated at -20°C for 20 min followed by centrifugation at 18,000 x *g* at 4°C for 15 min. The

supernatants were collected for UHPLC-MS/MS analysis, and samples were kept at 4°C prior to column injection. Analytes were separated by ultra-high-performance liquid chromatography (Agilent 1290 Infinity LC Injector; Agilent, Santa Clara, CA) using a Kinetex 2.6 µm C18 100Å Reversed Phase LC Column, 50 x 3 mm (Phenomenex, Torrance, CA) following sample injection (40 µL per sample). A mobile phase of 2mM ammonium acetate in 9:1 H₂O:ACN (v/v) adjusted to pH 4.15 (A) and equal parts ACN:C₃H₈O:H₂O (1:1:1) (B) was used with an elution gradient of 10% B at a flow rate of 0.5 mL/min from 0-1 min, 10-70% B at 0.6 mL/min from 1-9 min, 70-80% B at 0.5 mL/min from 9-10 min, and 80-10% B at 0.5 mL/min from 10-12 min, with a wash period at 10% B from 12-15 min at a flow rate 0.5mL/min. The heated electrospray ionization source of the triple quadrupole mass spectrometer (Finnigan TSQ Quantum Ultra; Thermo Fisher Scientific) was operated in negative mode (4500V, 350°C) with collision energies listed in Table 4.1. Sheath gas pressure was set to 45 psi, auxiliary gas pressure was 15 psi, and capillary temperature was 350°C. Multiple reaction monitoring was performed using mass-to-charge ratio transitions and retention times are listed in Table 4.1. Calibration curves were linear with concentrations between 0 and 50 µM. Interday accuracy and precision were 18.5% and 22.1% respectively. The lower limits of quantification were between 10 and 50 nM.

Table 4.1. Bile acid mass spectrometry parameters

	Parent mass (g/mol)	Product mass (g/mol)	CE (eV)	RT (min)
DCA	391.285	Parent quantified	10	6.65
α MCA	407.280	Parent quantified	10	4.96
β MCA	407.300	Parent quantified	10	5.02
CA	407.370	Parent quantified	10	5.80
TDCA	498.280	80.11	80	4.71
T α β MCA	514.300	80.11	80	3.20
TCA	514.380	80.11	80	3.85
TCA-d5	519.420	80.11	80	3.20

CE: collision energy (eV: electron volts), RT: retention time (minutes)

4.2.6 Quantification of mRNA in mouse tissues

Liver, kidney, and terminal ileum sections were isolated from mice immediately following isoflurane overdose. RNA was extracted using TRIzol reagent (Life Technologies, Carlsbad, CA). RNA was reverse transcribed to cDNA using random hexamers (Multiscribe; Applied Biosystems, Foster City, CA).

Quantitative polymerase chain reaction using SYBR Green (7500 system; Applied Biosystems) was used to determine relative mRNA levels of genes involved in bile acid disposition, including synthesis enzymes and transporters. Target mRNA levels were normalized to those of 18S ribosomal RNA using TaqMan reagents (Applied Biosystems). Primer sequences are listed in Table 4.2.

Table 4.2. Primers used for qPCR

Mouse Gene	Protein	Forward Primer	Reverse Primer
<i>Slc10a1</i>	NTCP	5'-GGCTTCCTGATGGGCTACATT-3'	5'-AGAGTTGGACGTTTTGGAATCC-3'
<i>Slc10a2</i>	ASBT	5'-CCATGGGGTATCTTCGTGGG-3'	5'-GTTCCCGAGTCAACCCACAT-3'
<i>Slco1a1</i>	OATP1A1	5'-GTGCATACCTAGCCAAATCACT-3'	5'-CCAGGCCATAACCACACA-3'
<i>Slco1a4</i>	OATP1A4	5'-CCCAGAGCTCTCCAGTTTTG-3'	5'-TCCCATGTTGTTCTTCTGATTG-3'
<i>Slco1b2</i>	OATP1B2	5'-TGGGCATTGGGAGTATTCTGA-3'	5'-CCAGGTGTATGAGTTGGACCC-3'
<i>Abcb1a</i>	MDR1A (P-gp)	5'-CTCTTTGACTCGGGAGCAGAA-3'	5'-CGGAAACAAGCAGCATAAGAAA-3'
<i>Abcb11</i>	BSEP	5'-CTGCCAAGGATGCTAATGCA-3'	5'-CGATGGCTACCCTTTGCTTCT-3'
<i>Abcc2</i>	MRP2	5'-CTGAGTGCTTGGACCAGTGA-3'	5'-CAAAGTCTGGGGGAGTGTGT-3'
<i>Abcc3</i>	MRP3	5'-CTGGGTCCCCTGCATCTAC-3'	5'-GCCGCTTGAGCCTGGATAAC-3'
<i>Abcc4</i>	MRP4	5'-GAACAAGCAAGGTGCACTGA-3'	5'-TGCATCAAACAGCTCCTGAC-3'
<i>Slc51a</i>	OST α	5'-CACTGGCTCAGTTGCCATTT-3'	5'-GCATACGGCATAAAACGAGGT-3'
<i>Slc51b</i>	OST β	5'-GCAAACAGAAATCGAAAGAAGC-3'	5'-TCTGGCAGAAAGACAAGTGAT-3'
<i>Nr0b2</i>	SHP	5'-CGATCCTCTTCAACCCAGATG-3'	5'-AGGGCTCCAAGACTTCACACA-3'
<i>Fgf15</i>	FGF15	5'-GCCATCAAGGACGTCAGCA-3'	5'-CTTCCTCCGAGTAGCGAATCAG-3'
<i>Cyp7a1</i>	CYP7A1	5'-AACAACCTGCCAGTACTAGATAGC-3'	5'-GTGTAGAGTGAAGTCCTCCTTAGC-3'
<i>Cyp8b1</i>	CYP8B1	5'-GCCTTCAAGTATGATCGGTTCT-3'	5'-GATCTTCTTGCCCGACTTGTAGA-3'
<i>Cyp27a1</i>	CYP27A1	5'-CTGCGTCAGGCTTTGAAACA-3'	5'-TCGTTAAGGCATCCGTGTAGA-3'

4.2.7 Mouse necropsy

Five male *Slc10a1*^{-/-} mice that failed to thrive were euthanized at ages 4-6 weeks due to hunched posture, reduced locomotion, and occasional blood in the urine. Veterinary pathologists examined them to determine potential causes of failure to thrive. Tissues examined by histology included kidneys, heart, lung, esophagus, trachea, small intestine, large intestines, stomach, liver, thyroid gland, gallbladder, urinary bladder, bone marrow, skeletal muscle, uterus, testicle, and spleen.

4.2.8 Rosuvastatin studies

Control and *Slc10a1*^{-/-} mice were fasted 16 hr prior to oral gavage of rosuvastatin (10 mg/kg body weight) dissolved in 1x PBS. Mice were sacrificed 2 hr after rosuvastatin administration, blood was collected via cardiac puncture, and livers were harvested. The concentrations of rosuvastatin in serum and liver were determined using an adapted LC-MS/MS described below (DeGorter et al., 2012). Livers were diluted in acetonitrile (1:1 w/v) containing the internal standard d6-rosuvastatin. Livers were homogenized using a VeriSonic ultrasonic tissue homogenizer using ten, one-second pulses at eight watts at room temperature. The homogenates were centrifuged for 20 min at 10,000 x *g* at 4°C. Proteins in serum samples were precipitated by the addition of acetonitrile (1:1 v/v) containing the internal standard d6-rosuvastatin diluted to a final concentration of 20 ng/mL and centrifuged for 20 min at 10,000 x *g* at 4°C. A volume of 100 µL supernatant from serum or liver samples was added to a volume of 200 µL

0.05% formic acid (1:2 dilution (v/v) and analyzed by LC-MS/MS. Solutes were separated by reversed-phase chromatography using a TLX2 high-performance liquid chromatography system (Thermo Fisher Scientific). A 50 μ L aliquot of the diluted serum or liver sample containing internal standard was injected onto a Hypersil GOLD C18 column (50 \times 3 mm, 5 μ m; Thermo Fisher Scientific) and analytes were separated using a 0.05% formic acid and acetonitrile solvent gradient from a ratio of 70:30 v/v to 10:90 v/v. After electrospray ionization, positive mode mass spectrometric detection was carried out using the TSQ Vantage triple quadrupole mass spectrometer (Thermo Fisher Scientific) with a HESI II probe (Thermo Fisher Scientific). Mass-to-charge transitions were 482.1 \rightarrow 258.2 m/z for rosuvastatin and 488.0 \rightarrow 264.3 m/z for d6-rosuvastatin. Calibration curves were created with blank mouse serum and blank mouse liver homogenates from wild type C57BL/6 mice, with rosuvastatin concentrations in the linear range between 100 to 2000 ng/mL for liver samples, and 1 to 100 ng/mL for serum samples. Interday accuracy and precision were 5.8% and 8.9%, respectively, and the lower limit of quantitation was 1 ng/mL.

4.2.9 Statistics

Mann-Whitney tests were used to determine statistical differences between two groups where normal distribution was not observed. Student's t tests were used to determine statistical differences between two groups where normal distribution was observed. One-way ANOVA with Tukey's multiple comparison tests were used to determine statistical differences between three groups. Serum bile acids

and mRNA levels for control, normocholanemic *Slc10a1*^{-/-}, and hypercholanemic *Slc10a1*^{-/-} mice were quantified in four- to six-week old mice (n=4-5 male mice per group). Rosuvastatin studies and associated qPCR were conducted in ten-week-old mice (n=3-5 male mice per group). LC-MS/MS measurements for individual bile acids and rosuvastatin were performed once per mouse sample, and results are presented as mean \pm SD. Total bile acid measurements were performed in duplicate and quantitative PCR was performed in triplicate; these results are presented as mean \pm SEM. All statistical analyses were conducted using GraphPad Prism 6 (La Jolla, CA) and statistical significance was deemed at $P < 0.05$.

4.3 Results

4.3.1 Mouse phenotype

Relative mRNA levels were quantified to infer the extent of *Slc10a1* gene transcription in these mice. Relative to control animals, *Ntcp* (*Slc10a1*) mRNA levels were reduced 2-fold in heterozygous *Slc10a1*^{+/-} mice ($P < 0.0001$, Fig. 4.2) and >15 fold in homozygous *Slc10a1*^{-/-} mice ($P < 0.0001$, Fig. 4.2).

In *Slc10a1*^{-/-} mice, a bimodal phenotype was observed. Overall, approximately 45% of *Slc10a1*^{-/-} mice failed to thrive beginning at four weeks of age and died by seven weeks of age (Fig. 4.3). Between the ages of four and eight weeks, these mice appeared lethargic as subjectively observed by reduced locomotion and hunched posture. These mice also appeared dehydrated by reduced ability of skin to return to normal shape after pinching, and blood was detected in urine of some of these mice. No discernable pattern was observed in survival of these mice based on the breeding pair or litter. In some litters, all *Slc10a1*^{-/-} mice would survive. In other litters, 15-100% of *Slc10a1*^{-/-} mice would fail to thrive and succumb by seven weeks of age. This is the first report of mortality in a subset of *Slc10a1*^{-/-} mice.

Five male mice that appeared hunched with reduced locomotion, dehydration, and blood in urine were euthanized between the ages of four and six weeks for preliminary necropsies. Findings indicated that these *Slc10a1*^{-/-} mice were small for their age, with thin bodies and slightly jaundiced body cavities. Gallbladders were enlarged, bile ducts were not prominent, and compression of the gallbladder did not release bile into the duodenum. This

usually occurs subsequent to obstruction or from a congenital lack of a portion of the ductal wall, known as cholangiectasis. Bilirubin was found in the urine which may indicate diseased liver. Upon histological analysis, mice were found to have hyperplasia of the gallbladder, tubular degeneration in the kidneys, and bile acid depositions in the kidney resulting in bile cast nephropathy. Bile acid deposits were also observed in the bile canaliculi of the liver. Some hepatocyte swelling and necrosis were observed. Low body fat and may reflect decreased nutritional absorption. Subcutaneous administration of saline reversed this failure to thrive phenotype in mice. In mice that appeared lethargic and dehydrated between the ages of four and seven weeks, daily subcutaneous saline injections allowed mice to recover from this morbid phenotype and survive passed eight weeks of age. The full necropsy reports for these mice can be found in Appendix B. No abnormal phenotype was observed in heterozygous or control animals.

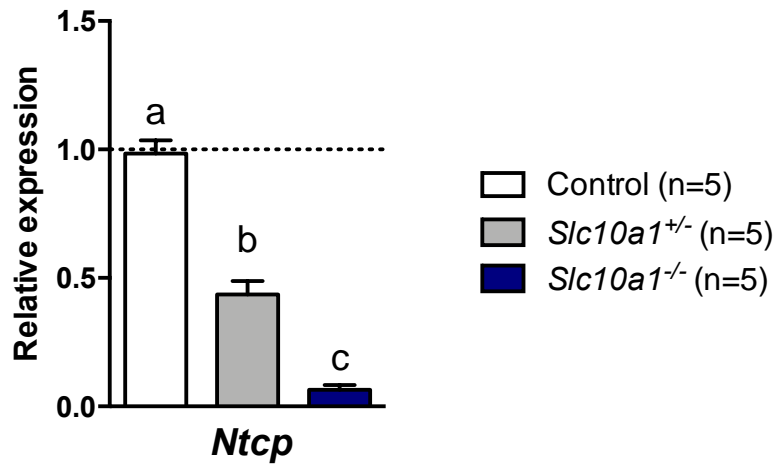


Figure 4.2. Relative mRNA levels in the livers of floxed control mice, *Slc10a1*^{+/-} mice, and *Slc10a1*^{-/-} mice.

Hepatic *Ntcp* (*Slc10a1*) mRNA expression was determined using qPCR. Experiments were performed in triplicate and results are presented as mean ± SEM (n=5 mice per group).

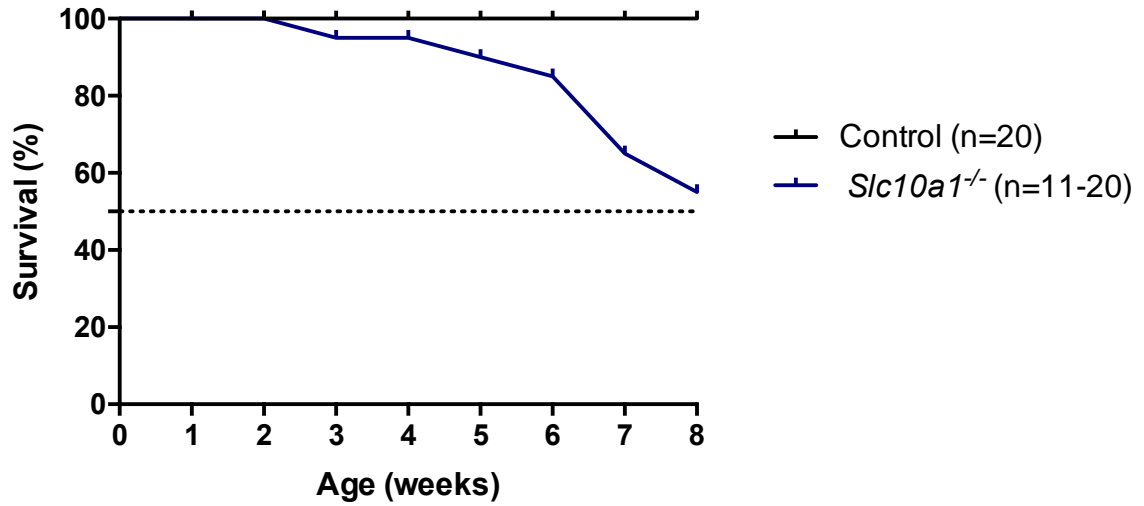
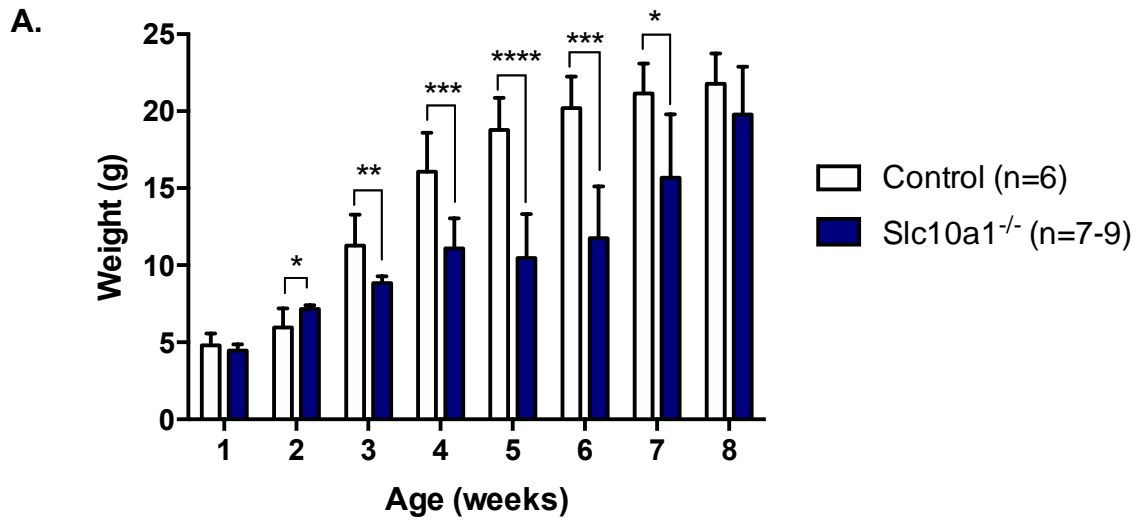


Figure 4.3. Mouse survival over the first eight weeks of life

Control mice: n=20. *Slc10a1*^{-/-} mice: 0-3 weeks of age, n=20; 3-5 weeks of age, n=19; 5-6 weeks of age, n=18; 6-7 weeks of age, n=17; 7-8 weeks of age, n=13; 8-9 weeks of age, n=11.

Altered bile acid signaling may result in nutrient malabsorption at the intestinal level. Body weights of control and *Slc10a1*^{-/-} mice were recorded weekly until eight weeks of age and are reported in Figure 4. Consistent with previous studies (Slijepcevic et al., 2015; Mao et al., 2019), between three and seven weeks of age, body weights for all *Slc10a1*^{-/-} mice in our study were significantly reduced relative to controls (Fig. 4.4, $P < 0.05$). This was observed in *Slc10a1*^{-/-} mice irrespective of phenotype, occurring in mice that failed to thrive and also in *Slc10a1*^{-/-} mice that survived past eight weeks of age. For mice that survived, their body weights normalized with body weights of control mice by 8 weeks of age (Fig. 4.4).



B.

Weight (grams ± SD)		
Week	Control (n=6)	<i>Slc10a1</i> ^{-/-} (n=7-9)
1	4.8 ± 0.8	4.5 ± 0.2
2	6.0 ± 1.2	7.2 ± 0.3
3	11.3 ± 2.0	8.8 ± 0.3
4	16.1 ± 2.5	11.1 ± 0.2
5	18.8 ± 2.1	10.5 ± 0.2
6	20.2 ± 2.0	11.8 ± 2.3
7	21.2 ± 1.9	15.7 ± 3.6
8	21.8 ± 2.0	19.8 ± 3.2

Figure 4.4. Weekly mouse body weights from week one to week eight

Control mice: n=6, *Slc10a1*^{-/-} mice: n=9 mice for weeks 1-6 and n=7 mice for weeks 7 & 8.

Statistical significance was determined using Mann Whitney tests, * P < 0.05, ** P < 0.001, *** P < 0.0001, **** P < 0.0001.

4.3.2 Serum total bile acid concentrations

To determine potential differences in bile acid disposition in mice four to six weeks of age, total serum bile acid concentrations were quantified. Mean serum bile acid concentrations for control mice were within the normal physiological range ($<16\mu\text{M}$) at $3.5 \pm 1.3 \mu\text{M}$, which were significantly lower than mean serum bile acid concentrations for *Slc10a1*^{-/-} mice ($249.0 \pm 79.2 \mu\text{M}$, $P = 0.0056$, Fig. 4.5 A). Similar to the two published *Slc10a1*^{-/-} mouse models, a bimodal bile acid phenotype was observed in our *Slc10a1*^{-/-} mice (Fig. 4.5 A). For the remainder of this study, *Slc10a1*^{-/-} mice were divided into subgroups based on total bile acid concentrations (Fig. 4.5 B). Total serum bile acids for *Slc10a1*^{-/-} normocholanemic mice were $16.2 \pm 5.8 \mu\text{M}$ and were not significantly different than controls. Total serum bile acids for *Slc10a1*^{-/-} hypercholanemic mice were $435.3 \pm 55.0 \mu\text{M}$, highly elevated relative to both control and *Slc10a1*^{-/-} normocholanemic mice ($P < 0.0001$, Fig. 4.5 B).

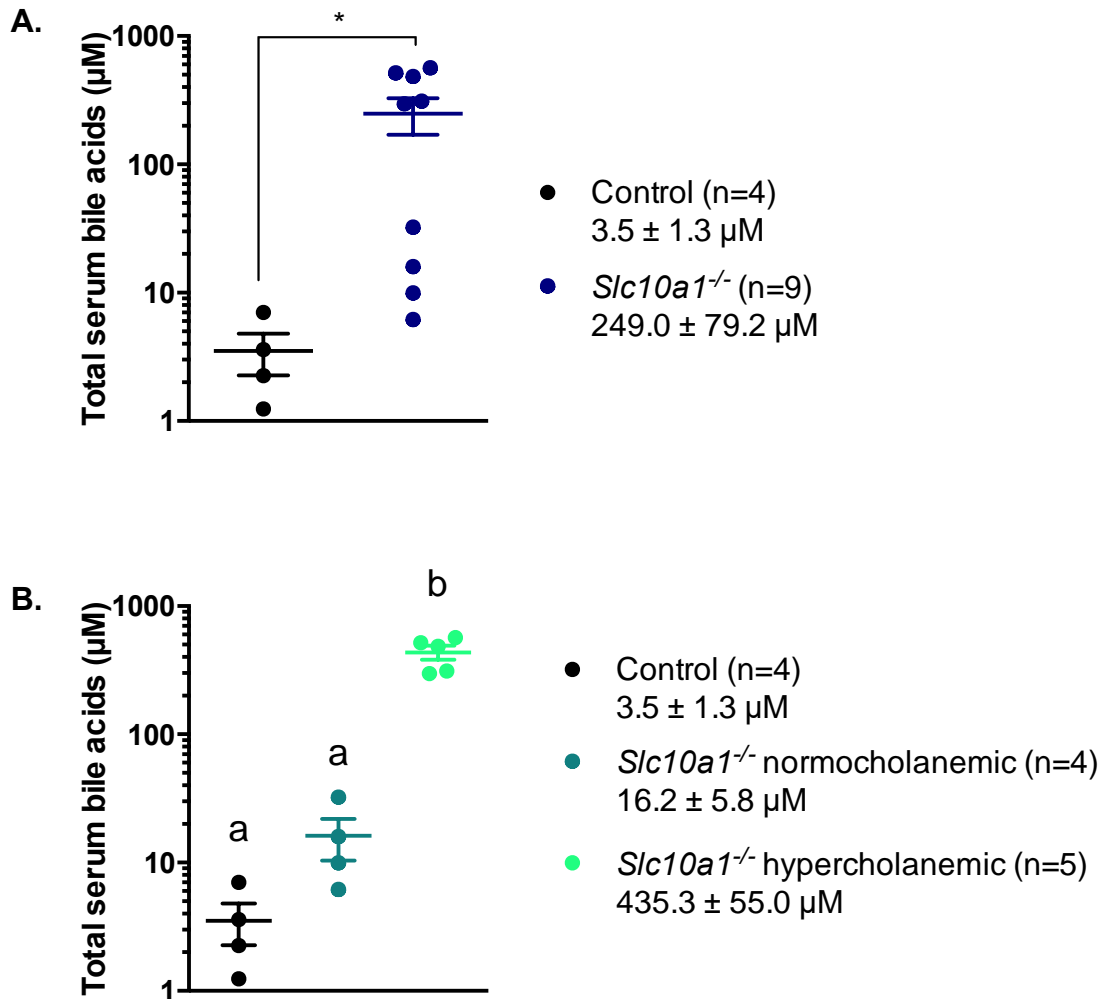


Figure 4.5. Total serum bile acid concentrations

A. Total serum bile acids in control (n=4) and *Slc10a1*^{-/-} mice (n=9), showing a bimodal bile acid phenotype in *Slc10a1*^{-/-} mice. Results are presented as mean \pm SEM. Statistical significance was determined using Mann-Whitney test, * $P < 0.05$. B. Total serum bile acid concentrations in mice divided by subpopulations: control (n=4), *Slc10a1*^{-/-} normocholanemic (n=4) and *Slc10a1*^{-/-} hypercholanemic (n=5) mice. Results are presented as mean \pm SEM and statistical significance was determined by one-way ANOVA with Tukey's multiple comparison tests, statistical differences between a and b: $P < 0.0001$.

4.3.3 Serum conjugated and unconjugated bile acids

Composition of the bile acid pool can be indicative of disruptions in specific bile acid genes and can provide insight into the relative toxicity profiles of bile acids within the serum. To investigate potential differences in the composition of circulating bile acid pools in mice four-to-six weeks of age, concentrations of individual bile acid species were quantified in the sera (Figure 4.6).

Hypercholanemic mice had significantly elevated taurocholic acid (TCA) concentrations in the serum ($282.8 \pm 170.5 \mu\text{M}$) relative to normocholanemic ($1.6 \pm 1.2 \mu\text{M}$) and control ($0.3 \pm 0.1 \mu\text{M}$) mice (Fig. 4.6 A & C, $P < 0.019$). Apparent differences in additional conjugated species T α β MCA and TDCA did not reach statistical significance ($P < 0.081$ and $P < 0.25$, respectively). None of the quantified unconjugated bile acid were significantly different between groups (Fig. 4.6 B).

To further determine the relative composition of unconjugated and conjugated bile acids in the sera, unconjugated and conjugated species are represented as percentage of the total bile acid pool in Figure 7. The sums of unconjugated bile acids α MCA, β MCA, CA, and DCA in the sera of mice were not significantly different between groups and ranged from $1.6 - 17.0 \pm 0.5 - 17.6 \mu\text{M}$ per group. The sum of conjugated bile acids T α β MCA, TCA, and TDCA was significantly elevated in *Slc10a1*^{-/-} hypercholanemic mice ($275.3 \pm 187.2 \mu\text{M}$) relative to *Slc10a1*^{-/-} normocholanemic ($2.9 \pm 2.4 \mu\text{M}$) and control mice ($0.5 \pm 0.1 \mu\text{M}$) ($P < 0.016$, Fig. 4.7). These elevations in conjugated bile acids in

hypercholanemic mice altered the overall ratio of unconjugated to conjugated bile acids. Serum bile acids in control and normocholanemic mice were ~20-25% conjugated species, whereas bile acids were 94% conjugated in hypercholanemic mice (Fig. 4.7).

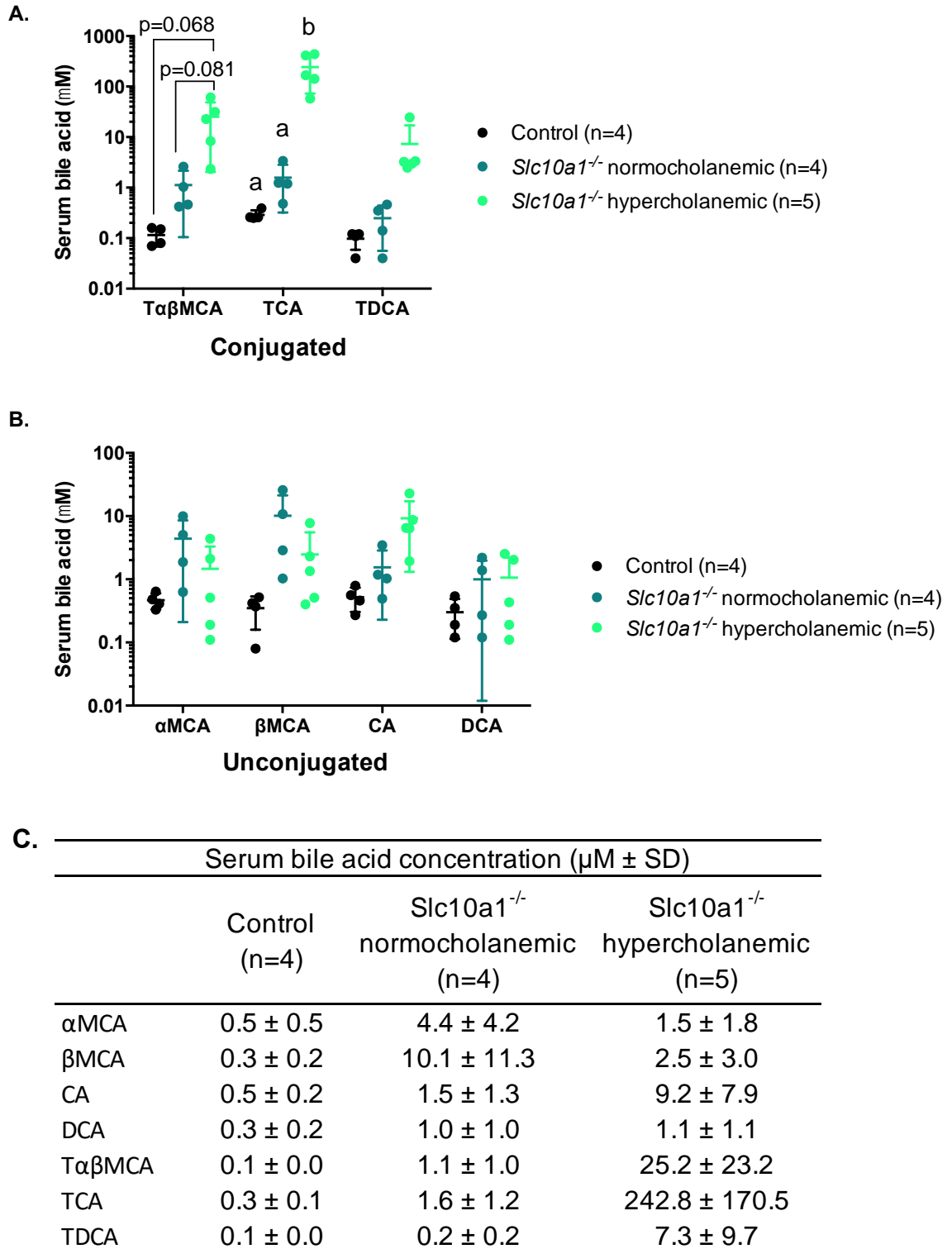


Figure 4.6. Individual serum bile acid concentrations

A. Conjugated bile acids species. B. Unconjugated bile acid species: C. Concentrations of each bile acid organized by group. Results are presented as mean \pm SD (n=4-5 mice per group) and statistical significance was determined using one-way ANOVA with Tukey's multiple comparison test, statistical differences between a and b: $P < 0.02$.

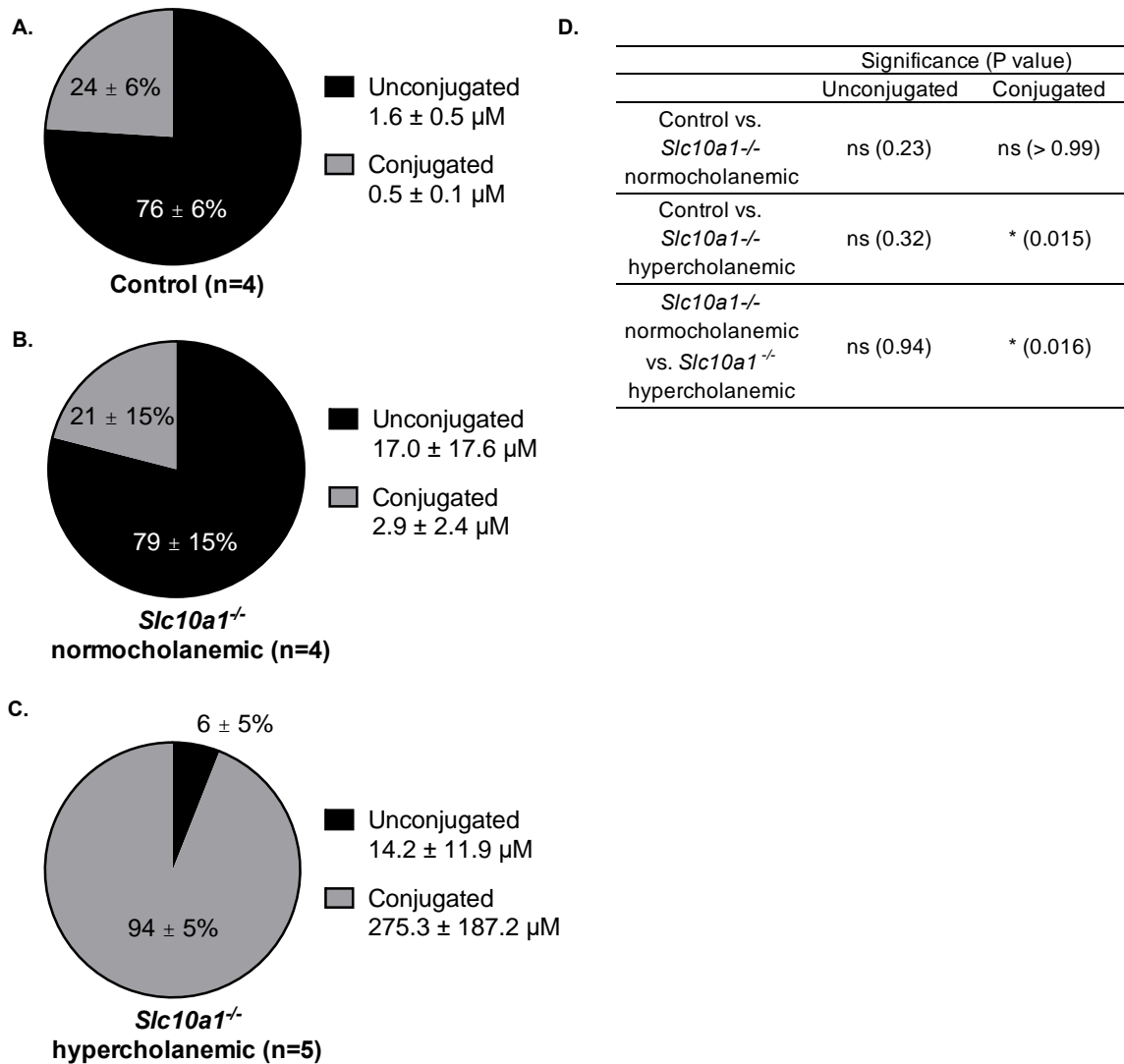


Figure 4.7. Percentages of unconjugated and conjugated bile acids

A-C. Unconjugated bile acids represent the sum of αMCA, βMCA, CA, and DCA. Conjugated bile acids represent the sum of TαβMCA, TCA, and TDCA. D. Summary of statistical differences between groups. Results are presented as mean ± SD (n=4-5 mice per group) and statistical significance was assessed using one-way ANOVA with Tukey's multiple comparison test, * P < 0.05.

To assess the relative toxicity of the serum bile acid pools in four- to six-week-old mice, compositions of cholic acid-derived species and muricholic acid-derived species were determined. Cholic acid species are more toxic whereas muricholic acids are more hydrophilic and less toxic (Chiang, 2017).

The sums of muricholic acids in the sera of mice ranged from $0.9 - 29.1 \pm 0.1 - 22.8 \mu\text{M}$ and were not significantly different between groups (Fig. 4.8). However, the sum of cholic acids was significantly elevated in *Slc10a1*^{-/-} hypercholanemic mice ($260.4 \pm 182.7 \mu\text{M}$) relative to *Slc10a1*^{-/-} normocholanemic ($2.2 \pm 3.6 \mu\text{M}$) and control mice ($1.2 \pm 0.4 \mu\text{M}$) ($P < 0.020$, Fig. 4.8). These elevations in cholic acids in hypercholanemic mice alter the ratio of muricholic acids to cholic acids. Cholic acids dominate the bile acid pool in hypercholanemic mice (89%), in contrast to normocholanemic and control mice, whose bile acid compositions were 29 and 56% cholic acid species, respectively (Fig. 4.8 A-C). These results suggest that hypercholanemic mice may have more toxic bile acid species in their sera than do control and normocholanemic mice.

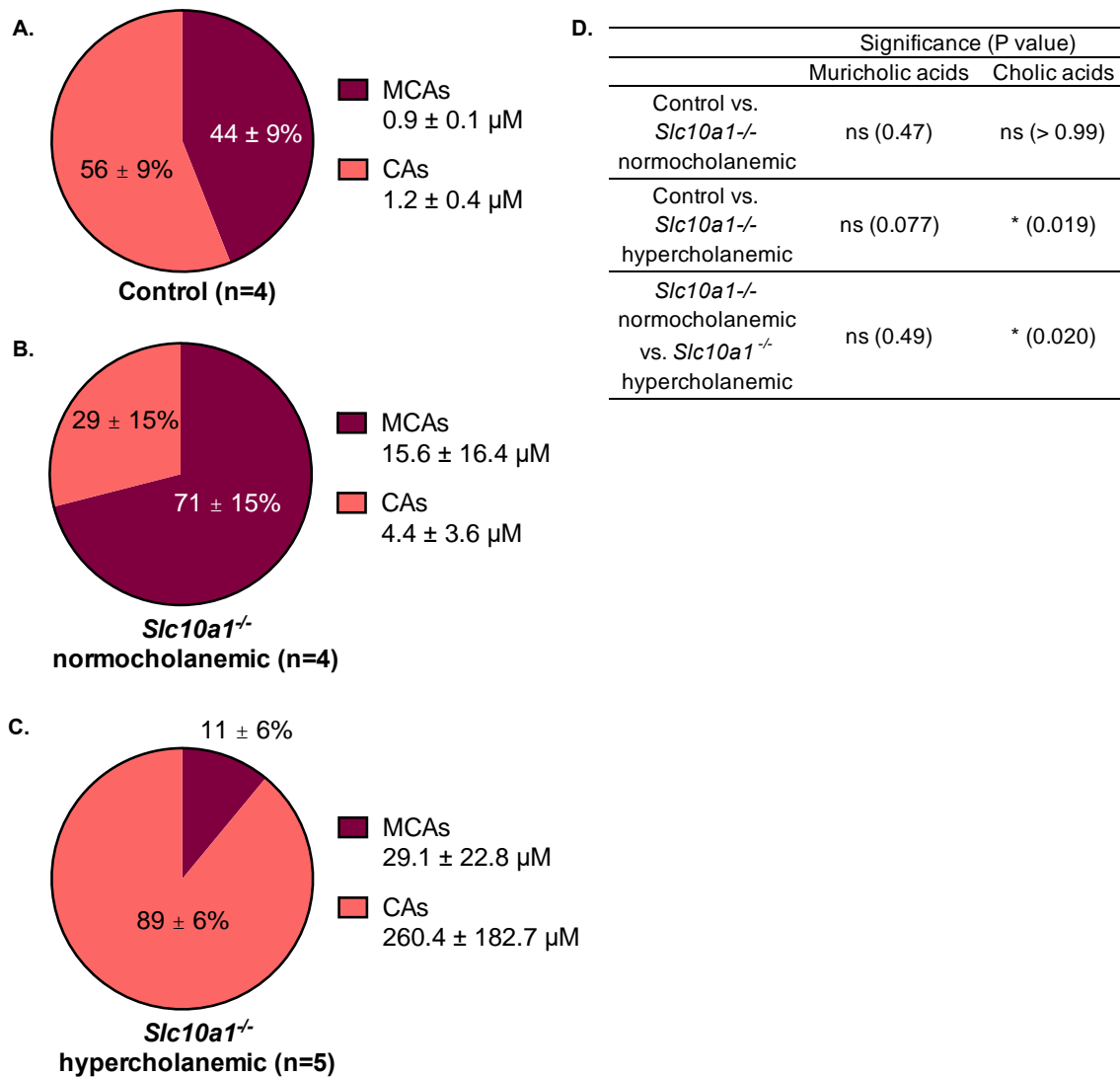


Figure 4.8. Percentages of muricholic acid and cholic acid species

A-C. Muricholic acids (MCAs) represent the sum of αMCA, βMCA, and TαβMCA. Cholic acids (CAs) represent the sum of CA, DCA, TCA, and TDCA. D. Summary of statistical differences between groups. Results are presented as mean ± SD (n=4-5 mice per group) and statistical significance was assessed using one-way ANOVA with Tukey's multiple comparison test, * P < 0.05.

4.3.4 Relative mRNA levels of hepatic bile acid uptake transporters

Serum hypercholanemia may be the result of reduced uptake of bile acids into hepatocytes. Therefore, expression levels of hepatic genes involved in bile acid uptake were evaluated in four- to six-week-old mice.

Relative mRNA levels of *Ntcp* were significantly reduced in both normocholanemic and hypercholanemic *Slc10a1*^{-/-} mice (Fig. 4.9 B, $P < 0.0001$). Hepatic mRNA expression of *Oatp1b2* was unchanged between groups (Fig. 9 C). Expression levels of *Oatp1a1* were significantly decreased in hypercholanemic mice relative to normocholanemic and control mice ($P < 0.033$, Fig. 4.9 D); *Oatp1a1* mRNA was nearly undetectable in all hypercholanemic mice. Relative mRNA levels of *Oatp1a4* were increased ~15-fold in hypercholanemic mice relative to normocholanemic and control mice ($P < 0.0030$, Fig. 4.9 E).

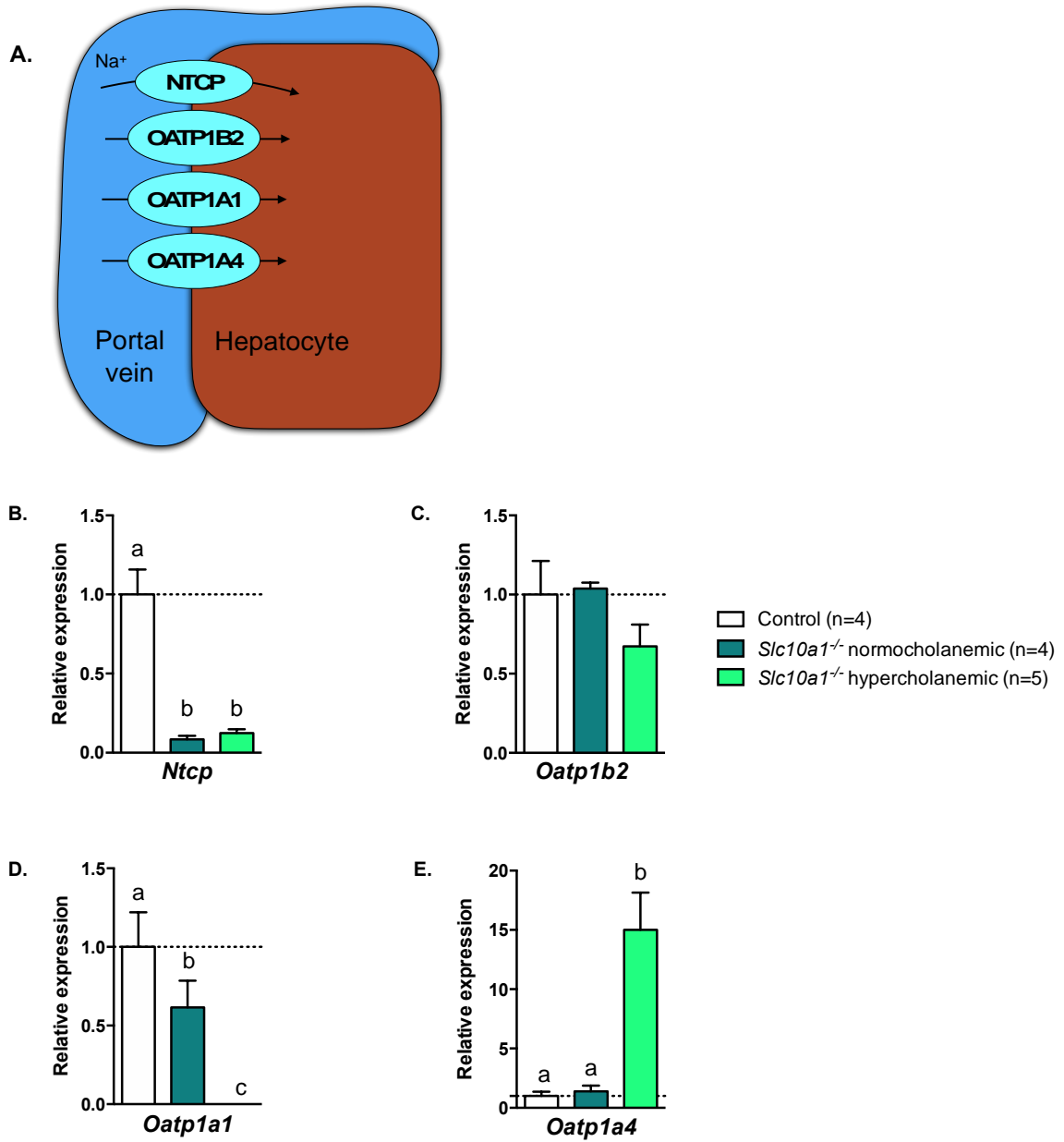


Figure 4.9. Relative mRNA expression of bile acid uptake transporters in the liver
 A. Localization of uptake transporters at the basolateral membrane of hepatocytes. Expression of B. Na⁺-taurocholate co-transporting polypeptide (*Ntcp*), and C-E. Organic anion transporting polypeptide (*Oatp*) isoforms *1b2*, *1a1*, and *1a4*. Results are presented as mean ± SEM (n=4-5 mice per group) and statistical significance was determined using one-way ANOVA with Tukey's multiple comparison tests, statistical differences between a, b, and c: P < 0.04.

4.3.5 Relative mRNA levels of bile acid efflux transporters

Expression of transporter genes that export bile acids into the bile canaliculi were also assessed in four- to six-week-old mice. The main canalicular membrane bile acid efflux transporter is bile salt export pump (BSEP), whereas multidrug resistance-associated protein 2 (MRP2) plays a more minor role and transports mainly sulfated bile acids.

Relative to control and normocholanemic mice, *Bsep* mRNA levels were reduced approximately 2 to 3-fold in hypercholanemic mice (Fig. 4.10 B, $P < 0.01$ and $P < 0.0001$, respectively). Normocholanemic mice displayed increased mRNA levels of *Bsep* compared to controls (Fig. 4.10 B, $P < 0.01$). No detectable differences were observed in *Mrp2* mRNA levels between groups (Fig. 4.10 C).

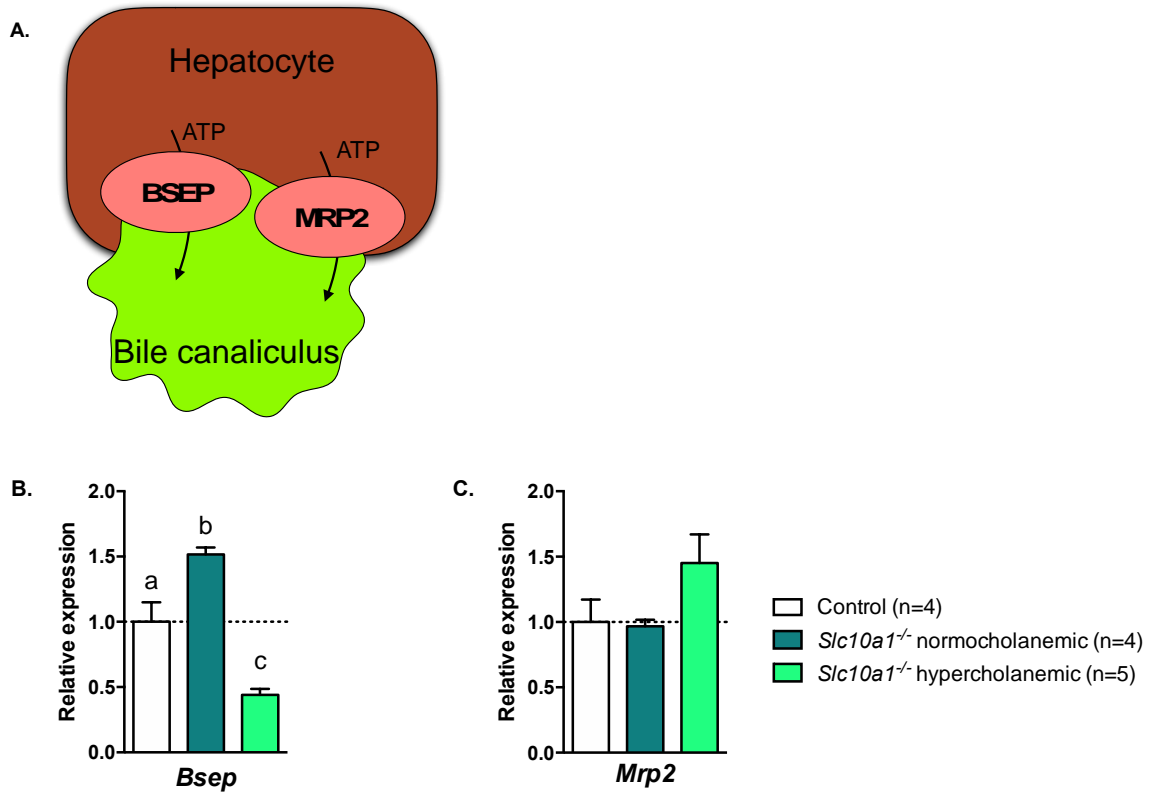


Figure 4.10. Relative mRNA expression of canalicular efflux transporters in the liver
 A. Localization of efflux transporters at the bile canalicular membrane of hepatocytes. Expression of B. Bile salt export pump (*Bsep*), and C. Multidrug resistance-associated protein 2 (*Mrp2*). Results are presented as mean \pm SEM (n=4-5 mice per group). Statistical significance was determined using one-way ANOVA with Tukey's multiple comparison test, statistical differences between *a*, *b*, and *c*: $P < 0.01$.

Under physiological conditions, basolateral efflux transporters organic solute transporters α and β (OST $\alpha\beta$) and multidrug resistance-associated protein 4 (MRP4) are not highly expressed in the liver. However, both OST $\alpha\beta$ and MRP4 can become upregulated upon dysregulated nuclear receptor signaling arising from pathology (Boyer et al., 2006; Slitt et al., 2007).

In hypercholanemic *Slc10a1*^{-/-} mice, both *Ost β* and *Mrp4* mRNA levels were significantly higher than what were detected for normocholanemic and control mice (Fig. 4.11 B & C, P < 0.05). Levels of *Ost α* mRNA were undetectable in all liver samples.

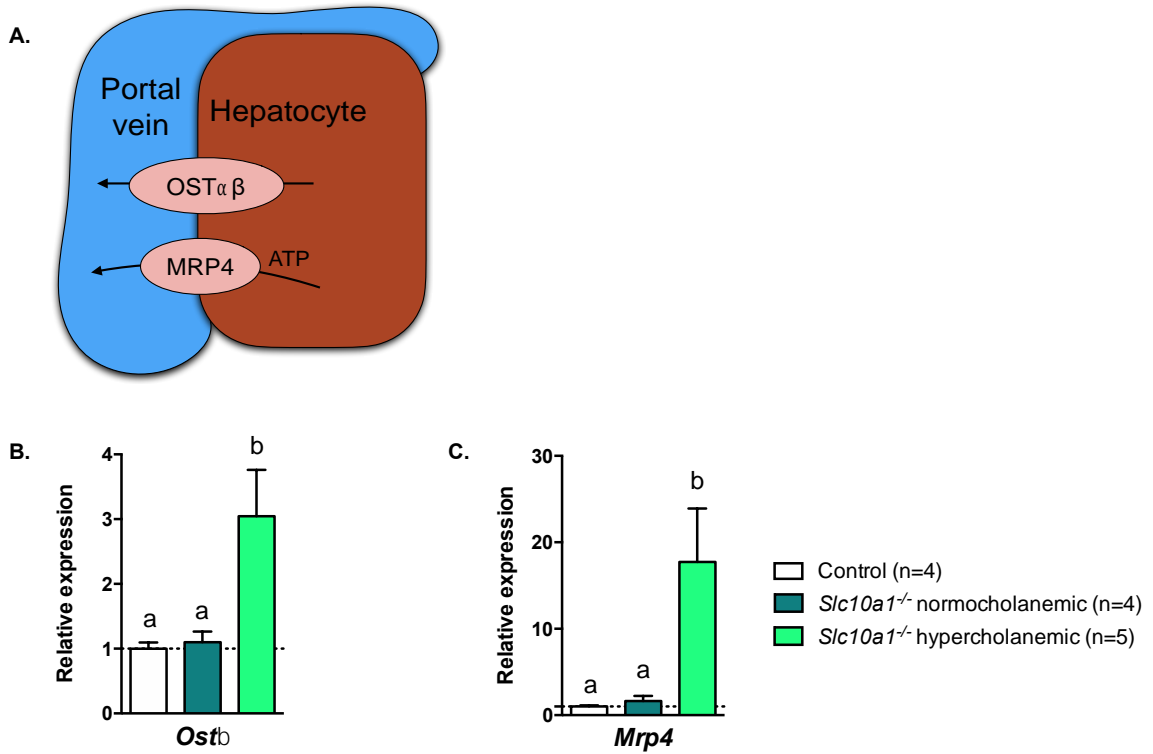


Figure 4.11. Relative mRNA expression of basolateral efflux transporters in the liver

A. Localization of efflux transporters at the basolateral membrane of hepatocytes. Expression of B. Organic solute transporter β (*Ost\beta*) and C. Multidrug resistance-associated protein 4 (*Mrp4*). Results are presented as mean \pm SEM (n=4-5 mice per group) and statistical significance was determined using one-way ANOVA with Tukey's multiple comparison test, statistical differences between a and b, $P < 0.05$.

4.3.6 Relative mRNA levels of hepatic bile acid synthesis genes

In addition to differences in hepatic transporter genes, disruption of *Slc10a1* may alter bile acid synthesis. Relative mRNA levels of the three main hepatic bile acid synthesis genes, *Cyp7a1*, *Cyp8b1*, and *Cyp27a1*, and of the transcriptional repressor of bile acid synthesis, small heterodimer partner (*Shp*), were quantified in mice four to six weeks of age.

Relative mRNA levels of *Shp* and *Cyp7a1* decreased and increased, respectively, in hypercholanemic mice compared to normocholanemic mice compared to normocholanemic mice ($P = 0.011$, Fig. 4.12 C and $P = 0.042$, Fig. 4.12 B). No significant differences in *Shp* or *Cyp7a1* mRNA levels were detected between control and hypercholanemic mice. Further, no differences were observed in *Cyp8b1* or *Cyp27a1* mRNA levels between groups (Fig. 4.12 D-E).

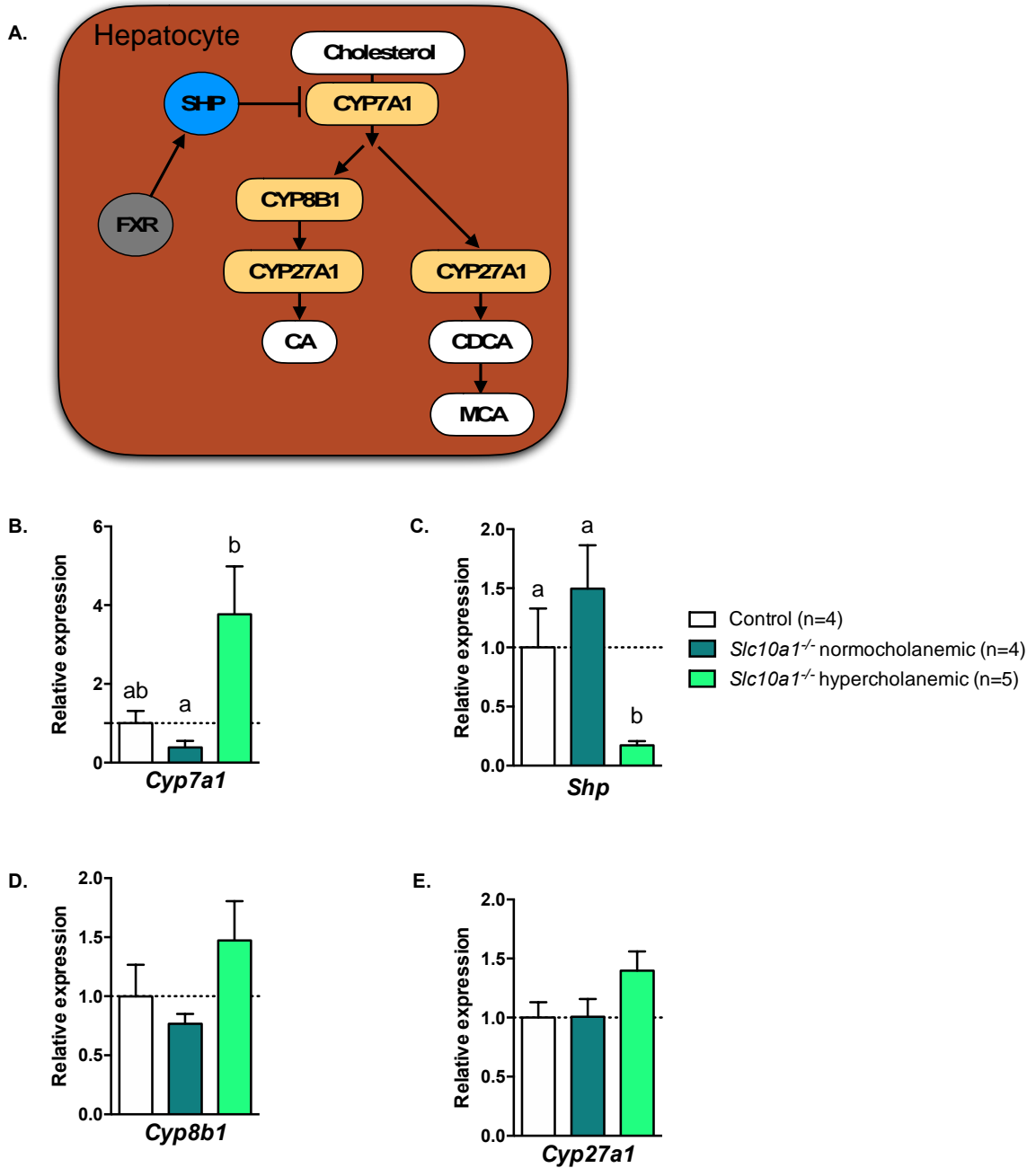


Figure 4.12. Relative mRNA levels of bile acid synthesis genes in the liver

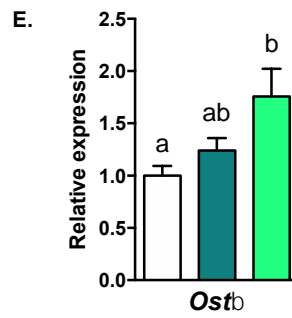
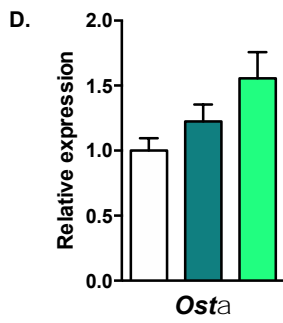
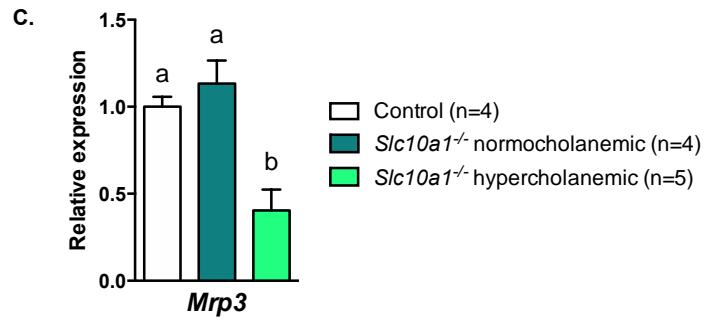
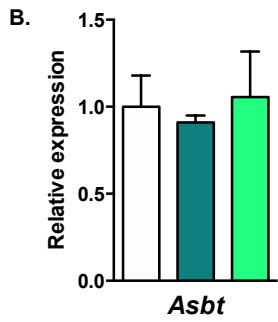
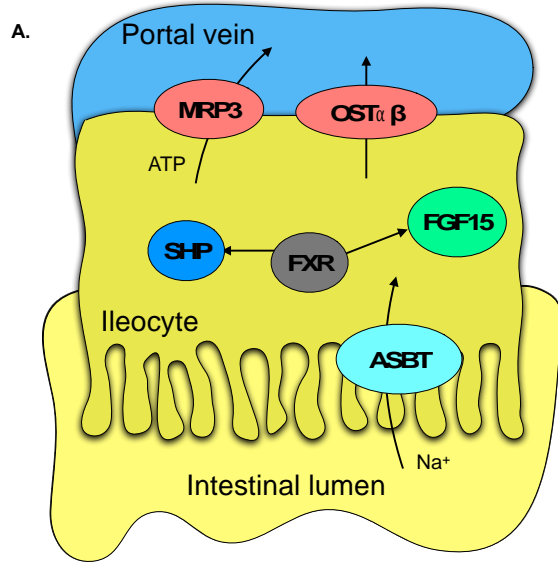
A. Bile acid synthesis occurs through CYP7A1 (rate-limiting enzyme), CYP8B1 (responsible for cholic acid (CA) synthesis), and CYP27A1 (involved in synthesis of CA and chenodeoxycholic acid (CDCA)). Bile acid-mediated activation of the nuclear receptor farnesoid X receptor (FXR) induces the production of the transcription factor small heterodimer partner (SHP), which indirectly represses *Cyp7a1*. Relative mRNA expression of B. *Cyp7a1*, C. *Shp*, D. *Cyp8b1*, and E. *Cyp27a1*. Results are presented as mean \pm SEM (n=4-5 mice per group) and statistical significance was determined using one-way ANOVA with Tukey's multiple comparison test, statistical differences between a, and b: P < 0.05.

4.3.7 Relative mRNA levels of bile acid genes in the ileum

Aside from the important role of the liver in bile acid synthesis and transport, the terminal ileum is responsible for the majority of active bile acid reuptake in the intestine. Thus, the effects of *Slc10a1* disruption on mRNA levels in the terminal ileum were assessed in four- to six-week-old mice.

Relative mRNA levels of the bile acid uptake transporter apical sodium-dependent bile acid transporter (*Asbt*) were not significantly different between groups (Fig. 4.13 B). Levels of multidrug resistance-associated protein 3 (*Mrp3*) were reduced in hypercholanemic mice relative to control and normocholanemic mice ($P < 0.0085$, Fig. 4.13 C). No detectable differences were observed in *Osta* mRNA levels between groups. However, *Ost β* expression was increased in hypercholanemic mice relative to control mice ($P = 0.048$, Fig. 4.13 D & E).

Bile acid activation of FXR in ileocytes induces *Shp* and *Fgf15*, which signal to repress bile acid uptake and synthesis in enterocytes and hepatocytes. Although *Shp* and *Fgf15* mRNA levels appear higher in hypercholanemic mice relative to controls and normocholanemic mice, there were no significant differences detected between groups (Fig. 4.13 F & G).



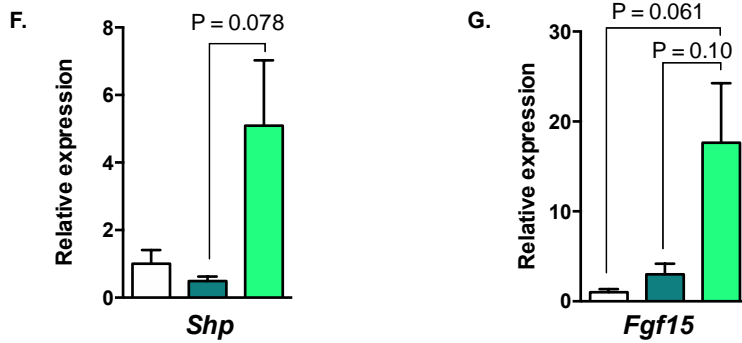


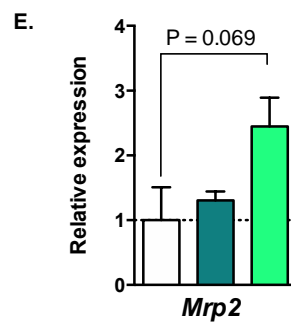
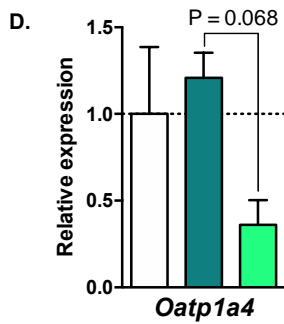
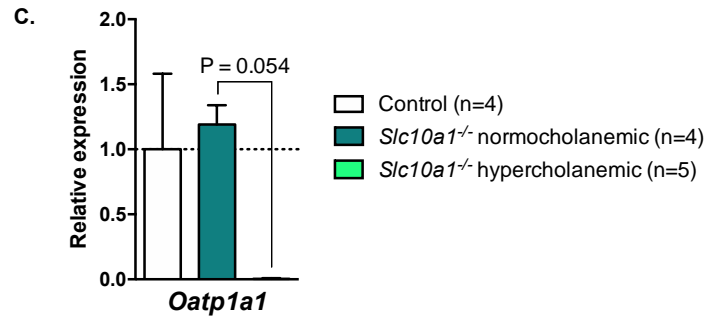
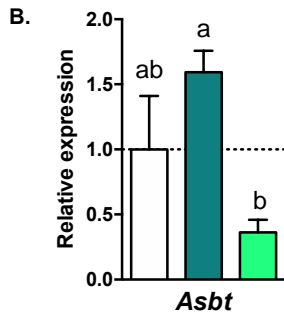
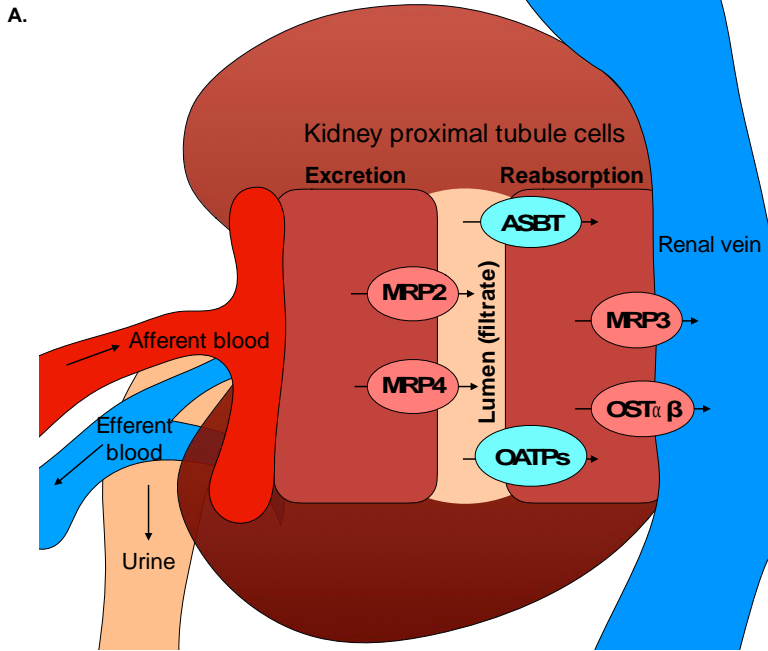
Figure 4.13. Relative mRNA levels of transporters and repressors of bile acid synthesis and uptake in the ileum

A. Bile acid uptake from the intestinal lumen occurs through apical sodium-dependent bile acid transporter (ASBT), and efflux into blood occurs through multidrug resistance-associated protein 3 (MRP3) and organic solute transporter $\alpha\beta$ (OST $\alpha\beta$). Bile acid-mediated activation of the nuclear receptor farnesoid X receptor (FXR) induces the production of the transcription factor small heterodimer partner (SHP) and the hormone fibroblast growth factor 15 (FGF15), which repress bile acid uptake and synthesis. B-G. Relative mRNA expression of B. *Asbt*, C. *Mrp3* D. *Ost α* , E. *Ost β* , F. *Shp*, and G. *Fgf15*. Results are presented as mean \pm SEM (n=4-5 mice per group) and statistical significance was determined using one-way ANOVA with Tukey's multiple comparison test, statistical differences between a and b: P < 0.05.

4.3.8 Relative mRNA levels of bile acid transporter genes in the kidney

Bile acids are minimally excreted in the urine under physiological conditions, however hypercholanemia can increase renal filtration and excretion (Alnouti, 2009). Furthermore, our hypercholanemic mice displayed signs of dehydration and blood in urine, which could be indicative of kidney damage. Relative mRNA levels of bile acid transporters in the kidney were therefore assessed in four- to six-week-old mice.

Relative mRNA levels of the uptake transporter *Asbt* were significantly reduced in hypercholanemic mice relative to normocholanemic mice (Fig. 4.14 B, $P < 0.012$). However, no significant differences were detected in relative mRNA levels for uptake transporters *Oatp1a1* and *Oatp1a4* (Fig. 4.14 C & D). No significant differences were observed between groups for mRNA levels of efflux transporters *Mrp2* and *Mrp4*, which export bile acids from renal cells into the filtrate for urinary excretion. Relative mRNA levels of efflux transporters *Ost α* , *Ost β* , and *Mrp3*, which favour secretion of bile acids from renal cells back into the blood, were significantly increased in hypercholanemic mice relative to normocholanemic and control mice (Fig. 4.14 G-I, *Ost α* and *Ost β* : $P < 0.001$, *Mrp3*: $P < 0.05$).



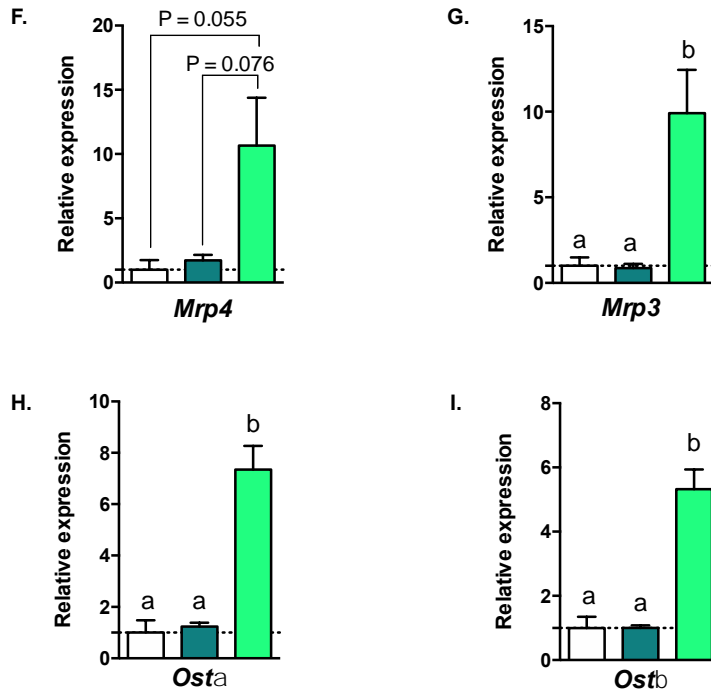


Figure 4.14. Relative mRNA levels of bile acid transporters in the kidney

A. Bile acid filtration at the kidney. Bile acids are excreted into the tubule lumen for urinary excretion by multidrug resistance-associated proteins 2 and 4 (MRP2 and MRP4). From the lumen, bile acids can be reabsorbed into proximal tubule cells by apical sodium-dependent bile acid transporter (ASBT) and organic anion transporting polypeptides (OATP1A1 and OATP1A4). Bile acids are exported back into the blood by organic solute transporters $\alpha\beta$ (OST $\alpha\beta$) and MRP3. B-I. Relative mRNA expression of B. *Asbt*, C. *Oatp1a1* D. *Oatp1a4*, E. *Mrp2*, F. *Mrp4*, and G. *Mrp3*, H. *Osta*, I. *Ostb* Results are presented as mean \pm SEM (n=4-5 mice per group) and statistical significance was determined using one-way ANOVA with Tukey's multiple comparison test, statistical differences between a, and b: P < 0.05.

4.3.9 Hepatic uptake of rosuvastatin

In human hepatocytes, NTCP is responsible for ~35% of rosuvastatin uptake (Ho et al., 2006; Bi et al., 2013). To determine the effect of *Slc10a1* disruption on hepatic uptake of rosuvastatin, a single dose of 10 mg/kg rosuvastatin was administered to ten-week-old mice by oral gavage. Two hours after rosuvastatin administration, mice were euthanized; blood was collected via cardiac puncture, and livers were harvested.

Serum rosuvastatin concentrations were 25.6 ± 13.7 ng/mL and 19.0 ± 10.6 ng/mL in *Slc10a1*^{-/-} and control mice, respectively (Fig. 4.15 A). Liver rosuvastatin concentrations were 861.9 ± 279.6 ng/g and 1028 ± 511.2 ng/g in *Slc10a1*^{-/-} and control mice, respectively (Fig. 4.15 B). No significant differences were observed in serum or liver concentrations of rosuvastatin between the two mouse genotypes (Figure 4.15 A & B). The liver-to-serum concentration ratios, which are important determinants of reliance on hepatic transport processes, were not significantly different, at 42.8 and 60.3 in *Slc10a1*^{-/-} mice and control animals, respectively (Fig. 4.15 C, P = 0.34).

To determine whether *Slc10a1*^{-/-} disruption affected bile acid transporter expression in these mice, mRNA levels for hepatic transporters were evaluated. Aside from the expected difference in *Ntcp* mRNA expression (P = 0.0040, Fig. 4.16 A), no significant differences were observed in hepatic uptake or efflux transporters between ten-week-old control and *Slc10a1*^{-/-} mice (Fig. 4.16 A & B).

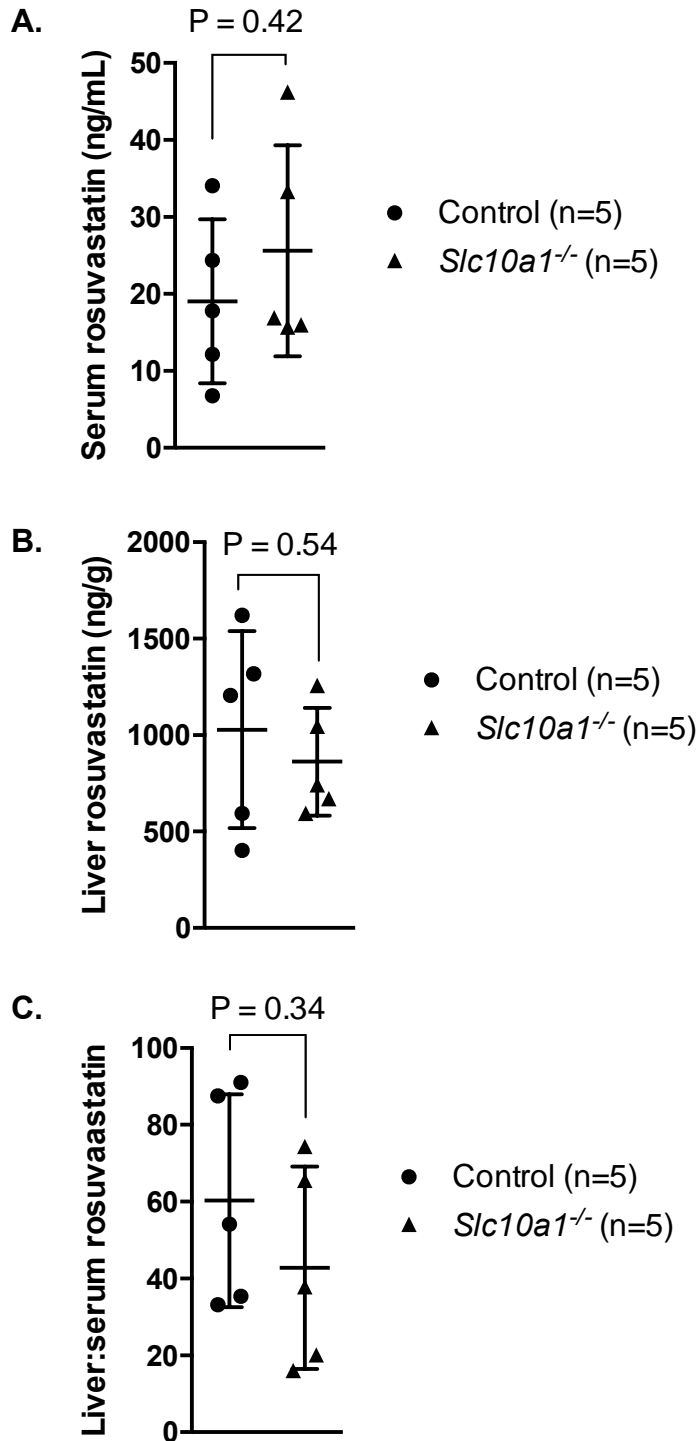


Figure 4.15. Hepatic disposition of orally administered rosuvastatin (10mg/kg) in control and *Slc10a1*^{-/-} mice.

A. Concentrations of rosuvastatin in serum, expressed as ng/mL. B. Concentrations of rosuvastatin in liver, expressed as ng rosuvastatin per g liver tissue. C. Liver-to-serum ratio of rosuvastatin, an important indicator of rosuvastatin uptake by hepatic transporters. Results are presented as mean \pm SD (n=5 mice per group) and statistical differences were determined using Student's t tests.

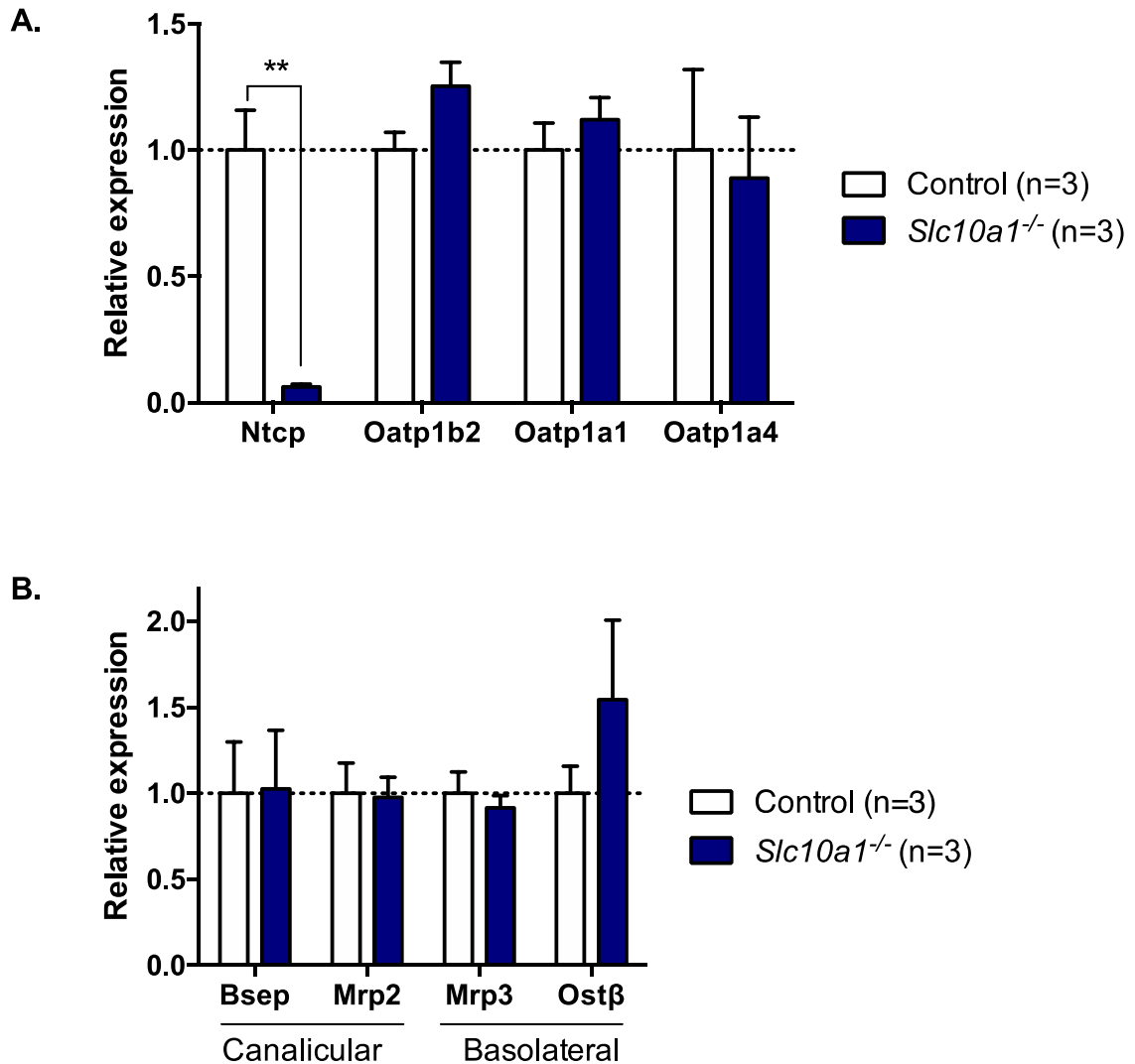


Figure 4.16. Hepatic mRNA expression of bile acid uptake and efflux transporters in ten-week-old mice

A. Bile acid uptake transporter at the basolateral membrane of hepatocytes. B. Bile acid efflux transporters at the canalicular (*Bsep*, *Mrp2*) and basolateral (*Mrp3* and *Ostβ*) membranes of hepatocytes. Results are presented as mean \pm SEM (n=3 mice per group) and statistical differences were assessed using Student's t tests.

4.4 Discussion

NTCP (encoded by gene *SLC10A1*) is the key bile acid uptake transporter on the basolateral membrane of hepatocytes (Dawson et al., 2009) and may be important for the hepatic uptake of rosuvastatin (Ho et al., 2006; Bi et al., 2013). However, limited information exists regarding bile acid dynamics and gene expression in mouse models of *Slc10a1* disruption, and hepatic uptake of rosuvastatin has not been evaluated in *Slc10a1*^{-/-} mice. This study assessed serum bile acid composition, mRNA expression in the liver, ileum, and kidney, and hepatic uptake of rosuvastatin in *Slc10a1*^{-/-} mice.

A bimodal bile acid phenotype was observed in our *Slc10a1*^{-/-} mice. Approximately 55% of *Slc10a1*^{-/-} mice exhibited decreased body weights from three to seven weeks of age, which normalized with control body weights by eight weeks of age. Serum bile acids were not significantly elevated in these mice, no additional phenotypic traits were observed, and gene expression was comparable to what was observed in control mice. Conversely, serum hypercholanemia was observed in approximately 45% of *Slc10a1*^{-/-} mice, and these mice failed to thrive passed seven weeks of age.

Mendelian frequencies were not observed in the proportions of hypercholanemic and normocholanemic mice in any given litter, suggesting that disruption of *Slc10a1*^{-/-} is associated with incomplete penetrance. Reduced penetrance is also observed in the inherited bile acid condition Familial Hypercholanemia. Three individuals homozygous for mutations in the *TJP2* gene, which is important in tight junction formation between hepatocytes and

cholangiocytes of the bile ducts, were unaffected by this genetic deficiency.

However, their siblings suffered from fat malabsorption, rickets, and deficiency of vitamin K subsequent to reduced bile acids in the intestinal lumen (van Mil et al., 2005).

Mice that failed to thrive displayed striking elevations in conjugated and cholic acid species. The prototypical NTCP substrate, taurocholic acid, was highly elevated in hypercholanemic *Slc10a1*^{-/-} mice. Increased cholic acid species in mouse serum may suggest greater toxicity in the bile acid pools of hypercholanemic *Slc10a1*^{-/-} mice. However, hepatic concentrations of bile acids were not quantified, and mRNA expression of the *Cyp8b1*, the precursor to cholic acid synthesis, was no different between control and hypercholanemic mice. Therefore, it remains unclear whether the hepatic composition of bile acids is also dominated by cholic acid species. Regardless of the composition of serum bile acids in these mice, the extent of hypercholanemia likely results in bile acid spillover into the kidney in these mice. The decreased mRNA expression of uptake transporter genes and increased mRNA expression of efflux transporter genes in the kidney are indicative of elevated bile acids in the kidney (Slitt et al., 2007).

Our findings of reduced survival in hypercholanemic mice are inconsistent with previous reports of *Slc10a1*^{-/-} mice, where mortality was not observed (Slijepcevic et al., 2015; Mao et al., 2019). As serum bile acid concentrations in our hypercholanemic mice were comparable or even lower than concentrations observed in the alternative studies, it remains unclear why our mice were unable

to thrive. However, the enlarged gallbladders, bile deposits in bile canaliculi, and lack of prominent bile ducts in hypercholanemic mice suggest disruption of gallbladder emptying. This would decrease bile acid levels within the intestinal lumen, limiting food emulsification and decreasing absorption of vital nutrients.

Numerous changes in mRNA expression levels of bile acid transporters and synthesis genes were observed in hypercholanemic *Slc10a1*^{-/-} mice relative to normocholanemic *Slc10a1*^{-/-} mice and controls. Hepatic mRNA levels of *Cyp7a1*, *Oatp1a4*, *Ostβ*, and *Mrp4*, were increased, whereas *Oatp1a1*, *Bsep* and *Shp* were decreased in hypercholanemic mice. The rodent transporter OATP1A1 is important in hepatic bile acid uptake transport in mice, especially in the absence of NTCP (Slijepcevic et al., 2015). Levels of *Oatp1a1* mRNA were nearly undetectable in our hypercholanemic mice. Consistent with reports from Slijepcevic et al., we speculate that hypercholanemia results from absence of OATP1A1 and NTCP in these mice. Simulations by Cravetto et al. showed that reduced hepatic extraction of bile acids is likely the most important contributor to elevated serum bile acids (Cravetto et al., 1988).

The major nuclear receptor involved in bile acid homeostasis is FXR (Li and Chiang, 2013). Nuclear receptors PXR and CAR also act as complementary pathways for bile acid homeostasis and detoxification, especially in cases of disrupted FXR signaling (Schuetz et al., 2001; Guo et al., 2003; Wagner et al., 2005). Hepatic nuclear receptors are regulated by the fasted and fed states. Activity of FXR and VDR is reduced during the fasted state, whereas activity of PXR and CAR is enhanced in the fasted state (Ding et al., 2006; Wieneke et al.,

2007; Grasfeder et al., 2009; Preidis et al., 2017; Aatsinki et al., 2019). Relative mRNA expression of genes in our hypercholanemic mice reflected changes that occur during fasting; levels of hepatic mRNA for direct FXR target genes *Bsep* and *Shp* were decreased in hypercholanemic mice. Furthermore, consistent with PXR activation in the fasted state, *Oatp1a1* mRNA was reduced and *Oatp1a4* was increased in hypercholanemic mice. The increase in *Mrp4* mRNA observed in livers of our hypercholanemic mice may be the result of increased activity of CAR. Significantly decreased mRNA levels of *Mrp3* in the ileum are consistent with reduced VDR activity in the fasted state.

In our hypercholanemic mice, significantly elevated mRNA levels of the major bile acid synthesis gene *Cyp7a1* are consistent with reduced expression of its repressor, *Shp*. However, these observations are inconsistent with the trends of mRNA expression of *Shp* and *Fgf15* observed in the ilea of our hypercholanemic mice. One possible explanation is increased retention of bile acids in ileocytes, which has been reported in cases where intestinal cells sense low levels of bile acids within the intestinal lumen. The cells react by conserving intracellular stores of bile acids (Hofmann, 2003; Lanzini et al., 2003), which would explain enhanced *Shp* and *Fgf15* mRNA levels. However, recent studies have also indicated enterocytes can sense high serum bile acid concentrations, resulting in induction of FGF15/19 signaling (Slijepcevic et al., 2017). To determine the bases for these inconsistencies, further evaluation of serum FGF15 concentrations and FGF15 signaling at the hepatocyte is warranted.

In mice ten weeks of age, no significant differences were observed in the serum or liver concentrations of rosuvastatin, nor in the serum-to-liver ratio of rosuvastatin in *Slc10a1*^{-/-} mice. Expression of mRNA levels for hepatic transporters were no different between ten-week-old control and *Slc10a1*^{-/-} mice. Although serum bile acids were not quantified in these mice, the absence of differences in transporter expression suggest these mice were normocholanemic.

Important species differences in hepatic uptake of bile acids should be considered when interpreting findings from mouse models. Human OATP1B1 and OATP1B3 are hepatocyte-specific transporters that are highly expressed in the liver and possess a single murine ortholog, OATP1B2 (Roth et al., 2012). In addition, OATP1A1 and OATP1A4 localize to the basolateral membrane of mouse hepatocytes (Geier et al., 2007), however the human ortholog, OATP1A2, is not abundant in human hepatocytes (Lee et al., 2005).

In the context of bile acid uptake, murine OATP1A1 is an important rodent bile acid transporter and shares a similar substrate profile with NTCP (Hata et al., 2003). Although the repression of *Oatp1a1* in hypercholanemic mice cannot be directly translated to humans, findings may still be indicative of overall hepatic nuclear receptor signaling during hypercholanemia. This is supported by clinical studies describing vitamin D deficiency in individuals with homozygous loss of function genetic variation in *SLC10A1* (Vaz et al., 2015; Deng et al., 2016; Liu et al., 2017; Qiu et al., 2017).

In the context of rosuvastatin uptake, murine OATP1A1 and OATP1A4 act along with OATP1B2 to mimic the hepatic uptake functions of human OATP1B1

and OATP1B3 (Iusuf et al., 2012). Previous studies in mouse models of OATP deficiency have found that murine isoforms of OATP1A and OATP1B are important in hepatic rosuvastatin uptake in mice (DeGorter et al., 2012; Iusuf et al., 2013). Importantly, in *Oatp1a/1b*^{-/-} mice, systemic concentrations of rosuvastatin were ~8-fold higher in *Oatp1a/1b*^{-/-} mice compared to controls, however hepatic concentrations were unchanged between groups. This suggests that in the event of OATP1A/1B deficiency, there are additional hepatic uptake transporters with lower affinity for rosuvastatin that can maintain some degree of hepatic rosuvastatin uptake. The presence of OATP1A isoforms in mouse hepatocytes but not human hepatocytes is a major species difference that could negate a potential relevance of NTCP to rosuvastatin transport in mice. The absence of OATP1A isoforms in human hepatocytes likely provides a more important role for NTCP in statin disposition in humans. This is especially true in the context of genetic deficiency or pharmacological inhibition of OATPs, which is relatively common. Evidence suggests that NTCP is important in the hepatic uptake of pravastatin in humans, another hydrophilic statin (Lu et al., 2016).

Taken together, hypercholanemic *Slc10a1*^{-/-} mice display hepatic gene expression that is consistent with nuclear receptor activity observed in the fasted state. This is supported by enlarged gallbladders and lack functional bile ducts, which may decrease bile acid concentrations in the intestinal lumen. Additionally, transporter expression and bile casts in the kidneys of hypercholanemic mice suggest that excessive renal accumulation of bile acids may lead to their demise. Failure of adequate compensatory bile acid uptake via OATP1A1 may represent

the basis for profound hypercholanemia observed in a subset of *Slc10a1*^{-/-} mice. Despite differences in hepatic uptake transporters between mice and humans, our findings of likely altered hepatic nuclear receptor signaling in the liver merit investigation in humans. In terms of pharmacotherapy, NTCP does not appear important in hepatic rosuvastatin uptake in mice, however the relevance of NTCP to human hepatic rosuvastatin disposition should be investigated.

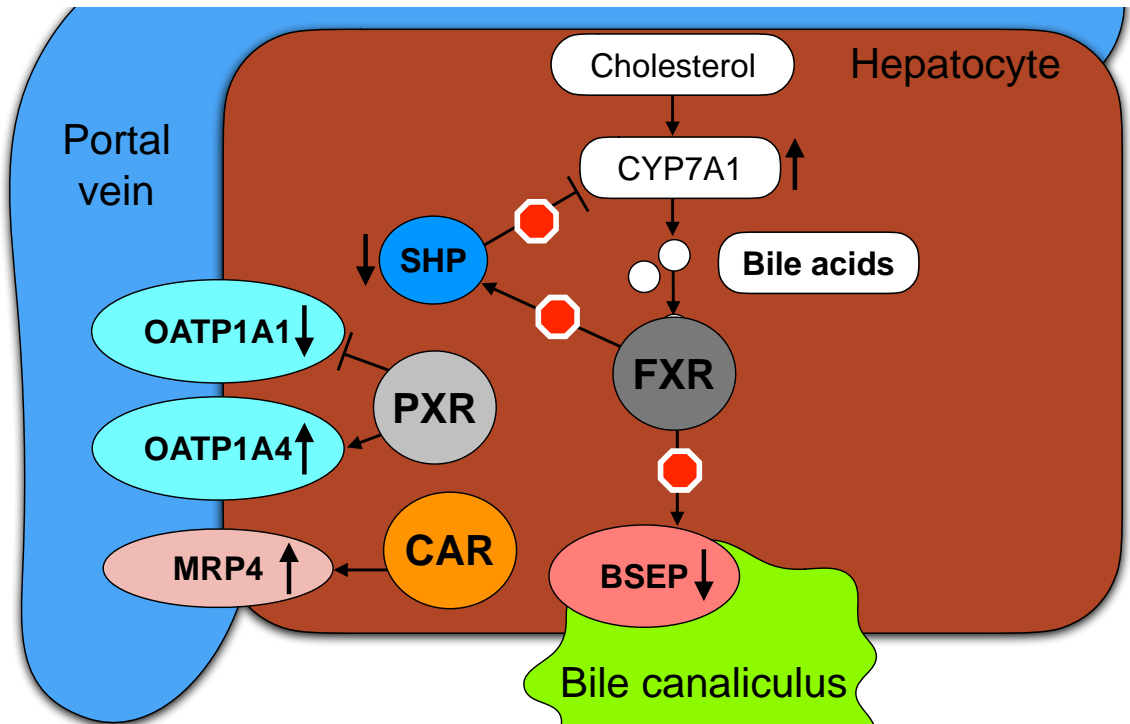


Figure 4.17. Hypothesized alterations in nuclear receptor signaling in our hypercholanemic *Slc10a1*^{-/-} mice

The major findings in our hypercholanemic mice are reduced *Oatp1a1*, *Bsep*, and *Shp* expression, along with elevated *Oatp1a4* and *Mrp4* expression. These changes are consistent with upregulated PXR and CAR and downregulated FXR observed in the fasted state. Together with reduced body weights, enlarged gallbladders, and serum hypercholanemia, it is likely that reduced bile acids in the lumen of the intestine diminishes nutrient absorption in hypercholanemic *Slc10a1*^{-/-} mice, resulting in fasted state gene expression in the liver.

4.5 References

- Aatsinki SM, Elkhwanky MS, Kummu O, Karpale M, Buler M, Viitala P, Rinne V, Mutikainen M, Tavi P, Franko A, Wiesner RJ, Chambers KT, Finck BN, and Hakkola J (2019) Fasting-Induced Transcription Factors Repress Vitamin D Bioactivation, a Mechanism for Vitamin D Deficiency in Diabetes. *Diabetes* **68**:918-931.
- Alnouti Y (2009) Bile Acid sulfation: a pathway of bile acid elimination and detoxification. *Toxicol Sci* **108**:225-246.
- Bi YA, Qiu X, Rotter CJ, Kimoto E, Piotrowski M, Varma MV, Ei-Kattan AF, and Lai Y (2013) Quantitative assessment of the contribution of sodium-dependent taurocholate co-transporting polypeptide (NTCP) to the hepatic uptake of rosuvastatin, pitavastatin and fluvastatin. *Biopharm Drug Dispos* **34**:452-461.
- Boyer JL, Trauner M, Mennone A, Soroka CJ, Cai SY, Moustafa T, Zollner G, Lee JY, and Ballatori N (2006) Upregulation of a basolateral FXR-dependent bile acid efflux transporter OSTalpha-OSTbeta in cholestasis in humans and rodents. *Am J Physiol Gastrointest Liver Physiol* **290**:G1124-1130.
- Chen C, Stock JL, Liu X, Shi J, Van Deusen JW, DiMattia DA, Dullea RG, and de Morais SM (2008) Utility of a novel Oatp1b2 knockout mouse model for evaluating the role of Oatp1b2 in the hepatic uptake of model compounds. *Drug Metab Dispos* **36**:1840-1845.
- Chiang JY (2013) Bile acid metabolism and signaling. *Compr Physiol* **3**:1191-1212.
- Chiang JY (2017) Recent advances in understanding bile acid homeostasis. *F1000Res* **6**:2029.
- Cravetto C, Molino G, Hofmann AF, Belforte G, and Bona B (1988) Computer simulation of portal venous shunting and other isolated hepatobiliary defects of the enterohepatic circulation of bile acids using a physiological pharmacokinetic model. *Hepatology* **8**:866-878.
- Dawson PA, Lan T, and Rao A (2009) Bile acid transporters. *J Lipid Res* **50**:2340-2357.
- DeGorter MK, Tirona RG, Schwarz UI, Choi YH, Dresser GK, Suskin N, Myers K, Zou G, Iwuchukwu O, Wei WQ, Wilke RA, Hegele RA, and Kim RB (2013) Clinical and pharmacogenetic predictors of circulating atorvastatin and

- rosuvastatin concentrations in routine clinical care. *Circ Cardiovasc Genet* **6**:400-408.
- DeGorter MK, Urquhart BL, Gradhand U, Tirona RG, and Kim RB (2012) Disposition of atorvastatin, rosuvastatin, and simvastatin in *oatp1b2*^{-/-} mice and intraindividual variability in human subjects. *J Clin Pharmacol* **52**:1689-1697.
- Deng M, Mao M, Guo L, Chen FP, Wen WR, and Song YZ (2016) Clinical and molecular study of a pediatric patient with sodium taurocholate cotransporting polypeptide deficiency. *Exp Ther Med* **12**:3294-3300.
- Ding X, Lichti K, Kim I, Gonzalez FJ, and Staudinger JL (2006) Regulation of constitutive androstane receptor and its target genes by fasting, cAMP, hepatocyte nuclear factor alpha, and the coactivator peroxisome proliferator-activated receptor gamma coactivator-1alpha. *J Biol Chem* **281**:26540-26551.
- Geier A, Wagner M, Dietrich CG, and Trauner M (2007) Principles of hepatic organic anion transporter regulation during cholestasis, inflammation and liver regeneration. *Biochim Biophys Acta* **1773**:283-308.
- Grasfeder LL, Gaillard S, Hammes SR, Ilkayeva O, Newgard CB, Hochberg RB, Dwyer MA, Chang CY, and McDonnell DP (2009) Fasting-induced hepatic production of DHEA is regulated by PGC-1alpha, ERRalpha, and HNF4alpha. *Molecular endocrinology (Baltimore, Md)* **23**:1171-1182.
- Guo GL, Lambert G, Negishi M, Ward JM, Brewer HB, Jr., Kliewer SA, Gonzalez FJ, and Sinal CJ (2003) Complementary roles of farnesoid X receptor, pregnane X receptor, and constitutive androstane receptor in protection against bile acid toxicity. *J Biol Chem* **278**:45062-45071.
- Hata S, Wang P, Eftychiou N, Ananthanarayanan M, Batta A, Salen G, Pang KS, and Wolkoff AW (2003) Substrate specificities of rat *oatp1* and *ntcp*: implications for hepatic organic anion uptake. *Am J Physiol Gastrointest Liver Physiol* **285**:G829-839.
- Ho RH, Tirona RG, Leake BF, Glaeser H, Lee W, Lemke CJ, Wang Y, and Kim RB (2006) Drug and bile acid transporters in rosuvastatin hepatic uptake: function, expression, and pharmacogenetics. *Gastroenterology* **130**:1793-1806.
- Hofmann AF (2003) Inappropriate ileal conservation of bile acids in cholestatic liver disease: homeostasis gone awry. *Gut* **52**:1239-1241.
- Iusuf D, van de Steeg E, and Schinkel AH (2012) Functions of OATP1A and 1B transporters in vivo: insights from mouse models. *Trends in pharmacological sciences* **33**:100-108.

- Iusuf D, van Esch A, Hobbs M, Taylor M, Kenworthy KE, van de Steeg E, Wagenaar E, and Schinkel AH (2013) Murine Oatp1a/1b Uptake Transporters Control Rosuvastatin Systemic Exposure Without Affecting Its Apparent Liver Exposure. *Molecular Pharmacology* **83**:919.
- Kosters A and Karpen SJ (2008) Bile acid transporters in health and disease. *Xenobiotica* **38**:1043-1071.
- Lanzini A, De Tavonatti MG, Panarotto B, Scalia S, Mora A, Benini F, Baisini O, and Lanzarotto F (2003) Intestinal absorption of the bile acid analogue ⁷⁵Se-homocholeic acid-taurine is increased in primary biliary cirrhosis, and reverts to normal during ursodeoxycholic acid administration. *Gut* **52**:1371-1375.
- Lee W, Glaeser H, Smith LH, Roberts RL, Moeckel GW, Gervasini G, Leake BF, and Kim RB (2005) Polymorphisms in human organic anion-transporting polypeptide 1A2 (OATP1A2): implications for altered drug disposition and central nervous system drug entry. *J Biol Chem* **280**:9610-9617.
- Li J and Dawson PA (2019) Animal models to study bile acid metabolism. *Biochim Biophys Acta Mol Basis Dis* **1865**:895-911.
- Li T and Chiang JY (2013) Nuclear receptors in bile acid metabolism. *Drug Metab Rev* **45**:145-155.
- Link E, Parish S, Armitage J, Bowman L, Heath S, Matsuda F, Gut I, Lathrop M, Collins R, and Grp SC (2008) SLCO1B1 variants and statin-induced myopathy - A genomewide study. *New Engl J Med* **359**:789-799.
- Liu R, Chen C, Xia X, Liao Q, Wang Q, Newcombe PJ, Xu S, Chen M, Ding Y, Li X, Liao Z, Li F, Du M, Huang H, Dong R, Deng W, Wang Y, Zeng B, Pan Q, Jiang D, Zeng H, Sham P, Cao Y, Maxwell PH, Gao ZL, Peng L, and Wang Y (2017) Homozygous p.Ser267Phe in SLC10A1 is associated with a new type of hypercholanemia and implications for personalized medicine. *Sci Rep* **7**:9214.
- Lu XF, Zhou Y, Bi KS, and Chen XH (2016) Mixed effects of OATP1B1, BCRP and NTCP polymorphisms on the population pharmacokinetics of pravastatin in healthy volunteers. *Xenobiotica* **46**:841-849.
- Mao F, Liu T, Hou X, Zhao H, He W, Li C, Jing Z, Sui J, Wang F, Liu X, Han J, Borchers CH, Wang JS, and Li W (2019) Increased sulfation of bile acids in mice and human subjects with sodium taurocholate cotransporting polypeptide deficiency. *J Biol Chem* **294**:11853-11862.
- Medwid S, Li MMJ, Knauer MJ, Lin K, Mansell SE, Schmerk CL, Zhu C, Griffin KE, Yousif MD, Dresser GK, Schwarz UI, Kim RB, and Tirona RG (2019) Fexofenadine and Rosuvastatin Pharmacokinetics in Mice with Targeted

Disruption of Organic Anion Transporting Polypeptide 2B1. *Drug Metab Dispos* **47**:832-842.

Preidis GA, Kim KH, and Moore DD (2017) Nutrient-sensing nuclear receptors PPAR α and FXR control liver energy balance. *J Clin Invest* **127**:1193-1201.

Qiu JW, Deng M, Cheng Y, Atif RM, Lin WX, Guo L, Li H, and Song YZ (2017) Sodium taurocholate cotransporting polypeptide (NTCP) deficiency: Identification of a novel SLC10A1 mutation in two unrelated infants presenting with neonatal indirect hyperbilirubinemia and remarkable hypercholanemia. *Oncotarget* **8**:106598-106607.

Roth M, Obaidat A, and Hagenbuch B (2012) OATPs, OATs and OCTs: the organic anion and cation transporters of the SLCO and SLC22A gene superfamilies. *Br J Pharmacol* **165**:1260-1287.

Schuetz EG, Strom S, Yasuda K, Lecureur V, Assem M, Brimer C, Lamba J, Kim RB, Ramachandran V, Komoroski BJ, Venkataramanan R, Cai H, Sinal CJ, Gonzalez FJ, and Schuetz JD (2001) Disrupted bile acid homeostasis reveals an unexpected interaction among nuclear hormone receptors, transporters, and cytochrome P450. *J Biol Chem* **276**:39411-39418.

Slijepcevic D, Abbing RLPR, Katafuchi T, Blank A, Donkers JM, van Hoppe S, de Waart DR, Tolenaars D, van der Meer JHM, Wildenberg M, Beuers U, Elferink RPJO, Schinkel AH, and van de Graaf SFJ (2017) Hepatic Uptake of Conjugated Bile Acids Is Mediated by Both Sodium Taurocholate Cotransporting Polypeptide and Organic Anion Transporting Polypeptides and Modulated by Intestinal Sensing of Plasma Bile Acid Levels in Mice. *Hepatology* **66**:1631-1643.

Slijepcevic D, Kaufman C, Wichers CG, Gilglioni EH, Lempp FA, Duijst S, de Waart DR, Elferink RP, Mier W, Stieger B, Beuers U, Urban S, and van de Graaf SF (2015) Impaired uptake of conjugated bile acids and hepatitis b virus pres1-binding in na(+)-taurocholate cotransporting polypeptide knockout mice. *Hepatology* **62**:207-219.

Slitt AL, Allen K, Morrone J, Aleksunes LM, Chen C, Maher JM, Manautou JE, Cherrington NJ, and Klaassen CD (2007) Regulation of transporter expression in mouse liver, kidney, and intestine during extrahepatic cholestasis. *Biochimica et Biophysica Acta (BBA) - Biomembranes* **1768**:637-647.

Stancu C and Sima A (2001) Statins: mechanism of action and effects. *Journal of cellular and molecular medicine* **5**:378-387.

van de Steeg E, Wagenaar E, van der Kruijssen CM, Burggraaff JE, de Waart DR, Elferink RP, Kenworthy KE, and Schinkel AH (2010) Organic anion

- transporting polypeptide 1a/1b-knockout mice provide insights into hepatic handling of bilirubin, bile acids, and drugs. *J Clin Invest* **120**:2942-2952.
- van Mil SWC, Houwen RHJ, and Klomp LWJ (2005) Genetics of familial intrahepatic cholestasis syndromes. *Journal of Medical Genetics* **42**:449.
- Vaz FM, Paulusma CC, Huidekoper H, de Ru M, Lim C, Koster J, Ho-Mok K, Bootsma AH, Groen AK, Schaap FG, Oude Elferink RP, Waterham HR, and Wanders RJ (2015) Sodium taurocholate cotransporting polypeptide (SLC10A1) deficiency: conjugated hypercholanemia without a clear clinical phenotype. *Hepatology* **61**:260-267.
- Wagner M, Halilbasic E, Marschall HU, Zollner G, Fickert P, Langner C, Zatloukal K, Denk H, and Trauner M (2005) CAR and PXR agonists stimulate hepatic bile acid and bilirubin detoxification and elimination pathways in mice. *Hepatology* **42**:420-430.
- Wieneke N, Hirsch-Ernst KI, Kuna M, Kersten S, and Püschel GP (2007) PPARalpha-dependent induction of the energy homeostasis-regulating nuclear receptor NR1i3 (CAR) in rat hepatocytes: potential role in starvation adaptation. *FEBS letters* **581**:5617-5626.
- Zaher H, Meyer zu Schwabedissen HE, Tirona RG, Cox ML, Obert LA, Agrawal N, Palandra J, Stock JL, Kim RB, and Ware JA (2008) Targeted disruption of murine organic anion-transporting polypeptide 1b2 (Oatp1b2/Slco1b2) significantly alters disposition of prototypical drug substrates pravastatin and rifampin. *Mol Pharmacol* **74**:320-329.

5 Investigating sex-related effects of *Slc10a1* disruption in mice on serum bile acids and hepatic bile acid gene expression

5.1 Introduction

Bile acids are synthesized from catabolism of cholesterol in the liver and therefore mediate an important route for cholesterol turnover. Key enzymes involved in bile acid synthesis include CYP7A1, CYP8B1, and CYP27A1. Bile acid synthesis is negatively regulated by bile acid signaling. Bile acids bind to ligand-activated nuclear receptors, which elicit transcriptional repression of genes involved in synthesis and cellular uptake and efflux of bile acids. This process is integral to maintain bile acid homeostasis; when disrupted, accumulation of bile can be toxic to cells (Boyer, 2013). Plasma membrane-bound proteins that mediate the cellular uptake and efflux of bile acids, known as bile acid transporters, control bile flow throughout the enterohepatic system. Disruption of these transporters can alter bile acid disposition, resulting in bile acid-mediated pathologies including hepatic cholestasis and serum hypercholanemia (Dawson et al., 2009).

Despite wide-spread knowledge of sex-related differences in bile acid synthesis (Phelps et al., 2019), transport (Klaassen and Cheng, 2005), and detoxification (Alnouti and Klaassen, 2011), many studies are conducted solely in male subjects. Specifically, studies in bile acid transporter-deficient mice have largely reported results from male mice (van de Steeg et al., 2010; Csanaky et al., 2011; Zhang et al., 2012; Slijepcevic et al., 2015; Slijepcevic et al., 2017). These biases in medical research have implications on understanding

pathogenesis of disease and response to pharmacological treatments (Holdcroft, 2007).

NTCP (*SLC10A1*) is an important bile acid and drug transporter localized to the basolateral membrane of hepatocytes. NTCP has long been considered the key hepatic bile acid uptake transporter and is essential to maintain conjugated bile acid uptake into hepatocytes (Dawson et al., 2009). Genetic disruption of *SLC10A1* in humans and mice has been associated with serum hypercholanemia and differential expression of bile acid transporters (Slijepcevic et al., 2015; Mao et al., 2019). Studies in *Slc10a1*^{-/-} mice suggest that serum hypercholanemia may persist in females more so than males (Mao et al., 2019). However, detailed sex-associated characterization of differences in bile acid composition and hepatic gene expression have not been evaluated in *Slc10a1*^{-/-} mice.

Further, expression of drug metabolizing enzymes and drug and bile acid transporters, including NTCP, is sexually dimorphic (Cheng et al., 2005; Yang et al., 2012). Notwithstanding the growing evidence for a role of biological sex in bile acid regulation, limited information exists regarding potential sex differences in bile acid synthesis, composition, and transport in the context of *SLC10A1* disruption. Therefore, our study analyzed sex-associated differences in serum bile acid composition and hepatic bile acid synthesis and transporter gene expression in *Slc10a1*^{-/-} mice.

5.2 Methods & Materials

5.2.1 Materials

Taurocholic acid and d5-taurocholic acid were purchased from Toronto Research Chemicals (Toronto, ON). All other chemicals, unless otherwise stated, were obtained from Millipore-Sigma (St. Louis, MO).

5.2.2 Animal use approval

All animal experiments were approved by the University of Western Ontario Animal Care Committee (Protocol No. 2015-011), according to regulations and guidelines of the Canadian Council on Animal Care. Approval is listed in Appendix C.

5.2.3 Liver-specific targeted disruption of *Slc10a1* in C57BL/6 mice

Liver-specific targeted disruption of *Slc10a1* in C57BL/6 mice using the Alb-cre/LoxP method was performed as described in Chapter 4.2.3.

5.2.4 Quantification of serum total bile acids by colorimetric assay

Quantification of serum total bile acids was performed as previously described in Chapter 4.2.4

5.2.5 Quantification of serum individual bile acids by LC-MS/MS

Quantification of serum individual bile acids by LC-MS/MS was performed as previously described in Chapter 4.2.4.

5.2.6 Quantification of hepatic mRNA expression by qPCR

Quantification of hepatic mRNA levels was performed as previously described in Chapter 4.5.6.

5.2.7 Control, normocholanemic, and hypercholanemic mice

In keeping with previous studies (Slijepcevic et al., 2015; Mao et al., 2019), and with observations in Chapter 4 of this thesis, we observed serum normocholanemic and hypercholanemic populations within our *Slc10a1*^{-/-} mice. For the entirety of this study, our *Slc10a1*^{-/-} mice are grouped as normocholanemic (total bile acids < 35 μ M) or hypercholanemic (total serum bile acids >35 μ M).

5.2.8 Statistics

Unpaired, two-tailed, Student's t tests were used to determine statistical differences between two groups. Student's t tests were therefore employed to determine sex differences within control, normocholanemic *Slc10a1*^{-/-}, and hypercholanemic *Slc10a1*^{-/-} groups. One-way ANOVA with Tukey's multiple comparisons tests were used to determine statistical significance between three

groups. Therefore, one-way ANOVA with Tukey's tests were employed to determine differences between control, normocholanemic *Slc10a1*^{-/-}, and hypercholanemic *Slc10a1*^{-/-} mice of the same biological sex. Statistical significance was deemed at $P < 0.05$. Studies were conducted using 3-9 mice per group. All statistical analyses were conducted using GraphPad Prism 6 (La Jolla, CA).

5.3 Results

5.3.1 Total serum bile acids

To determine whether total serum bile acids were elevated in hypercholanemic mice regardless of biological sex, mice were grouped by sex and by genotype and phenotype. Serum total bile acids were elevated in hypercholanemic *Slc10a1*^{-/-} mice relative to control and normocholanemic mice, irrespective of sex ($P < 0.0001$, Fig. 5.1 A & B). In males, serum total bile acids were $1.8 \pm 0.7 \mu\text{M}$ in control mice, $12.3 \pm 3.7 \mu\text{M}$ in normocholanemic mice, and $435.3 \pm 55.0 \mu\text{M}$ in hypercholanemic mice. In female animals, serum total bile acid concentrations were $3.8 \pm 1.1 \mu\text{M}$ in controls, $25.3 \pm 4.4 \mu\text{M}$ in normocholanemic mice, and $495.2 \pm 20.6 \mu\text{M}$ in hypercholanemic mice, respectively. Total serum bile acids were not significantly different between control and normocholanemic mice, regardless of sex.

Studies in multiple strains of wild type mice observe that serum bile acid concentrations are higher in females relative to males (Turley et al., 1998; Phelps et al., 2019). To assess whether this trend is maintained in *Slc10a1*^{-/-} mice, differences were evaluated between males and females of the same genotype and phenotype (Fig. 5.1 C). Total serum bile acid concentrations were higher in female normocholanemic *Slc10a1*^{-/-} mice relative to male normocholanemic *Slc10a1*^{-/-} mice (25.3 ± 4.4 versus 12.3 ± 3.7 , $P = 0.047$, Fig. 5.1 C). No sex-related differences were observed in total serum bile acids in control and hypercholanemic *Slc10a1*^{-/-} mice.

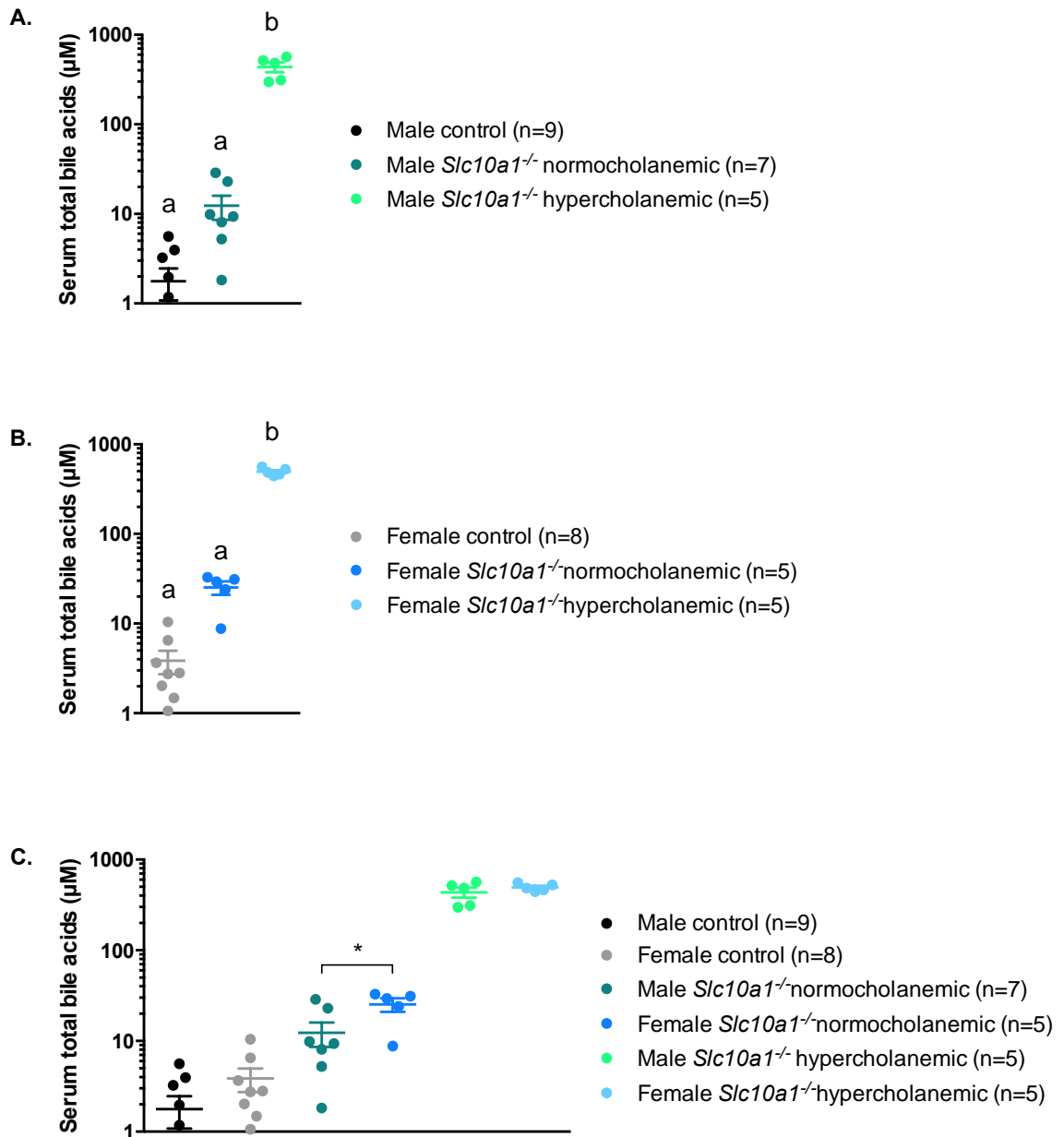


Figure 5.1. Total serum total bile acid concentrations grouped by biological sex

Evaluating serum total bile acids between genotype and phenotype for A. Male mice (n=5-9 mice per group) B. Female mice (n=5-8 mice per group). Results are presented as mean \pm SEM.

Statistical differences were determined using one-way ANOVA with Tukey's tests. Statistical significance between a and b: $P < 0.0001$. C. Evaluating sex-related differences within genotype and phenotype groups. Bile acid measurements in five control male mice were $< 0.1 \mu\text{M}$ therefore do not appear on the graphs. Experiments were performed in triplicate and results are presented as mean \pm SEM and statistical differences were determined using Student's t tests, * $P < 0.05$.

5.3.2 Individual serum unconjugated bile acids

To elucidate sex-associated differences in the effects of *Slc10a1* disruption on bile acid profiles in our mice, individual serum unconjugated bile acids were quantified.

No detectable differences in individual serum unconjugated bile acids were observed between control and normocholanemic mice, regardless of sex (Fig. 5.2 A & B). In hypercholanemic male mice, cholic acid was significantly elevated relative to control and normocholanemic mice ($9.2 \pm 7.9 \mu\text{M}$ versus $0.1 \pm 0.1 \mu\text{M}$ and $0.3 \pm 0.4 \mu\text{M}$ respectively, $P < 0.016$, Fig. 5.2 A). Although cholic acid appears elevated in hypercholanemic female mice relative to controls and normocholanemic animals, differences did not reach significance ($13.4 \pm 14.0 \mu\text{M}$ versus $0.4 \pm 0.3 \mu\text{M}$ and $0.4 \pm 0.4 \mu\text{M}$ respectively, $P < 0.17$, Fig. 5.2 B). No additional differences were observed for individual unconjugated bile acids between control, normocholanemic, and hypercholanemic mice of the same sex.

Sex differences were assessed for individual unconjugated bile acids in animals of the same genotype/phenotype. In control mice, deoxycholic acid was significantly elevated in females ($0.5 \pm 0.2 \mu\text{M}$) compared with males ($0.2 \pm 0.2 \mu\text{M}$) ($P = 0.0026$ Fig. 5.2 C). Deoxycholic acid was also higher in female normocholanemic mice relative to male normocholanemic mice (1.0 ± 0.3 versus $0.3 \pm 0.2 \mu\text{M}$, $P = 0.024$, Fig 5.2 C). No sex-related differences were observed in unconjugated bile acids of hypercholanemic mice (Fig. 5.2 C).

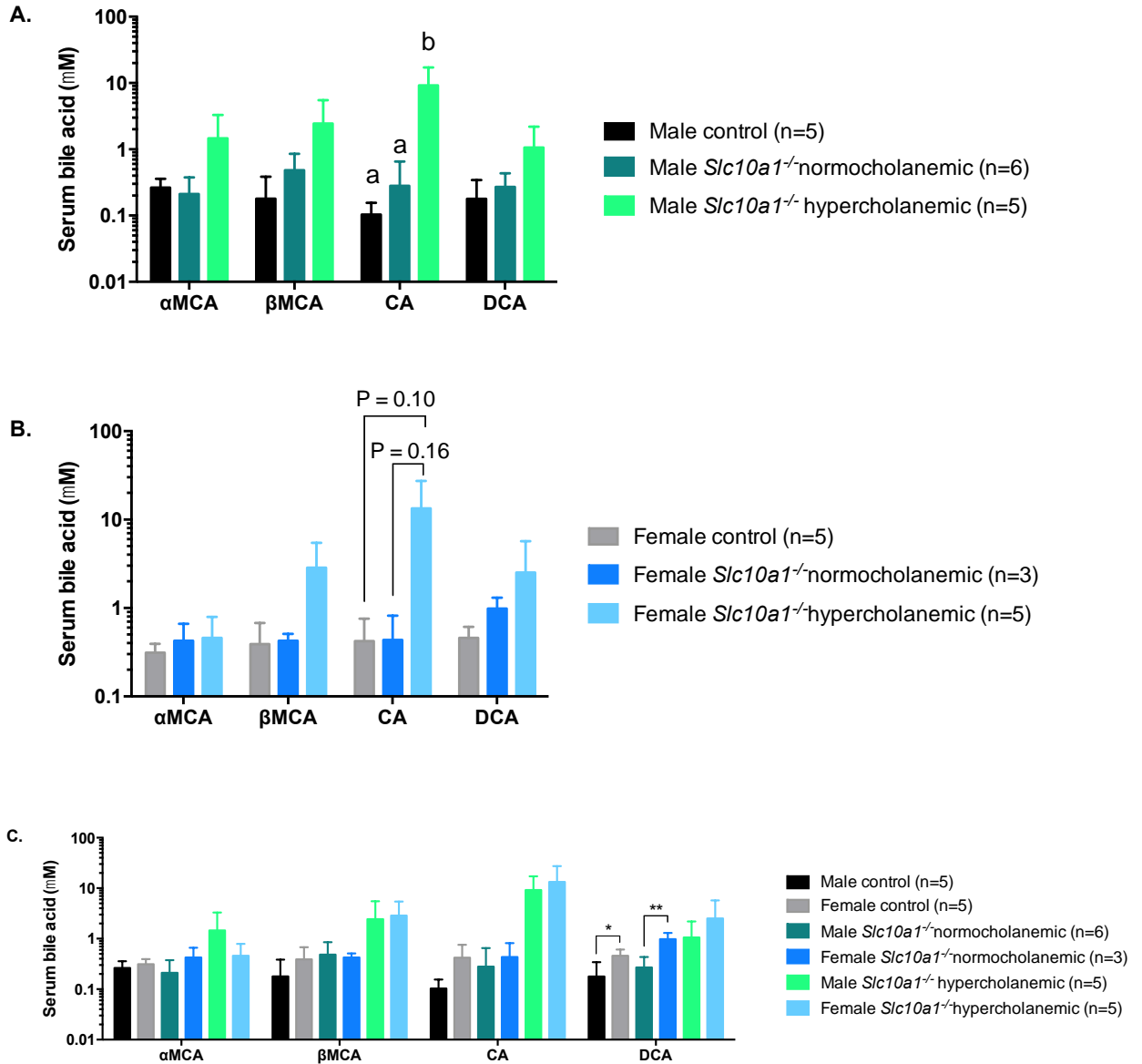


Figure 5.2. Individual unconjugated serum bile acid concentrations grouped by sex
 Comparing unconjugated bile acid species alpha muricholic acid (αMCA), beta muricholic acid (βMCA), cholic acid (CA), and deoxycholic acid (DCA) between genotype/phenotype for A. Males (n=5-6 mice per group). B. Females (n=3-5 mice per group). Results are presented as mean ± SEM. Statistical differences were determined using one-way ANOVA with Tukey's tests and statistical significance between a and b: P < 0.02. C. Evaluating sex-related differences within genotype/phenotype. Results are presented as mean ± SD. Statistical differences were determined using Student's t tests, * P < 0.05, ** P < 0.01.

5.3.3 Individual serum conjugated bile acids

As NTCP is the major hepatic conjugated bile acid transporter, effects of *Slc10a1* disruption on serum conjugated bile acid concentrations were evaluated.

In male mice, serum T α β MCA concentrations were significantly elevated in hypercholanemic animals relative to control and normocholanemic mice (25.2 \pm 23.2 μ M versus 0.03 \pm 0.03 μ M and 0.4 \pm 0.6 μ M respectively, $P < 0.022$, Fig. 5.3 A). Although serum tauro-alpha and tauro-beta muricholic acid (T α β MCA) concentrations appeared higher in female hypercholanemic mice relative to female control and normocholanemic mice, differences did not reach significance ($P < 0.14$). Serum taurocholic acid (TCA) concentrations were significantly elevated in hypercholanemic mice regardless of biological sex. In male hypercholanemic mice, serum TCA concentrations were 242.8 \pm 170.5 μ M, compared to 0.2 \pm 0.1 μ M and 1.6 \pm 2.4 μ M in male control and normocholanemic mice ($P < 0.036$, Fig. 5.3 A). In female hypercholanemic mice, serum TCA concentrations were 251.5 \pm 97.7 μ M, compared to 0.4 \pm 0.3 μ M and 6.4 \pm 6.7 μ M in female control and normocholanemic mice, respectively ($P < 0.0008$, Fig. 5.3 B). Taurodeoxycholic acid concentrations were not significantly different between males or females of different genotypes and phenotypes.

Sex differences were assessed for individual unconjugated bile acids in animals of the same genotype/phenotype. No significant sex-associated differences were observed for individual serum conjugated bile acids (Fig. 5.3 C).

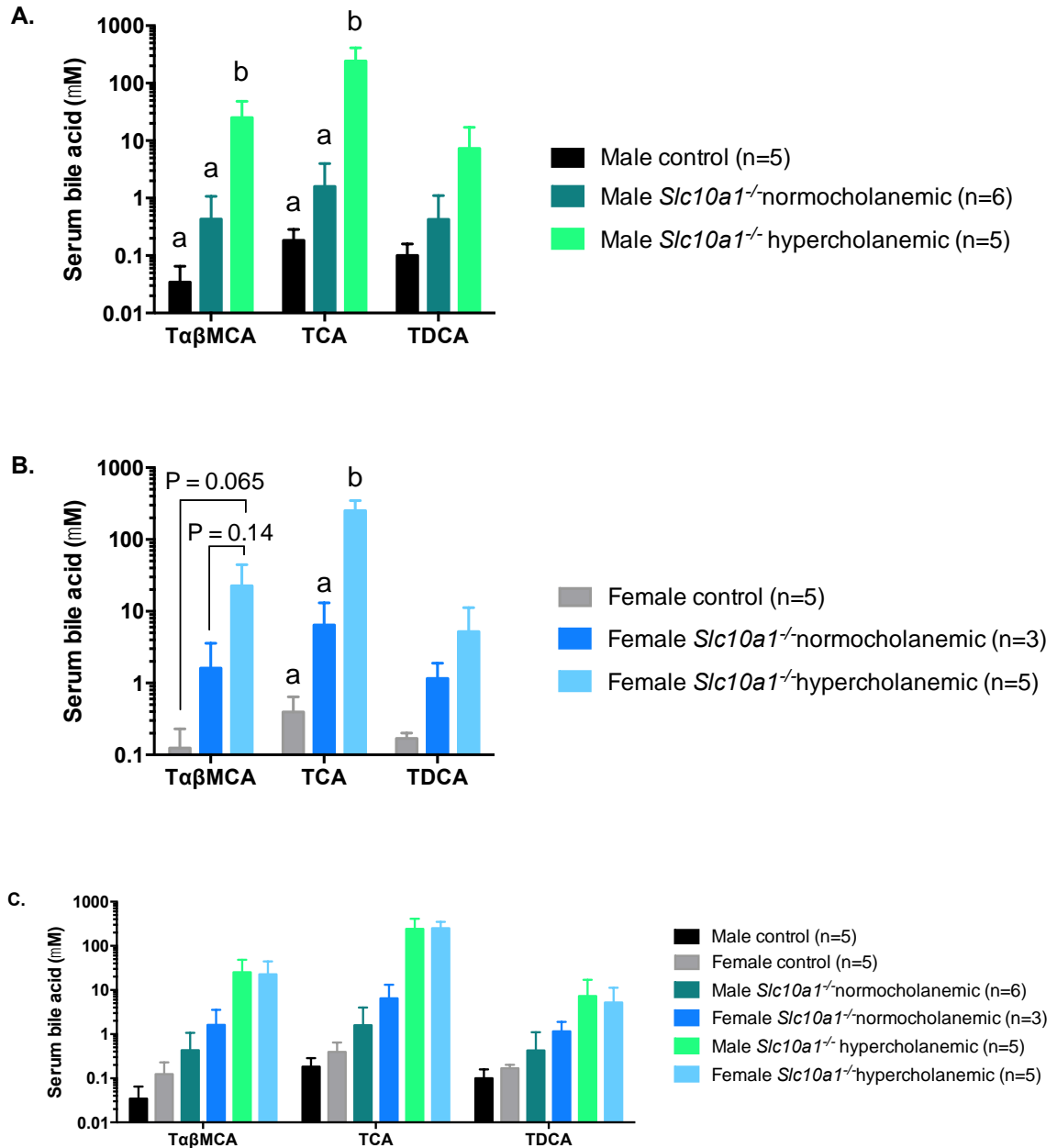


Figure 5.3. Individual conjugated serum bile acid concentrations grouped by sex
 Comparing conjugated bile acid species tauro-alpha and tauro-beta muricholic acids (TαβMCA), taurocholic acid (TCA), taurodeoxycholic acid (TDCA) between genotype/phenotype for A. Males (n=5-6 mice per group). B. Females (n=3-5 mice per group). Results are presented as mean ± SEM. Statistical differences were determined using one-way ANOVA with Tukey's tests, and statistical significance between a and b: P < 0.02. C. Evaluating sex-related differences within genotype and phenotype groups. Results are presented as mean ± SD. Significant differences were determined using Student's t tests, * P < 0.05. Taurine-conjugated αMCA and βMCA (TαMCA and TβMCA) are separate bile acids, however their concentrations were pooled as their mass-to-charge (m/z) ratios and retention times during mass spectrometry detection were indistinguishable, therefore they are represented together as TαβMCA.

5.3.4 Overall serum unconjugated and conjugated bile acid profiles

Based on total and individual bile acid measurements, our hypercholanemic *Slc10a1*^{-/-} mice have larger total bile acid pools than control, which appears to be mainly attributed to a rise in conjugated bile acids in the serum. To evaluate the relative abundance of conjugated bile acids in the sera, percentages of conjugated and unconjugated bile acid species were determined.

Serum bile acid compositions of control mice were 30-38 ± 5-16% conjugated (Fig. 5.4 A & B), whereas bile acids in normocholanemic mice were slightly more conjugated at 52-71 ± 17-32% (Fig. 5.4 C & D). The bile acid pools in the sera of hypercholanemic *Slc10a1*^{-/-} mice dominated by conjugated species (94 ± 4-5%, Fig. 5.4 E & F).

Differences in overall concentrations of unconjugated bile acids were determined by comparing the sums of αMCA, βMCA, CA, and DCA. Overall unconjugated bile acid concentrations were elevated in male hypercholanemic *Slc10a1*^{-/-} mice relative to control and normocholanemic males (14.2 ± 11.9 μM versus 0.6 ± 0.4 μM and 1.2 ± 0.7 μM respectively, P = 0.016, Fig. 5.4 A, C, D & Table 5.1). No significant differences were detected in overall unconjugated bile acids between control, normocholanemic, and hypercholanemic females.

Differences in overall concentrations of conjugated bile acids were determined by comparing the sums of TαβMCA, TCA, and TDCA. Overall conjugated bile acids were markedly higher in hypercholanemic mice, reaching significance in male and female groups. In males, conjugated bile acids in

hypercholanemic mice were $275 \pm 187.2 \mu\text{M}$, compared to $0.3 \pm 0.1 \mu\text{M}$ and 2.9 ± 4.0 in control and normocholanemic animals ($P < 0.0028$, Fig. 5.4 A, C, E & Table 5.1). In females, overall conjugated bile acids were $279.4 \pm 109.2 \mu\text{M}$ in hypercholanemic mice compared to $0.5 \pm 0.3 \mu\text{M}$ and $9.2 \pm 9.4 \mu\text{M}$ in control and normocholanemic animals respectively ($P < 0.009$, Fig. 5.4 B, D, F & Table 5.1). No significant differences were observed between control and normocholanemic mice of either sex.

With regard to sex-associated differences, no differences in overall conjugated or unconjugated bile acids were observed between male and female *Slc10a1*^{-/-} mice, regardless of bile acid phenotype (Table 5.2). In control mice, female unconjugated bile acids were significantly elevated relative to males ($0.5 \pm 0.3 \mu\text{M}$ versus $0.3 \pm 0.1 \mu\text{M}$ respectively, $P = 0.034$, Table 5.2). No sex differences in conjugated bile acids were observed in control mice (Table 5.2).

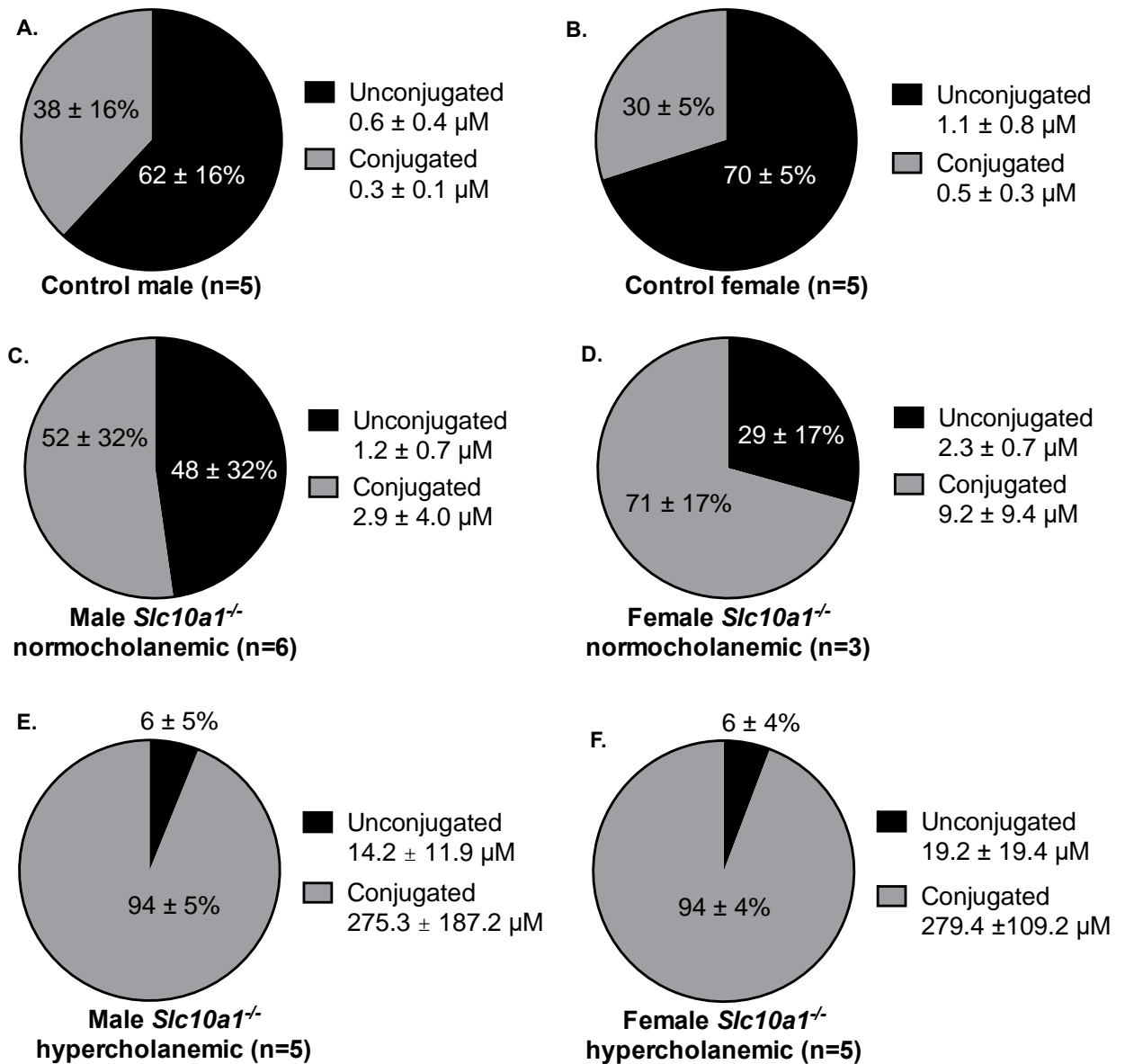


Figure 5.4. Overall serum unconjugated and conjugated bile acids

Unconjugated bile acids represent the sum of α MCA, β MCA, CA, and DCA. Conjugated bile acids represent the sum of T α β MCA, TCA, and TDCA. Percentages were derived from the mean micromolar concentrations of bile acids in the serum of mice \pm SD (denoted in the graph legends), n=3-6 mice per group.

Table 5.1. Statistical differences in serum unconjugated and conjugated bile acid species

Males	Significance (P value)		Females	Significance (P value)	
	Unconjugated	Conjugated		Unconjugated	Conjugated
Control vs. <i>Slc10a1</i> ^{-/-} normocholanemic	ns (0.99)	ns (0.99)	Control vs. <i>Slc10a1</i> ^{-/-} normocholanemic	ns (0.99)	ns (0.98)
Control vs. <i>Slc10a1</i> ^{-/-} hypercholanemic	* (0.016)	** (0.0028)	Control vs. <i>Slc10a1</i> ^{-/-} hypercholanemic	ns (0.11)	*** (0.00020)
<i>Slc10a1</i> ^{-/-} normocholanemic vs. <i>Slc10a1</i> ^{-/-} hypercholanemic	* (0.016)	** (0.0022)	<i>Slc10a1</i> ^{-/-} normocholanemic vs. <i>Slc10a1</i> ^{-/-} hypercholanemic	ns (0.19)	*** (0.00090)

Statistical differences were determined using one-way ANOVA with Tukey's tests, ns: not significant

Table 5.2. Sex-related differences in unconjugated and conjugated serum bile acids

Males vs. Females	Significance (P value)	
	Unconjugated	Conjugated
Control	* (0.034)	ns (0.066)
<i>Slc10a1</i> ^{-/-} normocholanemic	ns (0.055)	ns (0.15)
<i>Slc10a1</i> ^{-/-} hypercholanemic	ns (0.64)	ns (0.97)

Statistical differences were determined using Student's t tests, ns: not significant

5.3.5 Overall serum muricholic acid and cholic acid profiles

Muricholic acids are more hydrophilic bile acid species, are less toxic, and are weak agonists or antagonists of the master regulator of bile acid synthesis, farnesoid X receptor (FXR) (Sayin et al., 2013). Cholic acid species are more toxic and are more potent activators of FXR (Wang et al., 1999). The effects of *Slc10a1* disruption on serum muricholic acid and cholic acid species were therefore evaluated.

The serum bile acid pools of control and normocholanemic mice were composed of $22\text{-}35 \pm 2\text{-}18\%$ muricholic acids (Fig. 5.4 A-D). Serum bile acids of hypercholanemic mice comprised $8\text{-}11 \pm 6\text{-}7\%$ muricholic acid species (Fig. 5.4 E & F). Bile acid pools of hypercholanemic mice were therefore dominated by cholic acid species ($89\text{-}92 \pm 6\text{-}7\%$, Fig. 5.4 E & F).

Differences in overall concentrations of muricholic acids were determined by comparing the sums of α MCA, β MCA, and T α β MCA. Differences in overall concentrations of cholic acids were determined by comparing the sums of CA, TCA, and TDCA. In females and males, no significant differences were observed for concentrations of muricholic or cholic acids in control compared to normocholanemic mice (Fig. 5.5 A-D & Table 5.3). In males, overall concentrations of muricholic acids and cholic acids were significantly higher in hypercholanemic mice ($29.1 \pm 22.8 \mu\text{M}$ and $260.4 \pm 187.2 \mu\text{M}$) compared to control ($0.4 \pm 0.3 \mu\text{M}$ and $0.6 \pm 0.2 \mu\text{M}$) and normocholanemic mice ($1.2 \pm 0.7 \mu\text{M}$ and $2.9 \pm 3.3 \mu\text{M}$) ($P < 0.0086$, Fig. 5.5 & Table 5.3). In females, muricholic acids and cholic acids were elevated in hypercholanemic mice ($26.0 \pm 21.2 \mu\text{M}$

and $272.6 \pm 113.8 \mu\text{M}$) relative to control ($0.8 \pm 0.4 \mu\text{M}$ and $1.4 \pm 0.7 \mu\text{M}$) and normocholanemic mice ($2.5 \pm 2.2 \mu\text{M}$ and $9.0 \pm 7.6 \mu\text{M}$, Fig. 5.5). These differences were significant ($P < 0.035$ Fig. 5.5 & Table 4.3) with the exception of the differences in muricholic acids between female normocholanemic and hypercholanemic, which did not reach significance ($P = 0.088$).

The only sex-related difference observed when comparing concentrations of muricholic acids and cholic acids by genotype and phenotype was the significantly higher cholic acid concentrations in female control mice relative to male controls (1.4 ± 0.7 versus $0.6 \pm 0.2 \mu\text{M}$, $P = 0.030$, Table 5.4).

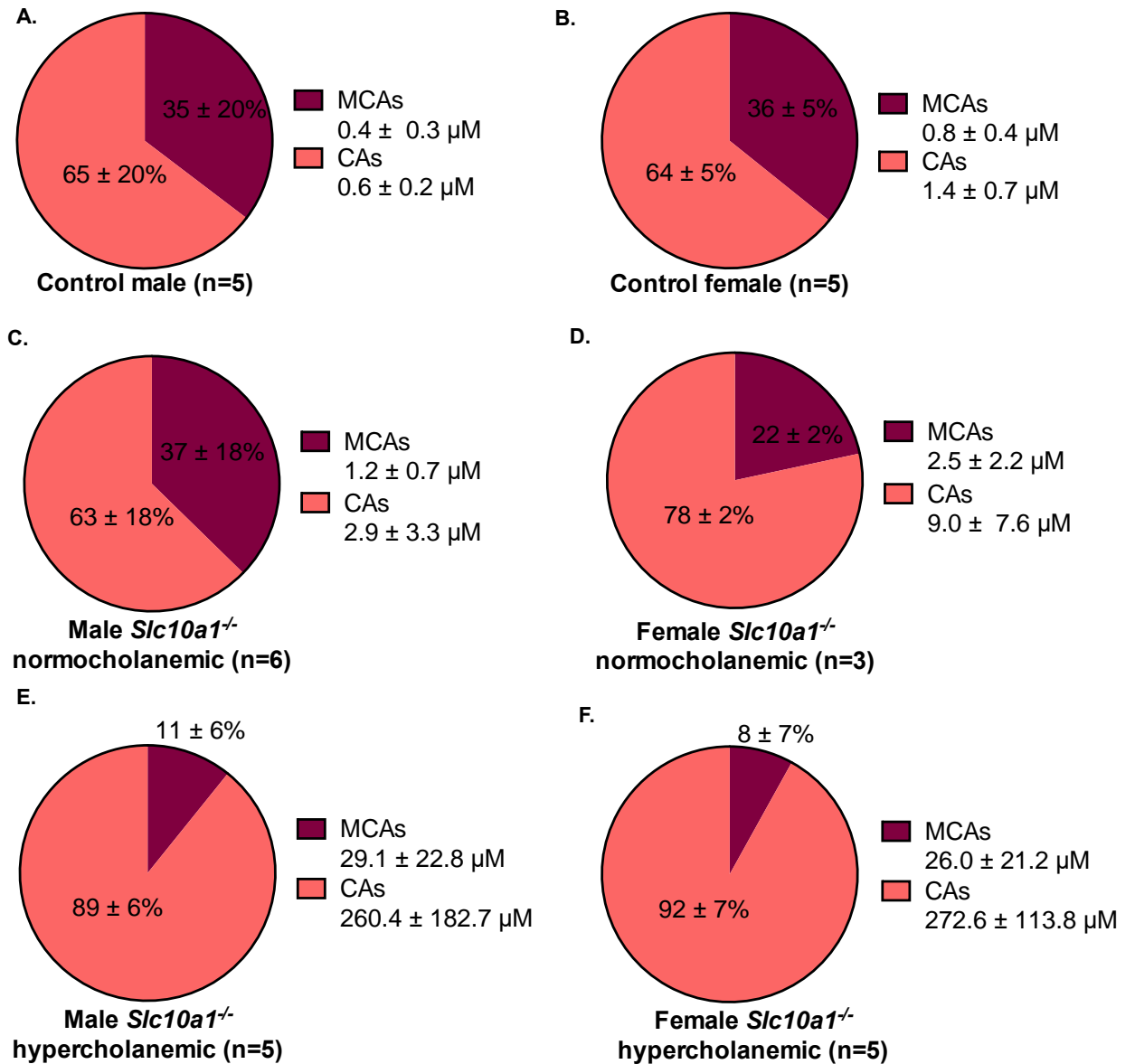


Figure 5.5. Overall serum muricholic acid species (MCAs) and cholic acid species (CAs)
 Muricholic acid species are derived from muricholic acid and, in our study, represent the sum of αMCA, βMCA, and TαβMCA. Cholic acid species are derived from cholic acid and represent, in our study, the sum of CA, DCA, TCA, and TDCA. Percentages were derived from the mean micromolar concentrations of bile acids ± SD, which are denoted in the graph legends.

Table 5.3. Statistical differences in overall serum muricholic acid and cholic acid species

Males	Significance (P value)		Females	Significance (P value)	
	Muricholic acids	Cholic acids		Muricholic acids	Cholic acids
Control vs. <i>Slc10a1</i> ^{-/-} normocholanemic	ns (0.99)	ns (0.99)	Control vs. <i>Slc10a1</i> ^{-/-} normocholanemic	ns (0.98)	ns (0.99)
Control vs. <i>Slc10a1</i> ^{-/-} hypercholanemic	** (0.0086)	** (0.0036)	Control vs. <i>Slc10a1</i> ^{-/-} hypercholanemic	* (0.035)	*** (0.00040)
<i>Slc10a1</i> ^{-/-} normocholanemic vs. <i>Slc10a1</i> ^{-/-} hypercholanemic	** (0.0074)	** (0.0028)	<i>Slc10a1</i> ^{-/-} normocholanemic vs. <i>Slc10a1</i> ^{-/-} hypercholanemic	ns (0.088)	** (0.0014)

Statistical differences were determined using one-way ANOVA with Tukey's tests, ns: not significant

Table 5.4. Sex-related differences in overall serum muricholic acid and cholic acid

Males vs. Females	Significance (P value)	
	Muricholic acids	Cholic acids
Control	ns (0.095)	* (0.030)
<i>Slc10a1</i> ^{-/-} normocholanemic	ns (0.17)	ns (0.10)
<i>Slc10a1</i> ^{-/-} hypercholanemic	ns (0.83)	ns (0.90)

Statistical differences were determined using Student's t tests, ns: not significant

5.3.6 Hepatic bile acid synthesis gene expression

Different bile acid pool composition could be due to differential expression of bile acid synthesis genes. In the liver, CYP7A1 is the rate-limiting enzyme for bile acid synthesis. Bile acid synthesis is repressed through negative feedback, where bile acid-binding to FXR induces production of small heterodimer partner (SHP). Small heterodimer partner is a transcription factor that inhibits *Cyp7a1* gene transcription (Chiang, 2009). Hepatic mRNA levels of genes involved in bile acid synthesis were assessed to determine potential differences between mouse groups.

No significant differences were observed in hepatic mRNA levels of *Cyp7a1* or *Shp* when comparing control and normocholanemic *Slc10a1*^{-/-} mice irrespective of sex (Fig. 5.6 A-D). In hypercholanemic mice, *Cyp7a1* was increased ~90-fold in male hypercholanemic mice relative to male control and male normocholanemic mice, however this difference did not reach significance ($P < 0.068$, Fig. 5.6 A). Levels of *Cyp7a1* were not different in female hypercholanemic mice relative to female control and female normocholanemic mice (Fig. 5.6 C). Expression of *Shp* mRNA was significantly decreased in both male and female hypercholanemic mice relative to control mice of the same sex ($P < 0.023$, Fig. 5.6 B & D). Relative to normocholanemic mice, *Shp* mRNA was decreased in male and female hypercholanemic mice. This difference was significant in female mice ($P = 0.025$, Fig. 5.6 D) however did not reach significance in males ($P = 0.070$, Fig. 5.6 B).

Sex-related differences were observed between male and female hypercholanemic mice. Levels of *Cyp7a1* mRNA were increased and *Shp* mRNA levels were decreased in male hypercholanemic mice relative to female hypercholanemic mice ($P < 0.016$, Fig. 5.6 E & F). Although *Cyp7a1* and *Shp* mRNA levels appeared elevated in female relative to male mice in control and normocholanemic groups, no significant sex-associated differences were detected (Fig. 5.6 E & F).

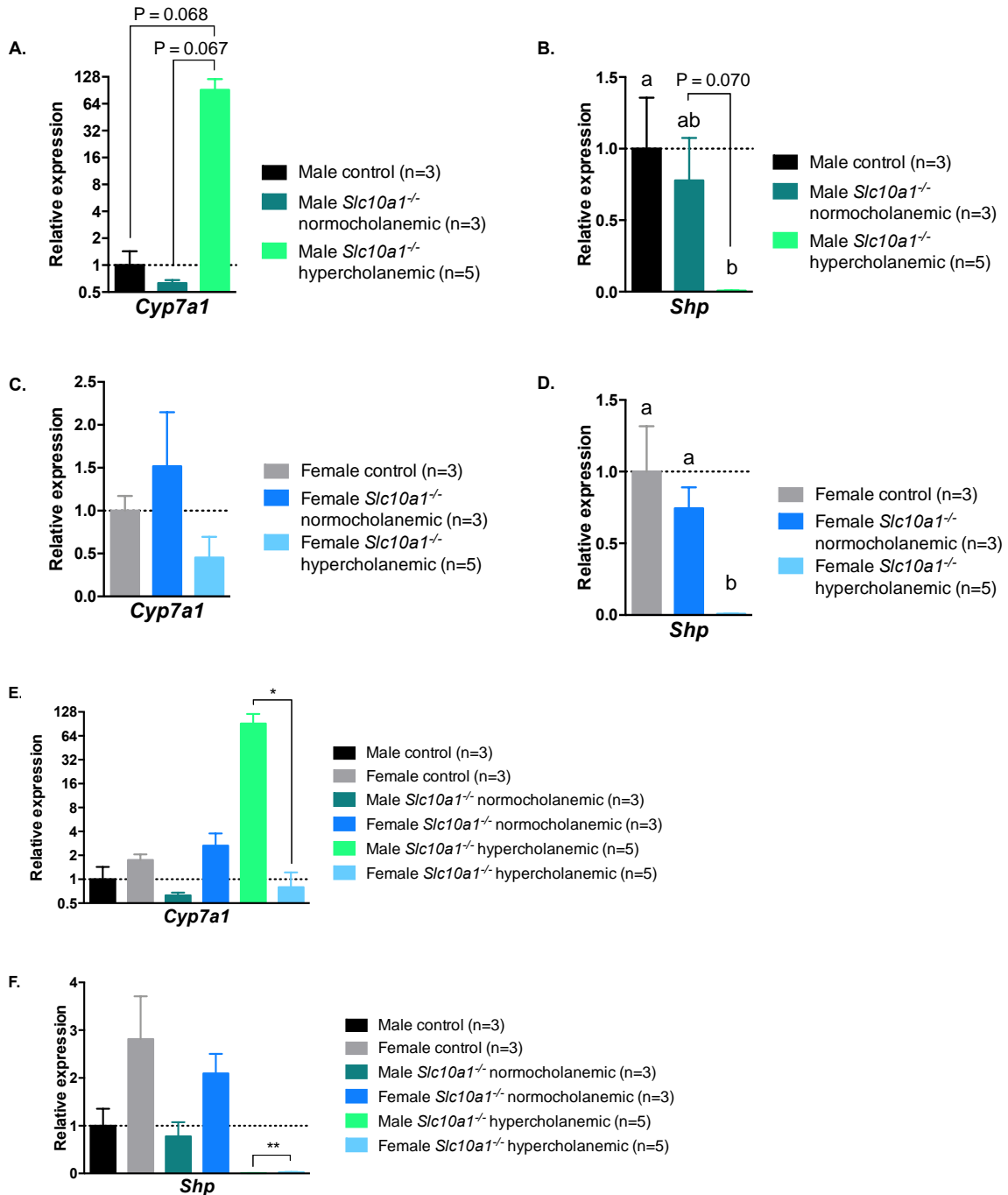


Figure 5.6. Hepatic mRNA expression of bile acid synthesis gene *Cyp7a1* its transcriptional repressor *Shp*

A. & B. Relative mRNA levels in male mice for A. *Cyp7a1* and B. *Shp*. C. & D. Relative mRNA levels in female mice for C. *Cyp7a1* and D. *Shp*. Experiments were performed in triplicate and results are presented as mean \pm SEM, n=3-5 mice per group. Statistical differences were detected using one-way ANOVA with Tukey's tests, and statistical significance between a and b: $P < 0.05$. E. & F. Sex-associated differences within genotype and phenotype groups for E. *Cyp7a1* expression. F. *Shp* expression. Experiments were performed in triplicate and results are presented as mean \pm SEM, n=3-5 mice per group. Statistical differences were determined using Student's t tests, * $P = 0.016$, ** $P = 0.0010$.

Within the liver, CYP8B1 is responsible for production of cholic acid, and CYP27A1 is involved in the production of both cholic acid and muricholic acids (Chiang, 2009). To elucidate whether differences in expression of these synthesis genes may contribute to increased cholic acid species in the serum of hypercholanemic mice, hepatic mRNA levels of *Cyp8b1* and *Cyp27a1* were quantified.

In male and female hypercholanemic mice, *Cyp8b1* mRNA levels were significantly reduced relative to normocholanemic males and females ($P < 0.019$, Fig. 5.7 A & C). Although *Cyp8b1* levels in hypercholanemic mice also appear decreased relative to *Cyp8b1* levels in control mice, these differences did not reach significance ($P = 0.053$, Fig. 5.7 A & C). Expression of *Cyp27a1* mRNA was significantly increased in hypercholanemic male mice relative to male control and normocholanemic mice ($P < 0.0004$, Fig. 5.7 B). In female hypercholanemic mice, the opposite was observed. Levels of *Cyp27a1* were decreased in female hypercholanemic mice relative females of different genotypes and phenotypes. This decrease was significant relative to normocholanemic females ($P = 0.011$, Fig 5.7 D), however the decrease in *Cyp27a1* mRNA observed between female hypercholanemic relative to female control mice did not reach significance ($P = 0.050$).

When assessing sex-related differences, both *Cyp8b1* and *Cyp27a1* were significantly decreased in female hypercholanemic mice relative to male hypercholanemic mice ($P = 0.0060$ & $P < 0.0001$ respectively, Fig. 5.7 E & F). No

sex-associated differences were detected in control or normocholanemic mice (Fig. 5.7 E & F).

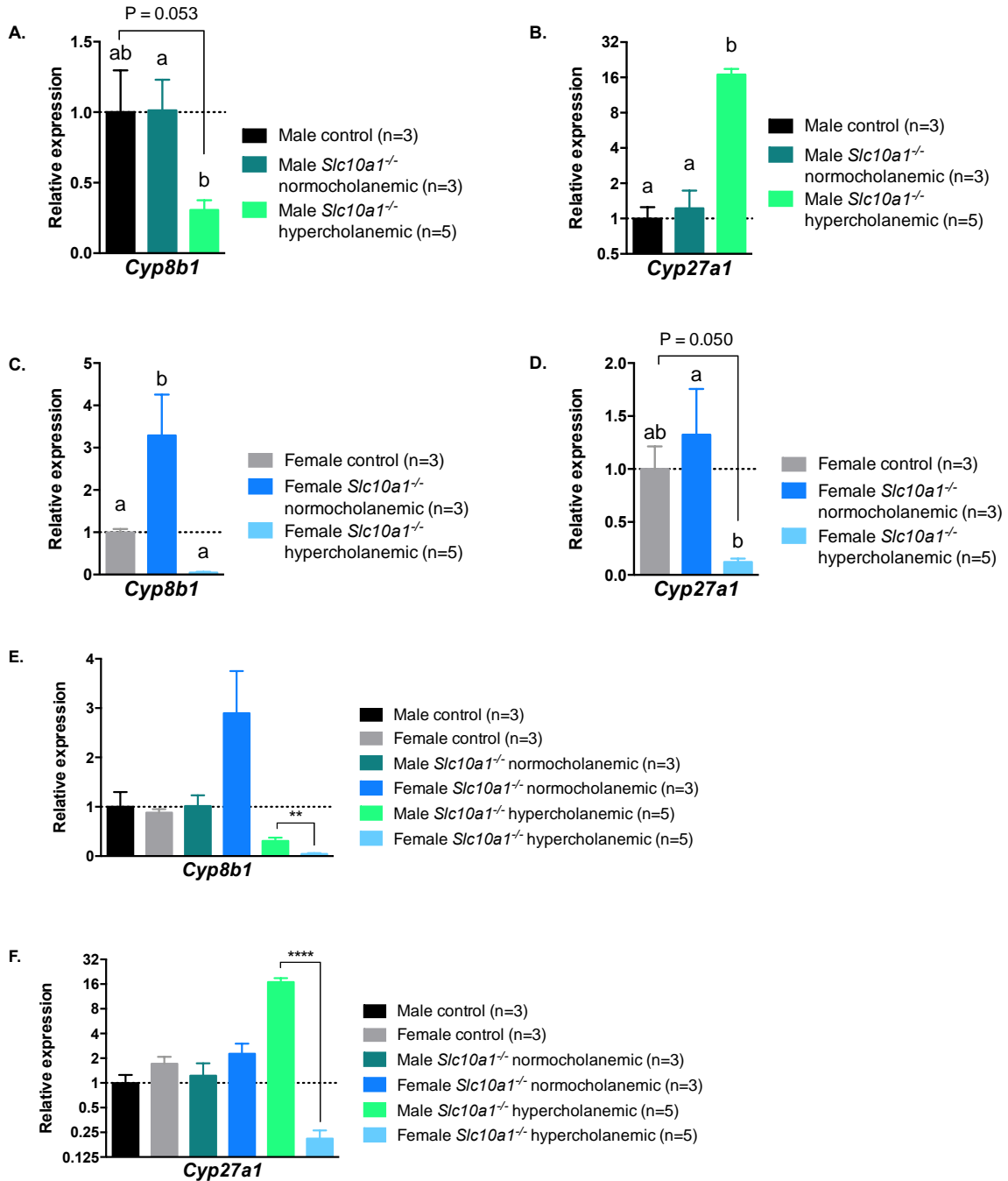


Figure 5.7. Hepatic mRNA expression of bile acid synthesis genes *Cyp8b1* and *Cyp27a1*
 A. & B. Relative mRNA levels in male mice for A. *Cyp8b1* and B. *Cyp27a1*. C. & D. Relative mRNA levels in female mice for C. *Cyp8b1* and D. *Cyp27a1*. Experiments were performed in triplicate and results are presented as mean \pm SEM, n=3-5 mice per group. Statistical differences were detected using one-way ANOVA with Tukey's tests, and statistical significance between a and b: P < 0.05. E. & F. Sex-associated differences within genotype and phenotype groups for E. *Cyp8b1* expression. F. *Cyp27a1* expression. Experiments were performed in triplicate and results are presented as mean \pm SEM, n=3-5 mice per group. Statistical differences were determined using Student's t tests, * P = 0.0060, ** P < 0.0001.

5.3.7 Hepatic expression of hepatic bile acid uptake transporters

Altered serum bile acid profiles may also be attributed to differential expression of genes involved in hepatic uptake of bile acids. Therefore, we determined expression of hepatic genes involved in bile acid uptake into the liver.

As expected, *Ntcp* mRNA levels were significantly decreased in normocholanemic and hypercholanemic *Slc10a1*^{-/-} mice relative to controls ($P < 0.044$, Fig. 5.8 A & C). No significant differences were observed in hepatic expression of *Oatp1b2* between mice of different genotypes & phenotypes for either sex (Fig. 5.8 B & D). No sex associated differences were observed for *Oatp1b2* expression within genotype and phenotype groups (Fig. 5.8 E). Within the hypercholanemic group, *Ntcp* mRNA expression was significantly decreased in females relative to males ($P = 0.021$, Fig. 5.8 F).

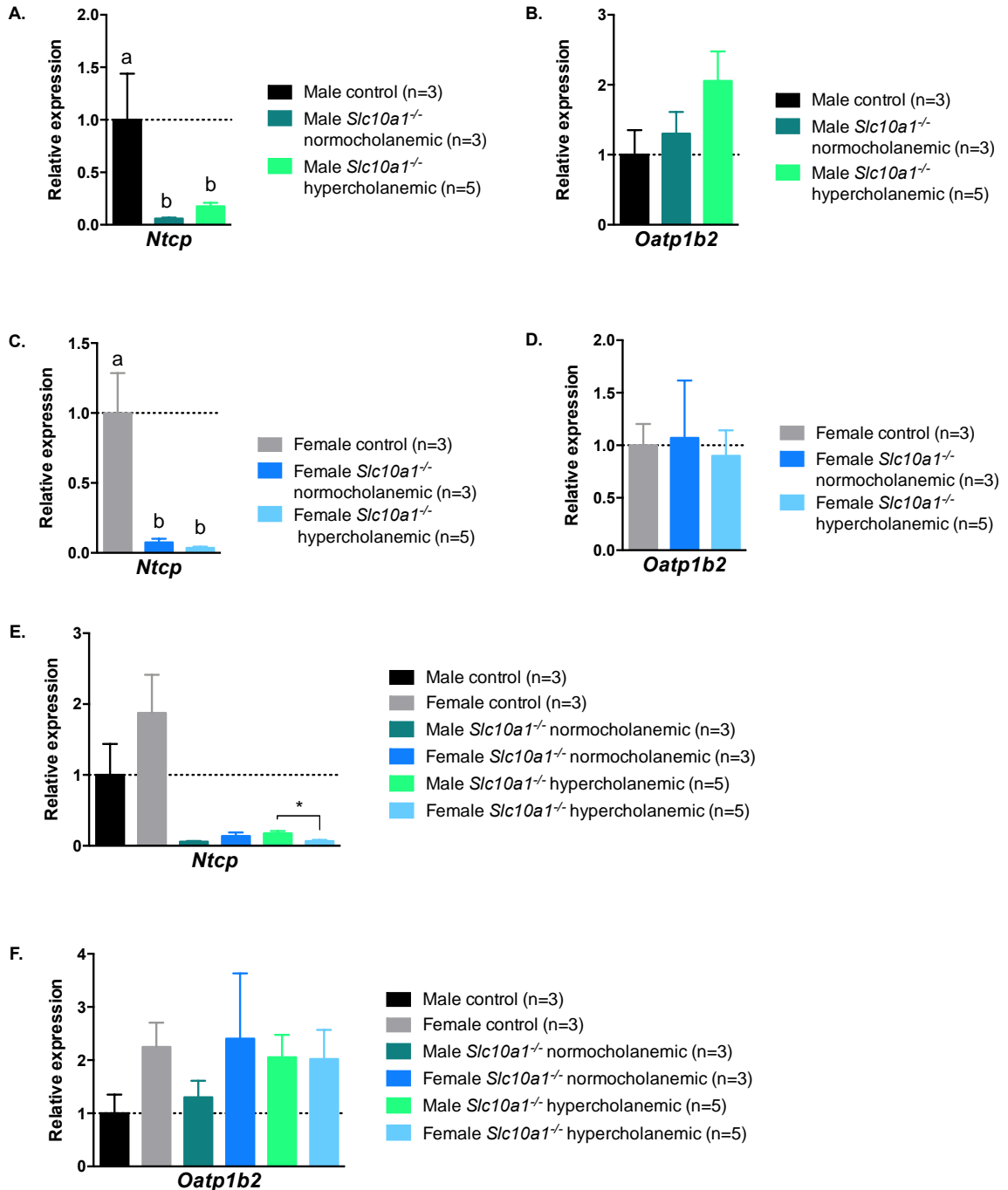


Figure 5.8. Hepatic mRNA expression of bile acid uptake transporter genes *Ntcp* and *Oatp1b2*

A. & B. Relative mRNA levels in male mice for A. *Ntcp* and B. *Oatp1b2*. C. & D. Relative mRNA levels in female mice for C. *Ntcp* and D. *Oatp1b2*. Experiments were performed in triplicate and results are presented as mean \pm SEM, n=3-5 mice per group. Statistical differences were detected using one-way ANOVA with Tukey's tests and statistical significance between a and b: $P < 0.05$. E. & F. Sex-associated differences within genotype and phenotype groups for E. *Ntcp* expression. F. *Oatp1b2* expression. Experiments were performed in triplicate and results are presented as mean \pm SEM, n=3-5 mice per group. Statistical differences were determined using Student's t tests, * $P = 0.021$.

Levels of the hepatic bile acid uptake transporter gene *Oatp1a1* mRNA were virtually undetectable in male and female hypercholanemic mice. The reduced expression of *Oatp1a1* mRNA was significant for male hypercholanemic mice relative to male controls and normocholanemic mice ($P < 0.034$, Fig. 5.9 A), however the observed decrease in *Oatp1a1* mRNA in female hypercholanemic mice relative to female control and normocholanemic mice did not reach significance ($P < 0.18, 0.036$, Fig. 5.9 C). Levels of *Oatp1a4* mRNA were significantly higher in male hypercholanemic mice relative to male control and normocholanemic animals ($P < 0.010$, Fig. 5.9 B). In female mice, the opposite trend was observed; *Oatp1a4* mRNA levels were decreased in hypercholanemic mice relative to control and normocholanemic animals, however these differences did not reach significance ($P < 0.078$, Fig. 5.9 D).

No detectable sex-related differences were observed for *Oatp1a1* mRNA expression within genotype and phenotype groups (Fig. 5.9 E). In control normocholanemic mice, *Oatp1a4* expression was higher in females than males. This sex difference was significant in control animals ($P = 0.011$, Fig. 5.9 F), however it did not reach significance for normocholanemic animals ($P = 0.19$, Fig. 5.9 F). The opposite was observed in hypercholanemic mice; *Oatp1a4* mRNA expression was significantly higher in males relative to females ($P = 0.0015$, Fig. 5.9 F).

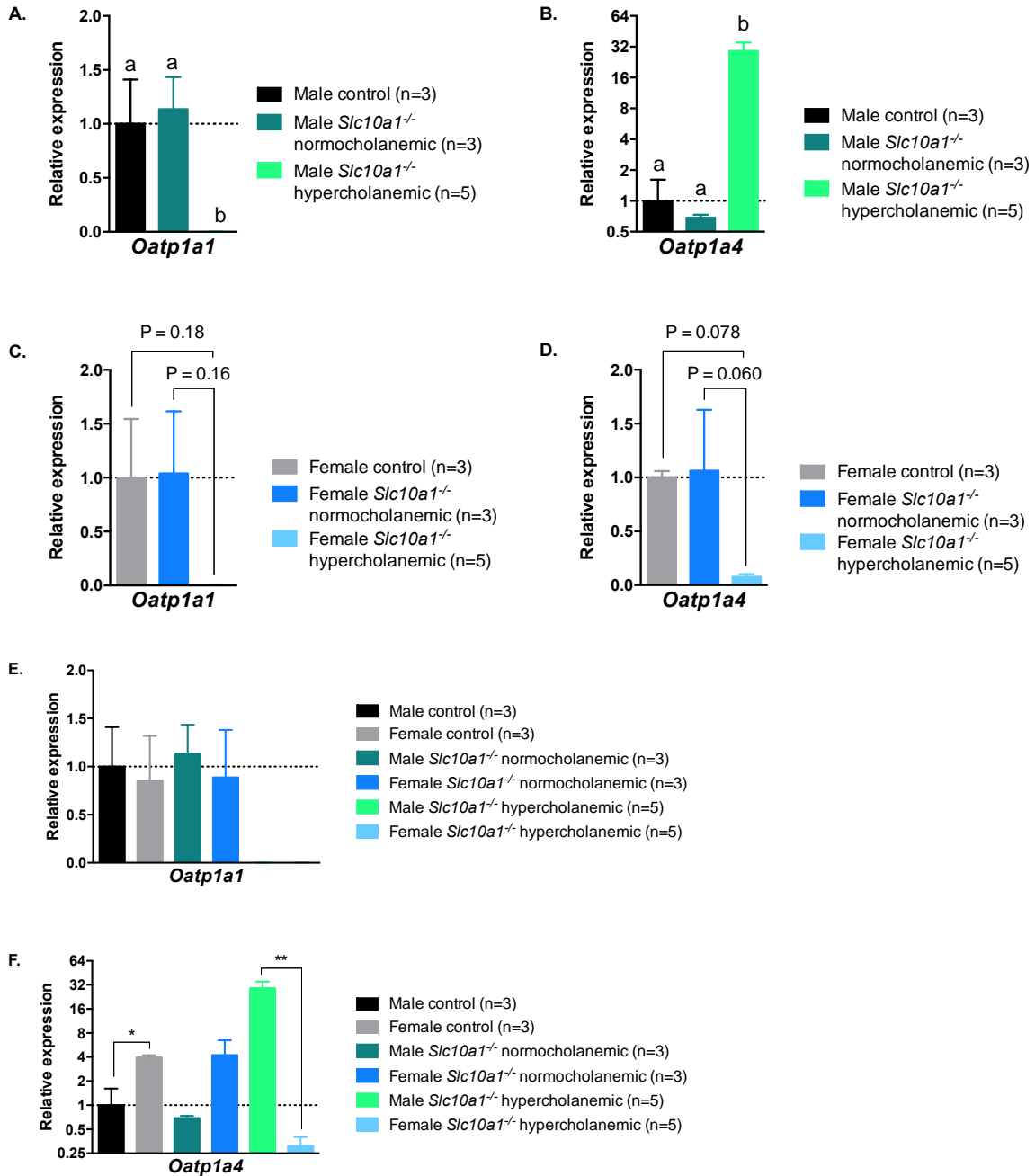


Figure 5.9. Hepatic mRNA expression of bile acid uptake transporter genes *Oatp1a1* and *Oatp1a4*

A. & B. Relative mRNA levels in male mice for A. *Oatp1a1* and B. *Oatp1a4*. C. & D. Relative mRNA levels in female mice for C. *Oatp1a1* and D. *Oatp1a4*. Experiments were performed in triplicate and results are presented as mean ± SEM, n=3-5 mice per group. Statistical differences were detected using one-way ANOVA with Tukey's tests and statistical significance between a and b: P < 0.04. E. & F. Sex-associated differences within genotype and phenotype groups for E. *Oatp1a1* expression and F. *Oatp1a4* expression. Experiments were performed in triplicate and results are presented as mean ± SEM, n=3-5 mice per group. Statistical differences were determined using Student's t tests, * P = 0.011, ** P = 0.0015.

5.3.8 Hepatic expression of hepatic bile acid efflux transporters

Hepatic bile acid efflux is also an important determinant to bile acid enterohepatic circulation and can affect serum bile acid concentrations. Differences in mRNA levels for transporters involved in hepatic bile acid efflux were therefore assessed.

With respect to canalicular efflux transporters, no significant differences were observed in *Bsep* mRNA levels between male control, normocholanemic, and hypercholanemic mice (Fig. 5.10 A). However, decreased *Bsep* mRNA levels were observed in hypercholanemic females relative to female control and normocholanemic mice ($P = 0.0009$, Fig. 5.10 C). Levels of *Mrp2* mRNA were decreased in male and female hypercholanemic mice relative to control and normocholanemic animals of the same sex. These differences were significant ($P < 0.05$) with the exception of the reduced *Mrp2* expression observed between male hypercholanemic and control animals, which did not reach significance ($P = 0.055$, Fig. 5.10 B).

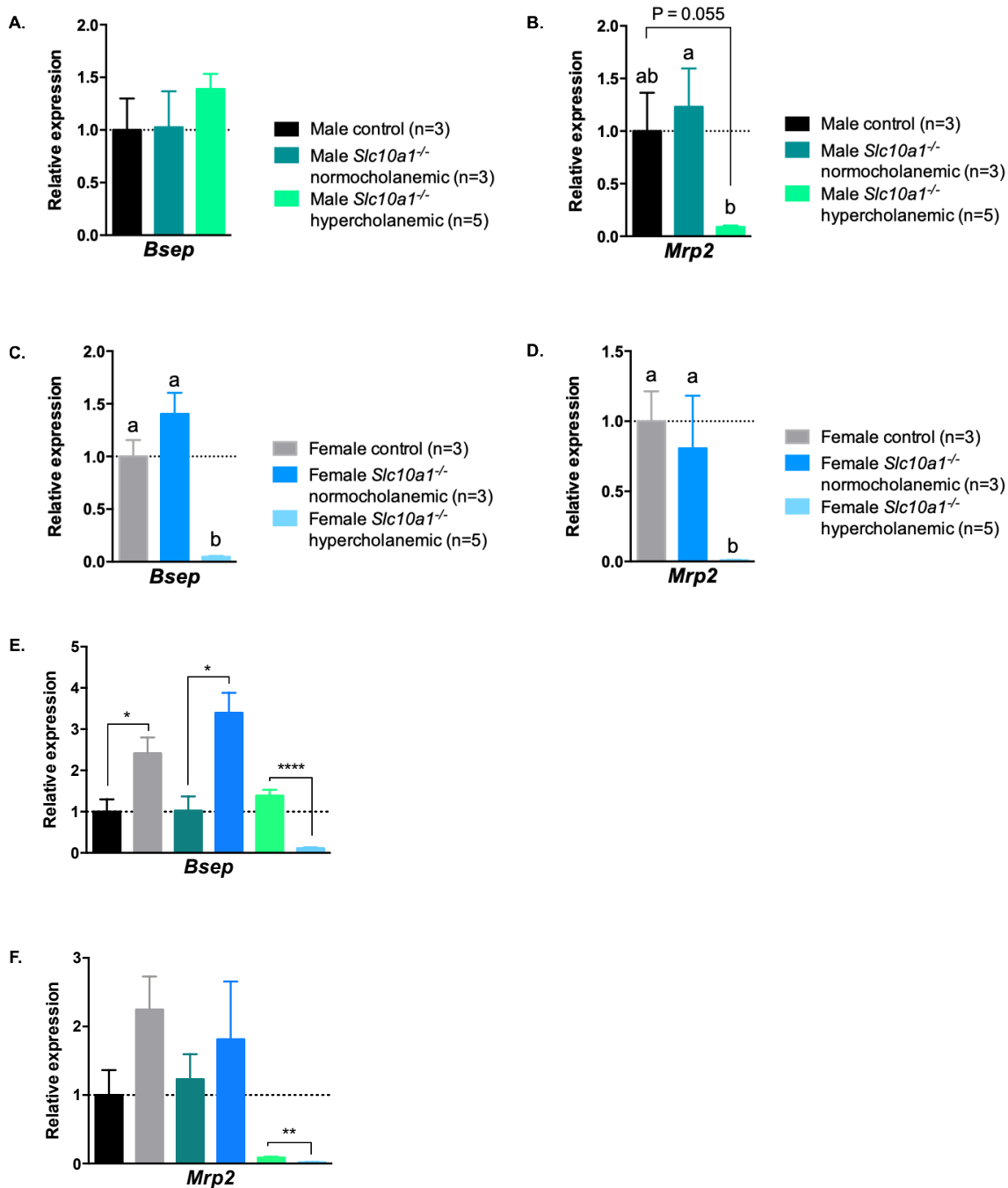


Figure 5.10. Hepatic mRNA expression of canalicular bile acid efflux transporter genes *Bsep* and *Mrp2*

A. & B. Relative mRNA levels in male mice for A. *Bsep* and B. *Mrp2*. C. & D. Relative mRNA levels in female mice for C. *Bsep* and D. *Mrp2*. Experiments were performed in triplicate and results are presented as mean ± SEM, n=3-5 mice per group. Statistical differences were detected using one-way ANOVA with Tukey's tests and statistical significance between a and b: P < 0.05. E. & F. Sex-associated differences within genotype and phenotype groups for E. *Bsep* expression and F. *Mrp2* expression. Experiments were performed in triplicate and results are presented as mean ± SEM, n=3-5 mice per group. Statistical differences were determined using Student's t tests, * P < 0.042, ** P = 0.0014, **** P < 0.0001.

Efflux transporters on the basolateral membranes of hepatocytes are also indicative of bile acid signaling and dynamics and can influence serum bile acid concentrations. In male hypercholanemic mice, although *Mrp3* mRNA appeared increased relative to male control and male normocholanemic mice, these differences did not reach significance ($p = 0.39$, Fig. 5.11 A). Conversely, *Mrp3* mRNA was nearly undetectable in livers of hypercholanemic female mice. Levels of *Mrp3* mRNA were significantly reduced in hypercholanemic female mice relative to female control mice ($P = 0.010$, Fig 5.11 C), however this reduction did not reach significance relative to control females ($P = 0.056$, Fig. 5.11 C). Expression of *Osta* was assessed, however mRNA levels were undetectable in all animals. No detectable differences were observed in expression of *Ost β* in male mice between genotype and phenotype groups (Fig. 5.11 B). However, *Ost β* mRNA levels were significantly increased in female hypercholanemic mice relative to female control and normocholanemic animals ($P < 0.0048$, Fig. 5.11 D).

With respect to sex-associated differences within genotype and phenotype groups, no significant differences were observed for *Mrp3*. Although *Mrp3* mRNA levels appear reduced in female hypercholanemic mice relative to male hypercholanemic mice, this difference did not reach significance (Fig 5.11 E). Sex differences were observed in *Ost β* mRNA levels, which were higher in female mice with respect to males of the same genotype and phenotype. These increases were significant in control and hypercholanemic animals ($P < 0.0089$, Fig. 5.11 F), however significance was not reached for differences for *Ost β*

mRNA levels between male and female normocholanemic mice ($P = 0.14$, Fig. 5.11 F).

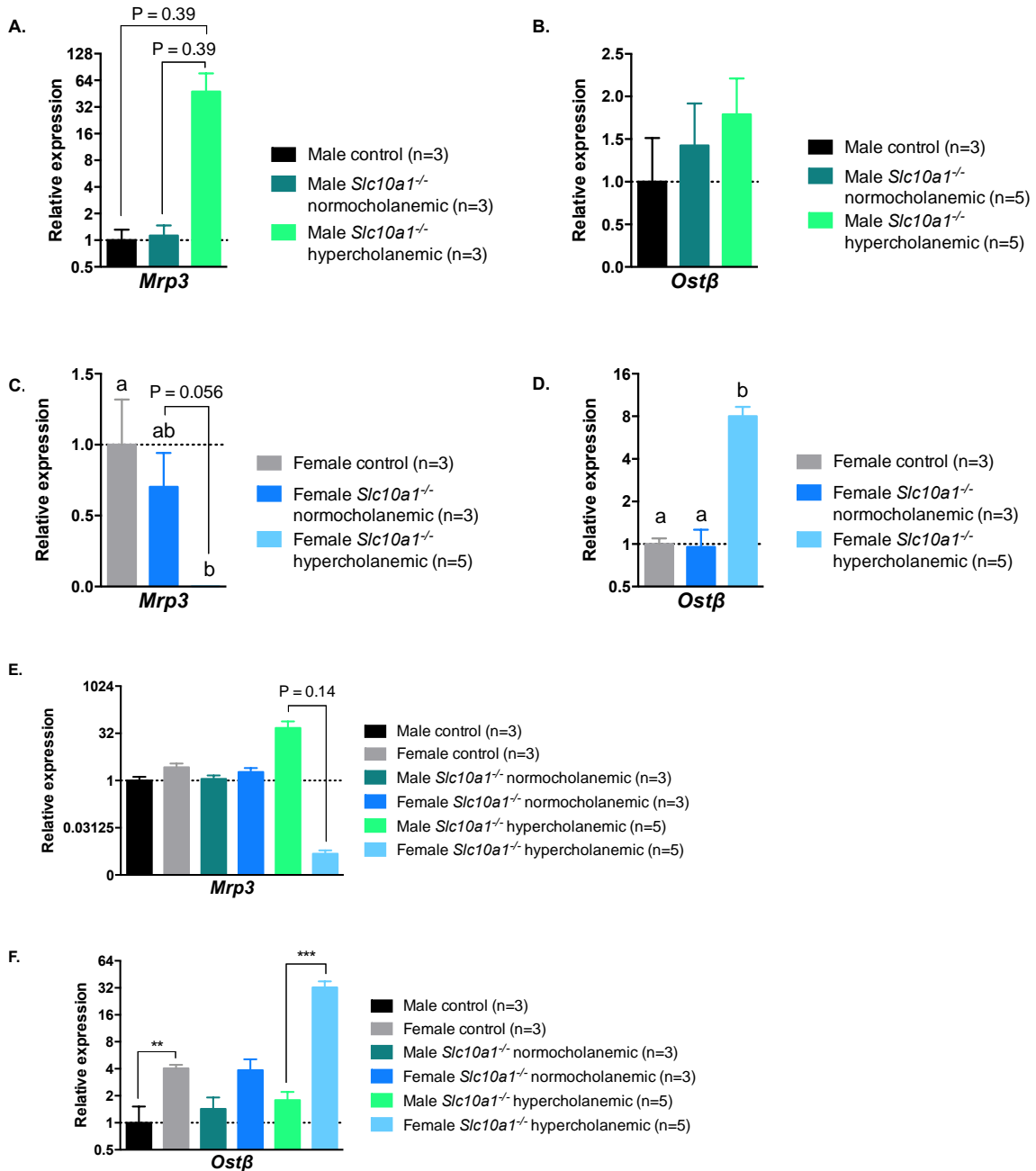


Figure 5.11. Hepatic mRNA expression of basolateral bile acid efflux transporter genes *Mrp3* and *Ostβ*

Expression of *Osta* was assessed but levels were undetectable in all mice. A. & B. Relative mRNA levels in male mice for A. *Mrp3* and B. *Ostβ*. C. & D. Relative mRNA levels in female mice for C. *Mrp3* and D. *Ostβ*. Experiments were performed in triplicate and results are presented as mean \pm SEM, n=3-5 mice per group. Statistical differences were detected using one-way ANOVA with Tukey's tests and statistical significance between a and b: P < 0.01. E. & F. Sex-associated differences within genotype and phenotype groups for E. *Mrp3* expression and F. *Ostβ* expression. Experiments were performed in triplicate and results are presented as mean \pm SEM, n=3-5 mice per group. Statistical differences were determined using Student's t tests, ** P = 0.0089, *** P = 0.0005

5.4 Discussion

Our study evaluated sex-dependent effects of *Slc10a1* disruption on serum bile acid composition and expression of hepatic bile acid synthesis and transport genes. We found that *Slc10a1* disruption results in excess serum conjugated bile acids and increases the abundance of both muricholic and cholic acid species in male and female hypercholanemic mice. No key differences were detected in overall bile acid composition between sexes. Expression of *Oatp1a1* mRNA was nearly undetectable in livers of male and female hypercholanemic mice. Sex-related differences within control and normocholanemic *Slc10a1*^{-/-} mouse groups are consistent with previous studies. In contrast, the sex differences in mRNA expression observed within hypercholanemic *Slc10a1*^{-/-} mice are opposite to what is reported in literature for wild type mice.

In wild type mice, serum bile acid concentrations are elevated in females (Uchida et al., 1983; Turley et al., 1998), which has been attributed to increased *Cyp7a1* expression in female animals (Schwarz et al., 2001). However, in our study, decreased hepatic mRNA levels of bile acid synthesis genes in female hypercholanemic mice suggests repression of bile acid synthesis. Interestingly, the opposite was observed in hypercholanemic male animals, who displayed significant elevations in *Cyp7a1* and *Cyp27a1* mRNA levels. Despite these differences, reduced mRNA levels of the transcriptional repressor *Shp* were observed in both male and female hypercholanemic mice. It is therefore unlikely that *Shp* is responsible for the differential *Cyp7a1* and *Cyp27a1* mRNA levels observed between male and female hypercholanemic mice.

We observed a shift toward cholic acid species in the sera of male and female hypercholanemic mice relative to control and normocholanemic mice. However, mRNA levels of the bile acid synthesis enzyme *Cyp8b1* were reduced in male and female hypercholanemic mice relative to normocholanemic and control animals. Thus, it is unlikely that the observed increase in cholic acids is due to increased *Cyp8b1* activity within the liver. The bile acid most highly elevated in sera of hypercholanemic mice was taurocholic acid, which is not surprising as TCA is the prototypical substrate of NTCP (Greupink et al., 2012). The striking increase in serum TCA concentrations in hypercholanemic mice is most likely a result of reduced hepatic uptake of conjugated bile acids in these animals. Contrary to findings by Mao et al., who observed persistently elevated conjugated bile acids in some female hypercholanemic *Slc10a1*^{-/-} mice relative to hypercholanemic males (Mao et al., 2019), no sex differences in serum conjugated bile acid concentrations were observed in our hypercholanemic *Slc10a1*^{-/-} animals.

Hepatic mRNA levels of many bile acid transporters were elevated in female control and normocholanemic mice relative to males of their respective genotypes and phenotypes. These sex related differences were significant for *Oatp1a4* and *Bsep* and *Ostβ*. This is consistent with previous studies, which indicate increased *Bsep*, *Oatp1a4*, and *Ostβ* expression in wild type female mice relative to males (Cheng et al., 2005; Sheng et al., 2017). Sexually dimorphic expression of these transporters is likely the result of differences in hormonal signaling (Cheng et al., 2006). Interestingly, sex associated differences in hepatic

bile acid gene expression in our hypercholanemic mice are opposite to what is observed in our control and normocholanemic mice and to what is reported in literature. Levels of hepatic *Cyp7a1*, *Cyp27a1*, *Oatp1a4*, and *Bsep* mRNA were significantly lower in livers of female relative to male hypercholanemic mice. This was not the case for *Ost β* , although it remains unclear why female biased *Ost β* is maintained in hypercholanemic mice whereas female biased expression of hepatic *Cyp7a1*, *Cyp27a1*, *Oatp1a4*, and *Bsep* are not.

Further studies will be necessary to elucidate exact pathways regulating these sex differences in gene expression. One possible hypothesis involves the interplays between bile acid signaling, the gut microbiome, sex hormones, and nuclear receptor activity. A symbiotic relationship is observed between bile acids and the gut microbiome. Bile acids modulate the gut microbiota through direct antimicrobial effects, which alters the composition of the gut microbiome (Begley et al., 2005). Alternatively, microbiota metabolize bile acids and, in doing so, contribute to FXR regulation (Inagaki et al., 2006). In mice, sex differences have been reported in the gut microbiome composition and in FXR signaling, which has been associated with sex differences in hepatic bile acid gene expression (Sheng et al., 2017).

Taken together, the likely reduction in bile acids in the intestine of *Slc10a1*^{-/-} mice may disrupt microbial composition and FXR signaling in a sex-dependent manner. An elegant study by Weger et al. evaluated gene expression in conventional and germ free mice and noted that the abolition of the gut microbiome induced a feminized gene expression pattern in livers of germ free

animals (Weger et al., 2019). Authors found that altered gut microbiomes in germ free mice resulted in disrupted sex and growth hormone signaling, which are imperative in establishing sexually dimorphic hepatic gene expression (Weger et al., 2019). This hypothesis is supported by Mao et al.'s observation of upregulated *Sult2e1* the major estrogen sulfotransferase, in livers of male hypercholanemic *Slc10a1*^{-/-} mice (Mao et al., 2019).

Despite our observations of differences in bile acid synthesis and transporter genes, similar overall phenotypes were observed for male and female hypercholanemic mice. As *Oatp1a1* mRNA levels are nearly absent in both male and female hypercholanemic mice, we suggest that the inability of OATP1A1 to compensate for absence of NTCP remains the driving factor for serum hypercholanemia in *Slc10a1*^{-/-} mice, regardless of biological sex.

In contrast to mice, bile acid concentrations in humans are generally higher in males (Trottier et al., 2011; Xiang et al., 2012; Frommherz et al., 2016). This is also reflected in human pathology by female-dominant gallstone formation (Fisher and Yousef, 1973; Bennion et al., 1978) and hormonal induction of cholestasis in genetically predisposed women (Wagner et al., 2009; Dixon and Williamson, 2016). Additionally, biological sex, rather than *CYP7A1* or *OATP1B1* genotype, was identified as the most important determinant of bile acid synthesis and composition in humans (Xiang et al., 2009).

Humans with inactive NTCP develop serum hypercholanemia and striking elevations in conjugated bile acids. These elevations are most prominent in early life (Vaz et al., 2015; Deng et al., 2016; Liu et al., 2017; Qiu et al., 2017), which

corresponds with the hypercholanemic phenotype observed in our juvenile *Slc10a1*^{-/-} mice. Studies have not assessed sex differences in human cases of NTCP deficiency, likely due to the rare nature of NTCP deficiency. However, the sex differences in mRNA expression of important bile acid synthesis and transport genes observed in our hypercholanemic mice suggest altered hormonal and nuclear receptor signaling, which warrant further investigation in humans. Importantly, many of these bile acid transporters are also central to drug disposition and response (Giacomini et al., 2010), therefore disruptions in their expression or function may alter drug disposition or predispose individuals to adverse drug events.

In conclusion, we identified normocholanemic and hypercholanemic serum bile acid phenotypes in male and female *Slc10a1*^{-/-} mice. We determined that biological sex does not influence bile acid pool composition in *Slc10a1*^{-/-} mice, regardless of normocholanemic or hypercholanemic phenotype. We observed that sex-associated differences in mRNA levels of bile acid synthesis and transport genes in control and normocholanemic mice reflect what is reported in literature. Importantly, however, many of the sex related differences observed in our hypercholanemic mice were opposite to what is found in wild type mice. Sex-related differences in hepatic gene expression in NTCP-deficient humans should be investigated to determine potential clinical relevance of our findings.

5.5 References

- Alnouti Y and Klaassen CD (2011) Mechanisms of gender-specific regulation of mouse sulfotransferases (Sults). *Xenobiotica* **41**:187-197.
- Begley M, Gahan CG, and Hill C (2005) The interaction between bacteria and bile. *FEMS microbiology reviews* **29**:625-651.
- Bennion LJ, Drobny E, Knowler WC, Ginsberg RL, Garnick MB, Adler RD, and Duane WC (1978) Sex differences in the size of bile acid pools. *Metabolism* **27**:961-969.
- Boyer JL (2013) Bile formation and secretion. *Compr Physiol* **3**:1035-1078.
- Cheng X, Maher J, Chen C, and Klaassen CD (2005) Tissue distribution and ontogeny of mouse organic anion transporting polypeptides (Oatps). *Drug Metab Dispos* **33**:1062-1073.
- Cheng X, Maher J, Lu H, and Klaassen CD (2006) Endocrine regulation of gender-divergent mouse organic anion-transporting polypeptide (Oatp) expression. *Mol Pharmacol* **70**:1291-1297.
- Chiang JY (2009) Bile acids: regulation of synthesis. *J Lipid Res* **50**:1955-1966.
- Csanaky IL, Lu H, Zhang Y, Ogura K, Choudhuri S, and Klaassen CD (2011) Organic anion-transporting polypeptide 1b2 (Oatp1b2) is important for the hepatic uptake of unconjugated bile acids: Studies in Oatp1b2-null mice. *Hepatology* **53**:272-281.
- Dawson PA, Lan T, and Rao A (2009) Bile acid transporters. *J Lipid Res* **50**:2340-2357.
- Deng M, Mao M, Guo L, Chen FP, Wen WR, and Song YZ (2016) Clinical and molecular study of a pediatric patient with sodium taurocholate cotransporting polypeptide deficiency. *Exp Ther Med* **12**:3294-3300.
- Dixon PH and Williamson C (2016) The pathophysiology of intrahepatic cholestasis of pregnancy. *Clinics and Research in Hepatology and Gastroenterology* **40**:141-153.
- Fisher MM and Yousef IM (1973) Sex differences in the bile acid composition of human bile: studies in patients with and without gallstones. *Canadian Medical Association journal* **109**:190-193.
- Frommherz L, Bub A, Hummel E, Rist MJ, Roth A, Watzl B, and Kulling SE (2016) Age-Related Changes of Plasma Bile Acid Concentrations in

Healthy Adults--Results from the Cross-Sectional KarMeN Study. *PLoS One* **11**:e0153959.

Giacomini KM, Huang S-M, Tweedie DJ, Benet LZ, Brouwer KLR, Chu X, Dahlin A, Evers R, Fischer V, Hillgren KM, Hoffmaster KA, Ishikawa T, Keppler D, Kim RB, Lee CA, Niemi M, Polli JW, Sugiyama Y, Swaan PW, Ware JA, Wright SH, Wah Yee S, Zamek-Gliszczyński MJ, Zhang L, and The International Transporter C (2010) Membrane transporters in drug development. *Nature Reviews Drug Discovery* **9**:215-236.

Greupink R, Nabuurs SB, Zarzycka B, Verweij V, Monshouwer M, Huisman MT, and Russel FGM (2012) In Silico Identification of Potential Cholestasis-Inducing Agents via Modeling of Na⁺-Dependent Taurocholate Cotransporting Polypeptide Substrate Specificity. *Toxicological Sciences* **129**:35-48.

Holdcroft A (2007) Gender bias in research: how does it affect evidence based medicine? *Journal of the Royal Society of Medicine* **100**:2-3.

Inagaki T, Moschetta A, Lee Y-K, Peng L, Zhao G, Downes M, Yu RT, Shelton JM, Richardson JA, Repa JJ, Mangelsdorf DJ, and Kliewer SA (2006) Regulation of antibacterial defense in the small intestine by the nuclear bile acid receptor. *Proceedings of the National Academy of Sciences of the United States of America* **103**:3920.

Klaassen CD and Cheng X (2005) *Age- and Gender-Related Differences in Xenobiotic Transporter Expression*. John Wiley & Sons, Inc.

Liu R, Chen C, Xia X, Liao Q, Wang Q, Newcombe PJ, Xu S, Chen M, Ding Y, Li X, Liao Z, Li F, Du M, Huang H, Dong R, Deng W, Wang Y, Zeng B, Pan Q, Jiang D, Zeng H, Sham P, Cao Y, Maxwell PH, Gao ZL, Peng L, and Wang Y (2017) Homozygous p.Ser267Phe in SLC10A1 is associated with a new type of hypercholanemia and implications for personalized medicine. *Sci Rep* **7**:9214.

Mao F, Liu T, Hou X, Zhao H, He W, Li C, Jing Z, Sui J, Wang F, Liu X, Han J, Borchers CH, Wang JS, and Li W (2019) Increased sulfation of bile acids in mice and human subjects with sodium taurocholate cotransporting polypeptide deficiency. *J Biol Chem* **294**:11853-11862.

Phelps T, Snyder E, Rodriguez E, Child H, and Harvey P (2019) The influence of biological sex and sex hormones on bile acid synthesis and cholesterol homeostasis. *Biol Sex Differ* **10**:52.

Qiu JW, Deng M, Cheng Y, Atif RM, Lin WX, Guo L, Li H, and Song YZ (2017) Sodium taurocholate cotransporting polypeptide (NTCP) deficiency: Identification of a novel SLC10A1 mutation in two unrelated infants

presenting with neonatal indirect hyperbilirubinemia and remarkable hypercholanemia. *Oncotarget* **8**:106598-106607.

Sayin SI, Wahlström A, Felin J, Jäntti S, Marschall HU, Bamberg K, Angelin B, Hyötyläinen T, Orešič M, and Bäckhed F (2013) Gut microbiota regulates bile acid metabolism by reducing the levels of tauro-beta-muricholic acid, a naturally occurring FXR antagonist. *Cell metabolism* **17**:225-235.

Schwarz M, Russell DW, Dietschy JM, and Turley SD (2001) Alternate pathways of bile acid synthesis in the cholesterol 7 α -hydroxylase knockout mouse are not upregulated by either cholesterol or cholestyramine feeding. *J Lipid Res* **42**:1594-1603.

Sheng L, Jena PK, Liu HX, Kalanetra KM, Gonzalez FJ, French SW, Krishnan VV, Mills DA, and Wan YY (2017) Gender Differences in Bile Acids and Microbiota in Relationship with Gender Dissimilarity in Steatosis Induced by Diet and FXR Inactivation. *Sci Rep* **7**:1748.

Slijepcevic D, Abbing RLPR, Katafuchi T, Blank A, Donkers JM, van Hoppe S, de Waart DR, Tolenaars D, van der Meer JHM, Wildenberg M, Beuers U, Elferink RPJO, Schinkel AH, and van de Graaf SFJ (2017) Hepatic Uptake of Conjugated Bile Acids Is Mediated by Both Sodium Taurocholate Cotransporting Polypeptide and Organic Anion Transporting Polypeptides and Modulated by Intestinal Sensing of Plasma Bile Acid Levels in Mice. *Hepatology* **66**:1631-1643.

Slijepcevic D, Kaufman C, Wichers CG, Gilglioni EH, Lempp FA, Duijst S, de Waart DR, Elferink RP, Mier W, Stieger B, Beuers U, Urban S, and van de Graaf SF (2015) Impaired uptake of conjugated bile acids and hepatitis b virus pres1-binding in na(+)-taurocholate cotransporting polypeptide knockout mice. *Hepatology* **62**:207-219.

Trottier J, Caron P, Straka RJ, and Barbier O (2011) Profile of serum bile acids in noncholestatic volunteers: gender-related differences in response to fenofibrate. *Clin Pharmacol Ther* **90**:279-286.

Turley SD, Schwarz M, Spady DK, and Dietschy JM (1998) Gender-related differences in bile acid and sterol metabolism in outbred CD-1 mice fed low- and high-cholesterol diets. *Hepatology* **28**:1088-1094.

Uchida K, Mizuno H, Hirota K, Takeda Ki, Takeuchi N, and Ishikawa Y (1983) Effects of spinasterol and sitosterol on plasma and liver cholesterol levels and biliary and fecal sterol and bile acid excretions in mice. *Jap J Pharmacol* **33**:103-112.

van de Steeg E, Wagenaar E, van der Kruijssen CM, Burggraaff JE, de Waart DR, Elferink RP, Kenworthy KE, and Schinkel AH (2010) Organic anion

transporting polypeptide 1a/1b-knockout mice provide insights into hepatic handling of bilirubin, bile acids, and drugs. *J Clin Invest* **120**:2942-2952.

- Vaz FM, Paulusma CC, Huidekoper H, de Ru M, Lim C, Koster J, Ho-Mok K, Bootsma AH, Groen AK, Schaap FG, Oude Elferink RP, Waterham HR, and Wanders RJ (2015) Sodium taurocholate cotransporting polypeptide (SLC10A1) deficiency: conjugated hypercholanemia without a clear clinical phenotype. *Hepatology* **61**:260-267.
- Wagner M, Zollner G, and Trauner M (2009) New molecular insights into the mechanisms of cholestasis. *Journal of Hepatology* **51**:565-580.
- Wang H, Chen J, Hollister K, Sowers LC, and Forman BM (1999) Endogenous Bile Acids Are Ligands for the Nuclear Receptor FXR/BAR. *Molecular cell* **3**:543-553.
- Weger BD, Gobet C, Yeung J, Martin E, Jimenez S, Betrisey B, Foata F, Berger B, Balvay A, Foussier A, Charpagne A, Boizet-Bonhoure B, Chou CJ, Naef F, and Gachon F (2019) The Mouse Microbiome Is Required for Sex-Specific Diurnal Rhythms of Gene Expression and Metabolism. *Cell metabolism* **29**:362-382.e368.
- Xiang X, Backman JT, Neuvonen PJ, and Niemi M (2012) Gender, but not CYP7A1 or SLCO1B1 polymorphism, affects the fasting plasma concentrations of bile acids in human beings. *Basic & clinical pharmacology & toxicology* **110**:245-252.
- Xiang X, Han Y, Neuvonen M, Pasanen MK, Kalliokoski A, Backman JT, Laitila J, Neuvonen PJ, and Niemi M (2009) Effect of SLCO1B1 polymorphism on the plasma concentrations of bile acids and bile acid synthesis marker in humans. *Pharmacogenet Genomics* **19**:447-457.
- Yang L, Li Y, Hong H, Chang CW, Guo LW, Lyn-Cook B, Shi L, and Ning B (2012) Sex Differences in the Expression of Drug-Metabolizing and Transporter Genes in Human Liver. *Journal of drug metabolism & toxicology* **3**:1000119.
- Zhang Y, Csanaky IL, Cheng X, Lehman-McKeeman LD, and Klaassen CD (2012) Organic anion transporting polypeptide 1a1 null mice are sensitive to cholestatic liver injury. *Toxicol Sci* **127**:451-462.

6 Summary, future directions & conclusions

Aim 1

The primary aim of this chapter was to characterize the transport activity and expression of missense human genetic variants of *SLC10A1 in vitro*. The secondary objective was to use this data to determine whether seven *in silico* prediction tools accurately predicted our observed *in vitro* NTCP transport activity. We hypothesized that genetic variation would decrease transport activity and expression of variant NTCP. We also hypothesized that predictions made by *in silico* tools would reflect *in vitro* taurocholic acid transport, and that the ADME-optimized tool would be the best predictor of rosuvastatin transport by variant NTCP.

Of thirty-five previously uncharacterized NTCP variants, we identified seven with nearly absent transport of the endogenous and drug substrates taurocholic acid and rosuvastatin. These seven genetic variants produced the following amino acid substitutions: P73T, L138P, F234L, S241F, R249W, R252S, R252C. Although variant NTCP protein was detected in whole cell lysates, their expression was virtually undetectable at the plasma membrane. Their absence at the plasma membrane likely explains their loss of substrate transport. Sequence alignments show that six of seven residues that were affected are located within highly conserved regions, indicating their relative importance in the protein function. Furthermore, in the case of these variants, mutant amino acid residues have different properties than the original amino acid residue, which suggests they may disrupt protein structure or function. Two variants, A3T and E342K,

showed modest but significant increases in taurocholic acid. Nearly 2-fold higher rosuvastatin uptake was observed for the T171I variant. Interestingly, the G191R variant show a substrate-specific effect; this variation did not affect TCA uptake, however rosuvastatin uptake was markedly reduced. This may indicate that this region or residue is important in rosuvastatin binding, whereas it is not important in taurocholic acid binding.

In silico tools were moderate to good predictors of *in vitro* taurocholic acid transport. Four of the seven employed tools accurately predicted deleterious activity for all of the seven loss of activity and loss of plasma membrane expression variants. The ADME-optimized *in silico* tool was no better than other tools for predicting uptake of rosuvastatin by variant forms of NTCP. These results suggest that *in silico* predictions are not robust enough to replace functional assessment of *SLC10A1* genetic variation *in vitro*.

Caveats of these *in vitro* characterization methodologies include the laborious nature of experiments relative to the number of rare variants revealed by next-generation sequencing. Novel, high-throughput methodologies that characterize function and expression of thousands of variants show promise for replacing these low throughput approaches (Matreyek et al., 2018). Additionally, although we can infer that reduced activity is the result of reduced plasma membrane expression, the exact mechanisms of decreased plasma membrane expression remain unclear. Understanding the cellular localization of the variant proteins that are not expressed at the plasma membrane could provide evidence into the mechanisms of reduced trafficking or stability of these proteins.

Currently, the appeal of using *in silico* functional predictions is to rank variants from large datasets, such as next-generation sequencing data, for functional characterization. One approach that may increase the utility of current *in silico* prediction tools could be to generate predictions from multiple tools and rank variants based on the number of tools that predict deleteriousness. Further optimization of algorithms will be required to increase confidence of their predictions.

A challenge of employing *in silico* tools to predict protein function is their relevance in terms of drug disposition. With the exception of few novel tools optimized using experimental data from drug studies, predictions are often based on data relevant to the endogenous function of a protein. Optimization for relevance to drug transport or metabolism is particularly challenging for multiple reasons, including substrate specificity. One approach could be to optimize a prediction tool based on known or predicted binding sites for a particular class of drug.

Taken together, these results identify previously uncharacterized genetic variants in human *SLC10A1* that result in altered taurocholic acid and rosuvastatin transport *in vitro*. The loss of function variants are likely the most directly transferrable findings from this study, as homozygous loss of function variation in *SLC10A1* is associated with serum hypercholanemia and may disrupt nutrient homeostasis. However, the variant that displays gain of rosuvastatin transport could be beneficial in humans on rosuvastatin therapy, owing to the potential increase in hepatic accumulation of rosuvastatin.

Next steps involve defining the roles of these genetic variants *in vivo*, and in particular, in human subjects. The variants characterized in this study are rare, with global minor allele frequencies less than 0.5%, which explains why such variants have not been previously characterized. However, frequencies of certain genetic variants in *SLC10A1* are higher in Asian populations (Ho et al., 2004; Pan et al., 2011), reaching upwards of 7.5% minor allele frequency. Therefore, the relevance of our findings may be of greater importance in individuals of Asian descent. The most frequent and widely characterized NTCP variant, p.S267F, was shown to have nearly abolished taurocholic acid transport *in vitro* (Ho et al., 2004), yet a 4-fold gain of rosuvastatin transport relative to wild type (Ho et al., 2006). These *in vitro* findings translate to humans homozygous for the p.S267F variant as serum conjugated hypercholanemia (Liu et al., 2017) and increased hepatic uptake of pravastatin (Lu et al., 2016), respectively. Our *in vitro* findings represent an important step in identifying variants of potential clinical importance, and future studies should evaluate the effects of these variations on bile acid dynamics and rosuvastatin transport in human subjects. A summary of how *in silico* and *in vitro* assays contribute to overall functional characterization of important human genetic variants is displayed in Figure 6.1 (Russell and Schwarz, 2020).

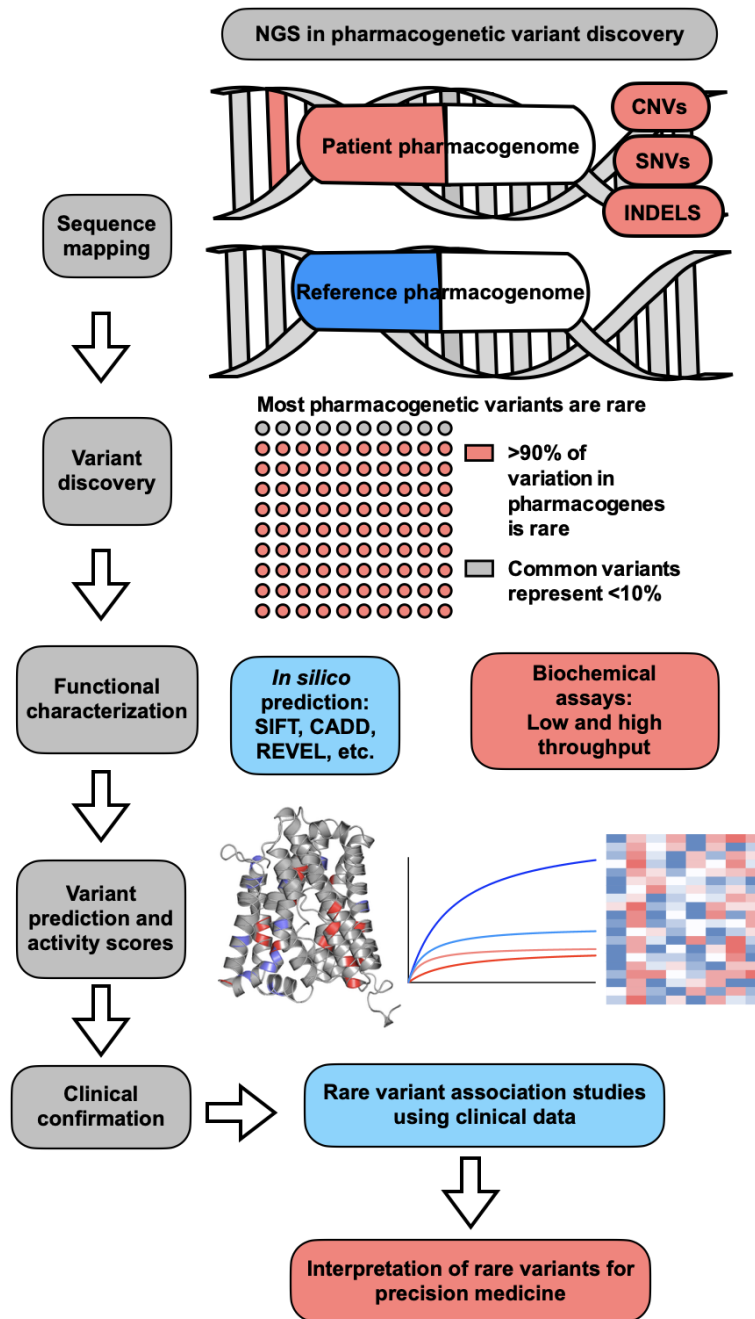


Figure 6.1. Rare genetic variant discovery and characterization: from next-generation sequencing to *in vivo* clinical relevance

First, next-generation sequencing is used to identify rare variants. This is done by sequence mapping, which helps discover variants by comparing the patient sequencing data to that of a reference genome. Using this approach, many rare variants of unknown clinical significance are identified. Subsequent to this, we can employ *in silico* tools to help predict the function of these rare variants, and low-throughput and high-throughput *in vitro* assays can be used to help elucidate functional effects of these genetic variants. Ultimately, this can help inform which variants should be tested *in vivo* for potential clinical relevance. Overall, the goal is to help identify rare genetic factors that might contribute to disease and drug response (Russell and Schwarz, 2020).

Aim 2

The primary objective of this chapter was to elucidate the effects of genetic disruption of *Slc10a1* in mice on serum bile acids and bile acid synthesis and transporter gene expression. The secondary objective of this chapter was to determine hepatic uptake of rosuvastatin in *Slc10a1*^{-/-} mice. We hypothesized that *Slc10a1* disruption would result in conjugated serum hypercholanemia due to a lack of compensatory hepatic bile acid uptake by non-NTCP transporters. We also hypothesized that disruption of *Slc10a1* would result in significantly reduced hepatic uptake of rosuvastatin.

A bimodal bile acid phenotype was observed in our *Slc10a1*^{-/-} mice, which was not surprising given that two independent research groups also noted this finding (Slijepcevic et al., 2015; Mao et al., 2019). In our study, bile acid concentrations in the serum were >25-fold higher than physiological concentrations in approximately 45% of *Slc10a1*^{-/-} mice. The enlarged gallbladders, bile deposits in bile canaliculi, and lack of prominent bile ducts in hypercholanemic mice suggest disruption of gallbladder emptying. This would decrease bile acid levels within the intestinal lumen, limiting food emulsification and decreasing absorption of nutrients, which may explain persistent reductions in body weights in these mice. The fasted state has been associated with increased activity of important hepatic nuclear receptors PXR and CAR, and decreased activity of FXR and VDR. Altered mRNA levels of bile acid genes in our hypercholanemic *Slc10a1*^{-/-} mice are consistent with these alterations in nuclear receptor signaling (Fig. 6.2).

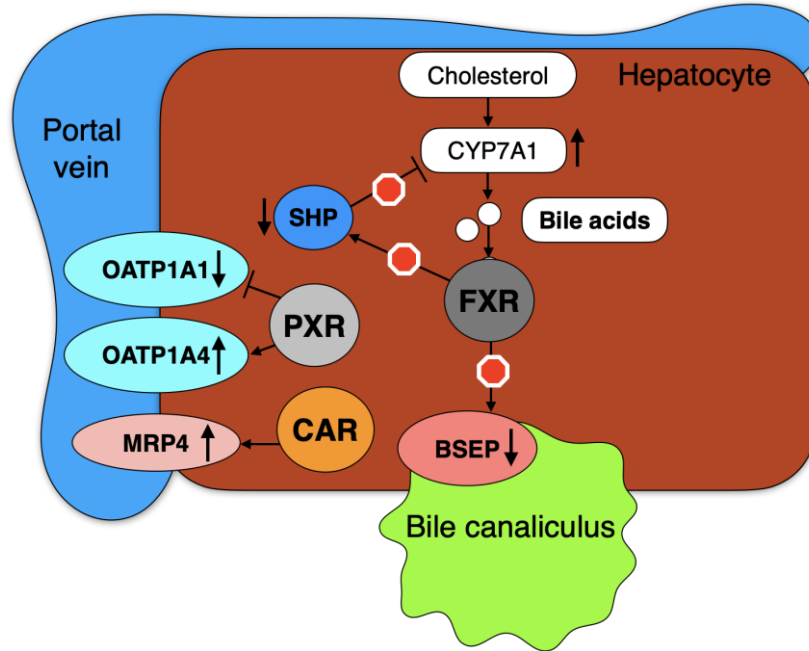


Figure 6.2. Hypothesized alterations in nuclear receptor signaling in our hypercholanemic *Slc10a1*^{-/-} mice

The major findings in our hypercholanemic mice are reduced *Oatp1a1*, *Bsep*, and *Shp* expression, along with elevated *Oatp1a4* and *Mrp4* expression. These changes are consistent with upregulated PXR and CAR and downregulated FXR observed in the fasted state. Together with reduced body weights, enlarged gallbladders, and serum hypercholanemia, it is likely that reduced bile acids in the lumen of the intestine diminishes nutrient absorption in hypercholanemic *Slc10a1*^{-/-} mice, resulting in fasted state gene expression in the liver.

Our hypothesis of serum conjugated hypercholanemia was therefore supported in this subset of *Slc10a1*^{-/-} mice. The virtual absence of hepatic *Oatp1a1* mRNA, an important bile acid transporter in rodents, supports the hypothesis that OATP1A1 is an important compensatory pathway in *Slc10a1*^{-/-} mice exhibiting profound hypercholanemia. Bile casts in the kidneys, increased renal expression of bile acid efflux transporters, and decreased renal expression of bile acid uptake transporters were observed in these mice. These findings suggest enhanced renal elimination of bile acids subsequent to accumulation of bile acids in the serum, which may result in kidney toxicity. It is important to note that a developmental defect in the formation of the bile duct system of hypercholanemic mice cannot be ruled out. This is supported by bile cast formation in the bile canaliculi, some hepatocyte swelling and necrosis, unformed bile ducts, and markedly enlarged gallbladders. Although we did not directly evaluate formation of the bile ducts in the present thesis, *SLC10A1* has been identified as a master regulator of genes in the liver (Yang et al., 2010) and its disruption could impair proper formation of the biliary system.

Implications of this fasted phenotype in hypercholanemic *Slc10a1*^{-/-} mice may be important in humans. In humans, serum hypercholanemia is most prominent in NTCP-deficient pediatrics (Vaz et al., 2015). Additionally, our hypothesis of upregulated PXR and CAR in hypercholanemic mice due to fasting could be important in humans with homozygous loss of function genetic variation in *SLC10A1*, although this remains to be tested. PXR and CAR are particularly important in drug metabolism (Wang et al., 2012), thus if these findings translate

to humans, NTCP deficient individuals may be susceptible to altered pharmacokinetics and pharmacodynamics for many drugs in clinical use. Such individuals may require an enhanced dose of drug due to rapid drug metabolism and inactivation. Conversely, for prodrugs, enhanced PXR or CAR-mediated metabolism to the active drug could render an individual more susceptible to toxicity or adverse drug events.

It remains unclear why only ~45% of *Slc10a1*^{-/-} mice display this fasted-like phenotype. The remaining 55% of mice appear moderately affected in early life, as observed by decreased body weights. However, their body weights normalize with those of control mice by eight weeks of age. A potential explanation for these major phenotypic differences is reduced maternal care in early life. This is supported by the notion that hypercholanemic mice are able to survive to ten weeks when hydrated with saline injections. It remains to be seen whether these mice would survive long-term, and if so, whether their hypercholanemia and altered gene expression would persist.

This aim relied on evaluating mRNA expression of bile acid genes to determine potential disruption of pathways in bile acid signaling. Although mRNA is a good first step in understanding which genes might be affected, additional methods are necessary to further validate these findings. Protein expression is an important indicator of bile acid transporter function. Additionally, hepatic concentrations of bile acids could assist in evaluating the extent of nuclear receptor activation in these animals. Furthermore, quantification and serum

biomarkers of bile acid synthesis and signaling would enhance our understanding of disruptions in bile acid physiology in *Slc10a1*^{-/-} mice.

For our secondary objective, our hypothesis of decreased hepatic rosuvastatin uptake in *Slc10a1*^{-/-} was not supported by our results. Liver-to-serum concentrations of rosuvastatin were no different in ten-week-old *Slc10a1*^{-/-} mice relative to age-matched controls. Although we did not quantify serum bile acids in these mice, these studies were conducted in ten-week-old mice. Our hypercholanemic mice did not naturally survive passed seven weeks of age, therefore we speculate that the *Slc10a1*^{-/-} mice in the rosuvastatin study were normocholanemic. Hepatic bile acid transporter mRNA expression in ten-week-old mice was no different in *Slc10a1*^{-/-} mice relative to controls, providing further evidence that these mice were normocholanemic. Normocholanemia.

The major limitations of extrapolating these results in the context of humans are species differences in rosuvastatin uptake transporters when comparing mice and humans. The presence of OATP1A isoforms in mouse hepatocytes but not human hepatocytes is a major species difference that may reduce the relevance of NTCP to rosuvastatin disposition in mice. Future studies could co-administer an NTCP inhibitor and rosuvastatin in *Oatp1a/1b*^{-/-} mice to determine whether hepatic uptake of rosuvastatin is maintained by additional transporters. Ultimately, studies should be performed in humans to determine whether rosuvastatin disposition is affected by inhibition of NTCP. Studies in humans with the p.S267F NTCP variation, which displays gain of statin transport relative to wild type, showed that this variant enhanced systemic clearance of

pravastatin, which is another hydrophilic statin (Lu et al., 2016). These results provide the basis to hypothesize that pharmacological inhibition or genetic deficiency in NTCP will alter hepatic uptake of rosuvastatin in humans.

In mice, OATP1A isoforms and OATP1B2 appear important for rosuvastatin disposition, whereas NTCP and OATP2B1 do not (DeGorter et al., 2012; Iusuf et al., 2013; Medwid et al., 2019). To determine the importance of NTCP to rosuvastatin transport in humans, clinical studies using coadministration of rosuvastatin and a selective inhibitor of the important rosuvastatin transporters, OATP1B1 and OATP1B3, will be required. It is likely that genetic deficiency or pharmacological inhibition of NTCP alone will not be clinically important to rosuvastatin disposition in humans, as OATP1B1 and OATP1B3 will maintain hepatic rosuvastatin uptake. However, the role of NTCP in rosuvastatin uptake into hepatocytes may become more important in genetic deficiency of hepatic OATPs or their pharmacological inhibition. Furthermore, as NTCP inhibitors are becoming important in treating hepatitis B and D, and further therapeutic indications relative to select forms of cholestasis or metabolic conditions are being evaluated, this may enhance the incidence of drug-transporter interactions involving NTCP and OATPs.

Aim 3

The objective of this aim was to examine sex-related differences in serum bile acid composition and hepatic bile acid gene expression in *Slc10a1*^{-/-} mice. Our first hypothesis was that mRNA expression of bile acid synthesis genes

would be elevated in female mice, resulting in increased serum bile acid concentrations. We also hypothesized that sex differences in bile acid transporter expression observed in wild type mice would be conserved in our *Slc10a1*^{-/-} mice. Our results did not support these hypotheses.

Overall, serum bile acid pool concentrations did not significantly differ between males and females. Sexual dimorphisms in bile acid synthesis and transporter mRNA expression in control and normocholanemic mice were consistent with literature (Cheng et al., 2005; Sheng et al., 2017). However, sex-associated expression of bile acid synthesis and transport genes in hypercholanemic mice were largely opposite of what was expected. Expression of *Cyp7a1*, which has been linked to increased bile acid synthesis in female mice (Schwarz et al., 2001), was increased in male hypercholanemic mice rather than female hypercholanemic mice. Additionally, *Oatp1a4* and *Bsep* are female-dominant genes, which was reflected in our control and normocholanemic mice. However, *Oatp1a4* and *Bsep* mRNA levels were significantly reduced in female hypercholanemic mice relative to male hypercholanemic mice. These findings suggest potentially dysregulated hormonal signaling in our hypercholanemic mice, resulting in feminization of liver gene expression in hypercholanemic males and defective sexual dimorphism in hypercholanemic females.

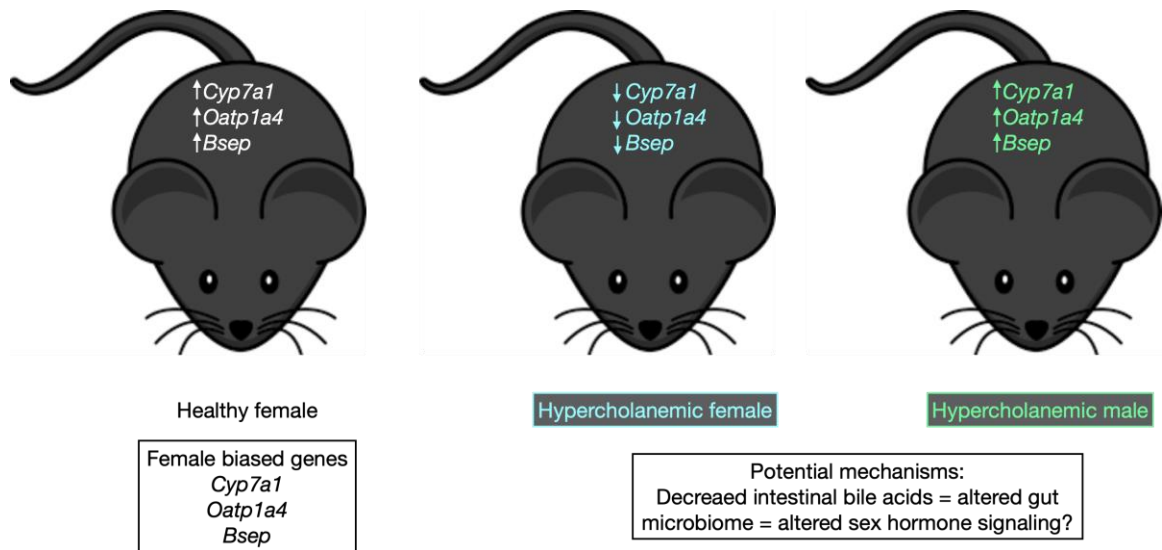


Figure 6.3. Female-dominant gene expression in healthy and hypercholanemic mice

In healthy, C57BL/6 mice and additional strains of mice, there is female-dominant expression of a variety of genes, including *Cyp7a1*, *Oatp1a4*, and *Bsep*. When tested in our *Slc10a1*^{-/-} mice, opposite sexual dimorphism was observed in our mice with hypercholanemia. Livers of female hypercholanemic *Slc10a1*^{-/-} mice show patterns consistent with male sex hormone expression, whereas livers of male hypercholanemic *Slc10a1*^{-/-} mice appear feminized by the increased expression of female-dominant genes. Although not tested directly in this thesis, potential explanations may involve altered bile acids within the intestine, which affect the gut microbiome and hormonal signaling.

Despite these differences, *Oatp1a1* mRNA was nearly undetectable in female and male hypercholanemic mice. Similarities in bile acid composition and concentrations, alongside virtually absent *Oatp1a1* mRNA, suggest that the sex differences in bile acid synthesis and transporter genes are not inherently important for the development of hypercholanemia in *Slc10a1*^{-/-} mice.

Although we speculate that reduced bile acids in the intestinal lumen may affect FXR and sex hormone signaling, additional studies are necessary to confirm this. Concentrations of estrogens and androgens should be measured in the serum and liver of these animals to determine potential alterations in sex hormones. Additionally, replicating hepatic concentrations of bile acids in hypercholanemic males and females and assessing the activation of estrogen and androgen receptors by these bile acid pools could reveal potential sex differences in bile acid signaling.

A high degree of variability was observed in serum bile acid concentrations and in mRNA levels of certain bile acid genes for mice within the same group. As the number of mice per group was relatively low (n=3-6 for the majority of comparisons), this variability could hinder potential significant differences in findings. Studies in larger cohorts of mice may be of more benefit to determine statistical differences.

Sex related differences have not been reported in human cases of NTCP deficiency, however there is a paucity of data surrounding NTCP deficient humans. In an aging study, Mao et al. determined that certain female *Slc10a1*^{-/-} mice remain hypercholanemic at 20 months of age, whereas this was not

observed in male *Slc10a1*^{-/-} mice. Our findings of sex-related differences in hepatic mRNA expression of bile acid and drug transporters in *Slc10a1*^{-/-} mice warrant studies to determine whether these changes translate to humans. The altered gene expression we see in these mice involve a variety of genes important in additional physiological functions, including drug metabolism.

6.1 Conclusions

The hypothesis of this study was that genetic variation in *SLC10A1* would decrease bile acid and rosuvastatin transport. Our hypothesis was both supported and refuted by *in vitro* data, where some variants are gain of function and others show loss of function to transport taurocholic acid or rosuvastatin. Our *in vivo* studies show that disruption of *SLC10A1* in mice reduced bile acid uptake and altered expression of a variety of important bile acid and drug disposition genes in a subset of *Slc10a1*^{-/-} mice. Our findings in *Slc10a1*^{-/-} mice also suggest that NTCP is not important for hepatic rosuvastatin uptake in mice.

NTCP is recognized as an important hepatic bile acid uptake transporter that is also capable of *in vitro* transport of rosuvastatin and integral to hepatitis B and D uptake into the liver (Ho et al., 2006; Dawson et al., 2009; Yan et al., 2012). Evidence suggests genetic variation in *SLC10A1* and pharmacological inhibition of NTCP mediate serum hypercholanemia and may potentiate malnutrition subsequent to altered bile flow (Vaz et al., 2015; Deng et al., 2016; Liu et al., 2017; Qiu et al., 2017; Blank et al., 2018). Bioinformatic analysis of

gene pathways in human liver samples have identified *SLC10A1* as a master regulator of gene expression for cytochrome P450 and bile acid synthesis enzymes (Yang et al., 2010). These important functions have heightened the interest in understanding effects of *SLC10A1* disruption on bile acid homeostasis and pharmacotherapy.

The studies in this thesis contribute to a better understanding of molecular changes observed in NTCP deficiency. Ultimately, these findings will provide the basis for subsequent evaluation of genetic deficiency and pharmacologic modulation of human NTCP and associated impacts on bile acid dynamics, nuclear receptor signaling, and substrate drug response.

6.2 References

- Blank A, Eidam A, Haag M, Hohmann N, Burhenne J, Schwab M, van de Graaf S, Meyer MR, Maurer HH, Meier K, Weiss J, Bruckner T, Alexandrov A, Urban S, Mikus G, and Haefeli WE (2018) The NTCP-inhibitor Myrcludex B: Effects on Bile Acid Disposition and Tenofovir Pharmacokinetics. *Clin Pharmacol Ther* **103**:341-348.
- Cheng X, Maher J, Chen C, and Klaassen CD (2005) Tissue distribution and ontogeny of mouse organic anion transporting polypeptides (Oatps). *Drug Metab Dispos* **33**:1062-1073.
- Dawson PA, Lan T, and Rao A (2009) Bile acid transporters. *J Lipid Res* **50**:2340-2357.
- DeGorter MK, Urquhart BL, Gradhand U, Tirona RG, and Kim RB (2012) Disposition of atorvastatin, rosuvastatin, and simvastatin in oatp1b2^{-/-} mice and intraindividual variability in human subjects. *J Clin Pharmacol* **52**:1689-1697.
- Deng M, Mao M, Guo L, Chen FP, Wen WR, and Song YZ (2016) Clinical and molecular study of a pediatric patient with sodium taurocholate cotransporting polypeptide deficiency. *Exp Ther Med* **12**:3294-3300.
- Ho RH, Leake BF, Roberts RL, Lee W, and Kim RB (2004) Ethnicity-dependent polymorphism in Na⁺-taurocholate cotransporting polypeptide (SLC10A1) reveals a domain critical for bile acid substrate recognition. *J Biol Chem* **279**:7213-7222.
- Ho RH, Tirona RG, Leake BF, Glaeser H, Lee W, Lemke CJ, Wang Y, and Kim RB (2006) Drug and bile acid transporters in rosuvastatin hepatic uptake: function, expression, and pharmacogenetics. *Gastroenterology* **130**:1793-1806.
- Iusuf D, van Esch A, Hobbs M, Taylor M, Kenworthy KE, van de Steeg E, Wagenaar E, and Schinkel AH (2013) Murine Oatp1a/1b Uptake Transporters Control Rosuvastatin Systemic Exposure Without Affecting Its Apparent Liver Exposure. *Molecular Pharmacology* **83**:919.
- Liu R, Chen C, Xia X, Liao Q, Wang Q, Newcombe PJ, Xu S, Chen M, Ding Y, Li X, Liao Z, Li F, Du M, Huang H, Dong R, Deng W, Wang Y, Zeng B, Pan Q, Jiang D, Zeng H, Sham P, Cao Y, Maxwell PH, Gao ZL, Peng L, and Wang Y (2017) Homozygous p.Ser267Phe in SLC10A1 is associated with a new type of hypercholanemia and implications for personalized medicine. *Sci Rep* **7**:9214.

- Lu XF, Zhou Y, Bi KS, and Chen XH (2016) Mixed effects of OATP1B1, BCRP and NTCP polymorphisms on the population pharmacokinetics of pravastatin in healthy volunteers. *Xenobiotica* **46**:841-849.
- Mao F, Liu T, Hou X, Zhao H, He W, Li C, Jing Z, Sui J, Wang F, Liu X, Han J, Borchers CH, Wang JS, and Li W (2019) Increased sulfation of bile acids in mice and human subjects with sodium taurocholate cotransporting polypeptide deficiency. *J Biol Chem* **294**:11853-11862.
- Matreyek KA, Starita LM, Stephany JJ, Martin B, Chiasson MA, Gray VE, Kircher M, Khechaduri A, Dines JN, Hause RJ, Bhatia S, Evans WE, Relling MV, Yang W, Shendure J, and Fowler DM (2018) Multiplex assessment of protein variant abundance by massively parallel sequencing. *Nat Genet* **50**:874-882.
- Medwid S, Li MMJ, Knauer MJ, Lin K, Mansell SE, Schmerk CL, Zhu C, Griffin KE, Yousif MD, Dresser GK, Schwarz UI, Kim RB, and Tirona RG (2019) Fexofenadine and Rosuvastatin Pharmacokinetics in Mice with Targeted Disruption of Organic Anion Transporting Polypeptide 2B1. *Drug Metab Dispos* **47**:832-842.
- Pan W, Song IS, Shin HJ, Kim MH, Choi YL, Lim SJ, Kim WY, Lee SS, and Shin JG (2011) Genetic polymorphisms in Na⁺-taurocholate co-transporting polypeptide (NTCP) and ileal apical sodium-dependent bile acid transporter (ASBT) and ethnic comparisons of functional variants of NTCP among Asian populations. *Xenobiotica* **41**:501-510.
- Qiu JW, Deng M, Cheng Y, Atif RM, Lin WX, Guo L, Li H, and Song YZ (2017) Sodium taurocholate cotransporting polypeptide (NTCP) deficiency: Identification of a novel SLC10A1 mutation in two unrelated infants presenting with neonatal indirect hyperbilirubinemia and remarkable hypercholanemia. *Oncotarget* **8**:106598-106607.
- Russell LE and Schwarz UI (2020) Variant discovery using next-generation sequencing and its future role in pharmacogenetics. *Pharmacogenomics* **21**:471-486.
- Schwarz M, Russell DW, Dietschy JM, and Turley SD (2001) Alternate pathways of bile acid synthesis in the cholesterol 7 α -hydroxylase knockout mouse are not upregulated by either cholesterol or cholestyramine feeding. *J Lipid Res* **42**:1594-1603.
- Sheng L, Jena PK, Liu HX, Kalanetra KM, Gonzalez FJ, French SW, Krishnan VV, Mills DA, and Wan YY (2017) Gender Differences in Bile Acids and Microbiota in Relationship with Gender Dissimilarity in Steatosis Induced by Diet and FXR Inactivation. *Sci Rep* **7**:1748.

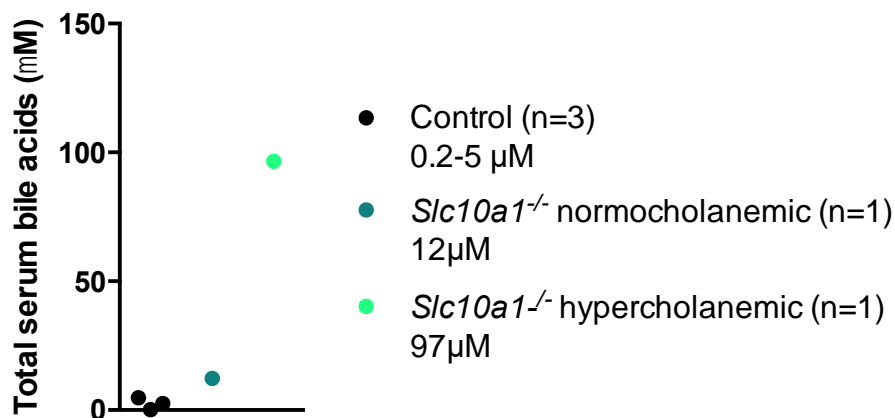
- Slijepcevic D, Kaufman C, Wichers CG, Gilgioni EH, Lempp FA, Duijst S, de Waart DR, Elferink RP, Mier W, Stieger B, Beuers U, Urban S, and van de Graaf SF (2015) Impaired uptake of conjugated bile acids and hepatitis b virus pres1-binding in na(+)-taurocholate cotransporting polypeptide knockout mice. *Hepatology* **62**:207-219.
- Vaz FM, Paulusma CC, Huidekoper H, de Ru M, Lim C, Koster J, Ho-Mok K, Bootsma AH, Groen AK, Schaap FG, Oude Elferink RP, Waterham HR, and Wanders RJ (2015) Sodium taurocholate cotransporting polypeptide (SLC10A1) deficiency: conjugated hypercholanemia without a clear clinical phenotype. *Hepatology* **61**:260-267.
- Wang Y-M, Ong SS, Chai SC, and Chen T (2012) Role of CAR and PXR in xenobiotic sensing and metabolism. *Expert opinion on drug metabolism & toxicology* **8**:803-817.
- Yan H, Zhong GC, Xu GW, He WH, Jing ZY, Gao ZC, Huang Y, Qi YH, Peng B, Wang HM, Fu LR, Song M, Chen P, Gao WQ, Ren BJ, Sun YY, Cai T, Feng XF, Sui JH, and Li WH (2012) Sodium taurocholate cotransporting polypeptide is a functional receptor for human hepatitis B and D virus. *Elife* **1**.
- Yang X, Zhang B, Molony C, Chudin E, Hao K, Zhu J, Gaedigk A, Suver C, Zhong H, Leeder JS, Guengerich FP, Strom SC, Schuetz E, Rushmore TH, Ulrich RG, Slatter JG, Schadt EE, Kasarskis A, and Lum PY (2010) Systematic genetic and genomic analysis of cytochrome P450 enzyme activities in human liver. *Genome Res* **20**:1020-1036.

7 Appendices

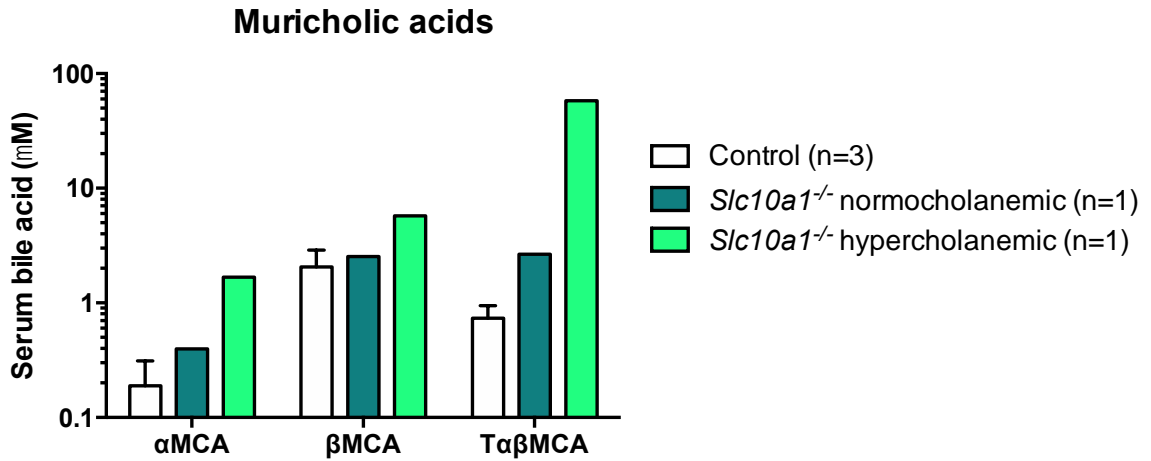
Appendix A. Supplemental data

Serum bile acids and gene array data for female *Slc10a1*^{-/-} mice

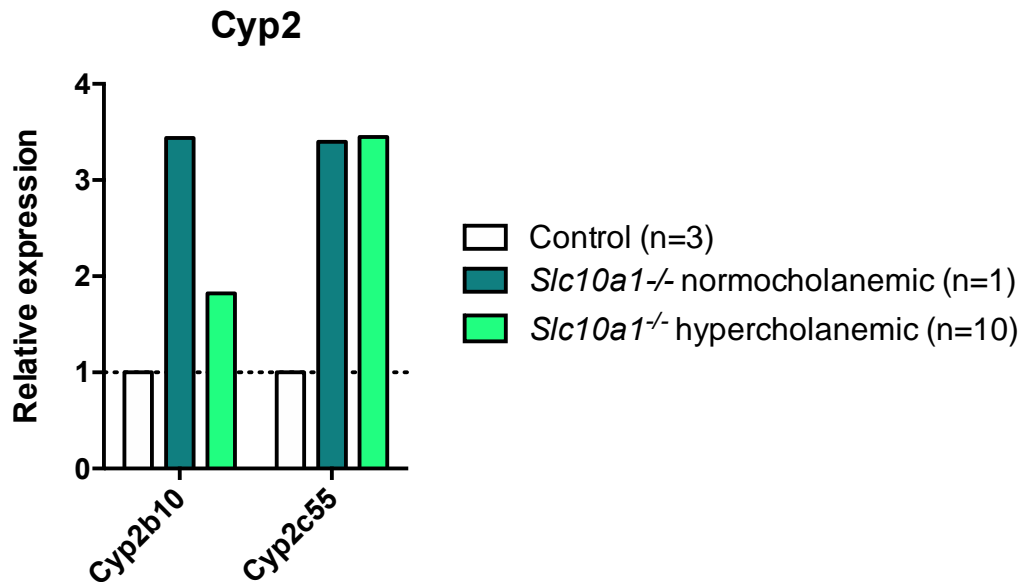
Description of female mice used in this study: One hypercholanemic KO mouse with low body weight, lethargy, hunched posture, and blood in urine was treated with subcutaneous fluids every two days for one week, from the age of five to six weeks postnatal. The condition of this mouse objectively improved, observed by increased body weight and increased locomotion. At 9 weeks of age, the total serum bile acid concentration for this mouse was 97 μ M. This mouse was deemed hypercholanemic and was sacrificed alongside a normocholanemic *Slc10a1*^{-/-} mouse that survived 9 weeks without subcutaneous intervention whose total serum bile acid concentration was 12 μ M. Additionally, three age-matched controls were sacrificed. RNA was extracted from livers of these five mice for subsequent gene array analysis by the Affymetrix GeneChip 2.0 at Robarts Research Institute. Bile acid concentrations and gene expression are presented below.



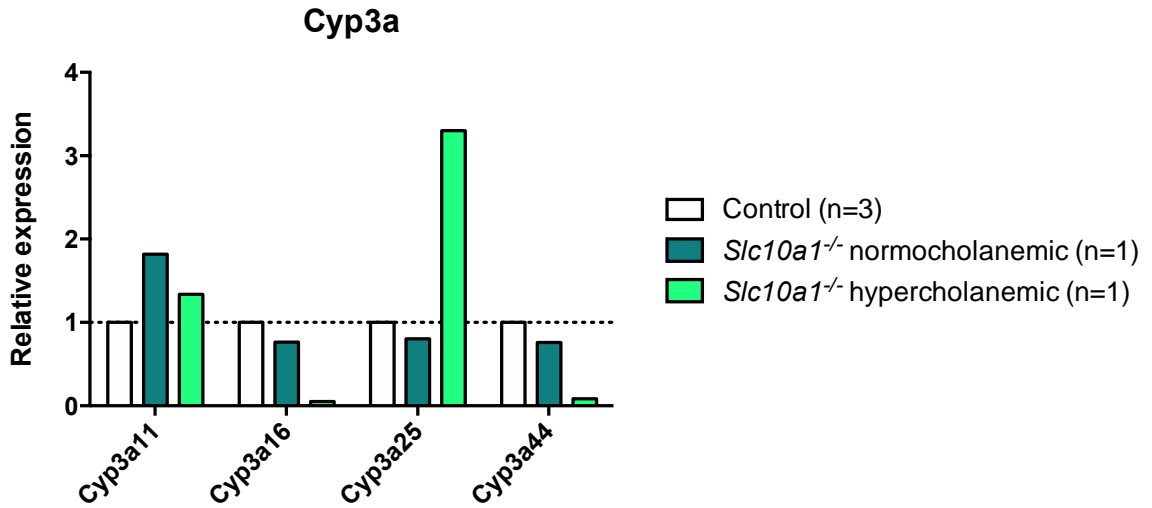
Appendix A. Figure 1. Total serum bile acid concentrations in 4-6-week-old control (n=3) and normocholanemic (n=1) and hypercholanemic (n=1) *Slc10a1*^{-/-} mice.



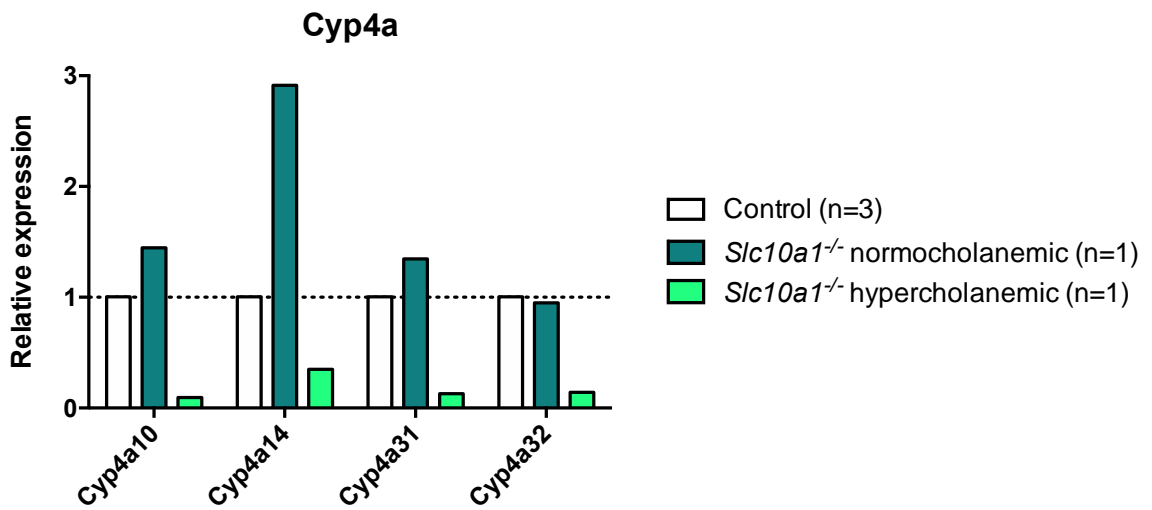
Appendix A Figure 2. Individual serum bile acid concentrations in 4-6-week-old control (n=3) and normocholanemic (n=1) and hypercholanemic (n=1) *Slc10a1*^{-/-} mice.



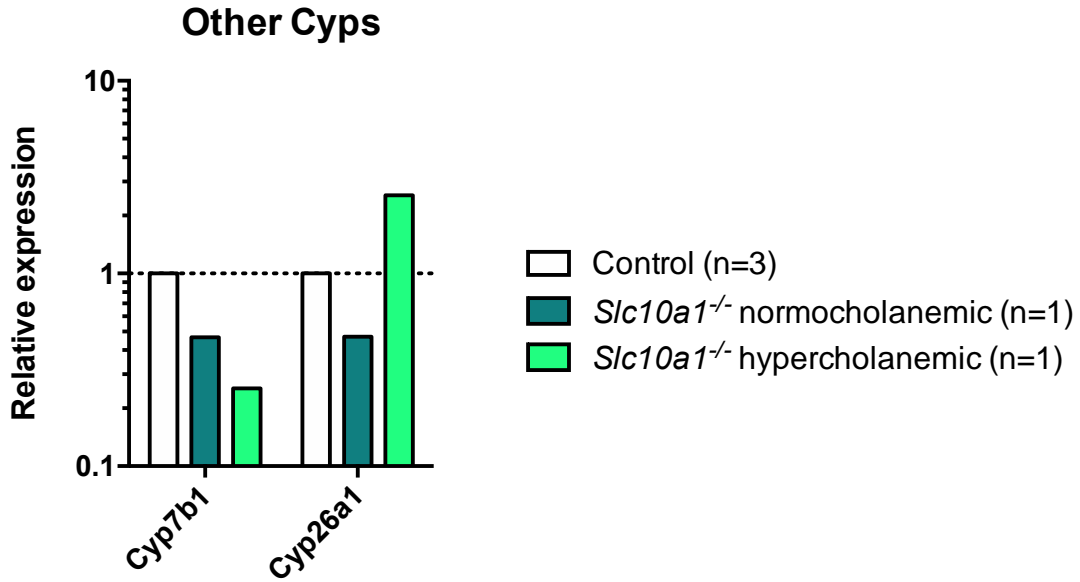
Appendix A. Figure 3. Gene transcript levels for *Cyp2a* genes in three control, one normocholanemic *Slc10a1*^{-/-} mouse (KO normocholanemic), and one hypercholanemic *Slc10a1*^{-/-} mouse (KO Hypercholanemic) determined by liver gene array.



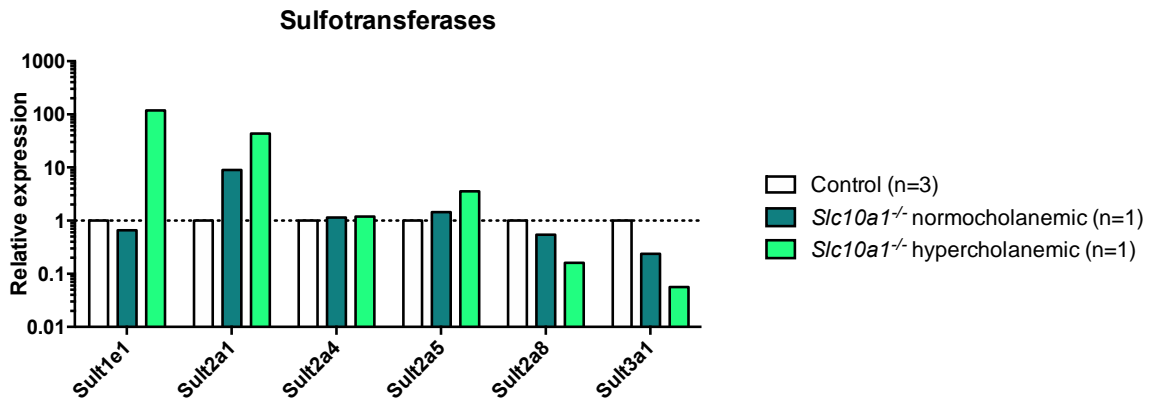
Appendix A. Figure 4. Gene transcript levels for *Cyp3a* genes in three control, one normocholanemic *Slc10a1*^{-/-} mouse (KO normocholanemic), and one hypercholanemic *Slc10a1*^{-/-} mouse (KO Hypercholanemic) determined by liver gene array.



Appendix A. Figure 5. Gene transcript levels for *Cyp4a* genes in three control, one normocholanemic *Slc10a1*^{-/-} mouse (KO normocholanemic), and one hypercholanemic *Slc10a1*^{-/-} mouse (KO Hypercholanemic) determined by liver gene array.



Appendix A. Figure 6. Gene transcript levels for additional *Cyp* genes in three control, one normocholanemic *Slc10a1*^{-/-} mouse (KO normocholanemic), and one hypercholanemic *Slc10a1*^{-/-} mouse (KO Hypercholanemic) determined by liver gene array.



Appendix A. Figure 7. Gene transcript levels for *Sult* genes in three control, one normocholanemic *Slc10a1*^{-/-} mouse (KO normocholanemic), and one hypercholanemic *Slc10a1*^{-/-} mouse (KO Hypercholanemic) determined by liver gene array.

Appendix B. Mouse necropsy reports

Western University
London, ON

Case #: 17-064918
AUP #/PI: 2015-011 /Kim
Clinical Vet: Dr. Emily Truscott

Received: August 14, 17 **Species:** mouse **Strain:** Ntcp ko Cre +/-
At Risk: newly weaned **Sex:** male **Age:** Mouse 1: DOB June 16/17 Mouse 2: DOB July 9/17

History: Mice are a C57BL6 background with a deletion of the bile acid transporter, Ntcp (Slco10a1). (The deletion is liver specific and was created by excising a portion of exon 2 via mating with Alb-Cre mice.) The knockout mice are similar to the controls at birth, but by 3-4 weeks they are much smaller than the controls. By 5-6 weeks many of the knockout mice are small, lethargic, hunched and have detectable bilirubin in their urine (identified on urine Chemstrips). They also have extremely high systemic bile acid levels. In extreme cases, there is also discoloration of the urine (likely bilirubinemia - no crystalluria present on microscopic examination). When these sick mice have died or have been sacrificed for experimental reasons we commonly observe enlarged gallbladders on necropsy. Many of these sick mice can recover if well monitored and given subcutaneous fluids regularly. By 8-9 weeks the knockout mice are able to gain weight and appear healthy.

Necropsy:

Both mice: smaller overall size versus littermates with a thin body condition. No evidence of external parasitism. The body wall/subcutaneous tissue appeared slightly jaundiced in both cases.

Mouse 1: The gall bladder was enlarged and pale yellow/white. There was an area of pale tissue/mesentery possibly related to the area of the pancreas/first bowel loop. Urine was collected and tested 1+ for bilirubin present.

Mouse 2: The gall bladder was enlarged and dark brown.

Histology: Tissues examined included: ~~kidneys, heart, lung, esophagus, trachea, small intestine, large intestines, stomach, liver, thyroid gland, gall bladder, urinary bladder, bone marrow, skeletal muscle, uterus, testicle, and spleen.~~ All tissues were interpreted to be within normal limits histologically, with the following exceptions:

Mouse 1 (slide 1):

Gall bladder: There is moderate diffuse papillary hyperplasia of the mucosa associated with patchy, cytoplasmic macrovesiculation of the distal tips of the villi. Many vacuoles are clear (likely contained fat), and many contain pale eosinophilic amorphous (hyaline) material (PAS stain negative). Multifocally, large tufts of the villus tips are degenerating and sloughing into the central lumen.

Kidney: Bilaterally, there is generalized deposition of amorphous eosinophilic to heterochromatic material within the distal and proximal tubules as well as within the collecting ducts, consistent with bile casts, some of which are mineralized

Liver: There is mild, generalized perinuclear rarefaction of hepatocytes.

Mouse 2 (slide 2):

Western University
London, ON

Case #: 17-064918
AUP #/PI: 2015-011 /Kim
Clinical Vet: [REDACTED]

Received: August 14, 17 **Species:** mouse **Strain:** ~~Ntcp ko Cre~~ +/-
At Risk: newly weaned **Sex:** male **Age:** Mouse 1: DOB June 16/17 Mouse 2: DOB July 9/17

History: Mice are a C57BL6 background with a deletion of the bile acid transporter, ~~Ntcp~~ (Slco10a1). (The deletion is liver specific and was created by excising a portion of exon 2 via mating with Alb-Cre mice.) The knockout mice are similar to the controls at birth, but by 3-4 weeks they are much smaller than the controls. By 5-6 weeks many of the knockout mice are small, lethargic, hunched and have detectable bilirubin in their urine (identified on urine ~~Chemstrips~~). They also have extremely high systemic bile acid levels. In extreme cases, there is also discoloration of the urine (likely bilirubinemia - no crystalluria present on microscopic examination). When these sick mice have died or have been sacrificed for experimental reasons we commonly observe enlarged gallbladders on necropsy. Many of these sick mice can recover if well monitored and given subcutaneous fluids regularly. By 8-9 weeks the knockout mice are able to gain weight and appear healthy.

Necropsy:

Both mice: smaller overall size versus littermates with a thin body condition. No evidence of external parasitism. The body wall/subcutaneous tissue appeared slightly jaundiced in both cases.

Mouse 1: The gall bladder was enlarged and pale yellow/white. There was an area of pale tissue/mesentery possibly related to the area of the pancreas/first bowel loop. Urine was collected and tested 1+ for bilirubin present.

Mouse 2: The gall bladder was enlarged and dark brown.

Histology: ~~Tissues examined included: kidneys, heart, lung, esophagus, trachea, small intestine, large intestine, stomach, liver, thyroid gland, gall bladder, urinary bladder, bone marrow, skeletal muscle, uterus, testicle, and spleen.~~ All tissues were interpreted to be within normal limits histologically, with the following exceptions:

Mouse 1 (slide 1):

Gall bladder: There is moderate diffuse papillary hyperplasia of the mucosa associated with patchy, cytoplasmic macrovesiculation of the distal tips of the villi. Many vacuoles are clear (likely contained fat), and many contain pale eosinophilic amorphous (hyaline) material (PAS stain negative). Multifocally, large tufts of the villus tips are degenerating and sloughing into the central lumen.

Kidney: Bilaterally, there is generalized deposition of amorphous eosinophilic to heterochromatic material within the distal and proximal tubules as well as within the collecting ducts, consistent with bile casts, some of which are mineralized

Liver: There is mild, generalized perinuclear rarefaction of hepatocytes.

Mouse 2 (slide 2):

Oct. 25, 2017

Necropsy report

Description: 2 juvenile male mice are presented live for necropsy and subsequently euthanized by isofluorane gas. Both are hunched, but ambulatory. Hair coat and skin are apparently normal. Teeth are aligned and show no malocclusion. Each mouse will be described below under 'small' and 'large' which denotes their relative size.


Small: The thymus is not apparent. The gall bladder is moderately distended and filled with green/brown clear fluid. The common bile duct is not prominent. The stomach is filled with ingesta and the intestines are filled with digesta with formed fecal material in the distal colon. There are no significant lesions of the major organs including the liver, spleen, kidney, adrenal glands, stomach, and intestines. There are likewise no significant lesions of the heart, lung, and brain. Body fat is minimal, but there is no apparent serous atrophy.

Large: The thymus is present. The gall bladder is markedly enlarged and filled with clear green to black fluid. The gall bladder extends approximately 3mm beyond the edge of the right medial lobe. The common bile duct is not prominent. The stomach is filled with ingesta and the intestines are filled with digesta with formed fecal material in the distal colon. Similar to the small mouse, there are no significant lesions of the major organs including the liver, spleen, kidney, adrenal glands, stomach, and intestines. There are likewise no significant lesions of the heart, lung, and brain. Body fat is minimal, but there is no apparent serous atrophy.

Preliminary diagnosis: Cholangiectasis

Interpretation: Consistent with reported previous findings, the gall bladder is enlarged. There are no secondary gross abnormalities that would suggest an ongoing severe pathologic process, such as inflammation. Lymph nodes are not prominent, which supports a non-reactive state. The gastrointestinal system contains abundant ingesta and digesta, which indicates robust appetite and digestive capability. The underconditioned state (low body fat) could reflect possible previous negative energy balance (i.e. off feed), conditions that prevents adequate nutritional absorption and/or a catabolic state. The reason for ill-thrift and hunched posture is not yet clear.

Thank you for the opportunity to necropsy the two mice. Please don't hesitate to contact me with any questions or comments.


Assistant Professor
Western University
Department of Pathology and Laboratory Medicine
Schulich School of Medicine & Dentistry
DSB4039
London ON N6A 3K7

Oct. 26, 2017

Necropsy report


Description: A female juvenile mouse is presented live for necropsy and subsequently euthanized by isofluorane gas. Similar to the mice necropsied on October 25th, 2017, this mouse is hunched, but ambulatory. Hair coat and skin are apparently normal. Teeth are aligned.

The thymus is present. The gall bladder is moderately enlarged and filled with clear green to black fluid. The common bile duct is not prominent. Compression of the gall bladder does not release bile into the duodenum. The stomach is filled with ingesta and the intestines are partially, but uniformly filled with digesta with formed fecal material in the distal colon. Similar to the previous necropsied mice, there are no significant lesions of the major organs including the liver, spleen, kidney, adrenal glands, stomach, and intestines. There are likewise no significant lesions of the heart, lung, and brain.

Preliminary diagnosis: Cholangiectasis

Interpretation: Consistent with the previous necropsies, the gall bladder is enlarged. Likewise, there are no secondary gross abnormalities that would suggest an ongoing severe pathologic process. Bile duct patency is difficult to test in small animals such as the mouse. The reason for ill-thrift and hunched posture is not yet clear.

Thank you for the opportunity to necropsy the mouse. Please don't hesitate to contact me with any questions or comments.


Assistant Professor
Western University
Department of Pathology and Laboratory Medicine
Schulich School of Medicine & Dentistry
DSB4039
London ON N6A 3K7

Oct. 30, 2017

Necropsy report


Description: A 4 week old male mouse is presented live for necropsy and subsequently euthanized by isofluorane gas. Similar to the mice necropsied on October 25 and 26, 2017, this mouse is hunched, but ambulatory. Subjectively, the mouse is more mobile than previous mice. Hair coat and skin are apparently normal. Teeth are aligned.

The thymus is present. The gall bladder is markedly enlarged, extending approximately 3mm from the edge of the right medial lobe, and filled with clear green to black fluid. The common bile duct is not prominent. The stomach is filled with ingesta and the intestines are partially, but uniformly filled with digesta with formed fecal material in the distal colon. Similar to the previous necropsied mice, there are no significant lesions of the major organs including the liver, spleen, kidney, adrenal glands, stomach, and intestines. There are likewise no significant lesions of the heart, lung, and brain.

Preliminary diagnosis: Cholangiectasis

Interpretation: Consistent with the previous necropsies, the gall bladder is enlarged. Likewise, there are no secondary gross abnormalities that would suggest an ongoing severe pathologic process. Histopathology may be helpful for assessing microscopic lesions. After fresh tissue harvesting for research purposes, organs were collected and infused with formalin when appropriate (intestines, lungs, heart). These tissues were placed in fixative for future trimming.

Thank you for the opportunity to necropsy the mouse. Please don't hesitate to contact me with any questions or comments.


Assistant Professor
Western University
Department of Pathology and Laboratory Medicine
Schulich School of Medicine & Dentistry
DSB4039
London ON N6A 3K7

Appendix C. Ethics & Animal Use Approvals



Office of Research Ethics

The University of Western Ontario
 Room 4180 Support Services Building, London, ON, Canada N6A 5C1
 Telephone: (519) 661-3036 Fax: (519) 850-2466 Email: ethics@uwo.ca
 Website: www.uwo.ca/research/ethics

Use of Human Subjects - Ethics Approval Notice

Principal Investigator: Dr. R.B. Kim

Review Number: 15586

Review Level: Full Board

Review Date: October 21, 2008

Protocol Title: Pharmacogenetics and drug response

Department and Institution: Medicine-Dept of, London Health Sciences Centre

Sponsor:

Ethics Approval Date: December 09, 2008

Expiry Date: November 30, 2012

Documents Reviewed and Approved: UWO Protocol, Letter of Information and Consent (v.6 Nov 2008)

Documents Received for Information:

This is to notify you that The University of Western Ontario Research Ethics Board for Health Sciences Research Involving Human Subjects (HSREB) which is organized and operates according to the Tri-Council Policy Statement: Ethical Conduct of Research Involving Humans and the Health Canada/ICH Good Clinical Practice Practices: Consolidated Guidelines; and the applicable laws and regulations of Ontario has reviewed and granted approval to the above referenced study on the approval date noted above. The membership of this REB also complies with the membership requirements for REB's as defined in Division 5 of the Food and Drug Regulations.

The ethics approval for this study shall remain valid until the expiry date noted above assuming timely and acceptable responses to the HSREB's periodic requests for surveillance and monitoring information. If you require an updated approval notice prior to that time you must request it using the UWO Updated Approval Request Form.

During the course of the research, no deviations from, or changes to, the protocol or consent form may be initiated without prior written approval from the HSREB except when necessary to eliminate immediate hazards to the subject or when the change(s) involve only logistical or administrative aspects of the study (e.g. change of monitor, telephone number). Expedited review of minor change(s) in ongoing studies will be considered. Subjects must receive a copy of the signed information/consent documentation.

Investigators must promptly also report to the HSREB:

- a) changes increasing the risk to the participant(s) and/or affecting significantly the conduct of the study;
- b) all adverse and unexpected experiences or events that are both serious and unexpected;
- c) new information that may adversely affect the safety of the subjects or the conduct of the study.

If these changes/adverse events require a change to the information/consent documentation, and/or recruitment advertisement, the newly revised information/consent documentation, and/or advertisement, must be submitted to this office for approval.

Members of the HSREB who are named as investigators in research studies, or declare a conflict of interest, do not participate in discussion related to, nor vote on, such studies when they are presented to the HSREB.

 Chair of HSREB

Ethics Officer to Contact for Further Information			
<input type="checkbox"/> Janice Sutherland (jsutherl@uwo.ca)	<input type="checkbox"/> Elizabeth Wambolt (ewambolt@uwo.ca)	<input type="checkbox"/> Grace Kelly (grace.kelly@uwo.ca)	<input checked="" type="checkbox"/> Denise Grafton (dgrafton@uwo.ca)

This is an official document. Please retain the original in your files.

cc: ORE File
 LHRI



Date: 18 October 2017

To: Richard Kim

Project ID: 5683

Study Title: Pharmacogenetics and drug response (REB# 15586)

Application Type: Continuing Ethics Review (CER) Form

Review Type: Delegated

FB Reporting Date: November 7, 2017

Date Approval Issued: 18/Oct/2017 11:31

REB Approval Expiry Date: 25/Nov/2018

Dear Richard Kim ,

The Western University Research Ethics Board has reviewed the application. This study, including all currently approved documents, has been re-approved until the expiry date noted above.

REB members involved in the research project do not participate in the review, discussion or decision.

Western University REB operates in compliance with, and is constituted in accordance with, the requirements of the TriCouncil Policy Statement: Ethical Conduct for Research Involving Humans (TCPS 2); the International Conference on Harmonisation Good Clinical Practice Consolidated Guideline (ICH GCP); Part C, Division 5 of the Food and Drug Regulations; Part 4 of the Natural Health Products Regulations; Part 3 of the Medical Devices Regulations and the provisions of the Ontario Personal Health Information Protection Act (PHIPA 2004) and its applicable regulations. The REB is registered with the U.S. Department of Health & Human Services under the IRB registration number IRB 00000940.

Please do not hesitate to contact us if you have any questions.

Sincerely,



AUP Number: 2015-011

PI Name: Kim, Richard


AUP Title: Phenotypic And Pharmacokinetic Evaluation Of An Ntcp Knockout Mouse Model

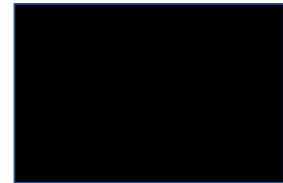
Approval Date: 06/16/2015

Official Notice of Animal Use Subcommittee (AUS) Approval: Your new Animal Use Protocol (AUP) entitled "Phenotypic And Pharmacokinetic Evaluation Of An Ntcp Knockout Mouse Model" has been APPROVED by the Animal Use Subcommittee of the University Council on Animal Care. This approval, although valid for four years, and is subject to annual Protocol Renewal.2015-011::1

1. This AUP number must be indicated when ordering animals for this project.
2. Animals for other projects may not be ordered under this AUP number.
3. Purchases of animals other than through this system must be cleared through the ACVS office. Health certificates will be required.

The holder of this Animal Use Protocol is responsible to ensure that all associated safety components (biosafety, radiation safety, general laboratory safety) comply with institutional safety standards and have received all necessary approvals. Please consult directly with your institutional safety officers.

Submitted by: 
on behalf of the Animal Use Subcommittee
University Council on Animal Care



The University of Western Ontario
Animal Use Subcommittee / University Council on Animal Care
Health Sciences Centre, • London, Ontario • CANADA – N6A 5C1
PH: 519-661-2111 ext. 86768 • FL 519-661-2028
Email: auspc@uwo.ca • <http://www.uwo.ca/animal/website/>

Appendix D. Permission to reproduce published articles

Dear Laura Russell,

Future Medicine Ltd. has approved your recent request. Before you can use this content, you must accept the license fee and terms set by the publisher.

Use this [link](#) to accept (or decline) the publisher's fee and terms for this order.

Request Summary:

Submit date: 02-Jun-2020

Request ID: 600015247

Publication: Pharmacogenomics

Title: Variant discovery using next-generation sequencing and its future role in pharmacogenetics.

Type of Use: Republish in a thesis/dissertation

Please do not reply to this message.

To speak with a Customer Service Representative, call +1-855-239-3415 toll free or +1-978-646-2600 (24 hours a day), or email your questions and comments to support@copyright.com.

Sincerely,

Copyright Clearance Center

Pharmacogenomics

Article Variant discovery using next-generation sequencing and its future role in pharmacogenetics.

GENERAL INFORMATION

Request ID	600015247	Request Date	02 Jun 2020
Request Status	Accepted	Price	0.00 CAD 

[> ALL DETAILS](#)

COMMENTS

 [Add Comment / Attachment](#)

02 Jun 2020 3:40:57 PM, by Laura Russell

I am hoping to reproduce the sections on Rare genetic variation and Computation predictions for my thesis, as I wrote these sections of the review and they are pertinent information for my PhD thesis



In Vitro Functional Characterization and in Silico Prediction of Rare Genetic Variation in the Bile Acid and Drug Transporter, Na⁻Taurocholate Cotransporting Polypeptide (NTCP, SLC10A1)

Author: Laura E. Russell, Yitian Zhou, Volker M. Lauschke, et al

Publication: Molecular Pharmaceutics

Publisher: American Chemical Society

Date: Apr 1, 2020

Copyright © 2020, American Chemical Society

PERMISSION/LICENSE IS GRANTED FOR YOUR ORDER AT NO CHARGE

This type of permission/license, instead of the standard Terms & Conditions, is sent to you because no fee is being charged for your order. Please note the following:

- Permission is granted for your request in both print and electronic formats, and translations.
- If figures and/or tables were requested, they may be adapted or used in part.
- Please print this page for your records and send a copy of it to your publisher/graduate school.
- Appropriate credit for the requested material should be given as follows: "Reprinted (adapted) with permission from (COMPLETE REFERENCE CITATION). Copyright (YEAR) American Chemical Society." Insert appropriate information in place of the capitalized words.
- One-time permission is granted only for the use specified in your request. No additional uses are granted (such as derivative works or other editions). For any other uses, please submit a new request.

Curriculum Vitae

Laura Russell

Post-secondary Education and Degrees:

The University of Western Ontario, London, Ontario, Canada
2015-2020: Ph.D., Physiology & Pharmacology

The University of Western Ontario, London, Ontario, Canada
2010-2015 Honours B.Sc., Major Medical Sciences, Major French Studies

Honours and Awards:

National Scholarship, Canadian Institutes of Health Research 2019 – 2020
Drug Safety and Effectiveness Cross-Disciplinary Training Program, Stream 2

National Scholarship, Canadian Institutes of Health Research 2018 – 2019
Drug Safety and Effectiveness Cross-Disciplinary Training Program, Stream 1

Clinical & Basic Pharmacology Poster Presentation Award, presented by
Western University at Physiology & Pharmacology Research Day in London,
Canada, November 5, 2019

Clinical & Basic Pharmacology Poster Presentation Award, presented by
Western University at Physiology & Pharmacology Research Day in London,
Canada, November 6, 2018

Rhoderic Reiffenstein Poster Presentation Award, presented by the Canadian
Society of Pharmacology & Therapeutics at the Joint Meeting of Canadian
Society of Pharmacology & Therapeutics, Canadian Society for Pharmaceutical
Sciences, and Canadian Chapter for Controlled Release Society in Toronto,
Canada, May 22-25, 2018

William Mahon Oral Presentation Award, presented by the Canadian Society of
Pharmacology & Therapeutics at the 2016 Safety Pharmacology
Society/Canadian Society of Pharmacology & Therapeutics/Japanese Safety
Pharmacology Society Joint Meeting in Vancouver, Canada, September 18-21,
2016

Publications:

Russell LE, Zhou Y, Lauschke VM, Kim RB. 2020. *In vitro* functional
characterization and *in silico* prediction of rare genetic variation in the bile acid

and drug transporter, Na⁺-taurocholate co-transporting polypeptide (NTCP, *SLC10A1*). *Mol Pharm* 17(4):1170-81.

Russell LE and Schwarz UI. 2020. Variant discovery using next-generation sequencing and its future role in pharmacogenetics. *Pharmacogenomics* 21(7):471-86.

Russell LE & Schleiff MA, Gonzalez E, Bart AG, Broccatelli F, Durmus S, Hartman JH, Humphreys WG, Lauschke VM, Martin I, Nichols C, Nwabufo C, Prasad B, Scott EE, Segall M, Takahashi R, Taub ME and Sodhi JK. 2020. Advances in the Study of Drug Metabolism – Symposium Report of the 12th Meeting of the International Society for the Study of Xenobiotics (ISSX). *Drug Metab Rev* 52(3):395-407.

Abstracts presented as oral presentations at conferences:

“Genetic variation in the hepatic bile acid and drug transporter, NTCP: expression, transport, and *in silico* functional prediction”, London Health Research Day, London, Canada, April 30, 2019

“Function & expression of rare genetic variants in bile acid and drug transporter NTCP”, Drug Safety and Effectiveness Cross-Disciplinary Training Program Annual Symposium, Toronto, Canada, April 10-12, 2019

“*In vitro* characterization of genetic variation in the bile acid transporter NTCP” Canadian Society of Pharmacology & Therapeutics Annual Meeting, Halifax, Canada, June 14- 16, 2017

“Elucidating the impact of genetic variation in bile acid transporters on bile acid and xenobiotic transport”, 2016 Safety Pharmacology Society/Canadian Society of Pharmacology & Therapeutics/Japanese Safety Pharmacology Society Joint Meeting, Vancouver, Canada, September 18-21, 2016

Abstracts presented as poster presentations at conferences:

“*In vitro* characterization and *in silico* prediction of rare genetic variants in bile acid and drug transporter, NTCP”. Physiology & Pharmacology Annual Research Day, Western University, London, Canada, November 5, 2019

“*In vitro* functional characterization of rare genetic variants in bile acid and drug transporter, NTCP”, International Society for the Study of Xenobiotics (ISSX) 12th International Meeting, Portland, Oregon, USA, July 28-31, 2019

“Investigating the mechanisms of bile acid-mediated organ toxicity in Ntcp (*Slc10a1*) knockout mice”, Physiology & Pharmacology Annual Research Day, Western University, London, Canada, November 6, 2018

“Investigating the effect of the gut microbiome on pharmacokinetics”, Genentech Intern Poster Day, South San Francisco, August 8, 2018

“Investigating the mechanisms of bile acid-mediated organ toxicity in Ntcp (*Slc10a1*) knockout mice”, Joint Meeting of Canadian Society of Pharmacology & Therapeutics, Canadian Society for Pharmaceutical Sciences, and Canadian Chapter for Controlled Release Society, Toronto, Canada, May 22-25, 2018

“*In silico* prediction of functional genetic variation in the hepatic bile acid transporter NTCP”, Joint Drug Safety & Effectiveness Cross-Training Program and the International Society for Pharmacoepidemiology, Toronto, Canada, April 22-25, 2018

“*In silico* prediction of functional genetic variation in the hepatic bile acid transporter NTCP”, Physiology & Pharmacology Research Day, Western University, London, Canada, November 7, 2017

“The functional role of genetic variation in the bile acid transporter NTCP”, London Health Research Day, London, Canada, March 28, 2017

“Elucidating the physiological impact of genetic variation in bile acid transporters”, Physiology & Pharmacology Research Day, Western University, London, Canada, November 1, 2016

Invited seminar presentations:

“Epigenetic regulation of bile acid transport”, Clinical Pharmacology Journal Club, Western University, London, Canada, March 26, 2020 *Cancelled due to COVID-19

“Biomarkers of Hepatic Drug Transporter Function: Improving Drug Development and Patient Therapy”, Drug Safety & Efficacy Cross Disciplinary Training Program Objective Structured Knowledge Translation Experience, Online, March 24, 2020

“Phosphorylation, bile acid homeostasis, and primary biliary cirrhosis”, Clinical Pharmacology Journal Club, Western University, London, Canada April 18, 2019

“Effective use of genomic data & applications for drug therapy”, Drug Safety & Efficacy Cross Disciplinary Training Program Objective Structured Knowledge Translation Experience, Online presentation, March 22, 2019

“Investigating the effect of the gut microbiome on pharmacokinetics: Genentech summer internship”, Clinical Pharmacology Grand Rounds, Western University, London, Canada, October 31, 2018

Discussing the journal article “FXR Agonists OCA and CDCA Increase Bile Acid Efflux in Sandwich-Cultured Human Hepatocytes: Functional Evidence and Mechanisms”, by Guo et al., Clinical Pharmacology Journal Club, Western University, London, Canada, March 22, 2018

“Elucidating the effects of genetic variation in hepatic bile acid & drug uptake transporter, NTCP”, Clinical Pharmacology Grand Rounds, Western University, London, Canada, March 7, 2018

Related Work Experience:

Genentech Summer Intern, June – September 2018

Research internship in the department of Drug Metabolism and Pharmacokinetics at Genentech, South San Francisco, USA.

Research project: determining the role of the gut microbiome on the pharmacokinetics and metabolism of two Genentech compounds in rodent models of gut microbiome depletion

Experience using Phoenix Win-Nonlin, antibiotic-induced knockdown of gut microbiome in mice and rats, germ-free mice, microsomal stability assays, aerobic and anaerobic stool culture incubations, LC/MS

Teaching Assistantships:

Physiology & Pharmacology 4980E: Seminar & Research Project, 2018 – 2020
A major laboratory project in Physiology or Pharmacology, which emphasizes experimental design, instrumentation, collection/analysis of data and communication of experimental results by oral, poster, and written presentations
Responsibilities: attend classes, presentations for class workshops, assist in developing research skills among students, grade assignments, administrative duties

Pharmacology 3620: Human Pharmacology & Therapeutic Principles, 2016 – 2018

Full year systems-based pharmacology course that examines drugs used to treat diseases that affect various organs of the body

Responsibilities as teaching assistant: Attend classes, answer student questions pertaining to course material, perform course review sessions, proctor exams

Pharmacology 2060: Introductory Pharmacology & Therapeutics, Jan. – Apr. 2016

Online course to assist in understanding fundamentals of drug action

Responsibilities: Answer student questions pertaining to lecture material, proctor exams